



## City Research Online

### City, University of London Institutional Repository

---

**Citation:** Kohl, C. (2017). Neural Substrates of Human Perceptual Decision-Making. (Unpublished Doctoral thesis, City, University of London)

This is the accepted version of the paper.

This version of the publication may differ from the final published version.

---

**Permanent repository link:** <https://openaccess.city.ac.uk/id/eprint/18904/>

**Link to published version:**

**Copyright:** City Research Online aims to make research outputs of City, University of London available to a wider audience. Copyright and Moral Rights remain with the author(s) and/or copyright holders. URLs from City Research Online may be freely distributed and linked to.

**Reuse:** Copies of full items can be used for personal research or study, educational, or not-for-profit purposes without prior permission or charge. Provided that the authors, title and full bibliographic details are credited, a hyperlink and/or URL is given for the original metadata page and the content is not changed in any way.

# Neural Substrates of Human Perceptual Decision-Making

Carmen Kohl

A thesis submitted for the degree of PhD in Psychology



City, University of London  
Department of Psychology  
Cognitive Neuroscience Research Unit

October 2017



# Table of Contents

Acknowledgements.....	10
Abstract.....	11
1. General Introduction.....	12
1.1. Sequential Sampling Models.....	12
1.1.1. Random-walk Models.....	13
1.1.2. Accumulator Models.....	15
1.2. Neural Correlates of the Decision Variable.....	18
1.2.1. Neural Activity in Non-human Primates.....	19
1.2.2. Activity in the Human Brain.....	22
1.2.2.1. Functional Magnetic Resonance Imaging.....	22
1.2.2.2. Electroencephalography and Magnetoencephalography.....	24
1.2.2.3. Transcranial Magnetic Stimulation.....	30
1.3. Model-based Analysis of Neural Signals.....	33
1.4. Current Project.....	37
2. Exploring Neural Correlates of Decision-Making under Speed/Accuracy Instructions.....	42
2.1. Experiment 1: EEG.....	48
2.1.1. Methods.....	49
2.1.1.1. Participants.....	49
2.1.1.2. Stimuli and Procedure.....	50
2.1.1.2.1. Stimuli and Experiment Setup.....	50
2.1.1.2.2. Difficulty Calibration.....	51
2.1.1.2.3. SAT Instructions.....	52
2.1.1.3. EEG Recording and Pre-processing.....	53
2.1.1.4. ERP Analysis.....	54
2.1.1.5. Model.....	55
2.1.1.5.1. Standard Model.....	56
2.1.1.5.2. Rescaled Model.....	57
2.1.1.5.3. Model Prediction.....	58
2.1.1.5.4. Bootstrap Comparison.....	59

2.1.2.	Results .....	60
2.1.2.1.	Behavioural Results .....	60
2.1.2.2.	ERP Results .....	62
2.1.2.3.	Model Results .....	63
2.1.3.	Discussion Experiment 1 .....	68
2.2.	Experiment 2: TMS .....	69
2.2.1.	Methods .....	71
2.2.1.1.	Participants .....	71
2.2.1.2.	Stimuli and Procedure .....	72
2.2.1.3.	Stimulation and Recording .....	72
2.2.1.4.	EMG/MEP Pre-processing .....	74
2.2.1.5.	MEP Smoothing .....	75
2.2.1.6.	Statistical Analysis .....	75
2.2.1.7.	Model .....	76
2.2.1.7.1.	Model Comparison .....	78
2.2.2.	Results .....	79
2.2.2.1.	Behavioural Results .....	79
2.2.2.2.	MEP Results .....	81
2.2.2.3.	Model Results .....	82
2.2.3.	Discussion Experiment 2 .....	86
2.3.	General Discussion .....	87
3.	Testing Different Neural Correlates of the Decision Variable .....	94
3.1.	Methods .....	104
3.1.1.	Participants .....	104
3.1.2.	Stimuli and Procedure .....	104
3.1.3.	EEG Recording and Analysis .....	106
3.1.3.1.	Event-related Potentials .....	107
3.1.3.1.1.	Centroparietal Positivity (CPP) .....	107
3.1.3.1.2.	Lateralised Readiness Potential (LRP) .....	108
3.1.3.2.	Time-Frequency Analysis .....	108
3.1.3.2.1.	Event-Related Beta Desynchronisation .....	109
3.1.3.3.	Statistical Analysis .....	109
3.1.3.4.	Exploratory Approach .....	110
3.2.	Results .....	111
3.2.1.	Behavioural Results .....	111

3.2.2.	Neural Results.....	113
3.2.2.1.	Centroparietal Positivity (CPP) .....	113
3.2.2.2.	Lateralised Readiness Potential (LRP) .....	113
3.2.2.3.	Event-Related Beta Desynchronisation .....	114
3.2.2.4.	Exploratory Approach .....	116
3.3.	Discussion .....	120
3.3.1.	Centroparietal Positivity (CPP) .....	121
3.3.2.	Lateralised Readiness Potential (LRP).....	123
3.3.3.	Event-related Beta Desynchronisation .....	124
3.3.4.	Exploratory Approach.....	126
3.3.5.	Summary.....	127
4.	Testing the CPP as a Decision Variable Signal by Manipulating Evidence Dynamics and Biases .....	129
4.1.	Experiment 1: Non-stationary Evidence.....	134
4.1.1.	Methods .....	137
4.1.1.1.	Participants.....	137
4.1.1.2.	Stimuli and Procedure .....	138
4.1.1.3.	EEG Recording and Pre-processing.....	141
4.1.1.3.1.	ERP Analysis .....	142
4.1.1.4.	Statistical Analysis .....	143
4.1.1.5.	Model Fit.....	144
4.1.1.6.	Model Prediction.....	148
4.1.2.	Results .....	150
4.1.2.1.	Behavioural Results.....	150
4.1.2.2.	ERP Results .....	152
4.1.2.3.	Model Fit.....	155
4.1.2.4.	Model Prediction.....	157
4.1.3.	Discussion Experiment 1 .....	160
4.2.	Experiment 2: Decision Bias .....	164
4.2.1.	Methods .....	167
4.2.1.1.	Participants.....	167
4.2.1.2.	Stimuli and Procedure .....	167
4.2.1.2.1.	EEG Recording and Pre-processing .....	169
4.2.1.2.2.	ERP Analysis .....	169
4.2.1.3.	Statistical Analysis .....	169

4.2.1.4.	Model Fit.....	170
4.2.1.5.	Model Prediction.....	173
4.2.2.	Results.....	173
4.2.2.1.	Behavioural Results.....	173
4.2.2.2.	ERP Results.....	175
4.2.2.3.	Model Fit.....	176
4.2.2.4.	Model Prediction.....	178
4.2.3.	Discussion Experiment 2.....	180
4.3.	General Discussion.....	184
5.	Multiple-Alternative Decision-Making.....	188
5.1.	Methods.....	196
5.1.1.	Participants.....	196
5.1.2.	Stimuli and Procedure.....	196
5.1.2.1.	Colour Calibration.....	197
5.1.2.2.	Stimuli and Experiment Setup.....	197
5.1.3.	Stimulation and Recording.....	201
5.1.4.	EMG Processing.....	202
5.1.4.1.	Pre-processing.....	202
5.1.4.2.	Re-categorisation.....	203
5.1.4.3.	Smoothing.....	206
5.1.4.4.	Statistical Analysis.....	207
5.1.5.	Model.....	208
5.1.5.1.	Model Fit.....	209
5.1.5.2.	Model Prediction.....	213
5.2.	Results.....	214
5.2.1.	Behavioural Results.....	214
5.2.2.	MEP Results.....	218
5.2.2.1.	Statistical Comparison.....	220
5.2.3.	Model.....	221
5.3.	Discussion.....	226
6.	General Discussion.....	234
6.1.	Summary.....	236
6.2.	Overall Findings.....	246
6.3.	Limitations and Future Directions.....	251
6.4.	Conclusion.....	253

7. Appendices.....	255
7.1. Appendix 1: Model Results for Normalised Data (Chapter 2, Experiment 1) .....	255
7.2. Appendix 2: Comparison of Two-choice 'within' and Two-choice 'between' Conditions (Chapter 5) .....	259
8. References .....	261

## Table of Figures

Figure 1.1: Diffusion model .....	14
Figure 1.2: Race model.....	16
Figure 1.3: Leaky competing accumulator (LCA) model .....	17
Figure 1.4: Typical decision-making experiment with non-human primates.....	20
Figure 1.5: CPP (Kelly & O’Connell, 2013) .....	29
Figure 2.1: Random dot motion task trial procedure .....	53
Figure 2.2: Race model.....	56
Figure 2.3: Behavioural results .....	61
Figure 2.4: CPP results.....	63
Figure 2.5: Model fit .....	66
Figure 2.6: Decision variable (empirical and simulated).....	67
Figure 2.7: EMG recording setup .....	73
Figure 2.8: MEP processing and simulation.....	78
Figure 2.9: Behavioural results .....	80
Figure 2.10: MEP results .....	82
Figure 2.11: Model fit .....	84
Figure 2.12: Decision variable (empirical and simulated).....	85
Figure 3.1: Simplified illustration of an accumulation process in a sequential sampling model framework .....	104
Figure 3.2: Random dot motion task trial procedure .....	106
Figure 3.3: Behavioural results .....	112
Figure 3.4: Neural results.....	115
Figure 3.5: ERP cluster.....	117
Figure 3.6: TFR cluster .....	119
Figure 4.1: Experiment 1 random dot motion task trial procedure .....	141
Figure 4.2: Race model.....	145
Figure 4.3: Race model applied to interruption and difficulty conditions .....	147
Figure 4.4: Behavioural results .....	151
Figure 4.5: CPP results.....	153
Figure 4.6: Model fit.....	157
Figure 4.7: Decision variable (empirical and simulated).....	159
Figure 4.8: Random dot motion task trial procedure .....	169
Figure 4.9: Race model applied to biased decisions.....	172
Figure 4.10: Behavioural results .....	174
Figure 4.11: CPP results.....	175
Figure 4.12: Model fit .....	178
Figure 4.13: Decision variable (empirical and simulated).....	179
Figure 5.1: Colour discrimination task.....	200
Figure 5.2: MEP categorisation.....	205
Figure 5.3: MEP processing.....	207
Figure 5.4: Standard LCA model .....	209

Figure 5.5: Model 1: LCA model applied to the current experiment .....	212
Figure 5.6: Behavioural results .....	216
Figure 5.7: MEP results (smoothed MEP signal for each muscle category) ...	219
Figure 5.8: MEP results (smoothed MEP signals for the difference between responding and non-responding muscles).....	220
Figure 5.9: Model fit .....	223
Figure 5.10: Decision variable (simulated).....	225
Figure 5.11: LCA Predictions of the difference between responding ('Correct') and non-responding ('Error 1') muscles .....	226
Figure 7.1: Model fit .....	257
Figure 7.2: Decision variable (empirical and simulated).....	258
Figure 7.3: MEP results (smoothed MEP signal for each muscle category) ...	260

## Table of Tables

Table 2.1: Model Comparison .....	64
Table 2.2: Estimated parameter values for the chosen model (Model 2) and its rescaled version .....	64
Table 2.3: Estimated parameter values for the chosen model (Model 2) and its rescaled version .....	83
Table 4.1: Model Comparison .....	155
Table 4.2: Estimated parameter values for the chosen model (Model 2) .....	155
Table 4.3: Model Comparison .....	177
Table 4.4: Estimated parameter values for the chosen model (Model 2) .....	177
Table 5.1: Model comparison .....	222
Table 5.2: Estimated parameter values for the chosen model (Model 1) .....	222
Table 7.1: Model Comparison .....	255
Table 7.2: Estimated parameter values for the chosen model (Model 2) and its rescaled version .....	256

## Acknowledgements

First and foremost, I would like to thank my supervisor Kielan Yarrow. He is a fantastic supervisor, and this project would not have been possible without his insight and expertise. His knowledge, but also his patience and serenity led me through this project, and I am very grateful to have worked with him.

I am equally indebted to Laure Spieser, who worked closely with me throughout these three years and, in fact, contributed as much as I did to this project. Her modelling work formed the backbone of our studies, and the discussions I had with her as well as Kielan were invaluable. Throughout these three years, the three of us made a fantastic team, and I am grateful for working in such a stimulating environment.

I would also like to thank my second and third supervisors, Bettina Forster and Sven Bestmann, as well as Leverhulme Trust for generously funding this project.

Lastly I would like to express my gratitude to my colleagues, friends, and family, and in particular my parents who have provided vital support throughout the years.

## Abstract

Perceptual decision-making describes the process of choosing one of at least two response alternatives based on sensory evidence. This sensorimotor process underlies a range of human behaviours and has been studied extensively by both psychologists and neuroscientists. There is now a consensus, that perceptual decision-making can be explained by sequential sampling models, which assume that we make decisions by accumulating sensory evidence over time until a decision threshold is reached and the response is executed. Although these models are designed to explain behavioural data, the accumulation-to-bound processes they predict have recently been shown to occur in the brain. In this project, we set out to explore these neural correlates of decision-making in the human brain by combining mathematical modelling with neuroimaging. We fitted sequential sampling models to human decision-making data collected in a number of paradigms and directly compared the associated accumulation profiles with neural signals, which were generated either by using electroencephalographic (EEG) recordings or through transcranial magnetic stimulation (TMS). We found that decision-related accumulation profiles can be observed using a parietal EEG signal, namely the event-related potential centroparietal positivity (CPP). Additionally, we showed that accumulation is fed forward to the motor system, where it can be measured using TMS-induced motor evoked potentials. We demonstrated that, under a number of manipulations, namely difficulty, response speed instructions, non-stationary evidence, decision biases, and number of alternatives, these signals display profiles similar to those predicted by sequential sampling models. Our findings support the notion that sequential sampling occurs in the human brain and demonstrate that a model-based approach in which sequential sampling models and neuroimaging are combined and inform each other, can shed light on the underlying mechanisms of human perceptual decision-making.

# 1. General Introduction

The ability to use information from the environment to quickly choose between two or more alternatives and guide our actions is a crucial part of human cognition. Whether we need to decide if it is safe to cross a road or which queue to join at the till, we constantly use sensory evidence to select appropriate motor responses countless times every day. In fact, it could be argued that virtually all human behaviour is based on perceptual decisions. The term 'perceptual decision' has been used for several decades and describes any decision (i.e. any choice between two or more alternatives) which is performed relatively quickly (typically within 1000 to 2000 ms) and is made based on sensory evidence (Krullee, Podell, & Ronco, 1954; Newsome, Britten, & Movshon, 1989; Ulehla, 1966).

Due to its central role in human cognition, a large body of research, in the fields of both psychology and neuroscience, has been dedicated to the understanding of perceptual decision-making, and a number of accounts have been suggested to explain the underlying mechanisms of how we make these decisions.

## 1.1. Sequential Sampling Models

One particularly influential concept in the field of perceptual decision-making has been that of sequential sampling models. This term describes a family of computational models which have a number of assumptions in common, at the core of which is the notion that perceptual decisions are made by sequentially integrating sensory stimuli and extracting decision-relevant information about the nature of the stimulus. This sensory evidence is accumulated over time and compared against a decision threshold. Once this threshold is reached, a decision is made and the appropriate response is initiated. While all sequential sampling models share the basic notion that sensory evidence is accumulated until a threshold is reached, there are a number of models that differ in important aspects, including complexity or the extent to which they are

neurophysiologically plausible. One aspect in which models within this framework differ is the nature of their stopping rule, which distinguishes between two types of models: random-walk models with a relative stopping rule, and accumulator models with an absolute stopping rule (Smith & Ratcliff, 2004).

### 1.1.1. Random-walk Models

Random-walk models typically assume that, in a binary decision, evidence for both alternatives is integrated in a single accumulator. The accumulation process begins at a starting point located midway between two thresholds, each associated with one of the response alternatives, and evidence is accumulated to a single total, with evidence in favour of alternative 'M' reflecting evidence against alternative 'N'.

One example of a random-walk model is the Diffusion model, which is arguably the most commonly applied of all sequential sampling models (Ratcliff, 1978; Ratcliff & McKoon, 2008; see Figure 1.1). In this model, a single accumulator with a threshold at a distance of  $a/2$  to either side of the starting point  $z$ , which is drawn from a uniform distribution with the range  $S_z$ , accumulates evidence over time according to a Wiener diffusion process. The accumulation profile is determined by the drift rate, which is drawn from a normal distribution with the mean  $\nu$  and the standard deviation  $\eta$ , as well as within-trial variability  $\sigma^2$ . Therefore, when the process is discretised, the accumulation at a certain time point corresponds to the sum of the information at the previous time point, a systematic amount of information  $I$  and Gaussian noise with mean 0 and standard deviation  $\sigma$ .

$$dx = I + N(0, \sigma^2) \quad (1.1.)$$

The reaction time (RT) is defined by the time taken for the accumulation to reach the threshold, plus a non-decision time  $T_{er}$  which is uniformly distributed with a range of  $S_{Ter}$  and accounts for any time used for sensory encoding and motor processing before and after the accumulation process respectively.

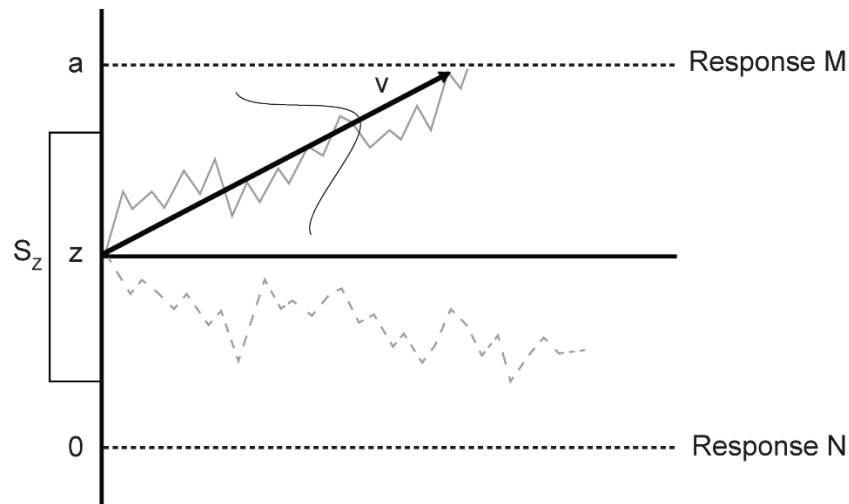


Figure 1.1: Diffusion model: a random-walk model in which accumulation begins at a starting point  $z$  and continues at an average rate  $v$ , towards one of two boundaries, each associated with a given response. The time taken to reach the boundary plus a non-decision time  $T_{er}$  determine the reaction time (RT). Additionally, the model assumes inter-trial variability, as  $z$  and  $T_{er}$  have a uniform distribution with the ranges  $S_z$  and  $S_{T_{er}}$ , and  $v$  is normally distributed with the standard deviation  $\eta$ . Note that accumulation can also follow a downward trajectory (dotted line), depending on which alternative receives more evidence.

The Diffusion model is one of the most prominent sequential sampling models and has been shown to account for behavioural data in a variety of paradigms, primarily in the context of perceptual decision-making tasks, such as lexical decision-making (Ratcliff, Gomez, & McKoon, 2004; Ratcliff, Thapar, & McKoon, 2010), and discriminations of brightness (Ratcliff & Rouder, 1998), direction (Ratcliff & McKoon, 2008), and orientation (Smith, Ratcliff, & Wolfgang, 2004), but has also been shown to account for RT distributions in value-based decisions (Krajbich & Rangel, 2011; Milosavljevic, Malmaud, & Huth, 2010), reinforcement learning (Frank et al., 2015), and memory tasks (Ratcliff, Thapar, & McKoon, 2004).

However, one of the major limitations of the Diffusion model is that, in its original form, it can only account for binary decisions and cannot be extended to choices with several alternatives. Since in a binary decision, evidence for both alternatives is integrated in a single accumulation process, it is not obvious how this model could account for more than two choices. A number of solutions have been suggested, most of which split the accumulation into several diffusion processes, each racing towards a boundary. This approach allows for the addition of an arbitrary number of processes. However, it does not follow the original assumptions as the inhibition between competing alternatives is lost

and has to be added to the model so that evidence added to one accumulator is subtracted from the other (Ratcliff, Smith, Brown, & McKoon, 2016).

Additionally, the Diffusion model has been criticised for not being neurophysiologically plausible as it assumes that accumulation can occur with both a positive and a negative mean slope. In its original formulation, the Diffusion model was designed to account for behavioural data and did not claim to model neural processes. However, more recent research makes increasing use of sequential sampling models to explore neural correlates of decision-making. Accumulation-to-bound processes like those predicted by sequential sampling models are now assumed to describe the activity of neural populations during decision-making (Smith & Ratcliff, 2004). Since this activity cannot drop below zero, or more specifically, can only drop to a limited extent based on the level of baseline activity, models which assume only positive accumulation are more appropriate to explain neural activity (Usher & McClelland, 2001). Overall, while the Diffusion model can account well for behavioural data in a range of decision-making tasks, it struggles to extend to more complex applications which are becoming increasingly relevant in the perceptual decision-making literature.

### **1.1.2. Accumulator Models**

The second type of sequential sampling model, namely the accumulator model, distinguishes itself from random-walk models primarily due to its absolute stopping rule. These models assume one accumulator for each response alternative, so that in a binary choice, evidence is accumulated in two separate totals. Both accumulators race towards a common threshold and the response is determined depending on which accumulator reaches the threshold first. Since accumulator models assume a separate accumulation process for each response alternative, they can easily be extended to decisions with any number of alternatives by simply adding accumulators.

In a typical accumulator model, such as what we refer to as a race model, the integration of evidence in each accumulator starts at a starting point  $z$ , drawn

from a uniform distribution with range  $S_z$ , and accumulates towards a threshold  $A$ . The rate at which the evidence accumulates differs across accumulators and is given by the drift rates  $v_m$  and  $v_n$  for accumulators associated with response ‘M’ and ‘N’ respectively, as well as noise  $\sigma^2$  (see Figure 1.2). The RT is defined by the time taken for the first accumulator to reach the threshold as well as a non-decision time  $T_{er}$ , drawn from a uniform distribution with the range  $S_{Ter}$ . At each point in time, a given accumulator  $m$  accumulates the input evidence supporting its alternative  $I_m$ , as well as noise so that the quantity accumulated at each time point is described by:

$$dx_m = I_m + N(0, \sigma^2) \quad (1.2.)$$

To remain physiologically plausible, this accumulation process is usually restricted to positive values at each time step.

$$x_m(t + 1) = \max(0, x_m(t) + dx_m) \quad (1.3.)$$

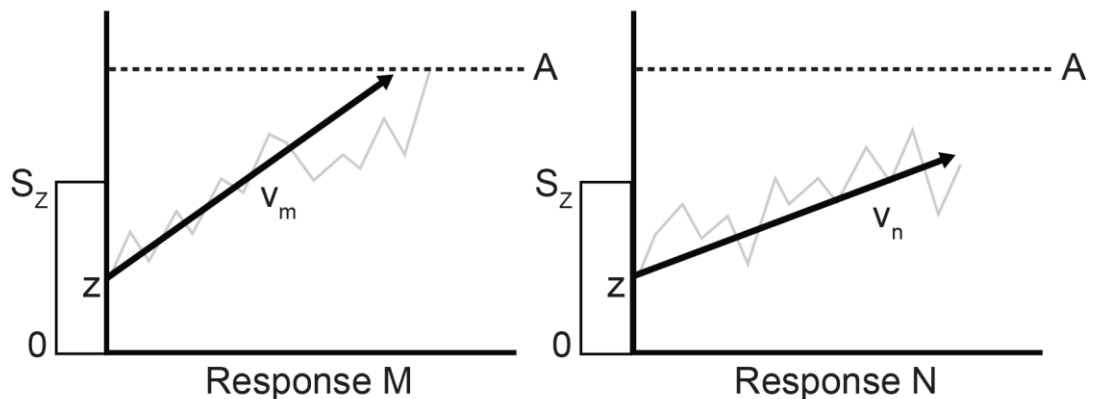


Figure 1.2: Race model: an accumulator model in which evidence for each alternative is accumulated in a separate accumulator. In both accumulators, accumulation begins at a starting point  $z$  (drawn from  $S_z$ ) and accumulates at a rate  $v$  (one for each accumulator) towards a threshold  $A$ . The response time is determined by the time required for the fastest accumulator to reach  $A$ , plus a non-decision time  $T_{er}$  (drawn from  $S_{Ter}$ ).

One of the most prominent examples of an accumulator model is the leaky competing accumulator model (LCA; Usher & McClelland, 2001). This model was designed to be as neurophysiologically plausible as possible and includes a leakage parameter, based on the finding that neural excitatory input currents decay over time (Abbott, 1991; Hodgkin & Huxley, 1990; Stein, 1967). Although this effect is decreased by recurrent self-excitation in populations of neurons, Usher and McClelland (2001) argued that his passive decay means that information is not integrated perfectly and that leaky integrators are a more physiologically plausible model of evidence accumulation. Additionally, the LCA

also implements physiological evidence suggesting lateral inhibition between neuronal populations (Desimone, 1998; Reynolds, Chelazzi, & Desimone, 1999), by including a parameter for mutual inhibition between accumulators (see Figure 1.3).

The model assumes that the integration of evidence in each accumulator starts at a starting point  $z$ , and races towards a threshold  $A$ . The quantity accumulated at each time point for a given accumulator  $m$  is therefore defined by the evidence input  $I_m$  (as described above,  $I_m$  and  $I_n$  are determined by the drift rates  $v_m$  and  $v_n$  for accumulators associated with response ‘M’ and ‘N’ respectively), the leakage over time  $k$ , inhibition from the other accumulator  $\beta$ , and noise  $\sigma^2$ :

$$dx_m = I_m - k x_m - \beta x_n + N(0, \sigma^2) \quad (1.4.)$$

In line with a typical accumulator model and to further strengthen the neural plausibility of the LCA, a threshold function is added to prevent accumulation from dropping below zero.

$$x_m(t + 1) = \max(0, x_m(t) + dx_m) \quad (1.5.)$$

Like most other models, the LCA defines the RT of a given decision by the sum of time taken to reach the threshold and a non-decision time  $T_{er}$ .

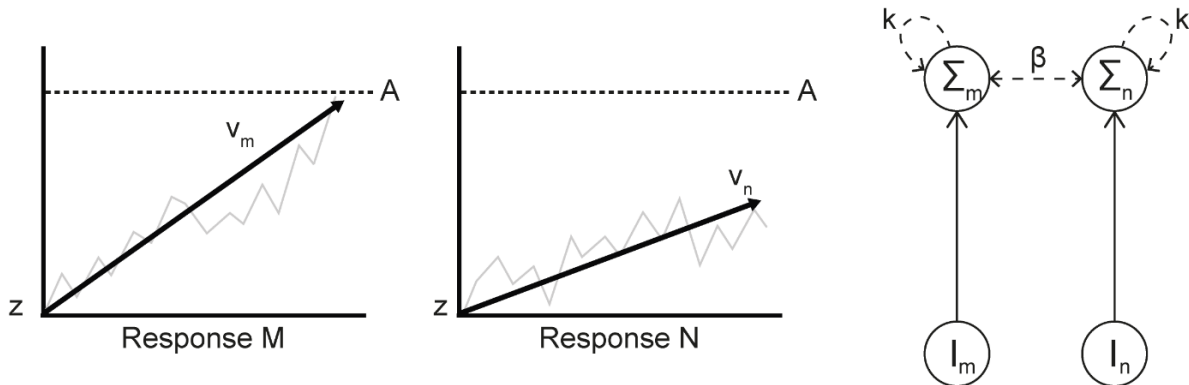


Figure 1.3: Leaky competing accumulator (LCA) model: Left: An accumulator model in which evidence for each alternative is accumulated in a separate accumulator. The accumulators start at a starting point  $z$  and race towards a threshold  $A$ , at rates of  $v_m$  and  $v_n$ . Right: Unlike the race model presented in Figure 1.2, the accumulators  $\Sigma_m$  and  $\Sigma_n$  are not independent but inhibit each other (inhibition defined by  $\beta$ ), and accumulated evidence input ( $I$ ) is subject to leakage ( $k$ ) over time. The response time is determined by the time required for the fastest accumulator to reach  $A$ , plus a non-decision time  $T_{er}$ .

The LCA has been shown to accurately describe perceptual decision-making in tasks such as length or motion discriminations (Gao, Tortell, & McClelland, 2011; Usher & McClelland, 2001), lexical decisions (Dufau, Grainger, & Ziegler,

2012), and value-based choices (Bogacz, Usher, Zhang, & McClelland, 2007), as well as choices with more than two alternatives (Niwa & Ditterich, 2008; Tsetsos, Usher, & Chater, 2010; Tsetsos, Usher, & McClelland, 2011).

However, the complexity of the LCA compared to other, more commonly used sequential sampling models, while increasing the biological plausibility of the model, also entails disadvantages, as it does not have a known likelihood function, which implies that the model can only be fitted through the slow process of simulating data for each proposed set of parameters (Turner & Sederberg, 2014). Additionally, since the LCA has a relatively large number of parameters which, although conceptually different, have similar effects on the simulated RT, there can be a trade-off between them (in particular between inhibition and leakage) which makes it difficult to recover accurate parameters, suggesting that the model may be formally non-identifiable (Miletic, Turner, Forstmann, & Van, 2017). Nevertheless, the LCA is a commonly applied model and is particularly useful for accounting for more complex decisions, as well as for linking sequential sampling to neural processes.

## **1.2. Neural Correlates of the Decision Variable**

Sequential sampling models were originally developed to account for RT and accuracy data and although some models, like the LCA, were designed to be physiologically plausible, the sequential sampling framework does not claim and was not developed to model neurobiology. Nevertheless, several neural signals have now been suggested to display characteristics of accumulation profiles similar to those predicted by sequential sampling models. Researchers now routinely explore the notion that sequential sampling occurs in the brain and reflects the neural mechanism underlying perceptual decision-making.

There are a number of characteristics that identify a signal as a correlate of the decision variable, i.e. as a signal reflecting the accumulation-to-bound process

as defined by sequential sampling models. The most fundamental ones include the assumption that the signal should display overall accumulation-to-bound dynamics, i.e. it must build up over the course of the decision-making process, and peak at the time of response. Specifically, the peak amplitude should reach a stereotyped level which is constant across decisions, indicating the crossing of a set threshold. Additionally, a neural correlate of decision-making should covary with the intensity of the physical stimulus. Decisions in which the quality of the sensory evidence is high (i.e. easy decisions) are, on average, associated with high drift rates and should therefore lead to steeper mean slopes in the neural signal and shorter RTs. There are a number of neural signals which have been suggested to meet these criteria and reflect an accumulation-to-bound process similar to the one predicted by sequential sampling models.

### **1.2.1. Neural Activity in Non-human Primates**

Neurophysiological research in non-human primates has been particularly successful at identifying such signals. This research provides rich data as it primarily makes use of single-unit recording, in which a microelectrode is inserted into the brain in order to record both spatially and temporally highly specific voltage changes, a method which is rarely applied in humans. A typical experiment exploring the decision-making process involves single-cell recording in behaving monkeys who engage in binary perceptual decisions and indicate their choices using saccadic eye-movements. A particularly commonly used perceptual decision-making task is the random dot motion task (see Figure 1.4). In this task, an array of moving dots is displayed on a screen, a proportion of which moves coherently in one direction while the remaining dots move in random directions. The monkey is trained to indicate the direction of the coherent motion by making a saccade into the same direction (Gold & Shadlen, 2000; Newsome et al., 1989; Palmer, Huk, & Shadlen, 2005).

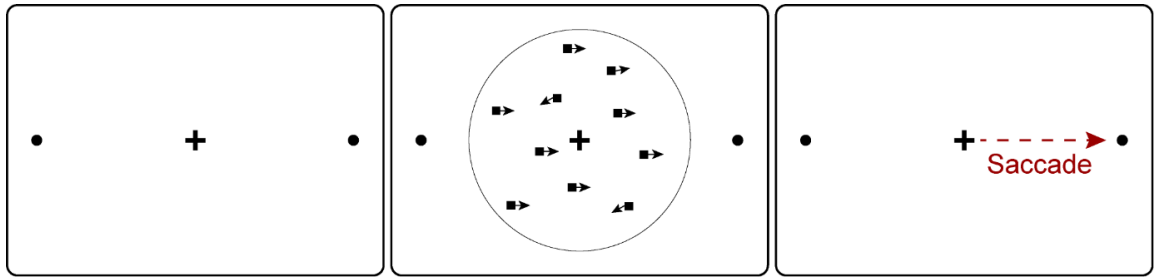


Figure 1.4: Typical decision-making experiment with non-human primates: after a fixation cross, the monkey is presented with a random dot motion task. In this task, a proportion of dots (here: 70%) move either to the left or to the right (here: right) while the rest of the dots move in random directions. The monkey identifies the direction of the perceived motion and indicates its response by making a saccadic eye-movement towards a target in the direction of the detected motion.

A number of structures have been found to be recruited during these saccadic decisions. The middle temporal area (MT) is associated with the detection of visual motion, while the lateral intraparietal area (LIP), the frontal eye field (FEF), and the superior colliculus (SC) are associated with the control and the initiation of eye movements (Bruce & Goldberg, 1985; Maunsell & van Essen, 1983; Segraves, 1992; Shadlen & Newsome, 1996). The firing rates of neurons in each of these areas have been associated with decision-related accumulation. For example, MT activity has been correlated with behavioural choice, i.e. a high firing rate in a given directionally selective MT neuron was shown to be related to an increased probability of the choice of that direction (Britten, Newsome, Shadlen, Celebrini, & Movshon, 1996). However, this relationship was found to be weak, and it has since been concluded that MT activity may represent the evidence, i.e. the input into the decision accumulators, rather than the decision variable itself (Ditterich, Mazurek, & Shadlen, 2003).

Activity in the FEF, which, like the SC and the LIP, is innervated by MT and controls the selection of visual targets as well as the appropriate saccadic movements (Schall, 2002, Bruce & Goldberg, 1985), has been found to predict responses by reaching a stereotyped maximum, suggesting accumulation-like dynamics (Hanes & Schall, 1996). Microstimulation studies have further supported the role of FEF activity as a correlate of decision-making (Gold & Shadlen, 2000), but only when a specific motor response is associated with each choice (Gold & Shadlen, 2003). Similar dynamics have been reported for

neuronal activity in the SC, which has been associated with dynamics simulated by the Diffusion model (Ratcliff, Cherian, & Segraves, 2003).

Similarly, a number of studies have suggested that activity in the LIP shows characteristics of the accumulation process predicted by sequential sampling models. Shadlen and Newsome (1996) recorded the activity of LIP neurons during a motion discrimination task and found that a subset of these neurons appeared neither sensory nor motor, but rather reflected the integration of decision-relevant sensory evidence. In a later study, the authors found that LIP activity predicted the saccadic eye movement the monkey used to indicate its decision, in both correct and incorrect trials. In those trials in which the motion was towards the response field of the LIP neurons, their activity built up over the course of the motion viewing and peaked at the time of the saccade. Additionally, the authors found that the magnitude of the build-up was dependent on the strength of the viewed motion, and concluded that these neurons accumulate sensory evidence to select an appropriate saccadic eye movement (Shadlen & Newsome, 2001). In a series of experiments, Shadlen and his colleagues strengthened this conclusion as they confirmed further characteristics of the decision variable to be consistent with LIP activity. For example, Huk and Shadlen (2005) found that briefly perturbing the strength of the decision-relevant evidence had a lasting impact, not only on the overt decision but also on the activity of LIP neurons, thereby supporting its role as the time integral of the sensory evidence. It was further found that LIP activity indicated the completion of the decision when it reached a stereotyped threshold (Roitman & Shadlen, 2002), even when further information was available (Kiani, Hanks, & Shadlen, 2008), that LIP activity may also reflect decision certainty (Kiani & Shadlen, 2009), and that it is linked to the speed-accuracy trade-off (Hanks, Kiani, & Shadlen, 2014). Activity in the LIP is therefore generally viewed as a neural substrate of the accumulation process suggested by sequential sampling models.

While research with non-human primates has provided valuable insights into the underlying mechanisms of perceptual decision-making, and has important advantages over research with human subjects, primarily due to the possibility

of employing invasive methods to record neural activity with great temporal and spatial resolutions, there are also clear limitations associated with animal research. While neurophysiological recordings in monkeys can give a unique insight into brain activity at a neuronal level, it provides no information about system-level activation. Since single-cell recordings can only measure changes at the targeted site while being blind to activity in even closely surrounding areas, this may give a false impression of the spatial selectivity of the neural substrates measured in this way. Additionally, monkeys have to be trained for a prolonged period of time in order to successfully perform even simple decision-making tasks, such as motion discrimination tasks. This research is therefore limited to comparatively simple designs with arguably low ecological validity. Importantly, there are limitations in the interpretability of monkey data as, besides anatomical differences between monkeys and humans, the monkey's behaviour may also differ as over-training may cause durable task-specific sensorimotor mappings which may cause monkeys to perform differently than they would in a spontaneous perceptual decision. Therefore, it is crucial to explore human perceptual decision-making directly.

## **1.2.2. Activity in the Human Brain**

Several lines of research have been dedicated to exploring perceptual decision-making and identifying potential neural correlates of the decision variable in the human brain. There are a number of methodologies available to study human brain activity, each providing different insights but also different limitations to explore decision-making.

### **1.2.2.1. Functional Magnetic Resonance Imaging**

One method which is commonly used to study human decision-making is functional magnetic resonance imaging (fMRI). Blood oxygenation level dependent (BOLD) fMRI is a non-invasive neuroimaging technique which measures brain activity by detecting local changes in blood oxygenation. As a given brain area becomes active, blood flow increases which in turn changes the ratio of oxyhaemoglobin to deoxyhaemoglobin. fMRI exploits the fact that

these two proteins have different magnetic properties in order to detect these local increases in relative blood oxygenation (Matthews & Jezzard, 2004).

Functional imaging-based approaches have been useful in decision-making research as this method has a very high spatial resolution on a system-wide level and allows researchers to identify discrete brain structures as well as whole networks involved in different cognitive processes. This has been used to identify a number of brain regions involved in perceptual decision-making. For example, the pre-supplementary motor area and the striatum have been associated with decisions under time pressure (Forstmann et al., 2008, 2010), while it has been suggested that the ventromedial prefrontal cortex is involved in the processing of decision biases (Chen, Jimura, White, Maddox, & Poldrack, 2015; Lopez-Persem, Domenech, & Pessiglione, 2016).

A number of brain areas have also been suggested to be directly involved in the accumulation of decision-related evidence, and arguably resemble the decision variable. For example, Heekeren, Marrett, Bandettini, and Ungerleider (2004), found characteristics of a decision-related accumulation process in the left dorsolateral prefrontal cortex (DLPFC), as greater activity was observed during easy compared to hard decisions. Other researchers have suggested the inferior frontal sulcus (Noppeney, Ostwald, & Werner, 2010), the right insula (Ho, Brown, & Serences, 2009), as well as inferior temporal, frontal, and parietal regions (Ploran et al., 2007; Tosoni, Galati, Romani, & Corbetta, 2008) to be involved in the decision-related accumulation of evidence. In a review of studies which combined fMRI approaches with sequential sampling models, Mulder, van Maanen, and Forstmann (2014) identified a frontoparietal network as associated with evidence accumulation. However, the authors also noted large variations in identified regions.

It is important to note that fMRI measures brain activity indirectly through changes in blood oxygenation, which respond slowly compared to electrophysiological signals. This low temporal resolution implies that signals have to last several seconds to be detected by fMRI, which makes it difficult to observe the dynamics of fast perceptual decisions, which usually do not take

longer than one second. To identify signals which may represent evidence accumulation, fMRI research therefore relies on a number of assumptions, which can make the interpretation of findings problematic. Specifically, it remains unclear how decision variable signals such as those identified in non-human primates would translate into BOLD response patterns. One particularly controversial assumption has been made by studies which claim that, since easier decisions are associated with steeper accumulation, the amplitude of the BOLD response in an accumulation-related region should be greater for easy compared to hard trials (Heekeren et al., 2004). Other authors have made the opposite assumption and argue that, given that activity falls off after a response is made, prolonged activity in hard decisions leads to a greater total activity and therefore a larger BOLD signal (Ho et al., 2009).

Although there seems to be a consensus regarding the involvement of frontal and parietal structures in the decision-related accumulation of evidence (Mulder et al., 2014), methodological inconsistencies and the associated large variety of brain regions suggested to be involved in accumulation make an interpretation difficult. Overall, fMRI provides the best spatial resolution in human imaging studies and is a useful tool to identify which brain regions are associated with decision-making. However, its comparatively poor temporal resolution makes fMRI less suitable to explore the dynamics of a decision variable which changes on a millisecond timescale.

#### **1.2.2.2. Electroencephalography and Magnetoencephalography**

An alternative to fMRI research is provided by electroencephalographic (EEG) and magnetoencephalographic (MEG) recordings. These techniques do not offer the same spatial resolution as fMRI data and are not able to identify specific brain regions. However, their high temporal resolution, which allows for the measurement of brain activity on a millisecond-by-millisecond basis, makes them a more appropriate choice to directly track decision variable signals which can build up and reach their maximum within hundreds of milliseconds.

EEG is a non-invasive technique, which, unlike fMRI, directly measures electrical activity in the brain, using electrodes on the scalp. A given individual

neuron receives and sends signals which are primarily electrical in nature. The neuron's electrical activity is comprised mainly of action potentials and postsynaptic potentials. Action potentials are discrete voltage spikes which are triggered in the cell body and travel, unchanged in amplitude, along the axon to the axon terminals where they cause the release of neurotransmitters into the synaptic cleft. When these neurotransmitters bind to the postsynaptic neuron, they alter the ion permeability of the membrane which leads to graded changes in voltage, called postsynaptic potentials. Both postsynaptic potentials and action potentials of individual neurons are far too small to be picked up by electrodes placed on the scalp. However, in the cerebral cortex, large numbers of pyramidal cells are oriented perpendicular to the cortical surface. Therefore, when a population of cells is active, postsynaptic potentials, which are more durable than action potentials, summate and can be recorded from the scalp. Typically, a total of 64 electrodes are placed on the scalp according to a 10-20 system (Jasper, 1958), which defines the location of the electrodes based on the distance between adjacent electrodes as either 10% or 20% of the front-back or left-right distance of the skull (although other systems, such as the equidistant montage, are also commonly used).

One of the most commonly applied ways to analyse EEG data is to segment it, time-lock each segment to a specific event, typically the stimulus onset, and take the mean of all segments in order to average out any activity which is not time-locked and therefore arguably not functionally related to the event. The resulting waveform is referred to as an event-related potential (ERP) and can be defined as a set of potential changes in response to a specific experimental variable (Donchin & Heffley, 1978). Alternatively to its temporal form, a Fourier transform can be used to analyse EEG data with regards to its spectral components. The Fourier transform is based on the notion that any waveform can be decomposed into a number of sinusoidal functions of different frequencies. In the context of EEG, the data are typically represented as a set of oscillations and interpreted in the context of a number of predefined frequency bands, namely the delta (< 4 Hz), theta (4-8 Hz), alpha (8-14 Hz, although low alpha frequencies are sometimes referred to as mu), beta (14-31 Hz), and gamma (> 31 Hz) bands.

MEG measures brain activity in a similar way to EEG and produces comparable data. However, instead of measuring electrical activity, it records magnetic fields produced by electrical currents. This can be advantageous as magnetic fields are less influenced by passing through the skull and other tissues. Nevertheless, MEG and EEG record very similar data which are commonly analysed in the same way, providing similar insights. Note that, in the following, we often refer only to EEG (primarily because it is the method we chose in this project), but the same signals and conclusions largely apply to MEG data.

A range of studies using both EEG and MEG have been conducted to explore decision-making. For example, a series of experiments by Philiastides and colleagues, who used face-car discrimination tasks, identified an early (170 ms) and a late (300 ms) ERP component as decision-relevant (Philiastides, Ratcliff, & Sajda, 2006; Philiastides & Sajda, 2007; Philiastides & Sajda, 2006). However, these components were interpreted as reflecting processes which occur prior to accumulation itself (Ratcliff, Philiastides, & Sajda, 2009). Additionally, results from regressor-based approaches have suggested, for example, that evidence accumulation correlates with spectral power in the theta band (van Vugt, Simen, Nystrom, Holmes, & Cohen, 2012), and that the encoding of decision-relevant evidence fluctuates with parietal oscillations in the delta band (Wyart, de Gardelle, Scholl, & Summerfield, 2012).

In the search for M/EEG correlates of the decision variable, a number of studies have explored signals which are associated with motor preparation. Contrary to previous formulations which assumed that response preparation followed the decision formation in a serial fashion (Donders, 1969; Sternberg, 1969), there is now considerable converging evidence to suggest that sensorimotor decisions can be observed in the same brain regions which prepare and execute the motor response, both from research using neurophysiological methods in non-human primates (Cisek & Kalaska, 2005; Romo, Hernandez, & Zainos, 2004), and human EEG signals (Donner, Siegel, Fries, & Engel, 2009; Kelly & O'Connell, 2013). These findings suggest that the level of accumulation at any

given time is continuously fed forward into the motor system and reflected in the level of response preparation.

This has led to the suggestion that event-related desynchronisation (ERD) in the beta frequency may correlate with decision-related accumulation (Donner et al., 2009). Oscillations of this frequency are known to decrease in power over the premotor cortex, primarily contralateral to the response, when a motoric response is prepared (Doyle, Yarrow, & Brown, 2005; Jasper & Penfield, 1949; Pfurtscheller, 1981; Zaepffel, Trachel, Kilavik, & Brochier, 2013). Since this signal is known to reflect the preparation of a motoric response, it should also reflect the decision-related accumulation of evidence, assuming that the decision variable is visible in the motor system. Donner et al. (2009) were able to demonstrate this by recording MEG during a random dot motion task. They found that activity in the beta frequency displayed a ramp-like profile, similar to the gradual build-up predicted by sequential sampling models and that this activity predicted the decision several seconds prior to the response. The significance of beta ERD in decision-making has since been supported in a number of studies, reporting its sensitivity to uncertainty (Tzagarakis, Ince, Leuthold, & Pellizzer, 2010), and bias (de Lange, Rahnev, Donner, & Lau, 2013), as well as its reaching of a stereotyped maximum before the response (Kubaneck, Snyder, Brunton, Brody, & Schalk, 2013).

Another EEG signal which has a known link to motor preparation and has been suggested to reflect accumulation is the lateralised readiness potential (LRP), an ERP component, recorded over the motor cortex (Ikeda & Shibasaki, 1992; Kornhuber & Deecke, 1965). The LRP is the lateralised part of the slow negativity which is observed during the preparation of a limb movement, which, like beta ERD, is stronger on the hemisphere contralateral to the movement, and has more recently been linked to decision-making (Noorbalooshi, Sharon, & McClelland, 2015; Rinkenauer, Osman, Ulrich, Muller-Gethmann, & Mattes, 2004). Importantly, it has also been suggested that the LRP closely follows an accumulation profile as predicted by sequential sampling models (Kelly & O'Connell, 2013; Polanía, Krajbich, Grueschow, & Ruff, 2014).

However, it is important to note that both signals, beta ERD and LRP, are signals of motor preparation and can only track the decision formation if the decision is associated with a specific motor response. Decisions which do not require overt, typically hand, movements, as well as decisions in which the stimulus-response mapping is not known during the accumulation process, cannot be explored using these signals (O'Connell, Dockree, & Kelly, 2012; Twomey, Kelly, & Connell, 2016). This dependence on the associated response demonstrates that these motor preparation signals can, at best, reflect a downstream process similar to accumulation, but that the accumulation process itself occurs in a different brain region.

One signal which has been proposed to reflect accumulation itself is an ERP component called centroparietal positivity (CPP; O'Connell et al., 2012). As the name suggests, this ERP is recorded over parietal electrodes and shows a large, slow positivity, which has been suggested to reflect the decision-related accumulation of evidence. O'Connell et al. (2012) used a gradual target detection task and found that the CPP displayed a profile which built up gradually over the course of the decision, before reaching a stereotyped maximum which predicted the response time. In a follow-up study using a random dot motion task with different levels of difficulty (i.e. different levels of motion coherence) it has also been shown that the rate at which the build-up occurs depends on the quality of the sensory evidence, further supporting the CPP's role as a decision variable signal (Kelly & O'Connell, 2013; O'Connell et al., 2012; see Figure 1.5). Importantly, the authors were able to fully dissociate the CPP from other EEG signals which are associated with sensory and motor processing, and found that, unlike sensory signals, the CPP displays the accumulation profile only when the sensory evidence is decision-related, and, unlike motor signals, does so even when no motor response is required (O'Connell et al., 2012; Twomey et al., 2016). Additionally, the CPP has been shown to display the same waveform in both visual and auditory decision-making. Together, these findings suggest that the CPP provides insight into the decision-related accumulation of evidence, independent of modality or stimulus-response mappings.

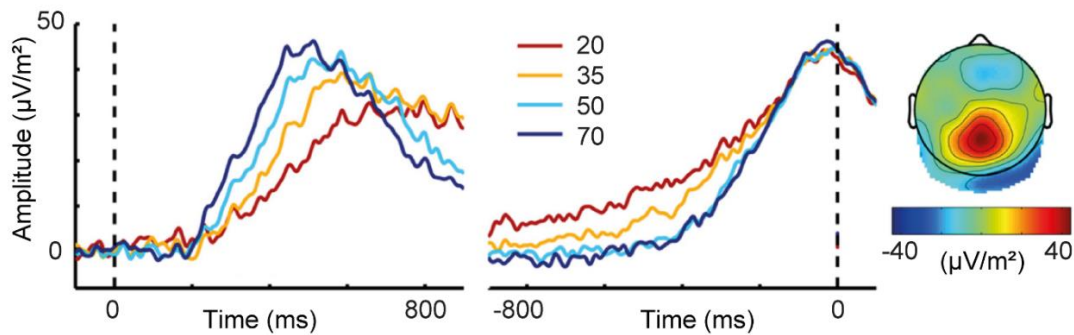


Figure 1.5: CPP (Kelly & O'Connell, 2013): from left to right: stimulus-locked CPP, response-locked CPP, and ERP topography. Waveforms in different colours are associated with different levels of difficulty (20%, 35%, 50%, and 70% coherence in a random dot motion task). The CPP builds up at a rate which depends on the level of difficulty and peaks at a stereotyped maximum at the time of response. The topoplot on the right shows the centroparietal location of the positivity (figure slightly edited from Kelly and O'Connell (2013)).

Note that the CPP has been suggested to be equivalent to the P300, a well-researched sensory-evoked centroparietal, positive ERP component which peaks between 300 and 600 ms after the onset of a task-relevant stimulus (Sutton, Braren, Zubin, & John, 1965; Twomey, Murphy, Kelly, & O'Connell, 2015). Although the P300 has been researched in the context of decision-making before, its exact functional relevance remained unclear, with most researchers merely arguing its involvement in stimulus processing (Nieuwenhuis, Aston-Jones, & Cohen, 2005; Pritchard, 1981). Although it is not yet clear whether all characteristics observed in studies utilising the P300 are consistent with accumulation-to-bound processes (Summerfield & Tickle, 2015), its potential equivalence with the CPP provides an interesting new perspective.

Although there is compelling evidence to suggest that the CPP is indeed an electrophysiological marker of evidence accumulation, alternative interpretations of the findings have been proposed. One contentious issue is that the CPP only predicts the time of the decision, but not the outcome, i.e. based on the CPP alone, choices for one alternative are indistinguishable from choices for another alternative. This led to the suggestion that the CPP may not reflect evidence accumulation, but rather confidence in the decision, as a decision variable is expected to predict the decision outcome, while confidence in the decision is non-selective (Urai & Pfeffer, 2014). However, it is important to note that the nature of EEG recordings does not allow us to distinguish between the activities of populations of neurons in close spatial proximity to each other. If

we hypothesise that a process close to that proposed by sequential sampling models is indeed taking place in centroparietal regions, an assumption which, due to its limited spatial resolution cannot be confirmed by EEG, we might assume that in a binary choice, there are two pools of neurons, one accumulating the evidence for each alternative. Even in this case of a true decision variable in centroparietal regions, volume conduction would lead EEG electrodes to record a summation of both accumulators, resulting in a signal not dissimilar to the CPP.

### **1.2.2.3. Transcranial Magnetic Stimulation**

Recently, a third approach to explore neural dynamics during decision-making in the human brain, namely transcranial magnetic stimulation (TMS), has become more relevant. TMS is a form of brain stimulation which can be used to disrupt activity in a given brain area and thereby identify its function. For example, Philiastides, Auksztulewicz, Heekeren, and Blankenburg (2011) used this approach to identify the DLPFC as a relevant region in the decision-making process. However, this TMS method can only provide insight into the involvement of a given brain region, and cannot track an evolving accumulation process over time.

Therefore, a different approach has recently been suggested. This approach uses TMS in order to measure the build-up of response preparation during decision-making. When TMS is applied over the motor cortex, it can induce electrical responses in the muscle associated with the stimulated region, called motor evoked potentials (MEPs). These responses were first observed during the 1980s using a technique called transcranial electric stimulation, which had similar effects to TMS, but large practical limitations, primarily because brief high-voltage electric shocks on the scalp made the procedure painful (Merton & Morton, 1980; Merton, Hill, Morton, & Marsden, 1982). Shortly thereafter, Barker, Jalinous, and Freeston (1985) developed TMS, in which a coil of wire is connected to an electrical capacitance, which, when discharged, causes a brief, large current pulse in the coil. This current causes a magnetic field oriented perpendicular to the coil, which in turn causes an electric field leading to current flows parallel to the coil in any conductive structures in close proximity. When

the coil is placed on the scalp, the magnetic field is only minimally impeded by the skull and is therefore able to produce currents in the brain. When a TMS coil is placed over the motor cortex and a current is produced in the primary motor cortex (M1), it can elicit contractions in contralateral, typically hand, muscles (Barker et al., 1985; Rothwell, Day, Thompson, Dick, & Marsden, 1987).

Importantly, the magnitude of these contractions can give insight into the level of motor preparation in M1 and adjacent premotor areas, as the MEP amplitude is a direct indicator of corticospinal excitability (Bestmann et al., 2008; Hadar, Makris, & Yarrow, 2012; Kiers, Fernando, & Tomkins, 1997). It has now been suggested that this measure of motoric preparation can be used to track the decision variable (Hadar, Rowe, Di Costa, Jones, & Yarrow, 2015). This claim is based on the same arguments that support tracking of motor-related EEG signals, such as the LRP, as a correlate of the decision variable, i.e. that response-related motoric activation does not follow the decision formation in a serial fashion as previously suggested (Donders, 1969; Sternberg, 1969), but instead occurs throughout the decision-making process, with accumulation constantly being fed forward into the motor system (Coles, Gratton, Bashore, Eriksen, & Donchin, 1985; Gluth, Rieskamp, & Büchel, 2013; Hadar et al., 2012; Michelet, Duncan, & Cisek, 2010; Servant, White, Montagnini, & Burle, 2015). Together, these findings imply that the level of accumulation for a given alternative at any given time point is reflected in the level of preparation of the corresponding response, which can be measured using recordings of MEPs.

Supporting this claim, Michelet et al. (2010) explored MEPs during an Eriksen flanker task, in which arrows indicating the appropriate response were either presented alone or surrounded either by congruent arrows which pointed in the same direction as the target arrow, or incongruent arrows, which pointed in the opposite direction and had to be ignored. TMS was applied at a number of time points throughout the decision-making process. It was found that, when the target arrow was not surrounded by incongruent arrows, the MEP size in the responding muscle increased over the course of the decision while the MEP size in the non-responding muscle decreased. In the incongruent condition, on the other hand, the same pattern was preceded by an initial increase in the non-

responding muscle. These findings suggest that MEP size reflects accumulation as it not only increases over the course of the decision but also dynamically tracks the evolution of the decision in incongruent trials. Importantly, the authors also found that MEP amplitudes reached a constant maximum immediately prior to the response across conditions, suggesting an accumulation-to-bound dynamic similar to the one predicted by sequential sampling models. Similarly, Klein-Flugge and Bestmann (2012) found that the difference in MEP amplitudes in the responding muscle compared to the non-responding muscle predicted the decision prior to the completion of the decision formation, and Klein, Olivier, and Duque (2012) found that MEP amplitudes were sensitive to decision biases, further supporting the potential role of corticospinal excitability as a correlate of the decision variable.

One limitation of using MEP amplitudes to track the accumulation process in this way is that stimulation can only occur at discrete time points and only one MEP at one time point can be retrieved from each decision-making process, which makes it difficult to reveal the continuous dynamics of a decision variable. Hadar et al. (2015) addressed this limitation. In a perceptual discrimination task in which participants were asked to categorise faces as either male or female, TMS pulses were applied at random time points throughout the decision-making process. Although only one MEP could be sampled per trial, MEPs from all trials were pooled, sorted by latency, and smoothed using a Gaussian kernel, allowing the authors to recover a continuous time-varying MEP signal, comparable to an ERP component. It was found that more difficult categorisations were associated with longer motoric activity in the responding muscle than easier ones. The authors also fitted a Diffusion model to their data and identified similarities between the simulated accumulation profile based on the model and the MEP signal, further supporting the conclusion that the MEP signal reflects decision-related accumulation.

This methodology to use TMS to induce MEPs and measure their amplitude as a correlate of decision-making is an interesting new approach to explore decision-making. However, to date, only a small number of studies have explored this MEP signal, and more research is needed to validate its role as a

decision variable. Nevertheless, it provides advantages over more established EEG or fMRI methods due to its spatial and temporal resolution. TMS methods provide great temporal resolution, although it is important to note that this is limited by the number of stimulations and their timing. Additionally, while EEG provides little information about the anatomical structures producing recorded signals, we can be confident that MEPs reflect activation in M1, and potentially also in premotor structures (Ahdab, Ayache, Brugières, Farhat, & Lefaucheur, 2016). However, its motor-specificity also implies that the MEP method can only give insight into decisions which involve a motor response, which limits its applicability. Nonetheless, initial findings suggest that it is a promising new method to track decision-making.

### **1.3. Model-based Analysis of Neural Signals**

As outlined above, perceptual decision-making has been studied extensively in the fields of experimental psychology, mathematical psychology, and cognitive neuroscience, each focusing on behavioural data, formal models, and neural data respectively, and contributing to our understanding of decision processes. More recently, however, the importance of combining all three approaches to gain better insights into perceptual decision-making has become increasingly apparent. This triangulation of methods (sometimes referred to as model-based cognitive neuroscience; Forstmann, Wagenmakers, Eichele, Brown, & Serences, 2011) provides several obvious advantages over traditional approaches. For example, mathematical models can break a complex cognitive process into several separate mechanisms, which are easier to test using neural data. An example of this is the introduction of bias in decision-making. Biased decisions are known to lead to faster RTs (Hick, 1952), but it is not clear how this difference in RT could be achieved in the brain, as possibilities include that sensory evidence which supports an existing bias could be integrated faster due to an attentional bias, or that decision processes could remain unchanged while only the biased response is prepared and therefore executed faster. Mathematical models, on the other hand, predict that biases are implemented

by reducing the amount of evidence required to form the decision (Bode et al., 2012; Gao, Zheng, & Wang, 2010; Leite & Ratcliff, 2011). Applying this knowledge to neuroimaging data allows for clear, testable predictions, and therefore greater insights into perceptual decision-making in the brain.

Conversely, neural data can be used to inform mathematical models. An example of this has been highlighted by Ditterich (2010), who set out to evaluate a variety of sequential sampling models and their ability to account for behavioural data in decisions with multiple alternatives. He found that a number of different models explained the data equally well while assuming different underlying mechanisms. However, it was emphasised that this does not render these models indistinguishable, as, while they make similar behavioural predictions, their internal dynamics displayed marked differences, necessitating the comparison to neural data to identify the best model.

To date, the majority of neuroimaging studies which explore perceptual decision-making, including those that aim to identify neural correlates of the decision variable, have not made use of this inter-disciplinary approach. While virtually all studies reported thus far have explored and evaluated neural signals in the context of the sequential sampling model framework, the vast majority of these studies have relied solely on conceptual predictions made by these models without applying them directly. fMRI research is arguably an exception as it commonly applies sequential sampling models and uses variations in model parameters to identify brain regions associated with accumulation (for a review, see Mulder et al., 2014). However, as outlined above, fMRI is not a suitable method to directly track the dynamically evolving decision variable.

M/EEG methods, on the other hand, are more useful to identify neural correlates of the accumulation process but have rarely been combined with mathematical modelling. Of course, any study exploring potential neural substrates of the decision variable, which is defined only by sequential sampling models, necessarily does so in the context of these models. However, many studies do not fit sequential sampling models to their data and instead, rely on a

conceptual understanding of the models to make solely intuitive predictions which are then tested using neural data.

For example, it is well-established that accumulation, as described by sequential sampling models, builds up gradually over the course of the decision and peaks at the time of response. Additionally, it has repeatedly been demonstrated that task difficulty, i.e. the quality of the sensory information during a perceptual decision, influences the drift rate in sequential sampling models, with easier decisions being associated with steeper accumulation profiles (Donkin, Averell, Brown, & Heathcote, 2009; Ratcliff & McKoon, 2008; Ratcliff & Rouder, 1998). These concepts have been used in a number of neuroimaging studies to identify neural correlates of the decision variable based on their shape, and without applying the models directly (Donner et al., 2009; O'Connell et al., 2012; Twomey et al., 2016).

While this approach has been successfully adding to our understanding of perceptual decision-making in the brain, it is difficult to apply to more complex designs. In simple and fast binary decisions based on stationary evidence, it is comparatively easy to predict the shape of the accumulation process, and the manipulation of decision difficulty has consistently been shown to have the same impact on the accumulation profile. However, more recently, research is moving on to more complex, more ecologically valid designs, as both neuroscience and modelling studies have showed increasing interest in designs including decisions under different levels of speed pressure, decision biases, and decisions with multiple alternatives (Bogacz, Wagenmakers, Forstmann, & Nieuwenhuis, 2010; Churchland, Kiani, & Shadlen, 2008; Mulder, Wagenmakers, Ratcliff, Boekel, & Forstmann, 2012; Summerfield & de Lange, 2014; Tsetsos et al., 2011).

To study these more complex forms of perceptual decision-making, the collaboration of disciplines is crucial. This is particularly important when neural data is used to explore the decision variable. With increasing complexity in the design, and importantly, increasing complexity in sequential sampling models, implementing nonlinearities such as inhibition between alternatives, it becomes

increasingly difficult to make intuitive predictions about the profile of the decision variable. With complex relationships between parameters, different, equally likely models can predict qualitatively different accumulation profiles which cannot be predicted by conceptual reasoning alone (Ditterich, 2010).

Additionally, even a specific model can make different predictions depending on how a specific paradigm is implemented. With the exception of the manipulation of difficulty, most experimental manipulations of decision-making can be explained by a given model in a number of different ways. An example of this is the implementation of response caution, which is modelled by varying the amount of evidence that needs to be accumulated to reach a decision (Brown & Heathcote, 2008; Marshall, Bogacz, & Gilchrist, 2012). While sequential sampling models, by convention, vary the decision threshold to achieve this effect, varying the starting point instead would lead to mathematically equivalent results, while producing different accumulation profiles. Therefore, it is important for studies investigating neural correlates of decision-making using complex designs to directly apply models to their data, rather than merely using the sequential sampling model framework as a basis for intuitive hypotheses.

A number of ways have been suggested to combine neuroimaging and sequential sampling models. For example, studies have fitted models to RT data and compared the resulting parameter values to specific properties in the signal (Gluth et al., 2013; Kelly & O'Connell, 2013). An arguably more informative approach is to use the estimated parameters to simulate the corresponding mean accumulation profile and directly compare its shape to the trajectory of the neural signal (Hadar et al., 2015; Twomey et al., 2015). Although this approach has been implemented in only a small number of studies to date, it allows for a direct comparison of the whole waveform with model predictions, without requiring speculations about the decision variable, and allows for a better evaluation of neural correlates of accumulation.

## 1.4. Current Project

In the light of this research, we set out to explore human perceptual decision-making and improve our understanding of sequential sampling in the human brain. Although perceptual decision-making has been researched for decades and in several disciplines, a number of questions remain unanswered, and a consensus regarding the neural mechanism underlying, particularly human, decision-making is yet to be reached. We therefore aimed to explore human brain activity during sensorimotor choices, shed light on some of the remaining questions, and improve our understanding of decision-making mechanisms.

Firstly, we aim to address the basic question of whether the accumulation process described by sequential sampling models (a mathematical abstraction) occurs concretely in the human brain. Sequential sampling models make no claims regarding neural processes and are instead designed to account only for behavioural data. Nevertheless, a large body of research has confirmed that accumulation-like processes can be tracked using firing rates of neurons in oculomotor structures in non-human primates. However, a similar consensus has not been reached regarding the human brain. Although we can speculate that neural processes in non-human primates are similar to those in the human brain, this speculation is questionable as monkeys require prolonged training to complete decisions which humans perform after simple instructions, which may lead to differences in sensorimotor mappings between humans and monkeys.

Nevertheless, neural correlates of the decision variable in the human brain have only recently become a topic of interest, not least because researchers are limited by the methodologies available for human research, and cannot track neural firing rates the way researchers can in non-human primates. Given the most commonly used methods of neuroimaging in humans, namely fMRI and M/EEG, researchers have to choose between good spatial and temporal resolution. While a high spatial resolution is important to identify structures involved in decision-making, a high temporal resolution is crucial to track the very fast evolving decision-variable, making M/EEG methods the most suitable

approach to study accumulation in the human brain. However, although this method has been used in this context for several years, and a number of signals have been proposed to be relevant, there is no consensus regarding which signal best reflects decision-related accumulation.

Overall, human research appears to lag behind research in non-human primates, in which a link between sequential sampling models and neural activity has already been established. We therefore aim to answer the primary question whether sequential sampling occurs in the human brain. We hypothesised that accumulation-to-bound dynamics like those predicted by sequential sampling models occur in the human brain and can be observed using EEG and TMS methods.

Secondly, given that decision-related accumulation can be tracked in the human brain we addressed the question of which signal best describes this process. In particular, we tested two signals which we deemed most promising, namely 1) the CPP and 2) the MEP signal reflecting excitability of motor areas. The CPP is of particular interest as claims have been made that it tracks the decision-related accumulation process directly and independently of sensory or motor processes (O'Connell et al., 2012). However, to date, it is not well-established and has not been tested under a large variety of manipulations. Additionally, it tracks accumulation as a whole and is not able to distinguish between response alternatives.

For the MEP signal, on the other hand, the claim is not that it displays accumulation directly, but instead, that it reflects a down-stream representation in the form of response preparation. We used a TMS method to generate smoothed MEP signals to track accumulation in the motor system, following the same approach as Hadar et al. (2015). This signal is not well-established but may be a promising tool, as its high temporal resolution implies that it can track the decision variable, without being limited in its spatial resolution like M/EEG signals. This implies that, to our knowledge, it is the only signal which allows us to track the evolution of individual responses in humans with more than two alternatives (there are EEG signals which reflect motor preparation and can be

used to track individual responses, but the very low spatial resolution of this method limits this to binary decisions).

Therefore, by exploring the question of which signals in the human brain track the decision-related accumulation of evidence, we not only tested the usefulness of different EEG signals, and in particular the CPP, but also explored whether accumulation is fed forward into motor systems. We hypothesised on the one hand, that the CPP can be used to track the decision variable, suggesting a parietal locus of accumulation, but on the other hand, that downstream accumulation can also be observed in motor areas which are related to the preparation of the response and can be tracked using MEP signals.

Thirdly, having established the validity of the chosen neural substrates of the decision variable, we explored the question of how the accumulation process reacts to a number of manipulations. Specifically, in the following chapters we tested the effect of the speed-accuracy trade-off, difficulty, non-stationary evidence, decision biases, and multiple alternatives on the neural accumulation profile. Each of these manipulations represents a step towards ecological validity as in everyday decisions we rarely choose between two well-defined and opposite alternatives the way decision-making is commonly operationalised in the lab. Some of these manipulations, such as the speed-accuracy trade-off have previously been explored but conclusions remain controversial (Hawkins, Wagenmakers, Ratcliff, & Brown, 2015; Heitz, 2014), while others, such as multi-alternative decision-making, have, to our knowledge, not yet been explored in the human brain. We hypothesised that the neural correlates of the decision variable are sensitive to these manipulations and display changes in their profile which are consistent with sequential sampling model parameter changes which explain the associated behavioural differences.

Fourthly, intertwined with these previous questions but perhaps of greatest importance, we address the question of exactly how similar the neural substrates of accumulation are to the accumulation predicted by sequential sampling models. As discussed in section 1.3, the evaluation of neural accumulation signals based on conceptual reasoning can only be informative

for basic paradigms. In order to understand the underlying mechanisms of perceptual decision-making, we need to make use of both neuroimaging and sequential sampling models. We therefore combined these approaches by fitting sequential sampling models to behavioural data and using the resulting parameter values to simulate accumulation profiles and directly compare them to the associated neural signals. In this way we set out to not only evaluate neural signals, but also, in return, to inform sequential sampling models, and gain a more holistic understanding of decision-making mechanisms. We hypothesised that the waveforms of both the CPP and the MEP signal would display strong qualitative similarities to the simulated accumulation profile predicted by sequential sampling models.

Overall, we explored human perceptual decision-making using both neurometric measures and sequential sampling modelling of behavioural data. We report our findings using the following structure. In Chapter 2, we explored the impact of the speed-accuracy trade-off on perceptual decision-making. In two experiments, we compared the predictions made by a race model to both the CPP, and an MEP signal. Since both neurometric signals contradicted model predictions in the same way, we proposed a novel implementation of the speed-accuracy trade-off in sequential sampling models which is able to account for both behavioural and neural findings. Since the shape of the CPP in Chapter 2 did not support the traditional implementation of the speed-accuracy trade-off in sequential sampling models, in Chapter 3 we tested the CPP's role as a correlate of accumulation using a more well-established manipulation, namely difficulty, and compared it to other EEG signals which have previously been suggested to reflect the decision variable. We concluded that the CPP does, in fact, reflect accumulation better than a number of other EEG signals. To further test the role of the CPP in decision-making, and test the effects of a range of conditions, in Chapter 4, we explored its shape using less commonly used manipulations, namely decisions with non-stationary evidence and biased decisions, and directly compared the resulting waveforms to simulated mean accumulation paths. Finally, in Chapter 5, we explored decision-making with multiple alternatives. To this end, we chose a TMS method due to its greater spatial selectivity compared to EEG measures. Using this method, we were able

to track the evolution of each of four response alternatives, which displayed great similarities with decision variable simulations made using the LCA model. We conclude in Chapter 6 and discuss the role of both of the neural correlates of the decision variable used here. We emphasise the importance of combining approaches from different disciplines in order to gain insights into human decision-making.

## 2. Exploring Neural Correlates of Decision-Making under Speed/Accuracy Instructions

Every day, we are faced with countless decisions, each requiring an appropriate compromise between speed and accuracy. Striving for accuracy necessitates lengthy deliberation, but environmental time pressures may force us to make quick, more error-prone decisions. This relationship, referred to as the speed-accuracy trade-off (SAT, Garrett, 1922; Hick, 1952; Wickelgren, 1977), has been demonstrated in a number of settings and appears to be a ubiquitous finding across experimental tasks and even species (Chittka, Dyer, Bock, & Dornhaus, 2003; Heitz & Schall, 2012; Ivanoff, Branning, & Marois, 2008).

The majority of research investigating the SAT has done so in the context of perceptual decision-making, partly because these comparatively simple, quick decisions allow for a great level of control in experimental settings, but importantly also because mathematical models of perceptual decision-making offer useful explanations for behavioural findings associated with the SAT. Perceptual decisions describe choices that are relatively fast (usually < 1000 ms) and based on sensory evidence (Newsome et al., 1989). According to a group of models called sequential sampling models, we make these decisions by accumulating sensory evidence over time, until a set decision threshold is reached. Once the threshold is reached, we make the decision and initiate the motor response associated with it.

Importantly, these accumulation-to-bound models are able to explain the shifts in behavioural data that are associated with the SAT, by simply adjusting the threshold parameter. A low threshold implies that less evidence needs to be accumulated to make a decision, which leads to faster, but also more error-prone decisions, as less evidence is accumulated and therefore less noise is averaged out. A high threshold, on the other hand, means that more evidence needs to be accumulated to reach a decision, which leads to longer reaction times (RTs) and fewer errors. With this simple threshold adjustment, sequential sampling models are able to account for accuracy rates and RT distributions for

correct and incorrect decisions in SAT tasks (Bogacz, Brown, Moehlis, Holmes, & Cohen, 2006; Brown & Heathcote, 2008; Smith & Ratcliff, 2004; Usher & McClelland, 2001).

Although sequential sampling models were designed to explain behavioural decision-making data and do so successfully, there is now substantial evidence from neural data to support their validity. Signals which display characteristics of the accumulation process predicted by sequential sampling models have been identified in electrophysiological data from non-human primates (Gold & Shadlen, 2000; Shadlen & Newsome, 1996, 2001) as well as electroencephalographic (EEG) /magnetoencephalographic (MEG) and functional resonance imaging (fMRI) recordings of human decision-making (Donner et al., 2009; Forstmann et al., 2008; O'Connell et al., 2012). The observation that the processes described by sequential sampling models closely resemble neural signals led to the testable prediction that threshold differences should be observable in neuroimaging data of SAT tasks.

A number of studies have attempted to explore the neural mechanisms of the SAT and test this hypothesis. The results have been mixed. There is, in fact, some evidence to support the role of the decision threshold as the neural mechanism to control the SAT. For example, van Veen, Krug, and Carter (2008) used fMRI to measure their participants' brain activity while they performed a Simon task (i.e. a task in which participants are presented with a square appearing left or right of the fixation cross and asked to respond to its colour, while ignoring its location) under instructions to emphasise either response speed or accuracy. They found an increase in baseline activity under speed instructions compared to accuracy instructions in a network of brain areas associated with decision-making, including premotor areas, the basal ganglia, the thalamus, the dorsolateral prefrontal cortex and the parietal cortex.

It is important to note that although sequential sampling models generally speak of a modulation of the threshold to explain SAT findings, the modulation of the baseline level of activity is mathematically equivalent to this claim. In fact, while, by convention, these models mention a threshold difference, sequential

sampling models are only able to predict a modulation in the baseline-threshold distance, but cannot give insight into whether this modulation is caused by a difference in baseline, threshold, or an interaction of the two, based on behavioural data alone. Therefore, van Veen et al. (2008) interpreted their findings of an increased baseline under speed instructions to support predictions of sequential sampling models.

Two further fMRI studies showed these increased levels of baseline activity in a number of areas, including the pre-supplementary motor area, for decisions under time pressure (Forstmann et al., 2008; Ivanoff et al., 2008; see Bogacz et al., 2010 for a review). Similarly, Wenzlaff, Bauer, Maess, and Heekeren (2011) found that speed stress led to higher activity in supplementary motor areas, as well as lower activation of the dorsolateral prefrontal cortex, using MEG. Together, these studies support sequential sampling models, not only by showing a modulation of baseline-threshold difference in the context of SAT, but also by identifying pre-motor areas, rather than sensory or primary motor areas, as the source of this modulation, supporting the claim that SAT mechanisms work at the level of the decision-making, not the level of encoding or motor execution (Bogacz et al., 2010).

Although initial fMRI findings are promising, other studies were not able to show a clear modulation of the baseline-threshold distance. Heitz and Schall (2012) trained macaque monkeys to perform a visual search task under either speed or accuracy pressure and recorded activity from frontal eye field (FEF) neurons, the firing rates of which have previously been associated with sequential sampling models (e.g. Gold & Shadlen, 2003). Their results suggest that the description of the SAT provided by sequential sampling models is incomplete as they identified several widespread changes associated with an emphasis on speed or accuracy. Specifically, they found that FEF activity during speed trials was not only raised during the baseline but also at the time of response, a finding which is inconsistent with traditional sequential sampling models. In a follow-up study, these results were strengthened, demonstrating that the SAT is a multifaceted phenomenon, associated with extensive and widespread modulations in activity (Heitz & Schall, 2013).

Similar studies were conducted with a focus on neurons in the lateral intraparietal area (LIP). Like FEF activity, firing rates of LIP neurons have previously been shown to display characteristics of the decision variable, i.e. the accumulation profile predicted by sequential sampling models, and may therefore be expected to show threshold differences (Paré & Wurtz, 2001; Shadlen & Newsome, 1996, 2001). However, a comparison of LIP activity in speed and accuracy regimes during a random dot motion task revealed no modulation in threshold levels (Hanks et al., 2014). Instead, additional evidence-independent activity was observed in the speed regime compared to the accuracy regime. This stronger activity was present from the beginning of the decision formation, thereby supporting previous fMRI findings (Forstmann et al., 2008; Ivanoff et al., 2008; van Veen et al., 2008). However, Hanks et al. (2014) showed that this stronger, speed-related, evidence-independent activity persisted throughout the decision-making process, suggesting that the initial difference in activation between the two regimes is not indicative of a pure modulation of the baseline-threshold distance, but rather due to an added urgency signal. A model with an urgency signal was also used by Thura and Cisek (2016) to explain their findings which indicated higher baseline activity as well as higher gain, but similar threshold levels in decision-related cells in speed compared to accuracy conditions.

In fact, the concept of an evidence-independent urgency signal has been a recurring theme throughout the SAT and sequential sampling model literature (Cisek, Puskas, & El-Murr, 2009; Hawkins, Forstmann, Wagenmakers, Ratcliff, & Brown, 2015; Milosavljevic et al., 2010; Thura, Beauregard-Racine, Fradet, & Cisek, 2012). It describes the idea that the accumulation of evidence is inflated by the addition of a signal which increases over time and ensures that a decision is made, even when no evidence is available. This urgency signal may increase faster under speed instructions compared to accuracy instructions, leading to faster, more error-prone responses, as the decision threshold is reached with less evidence. Note that this urgency signal is equivalent to the concept of collapsing bounds, which assumes that accumulation remains dependent on evidence alone throughout, but the decision thresholds are

dynamic and decrease towards the baseline over time, to ensure decision formation. However, it is important to note that standard sequential sampling models, without the addition of an urgency signal, have been supported across a large variety of paradigms, while there is only limited evidence to support models that do include this dynamic feature (see Hawkins et al., 2015 for a review). In fact, several studies were unable to support the concept of an urgency signal, suggesting instead that standard sequential sampling models can fully account for all behavioural data, including SAT data (Balci et al., 2011; Karsilar, Simen, Papadakis, & Balci, 2014).

Nevertheless, a recent study found support for an urgency signal as the driving force behind the SAT, by using EEG to record human brain activity during a random dot motion task under free response and deadline conditions (Murphy, Boonstra, & Nieuwenhuis, 2016). In this study, desynchronisation in the mu frequency band (8-14 Hz) was explored as a decision-related motor signal and results showed that, in the deadline condition, this signal was elevated towards the threshold (i.e. towards activity levels at response). While they showed that contralateral mu power at the time of the response remained the same across both conditions, indicating a common threshold, they found lower bilateral mu power prior to the stimulus onset, as well as lower ipsilateral power at the response in the deadline condition, suggesting the influence of an urgency signal. Further, Murphy et al. (2016) used measurements of pupil diameter to show that this urgency may be caused by a modulation of neural gain.

Together, these findings question the idea that the adjustment of the threshold in a sequential sampling process underlies the SAT on a neural level. While there is an overwhelming amount of evidence suggesting that the behavioural effects associated with the SAT are best accounted for by a change in threshold (Balci et al., 2011; Brown & Heathcote, 2008; Karsilar et al., 2014; Ratcliff & McKoon, 2008; Smith & Ratcliff, 2004; Usher & McClelland, 2001), neural data suggest that less specific changes are associated with the SAT, with most studies reporting a change in both baseline activation and gain.

In the light of this literature, and in particular the paucity of studies addressing the time-varying neurometric correlates of the SAT in humans, we set out to explore the neural mechanisms underlying the SAT in the context of sequential sampling models. In two experiments, we asked human subjects to complete a random dot motion task, while we recorded decision-related neural activity by either using EEG to record a centroparietal component which has previously been suggested to reflect accumulation, or transcranial magnetic stimulation (TMS) to record motor preparation. During the task, we manipulated the decision strategies by using 'speed' and 'accuracy' instructions, to explore their effects on the neural data. In addition, we manipulated the difficulty of the task as the impact of this manipulation has been researched extensively and it is well-established that both accumulation profiles predicted by sequential sampling models and neural correlates of decision-making vary in build-up rate as a result of varying difficulty. By fitting a sequential sampling model to the behavioural decision-making data and directly comparing the resulting model predictions to these neural signals, we aimed to gain new insights into the underlying mechanisms of the SAT.

In order to address the inconsistencies between the modelling and neuroimaging literature, we used two types of models, one of which used the typically reported variation in parameters to account for the SAT (i.e. varying threshold parameters across SAT conditions), and one in which we implemented a global modulation in activity. Specifically, we used the parameters estimated using varying thresholds as they have been shown to account well for behavioural data, and, without affecting the model fit, rescaled them to transfer the difference in thresholds over speed and accuracy regimes to all other parameters, modelling a widespread change in activity which has previously been reported in neural data (Heitz & Schall, 2012, 2013; Murphy et al., 2016). By directly comparing the predicted accumulation profiles of both models with two neural correlates of decision-making, we explored the mechanisms underlying decision-making in the context of the SAT and found evidence suggesting that the SAT is implemented in the human brain via a form of global gain modulation.

## 2.1. Experiment 1: EEG

EEG is a particularly suitable method to track perceptual decision-making in humans, since its high temporal resolution allows us to track the dynamically changing decision variable. To date, studies which used human EEG to directly test SAT mechanisms in the context of sequential sampling models are sparse. There are however, a number of EEG studies using human scalp potentials to explore the mechanisms of the SAT in a serial processing framework, where the locus of the SAT is placed on sensory, decision, or motor processes, which are thought of as non-overlapping intervals (Donders, 1969; Sternberg, 1969).

For example, studies focussing on the lateralised readiness potential (LRP), an event-related potential (ERP) indicating preparation of motor activity, measured the stimulus-LRP onset, and the LRP onset-response intervals separately in order to identify differences in sensory and motor processes respectively. These studies found that both LRP stages decrease in duration under speed instructions, suggesting both a sensory and motor locus of the SAT (Osman et al., 2000; Rinkenauer et al., 2004). Interestingly, by suggesting that post-decisional motor stages are affected by the SAT, these studies questioned the claim that the SAT is explained by a baseline-threshold difference alone. However, the notion of serial processing has since been rejected (Hadar, et al., 2015; see Experiment 2). Additionally, note that the LRP has previously been suggested to display characteristics of the accumulation profile predicted by sequential sampling models (Kelly & O'Connell, 2013) and, although not directly tested, does not seem to show an amplitude difference between SAT regimes at the time of response, further questioning the threshold effect (Osman et al., 2000; Rinkenauer et al., 2004).

Similarly, Osman et al. (2000) explored the ERP component P300, which may be equivalent to the centroparietal positivity (CPP), a component that has been shown to reflect the accumulation of evidence as suggested by sequential sampling models (Kelly & O'Connell, 2013; O'Connell et al., 2012; Twomey et al., 2015). In fact, like LIP firing rates in non-human primates, the CPP in the

human EEG has been shown to display accumulation-to-bound characteristics and described as the decision variable. For example, it has been demonstrated that the slope of the CPP scales with the strength of sensory evidence and predicts RT, and that its amplitude reaches a stereotyped level at response time, suggesting a fixed decision threshold (Kelly & O'Connell, 2013; O'Connell et al., 2012). Although Osman et al. (2000) explored the P300 under SAT conditions and found similar patterns as those observed in the LRP, they only tested peak latencies, to explore sensory and motor parts of the decision-making process and did not explore the P300 as a potential neural substrate of a decision variable. The effects of the SAT on the P300 were also explored by Perri, Berchicci, Spinelli, and Di Russo (2014), who found that fast compared to slow decisions led to an earlier and larger P300. However, in this study, no SAT instructions were given, and trials were divided into four different speed and accuracy conditions post hoc, which makes it difficult to compare findings. To our knowledge, the CPP has not been directly used to explore the effects of SAT on the decision variable.

In Experiment 1, we therefore set out to test the impact of SAT instructions on the CPP. As described above, we compared the resulting waveforms to two different models, one which makes use of a variation in the threshold parameter to model the SAT, and one which assumes a more global change in activity. We evaluated the resulting decision variables in the light of the CPP.

## **2.1.1. Methods**

### **2.1.1.1. Participants**

We recruited a total of 26 participants (nine males), with a mean age of 29.81 ( $SD = 7.24$ ). According to criteria that were established prior to the experiment, participants were excluded if they were unable to reach a calibrated coherence level of less than 90% for either of the difficulty conditions (see section 2.1.1.2.2). On this basis, we excluded three participants prior to the main experiment. The remaining sample consisted of 23 participants (eight males) with a mean age of 29.39 ( $SD = 7.47$ ), each of which participated in a single

two-hour session, completing 800 trials. Participants were recruited using poster advertisements and word of mouth, resulting in a sample which was primarily made up of students and staff at City, University of London. All participants were paid £8 per hour and an additional reward for task performance (up to £4 per session). The experiment was approved by the City, University of London Psychology Department Ethics Committee.

### **2.1.1.2. Stimuli and Procedure**

#### *2.1.1.2.1. Stimuli and Experiment Setup*

Participants completed a random dot motion task, in which they were presented with an array of moving dots. In each trial, a proportion of the dots moved coherently in one direction (either up or down) while the rest of the dots moved in random directions. Participants were asked to indicate the direction of the coherent motion. Trial difficulty was manipulated by varying the proportion of dots moving coherently, with larger coherence levels leading to easier decisions.

The task was displayed on a cathode ray tube screen (size: 41 cm x 30 cm), operating at a refresh rate of 85 Hz and a resolution of 1240 x 786 pixels. Participants were seated at a distance of 100 cm from the screen. In order to indicate their decision, participants held a digital response button interfaced via a 16 bit A/D card (National Instruments X-series PCIe-6323, sample rate 100,000 Hz) in each hand, and were instructed to press the right button to indicate the 'up' response, and the left button to indicate the 'down' response.

In each trial, a total of 300 white dots, 0.04 x 0.04 degrees visual angle (dva) in size, were displayed within a 5 dva circular aperture on a black background. A fixation cross (size: 0.33 x 0.33 dva) was located in the centre of the stimulus. All dots moved at a speed of 3.3 dva per second. While coherent dots moved either up or down, depending on the trial, the direction in which random dots moved was randomly selected for each dot and each frame. The position of all dots was randomised every five frames.

The trial procedure is displayed in Figure 2.1. Initially, participants were presented with a fixation cross for 500 ms (plus a jitter of up to 1000 ms, drawn from a uniform distribution). Then, 100% of the dots moved randomly for 1000 ms (plus a jitter of up to 1500 ms, drawn from a truncated gamma distribution with shape parameter 1 and scaling parameter 150)<sup>1</sup>. Since the onset of moving dots on the screen is likely to induce visual evoked potentials (VEPs) in the EEG, which may interfere with the recording of the CPP, this interval of random motion was introduced so that any VEPs occur before the stimulus onset (i.e. onset of coherent motion). This random motion was followed by the onset of coherent motion, when a proportion of dots started moving coherently either upwards or downwards, for up to 2000 ms, or until the response. Feedback was provided after each trial (see section 2.1.1.2.3). All stimuli were written in Matlab (The Mathworks, Natick, U.S.A.), using the Psychtoolbox extension (Brainard, 1997; Kleiner et al., 2007; Pelli, 1997) and run on a PC.

In this experiment, difficulty (easy, hard), direction (up, down), and instructions (speed, accuracy) were manipulated. The ‘speed’ and ‘accuracy’ conditions were blocked, while all other conditions were randomly intermixed. The order of the SAT blocks was counterbalanced across participants. Each participant completed a minimum of 100 practice trials. Practice trials started with a coherence level of 90%, i.e. 90% of dots moved in one direction while only 10% moved randomly, and became progressively more difficult.

#### 2.1.1.2.2. *Difficulty Calibration*

Once participants felt comfortable with the task, they completed a total of 200 staircase trials to calibrate the level of difficulty appropriate for the ‘easy’ and ‘hard’ conditions for each participant individually. To this end, we used the QUEST staircase procedure, implemented in Psychtoolbox, which estimated the coherence levels at which each participant responded correctly in 75% and 95% of trials (Watson & Pelli, 1983). These coherence levels were then used for the ‘hard’ and ‘easy’ conditions respectively. The stimulus presentation time

---

<sup>1</sup> A gamma distributed fore period with a shape parameter of 1 was chosen as it is associated with a uniform hazard function (Luce, 1986).

was reduced from 2000 ms to 1300 ms, and no feedback was provided during staircase trials. If a participant's performance led to estimated 'easy' and 'hard' coherence levels of more than 90%, the participant was excluded from the experiment. This procedure resulted in a mean coherence of 30.63% ( $SD = 18.69$ ) for 'hard' trials, and 67.67% ( $SD = 28.23$ ) for 'easy' trials.

#### 2.1.1.2.3. *SAT Instructions*

In order to enforce the SAT manipulations, participants were instructed to react as fast/accurately as possible in half of the trials. Additionally, feedback was provided after each trial to either reward participants (display of the word 'Correct' and a small monetary reward, adding up to a maximum of £4 per participant) for fast and correct/correct responses in 'speed'/ 'accuracy' trials, or provide negative feedback with the words 'TOO SLOW' or 'INCORRECT' in green letters on a red screen when the instructions were not followed. The inter-trial interval was increased by 1000 ms after each trial with negative feedback. Neutral feedback (no monetary reward, but a neutral screen with the words 'incorrect' or 'too slow') was shown when participants responded fast but incorrectly in the 'speed' condition or accurately but very slowly in the 'accuracy' condition. Whether a response was too slow or not was determined by a variable deadline which was initially set to 600 ms for the 'speed' and 1000 ms for the 'accuracy' condition. To optimise performance, the deadlines varied between 450 and 750 ms ('speed') and between 700 and 1300 ms ('accuracy') and were adjusted using separate QUEST staircase procedures, targeting accuracy levels of 75% for 'speed', and 90% for 'accuracy' conditions. Feedback was also provided when participants responded before the onset of the coherent motion ('too fast').

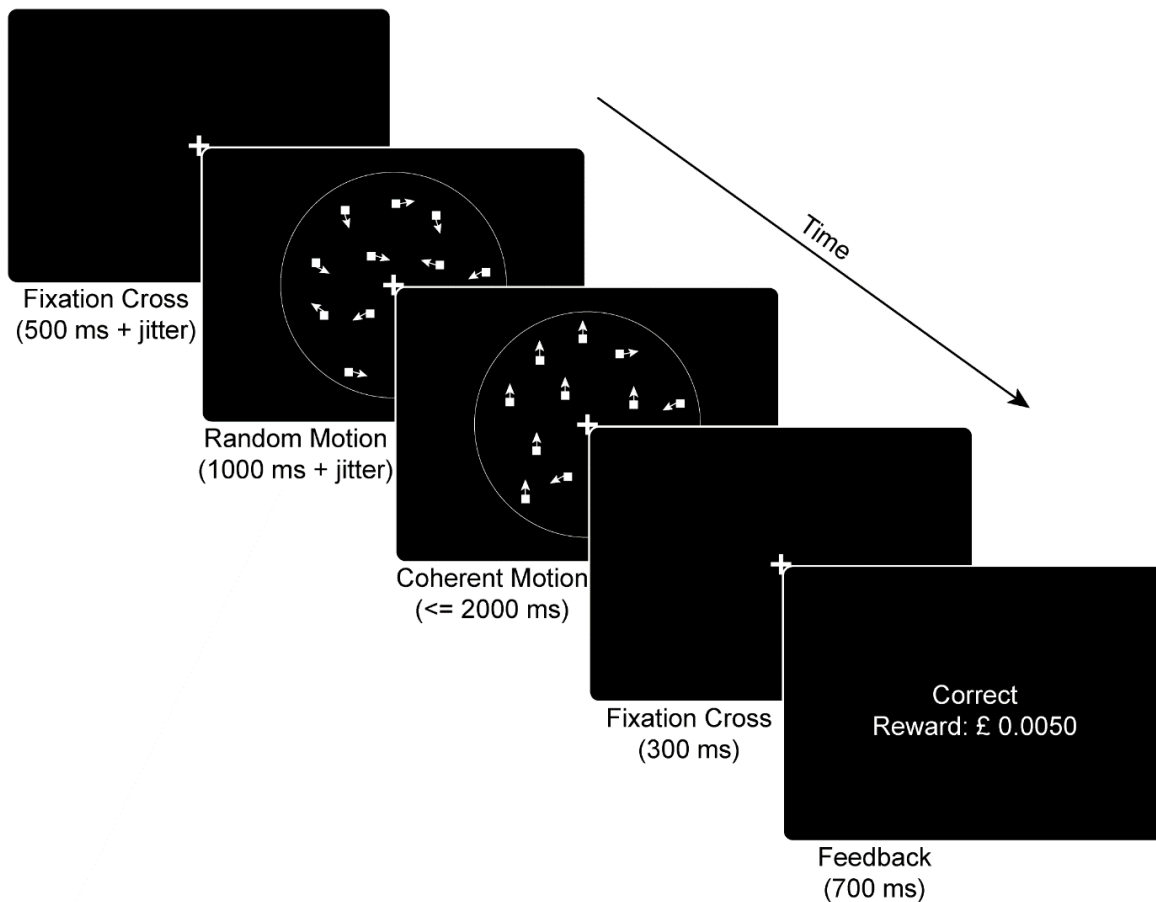


Figure 2.1: Random dot motion task trial procedure: after the presentation of a fixation cross, randomly moving dots were displayed on the screen for a minimum of 1000 ms. Then, a proportion of dots (defined by the level of coherence) moved coherently either up or down (here: up) and remained in this motion for up to 2000 ms or until the response. Each trial was followed by feedback after a short delay. Note that the size and number of dots have been adjusted for illustration.

### 2.1.1.3. EEG Recording and Pre-processing

Continuous EEG was recorded using 64 active electrodes, placed equidistantly on the scalp (EasyCap, M10 Montage) and referenced to the right mastoid. Using a BrainAmp amplifier (BrainProducts), data were recorded at a sampling rate of 1000 Hz and band-pass filtered from 0.016 – 1000 Hz. The data were then pre-processed and analysed using custom scripts in Matlab (The Mathworks, Natick, U.S.A.), drawing on functions from the EEGLAB toolbox (Delorme & Makeig, 2004).

EEG data were re-referenced to the average reference and filtered at 0.1 (low cut-off) and 45 Hz (high cut-off), using a Hamming windowed finite impulse response filter. To improve the signal-to-noise ratio, we initially visually

inspected the data to remove large muscle artifacts before applying independent component analysis to remove eye blink components. Any remaining artifacts were removed manually during a second visual inspection. Afterwards, spherical spline interpolation was used to reconstruct noisy channels, which were identified and rejected during the first visual inspection.

In line with the procedures used in previous CPP studies (Kelly & O'Connell, 2013; O'Connell et al., 2012), the data were converted to current source density (CSD) estimates to increase spatial selectivity. The CSD transformation was applied using the CSD toolbox, which uses a spherical spline algorithm, with the spline interpolation constant  $m$  set to its default value ( $m = 4$ ; Kayser & Tenke, 2006).

#### **2.1.1.4. ERP Analysis**

For the ERP analysis, we extracted both stimulus-locked (-200 to 2000 ms, relative to motion onset) and response-locked (-1000 to 100 ms, relative to the button press) epochs. All epochs were baseline corrected to the average over a 200 ms period preceding the motion onset. In order to collapse over 'up' and 'down' trials, the ERP topography of correct 'up' trials and incorrect 'down' trials (right button presses) was mirrored along the midline (i.e. activity recorded in electrodes on the left hemisphere was now associated with electrodes on the right hemisphere), so that all motor preparation appeared in the right hemisphere. Although this step was not strictly necessary to analyse the CPP, which is recorded from the midline, this mirroring allows for a better visualisation of activation across the scalp. The appropriate electrode to generate the CPP waveform was chosen individually, by visually inspecting each participant's averaged ERP topography to identify the centroparietal region of maximum amplitude (chosen electrodes: 1, 5, or 14, roughly equivalent to electrodes Cz, CPz, and Pz in the 10-20 system; see Figure 2.4). The activity in the selected electrodes was averaged for each condition and for stimulus and response-locked signals separately. Only correct trials were used in the ERP analysis.

In line with Kelly and O’Connell (2013), we measured the slope of the CPP for each participant, by fitting a straight line to the waveform from 200 to 350 ms in the stimulus-locked, and -250 to -100 ms in the response-locked data. Additionally, we compared the amplitudes of the ERP across different conditions at each time point between 0 and 1000 ms in the stimulus-locked and between -1000 and 0 ms in the response-locked data, using false discovery rate (FDR) controlled ANOVAs (Benjamini & Hochberg, 1995). In this procedure, the uncorrected  $p$ -values are sorted from lowest to highest ( $p_i$  refers to the  $i$ th lowest value out of  $m$  total  $p$ -values). The largest  $i$  for which  $p_i < \left(\frac{i}{m}\right) \alpha$  is identified and all  $p$ -values associated with  $i$ s smaller or equal to the identified  $i$  are considered significant.

#### 2.1.1.5. Model

We chose a race model to account for the behavioural data (Brown & Heathcote, 2008; Usher & McClelland, 2001). This model makes few assumptions about the decision-making process (e.g. it does not assume inhibition between accumulators) while still remaining somewhat physiologically plausible (e.g. it assumes noisy, positive accumulation; Brown & Heathcote, 2008; Usher & McClelland, 2001). According to this model (see Figure 2.2), a binary choice like the one used here is simulated using two accumulators, one associated with the correct, and one associated with the incorrect alternative. Both accumulators race towards a common decision threshold  $A$  and whichever accumulator reaches the threshold first determines the response.

Each accumulation process begins at a starting point  $z$ , drawn from a uniform distribution between 0 and the starting point parameter  $S_z$ . The profile of the accumulation process is determined by the drift rate  $v$  which determines the input  $I$  and the mean slope of the accumulation, as well as random noise  $N$ , drawn from a normal distribution with mean 0 and standard deviation  $\sigma$ , so that the quantity accumulated at each time point in accumulator  $m$  is described by:

$$dx_m = I_m + N(0, \sigma^2) \quad (2.1.)$$

Additionally, the accumulation process is restricted to positive values in order to remain physiologically plausible:

$$x_m(t + 1) = \max(0, x_m(t) + dx_m) \quad (2.2.)$$

The response time is defined as the time taken for the first accumulator to reach the threshold  $A$  plus a non-decision time which accounts for the duration of sensory and motor processing before and after the accumulation process respectively and is drawn from a uniform distribution with the width  $S_{Ter}$  and the centre  $T_{er}$ .

In a standard race model for a binary decision, this leads to a total of seven parameters ( $A, S_z, v_{correct}, v_{incorrect}, T_{er}, S_{Ter}, \sigma^2$ ). One parameter is chosen as a scaling parameter and fixed to an arbitrary value, resulting in a total of six free parameters.

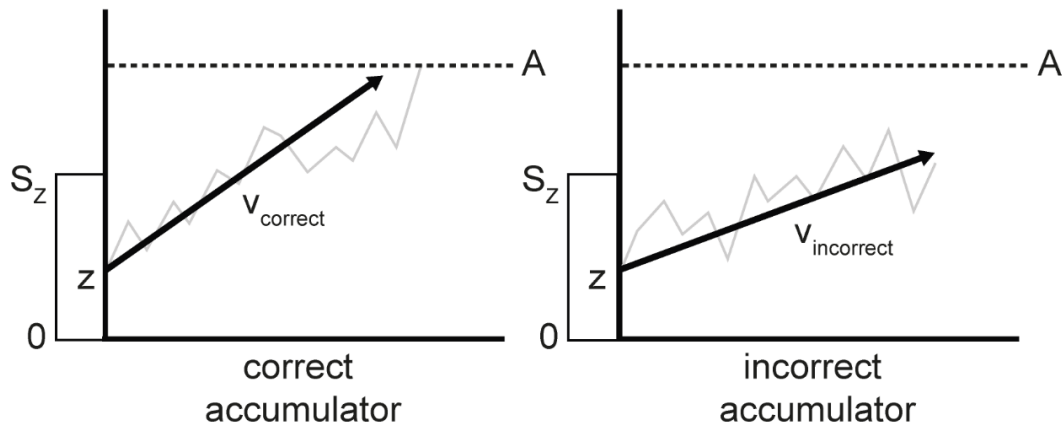


Figure 2.2: Race model: in a choice between two alternatives, two accumulators (one associated with the correct and one with the incorrect alternative) race towards a common threshold  $A$ . Each accumulation profile begins at a point randomly drawn from a uniform distribution between  $0$  and  $S_z$  and increases at a rate defined by the associated drift rate parameter ( $v_{correct}/v_{incorrect}$  for the correct/incorrect accumulator respectively), as well as noise. The modelled reaction time consists of the time taken for the first accumulator to reach  $A$ , as well as a non-decision time  $T_{er}$ , which accounts for sensory and motor processes.

#### 2.1.1.5.1. Standard Model

To apply this model to the data set in this experiment, we added drift rate parameters to account for the different difficulty conditions ( $v\text{-easy}_{correct}$ ,  $v\text{-easy}_{incorrect}$ ,  $v\text{-hard}_{correct}$ ,  $v\text{-hard}_{incorrect}$ ). This implementation of difficulty is well-established and has been validated using both behavioural and neural data (Mulder et al., 2014; Ratcliff & McKoon, 2008; Ratcliff & Rouder, 1998; Roitman & Shadlen, 2002; Twomey et al., 2015). In order to explain differences due to

SAT instructions, we added a threshold parameter. The threshold for ‘accuracy’ trials  $A_{accuracy}$  acted as a scaling parameter and was fixed to 1, while the threshold for the ‘speed’ condition,  $A_{speed}$ , was free to vary. We tested a total of three different models: one in which all remaining parameters were fixed across conditions (Model 1), one in which the starting point parameter  $S_z$  was free to vary across SAT conditions (Model 2), and one in which the non-decision time parameter  $T_{er}$  was free to vary across SAT conditions (Model 3; see Table 2.1).

Each model was fitted to the pooled RT data<sup>2</sup> (RTs faster than 180 ms or slower than 2000 ms (6.08%) were discarded). For each condition, RTs were simulated (in 10 ms time steps) based on the equations (2.1.) and (2.2.) and compared to RT data using Quantile Maximum Probability Estimation (Heathcote, Brown, & Mewhort, 2002). Parameter values were adjusted using a differential evolution algorithm implemented in Matlab (The Mathworks, Natick, U.S.A.; Price, Storn, & Jouni, 2005).

In order to compare the three models, we calculated the Bayesian information criterion (BIC, Schwarz, 1978) as well as the Akaike information criterion (AIC; Akaike, 1977). These measures describe the goodness of fit by considering both the likelihood of the model and the number of parameters, penalising complex models to resolve the problem of overfitting. The model with the best fit was then used to predict accumulation profiles.

#### 2.1.1.5.2. *Rescaled Model*

Although the SAT is typically implemented through a change in threshold as described above, more recent evidence suggests that behavioural changes due to SAT instructions are in fact caused by a more global change in activity (Heitz & Schall, 2012; Lo, Wang, & Wang, 2015; Murphy et al., 2016; Perri et al., 2014). We implemented this global gain modulation using a ‘rescaled’ model. For this, we used the best-fitting model described above and computed a new

---

<sup>2</sup> Note that the same analysis was repeated with normalised RT and EEG data and led to qualitatively identical results (see Appendix 7.1).

set of parameters for the ‘speed’ condition by simply dividing all parameters (apart from  $T_{er}$  and  $S_{Ter}$ ) by  $A_{speed}$ . This results in a model in which the threshold for both SAT conditions is 1 and the original difference between conditions is transferred onto all other parameters, modelling a global gain modulation. This rescaled model is mathematically equivalent to the standard model, but assumes different underlying processes and predicts a different accumulation path.

#### 2.1.1.5.3. *Model Prediction*

EEG is recorded from the scalp, and can therefore only measure the sum of all electrical brain activity underneath each electrode. Since we assume that each accumulation process occurs in a population of neurons in spatial proximity, we argue that an ERP recorded from the scalp above these neural populations, like the CPP, reflects the sum of both accumulators.

We chose the best-fitting model based on the BIC value and simulated 20,000 accumulation paths in 10 ms time steps. In order to create a signal similar to the CPP, accumulation profiles from the correct and incorrect accumulator associated with correct responses were summed and baseline corrected by subtracting the first data point from the entire accumulation profile. The resulting profiles were averaged for each condition separately and locked once to the stimulus and once to the response. Since the stimulus-locked signal includes varying time spans of post-decision stages, and we can only speculate about the behaviour of the accumulator after the response, we removed simulated trials from averaging after the response (i.e. after the crossing of the threshold plus  $T_i$ ; see below).

Since we averaged over all simulated accumulation traces per condition, we re-computed the CPP as an average rather than a grand average to compare the simulated accumulation profiles to the EEG signal. We also downsampled the CPP to 10 ms time steps and removed trials from the average once they reached their corresponding RT, to match the simulations.

In order to simulate the non-decision time in the model predictions, we added a brief sensory delay before the onset of the accumulation as well as a motor delay in which accumulation continued after the threshold was reached. We assume that this continuation of accumulation after the threshold is necessary as the participants continue to see the stimulus, and arguably continue to accumulate, during the brief period of time in which the threshold is reached but the button is not yet pressed. Since we fitted the non-decision time parameter  $T_{er}$  which contains the time interval for both sensory and motor processes, we divided it into  $T_e$  and  $T_r$ . The optimal division of  $T_{er}$  into these components was determined by calculating the mean squared error between the (re-computed) CPP and the simulated mean accumulation per condition, and using a differential evolution algorithm (Price et al., 2005) to minimise the mean squared error. The same procedure was used to match the arbitrary scale of the accumulation profile to the CPP's. Note that this optimisation of the scale and non-decision time division was performed separately for the standard and the rescaled model.

#### 2.1.1.5.4. *Bootstrap Comparison*

We then used a bootstrap procedure to compare the similarity of the neural signal and the model prediction between the standard and the rescaled model. In each of 1999 iterations, RT data were resampled with replacement within each condition ('speed easy', 'speed hard', 'accuracy easy', 'accuracy hard'). The resampled RT data sets were then used to fit the standard race model (the best-fitting model identified in section 2.1.1.5.1). To estimate the best-fitting parameters, a simplex algorithm (Lagarias, Reeds, Wright, & Wright, 1998), with the parameters obtained using the original data set as starting values, was used due to its relatively short computation time. The resulting parameters were then 'rescaled' in the same way as described in section 2.1.1.5.2. We then generated simulated accumulation profiles for both the standard and the rescaled model (as described in section 2.1.1.5.3). The predictions of each of the models were compared to the corresponding CPP (i.e. to the CPP generated using the same trials which were resampled to generate the resampled RT distribution) and the mean squared error was computed for each model. As for the original data (see section 2.1.1.5.3), the simulation of each iteration was adjusted to match the

corresponding CPP by fitting the scale and the proportion of sensory and motor delay using a differential evolution algorithm. The difference in mean squared error between the rescaled and the standard model of each iteration was then used to form a distribution around the difference in mean squared error between the models associated with the original data. We estimated the bias-corrected and accelerated (BCa) confidence interval and rejected the null hypothesis that both models resemble the CPP equally well if this interval did not include 0.

## 2.1.2. Results

### 2.1.2.1. Behavioural Results

In order to test the effects of difficulty and SAT instructions, data were collapsed over 'up' and 'down' trials. Trials with very short (< 180 ms) and very long ( $\geq$  2000 ms) RTs were excluded from the analysis (6.08% of trials). The remaining data are displayed in Figure 2.3.

To explore differences in correct RT, a 'Difficulty' ('easy'/'hard') x 'Instruction' ('speed'/'accuracy') ANOVA was conducted, and revealed a significant main effect of 'Difficulty',  $F(1, 22) = 120.12, p < .001, \eta_p^2 = .85$ , a significant main effect of 'Instruction',  $F(1, 22) = 102.77, p < .001, \eta_p^2 = .82$ , as well a significant interaction effect,  $F(1, 22) = 36.47, p < .001, \eta_p^2 = .62$ . As expected, RTs were faster in the 'speed' condition ( $M = 522$  ms) compared to the 'accuracy' condition ( $M = 673$  ms) in both 'easy',  $t(22) = -8.72, p < .001$ , and 'hard',  $t(22) = -9.74, p < .001$ , trials. RTs were also faster in 'easy' ( $M = 527$  ms) compared to 'hard' ( $M = 668$  ms) trials, an effect which was seen more strongly in the 'accuracy' condition,  $t(22) = 10.02, p < .001$ , than in the 'speed' condition,  $t(22) = 9.85, p < .001$ .

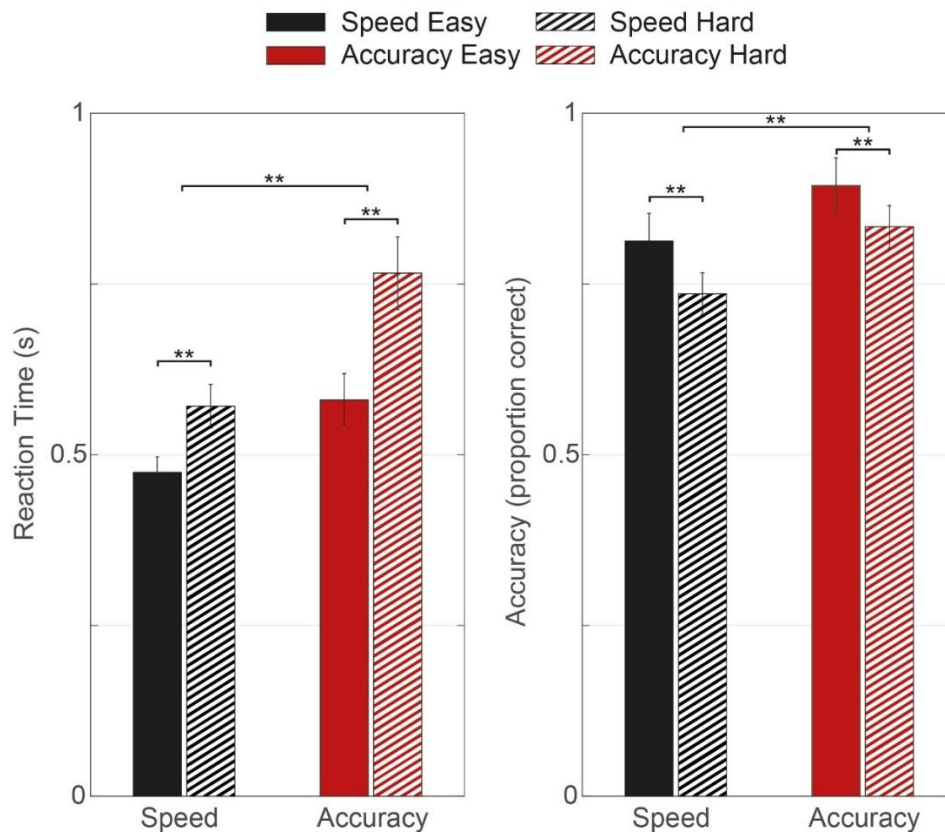


Figure 2.3: Behavioural results: reaction time (left) and accuracy scores (right) for each condition. Error bars indicate 95% Confidence Interval. \*\* indicates  $p < .001$ .

To explore these effects in the accuracy data, a generalised linear mixed-effects model with a logistic link function and binomial data model was used to account for the non-normal distribution. Using the ‘fitlme’ function in Matlab (The Mathworks, Natick, U.S.A.), parameter estimates were based on a maximum likelihood method using Laplace approximation. In this model, we used the ‘maximal’ random effects structure (Barr, Levy, Scheepers, & Tily, 2014), i.e. both manipulations, ‘Instruction’ and ‘Difficulty’, and their interaction were included as fixed effects, and both manipulations and their interactions within each participant were included as random effects (Wilkinson notation:  $\text{Accuracy} \sim 1 + \text{Instruction} * \text{Difficulty} + (1 + \text{Instruction} * \text{Difficulty} | \text{Participant})$ )<sup>3</sup>. Both ‘Difficulty’,  $t(88) = 4.68$ ,  $p < .001$ , and ‘Instruction’,  $t(88) = 7.76$ ,  $p < .001$ , were significant predictors, with higher accuracies observed in ‘easy’ ( $M = 85\%$ ) compared to

<sup>3</sup> The dispersion parameter of the model,  $\phi = .44$ , was calculated by dividing the sum of squared Pearson residuals by the residual degrees of freedom (Venables & Ripley, 2002), and indicates that there was no issue with overdispersion.

'hard' ( $M = 78\%$ ) trials and in 'accuracy' ( $M = 86\%$ ) compared to 'speed' ( $M = 77\%$ ) trials. The interaction between 'Difficulty' and 'Instruction' was not significant ( $p > .05$ ).

#### **2.1.2.2. ERP Results**

The CPP is displayed in Figure 2.4. 'Difficulty' ('easy'/'hard') x 'Instruction' ('speed'/'accuracy') ANOVAs were conducted to explore the effects of the manipulations on the build-up rate of the CPP. We found that, in both the stimulus-locked, and the response-locked waveforms, there was a significant main effect of 'Difficulty'  $F(1, 22) = 14.70, p = .001, \eta_p^2 = .40, F(1, 22) = 9.06, p = .006, \eta_p^2 = .29$ , with a higher slope in 'easy' compared to 'hard' trials. There was no main effect of 'Instruction', and no interaction effect in either of the time alignments ( $p > .26$ ).

Similarly, we used FDR-controlled ANOVAs to explore the CPP amplitude at each time step and found a main effect of 'Difficulty', with higher amplitudes in the 'easy' compared to the 'hard' conditions between 263 and 640 ms in the stimulus-locked CPP (corrected  $p < .049$ ). Again, we found no main effect of 'Instruction' and no interaction effect in the stimulus-locked CPP, and no effects were seen in the response-locked data (corrected  $p > .09$ ).

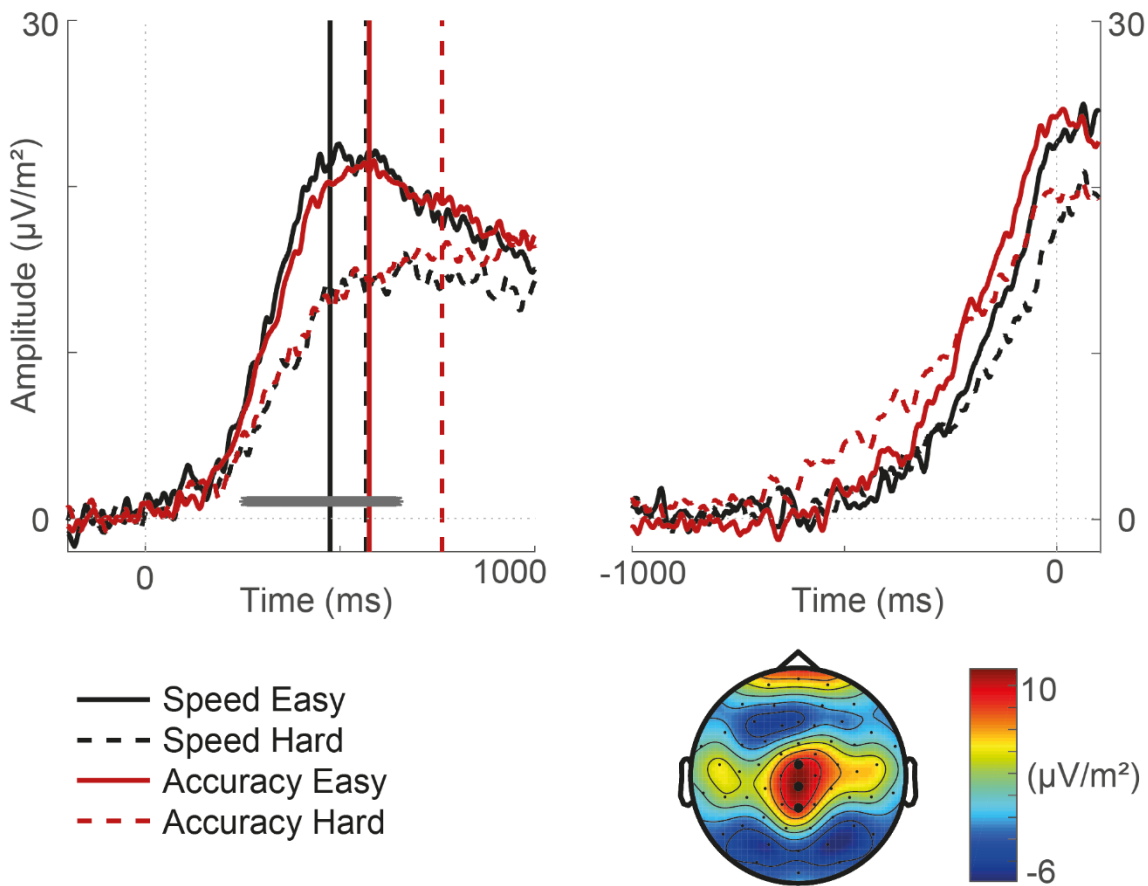


Figure 2.4: CPP results: stimulus-locked (left) and response-locked (right) CPP waveform for each condition. Vertical lines indicate mean RT for each condition. Note that mean RTs may differ slightly from those displayed in Figure 2.3, as only trials which were used to generate the waveform were included to calculate mean RTs. Grey dots at the bottom of the waveform indicate a significant main effect of 'Difficulty'. The bottom right panel shows the topography of the ERP, averaged over the stimulus-locked time interval of 0 to 1000 ms. Electrodes used to generate CPP waveforms are highlighted.

### 2.1.2.3. Model Results

We fitted three different race models to the RT data and compared their goodness of fit using the BIC (Schwarz, 1978; see Table 2.1). The best (lowest) BIC was associated with Model 2, a model in which drift rate varied across difficulty conditions, and both the threshold and the starting point distribution varied across SAT conditions. The parameters for this model, as well as its rescaled version are displayed in Table 2.2.

Table 2.1: Model Comparison: BIC and AIC values for each model and each experiment (best BIC and AIC values in bold).

Model	Number of parameters	Parameters	Experiment 1		Experiment 2	
			BIC	AIC	BIC	AIC
Model 1	9	$v\text{-easy}_{correct}, v\text{-easy}_{incorrect},$ $v\text{-hard}_{correct}, v\text{-hard}_{incorrect},$ $A_{speed},$ $S_z, T_{er}, S_{Ter}, \sigma^2$	62,466	62,398	44,933	44,868
Model 2	10	$v\text{-easy}_{correct}, v\text{-easy}_{incorrect},$ $v\text{-hard}_{correct}, v\text{-hard}_{incorrect},$ $A_{speed},$ $S_{z\text{-speed}}, S_{z\text{-accuracy}},$ $T_{er}, S_{Ter}, \sigma^2$	<b>62,464</b>	<b>62,389</b>	<b>44,932</b>	<b>44,859</b>
Model 3	10	$v\text{-easy}_{correct}, v\text{-easy}_{incorrect},$ $v\text{-hard}_{correct}, v\text{-hard}_{incorrect},$ $A_{speed},$ $T_{er\text{-speed}}, T_{er\text{-accuracy}},$ $S_z, S_{Ter}, \sigma^2$	62,479	62,404	44,937	44,865

Table 2.2: Estimated parameter values for the chosen model (Model 2) and its rescaled version: note that the response threshold  $A$  in the ‘accuracy’ condition was set to 1 as a scaling parameter.

Parameters		Standard Model: parameter values per SAT Instruction		Rescaled Model: parameter values per SAT Instruction	
		<i>accuracy</i>	<i>speed</i>	<i>accuracy</i>	<i>speed</i>
Starting point variability ( $S_z$ )		0.319	0.541	0.319	0.664
Response threshold ( $A$ )		1	0.815	1	
Non-decision time ( $T_{er}$ )		0.257		0.257	
Non-decision time variability ( $S_{Ter}$ )		0.229		0.229	
Diffusion constant ( $\sigma^2$ )		0.785		0.785	0.964
Drift rate ( $v$ )	correct	easy	2.475	2.475	3.038
		hard	1.350	1.350	1.656
	incorrect	easy	0.253	0.253	0.310
		hard	0.054	0.054	0.066

The estimated parameters of the standard model show that, as expected, higher drift rates were associated with ‘easy’ compared to ‘hard’ conditions, and lower thresholds were associated with ‘speed’ rather than ‘accuracy’ conditions. Additionally, higher starting point variability was estimated for the ‘speed’ condition, further decreasing the average baseline-threshold distance. In the rescaled parameters on the other hand, the threshold is equal in both conditions, while the difference between SAT conditions is passed on to all

other parameters (see Table 2.2). Note that the two models are nevertheless mathematically equivalent and produce the same fit to the RT data.

Figure 2.5 displays the quality of the model fit, which is identical for both the standard and rescaled model. The RT distribution is summarised by five quantile estimates (from left to right: 10%, 30%, 50%, 70%, 90%) for each condition separately, and the RT (x-axis) and proportion of data (y-axis) for each quantile is shown for both the empirical (circles) and simulated (lines and crosses) data. The overlap between empirical and modelled quantiles indicates that the model fitted the data well. The mean difference between predicted and recorded RT quantiles was approximately 15 ms for correct responses, confirming that the model was able to account for the RT data.

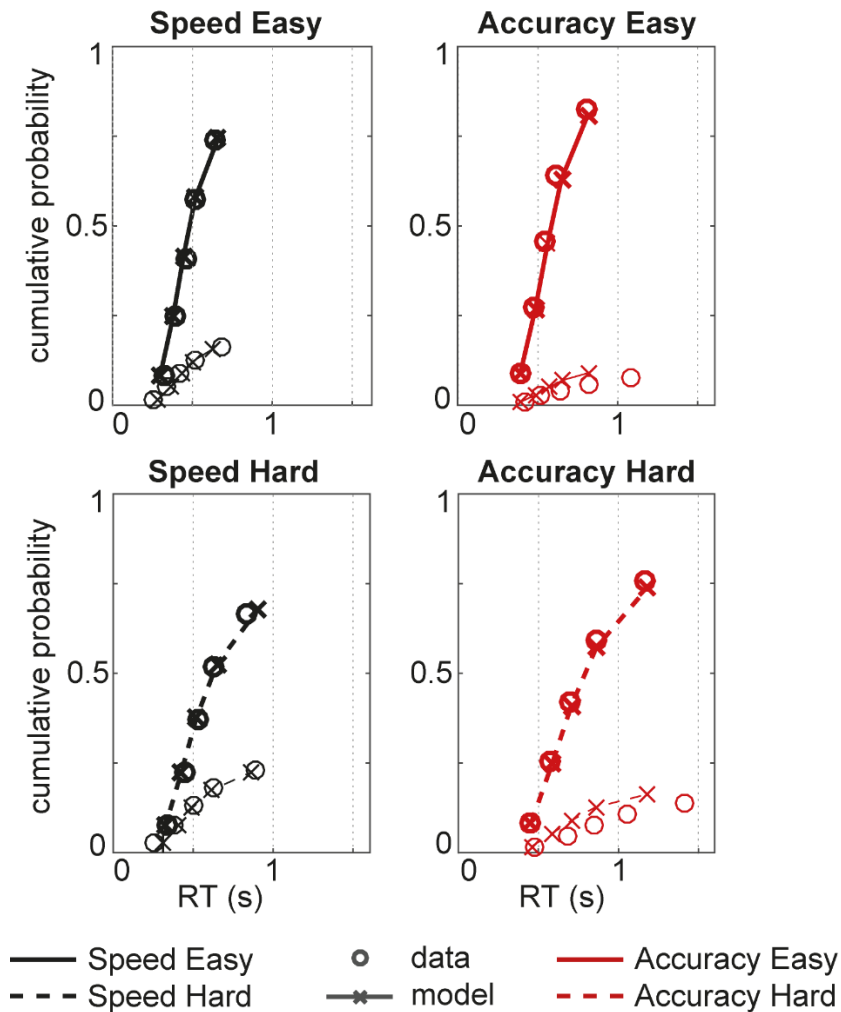
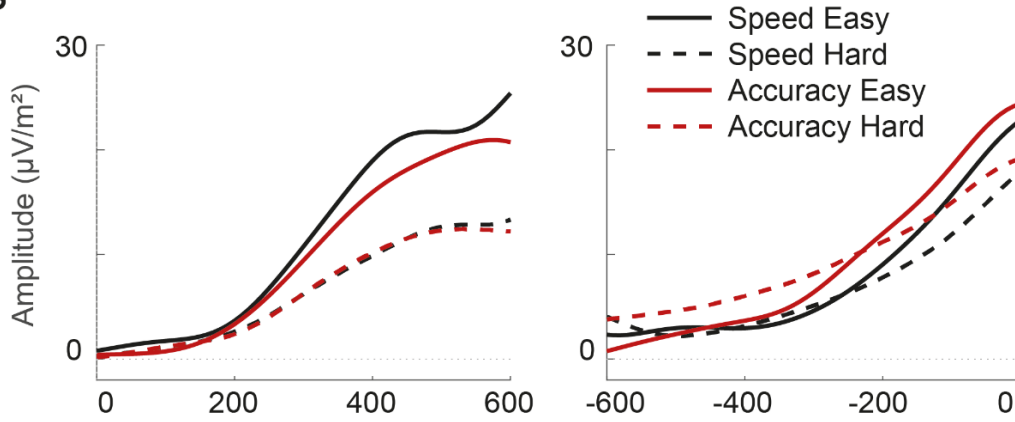


Figure 2.5: Model fit: quantiles estimated from behavioural data (circles) and Model 2 simulations (crosses and lines) for easy (top) and hard (bottom) decisions. For each condition, correct (thick) and incorrect (thin) quantiles are displayed separately. Note that the model fit is identical for the standard and the rescaled race model.

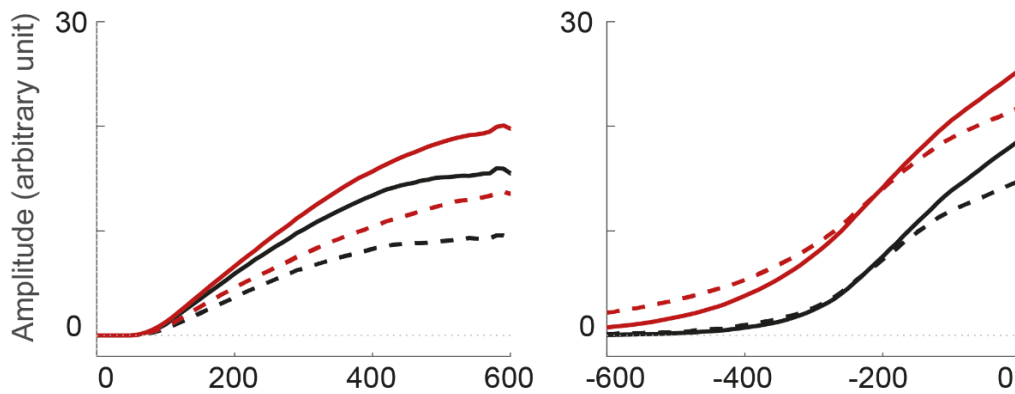
The simulated accumulation profile associated with the standard and the rescaled model parameters are displayed in Figure 2.6 b) and c) respectively. In both models, 'hard' profiles accumulate to a lower amplitude than 'easy' ones. However, there are marked differences between the standard and rescaled model in the way they predict the profiles associated with different SAT instructions. The standard race model predicts 'accuracy' profiles that accumulate much higher than 'speed' profiles in both stimulus-locked and response-locked signals. In the rescaled profiles on the other hand, like in the CPP waveforms (Figure 2.6 a), this difference is smaller in the response-locked signal and absent in the stimulus-locked profiles. The similarity of the rescaled model with the CPP was confirmed by a bootstrap procedure which showed that

the mean squared errors between the ERP and the simulation were significantly lower for the rescaled model than the standard model ( $p < .05$ ).

**a) CPP**



**b) Standard Model**



**c) Rescaled Model**

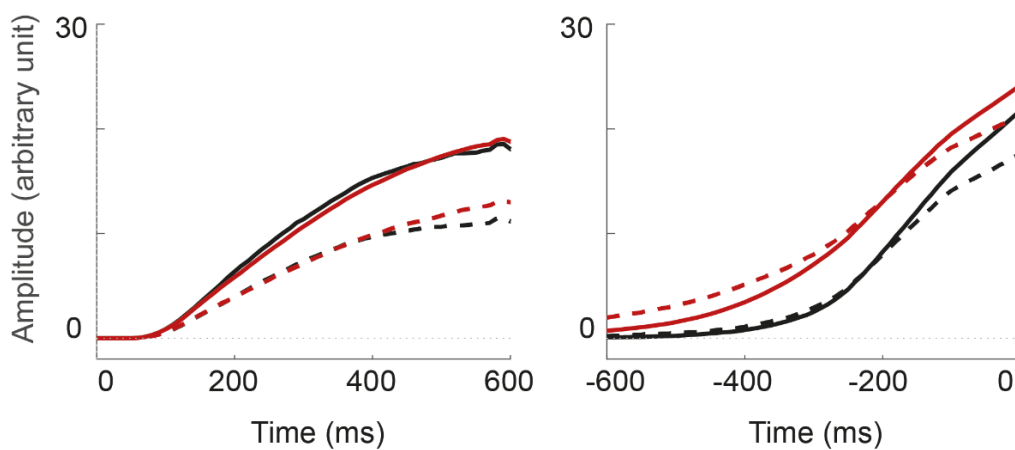


Figure 2.6: Decision variable (empirical and simulated): a) stimulus-locked (left) and response-locked (right) CPP for each condition. Note that the CPP here is a pooled average rather than a grand average and therefore differs from Figure 2.4. Additionally, the waveform has been low-pass filtered with a cut-off of 5 Hz for display only. b) stimulus-locked (left) and response-locked (right) accumulation profiles (correct and incorrect accumulator summed) per condition as predicted by the standard race model. c) stimulus-locked (left) and response-locked (right) accumulation profiles (correct and incorrect accumulator summed) per condition as predicted by the rescaled race model.

### 2.1.3. Discussion Experiment 1

In Experiment 1, we set out to test the CPP under SAT instructions, as well as test its similarity to two sequential sampling models representing two different implementations of the SAT. To this end, we recorded human EEG during a motion discrimination task with two levels of difficulty, and two different instructions, one emphasising response speed ('speed'), and one emphasising accuracy ('accuracy'). We found that these manipulations had the expected behavioural effects, with faster and more accurate decisions in 'easy' compared to 'hard' trials, and faster and less accurate decisions in 'speed' compared to 'accuracy' trials.

We chose to explore the CPP, as it has previously been suggested as a neural correlate of the decision variable (Kelly & O'Connell, 2013; O'Connell et al., 2012). In line with this notion, we found that the CPP built up over the course of the decision, before peaking at the response. Additionally, we found that the build-up had a steeper slope in 'easy', compared to 'hard' decisions, a typical finding for decision variables (Brown & Heathcote, 2008; Kelly & O'Connell, 2013; Ratcliff & McKoon, 2008; Roitman & Shadlen, 2002), supporting the role of the CPP as a neural correlate of decision-making. However, we observed no difference between waveforms associated with 'speed' and 'accuracy' trials. Since a difference in threshold would arguably translate into a difference in peak amplitudes in a neural substrate of the decision variable, this finding questions either the validity of the CPP as a neural correlate of the decision variable, or the validity of a variation in threshold as an explanation for the SAT.

To resolve this issue, two models with different implementations of the SAT were tested. A standard model which implemented a variation in threshold was associated with simulated accumulation profiles which displayed an amplitude difference between 'speed' and 'accuracy' conditions, and did not replicate the pattern observed in the CPP. The second model was a rescaled model which was mathematically identical to the standard model but transferred the difference in threshold onto other parameters, modelling a global change in

activity. The accumulation profiles predicted by this model were markedly more similar to the patterns shown in the CPP.

These findings suggest that the rescaled model provided a better account of the neural data than the standard model, indicating that the SAT may be implemented in the brain by a global change in activity (i.e. a change in both signal and noise). However, an alternative interpretation of these findings is that the SAT is in fact implemented in the brain via a specific change in the decision threshold, and that the CPP is not a valid neural substrate of the decision variable. Since there is relatively little research supporting the CPP's role as a decision-related signal, we additionally explored a different neural correlate of the decision variable to shed light on the underlying mechanisms of the SAT.

## **2.2. Experiment 2: TMS**

Experiment 1 indicated that sequential sampling models which vary in threshold in order to account for the SAT may paint an oversimplified picture of the neural mechanisms underlying this phenomenon. However, this finding is based on the validity of the CPP as a neural substrate of decision-making. In Experiment 2, we therefore set out to test the same paradigm using a different neural correlate of the decision variable.

One neurometric signal which has been suggested to display a decision-relevant accumulation of evidence is activity in the primary motor cortex (M1). Contrary to the assumption of serial processing (Donders, 1969; Sternberg, 1969), researchers have now suggested that response preparation occurs throughout the decision-making process, with the status of the accumulation process being continuously fed forward into the motor system (Coles et al., 1985; Gluth et al., 2013; Michelet et al., 2010). This implies that the progress of the accumulation of evidence can be tracked via the level of response preparation, reflected in the level of M1 activity. This concept has been used to track the decision variable using motor-related EEG signals, such as the LRP and event-related desynchronisation in the beta frequency band over motor areas (Donner et al., 2009; Kelly & O'Connell, 2013). A different approach to

track the excitability of M1 and adjacent premotor areas is the use of TMS (Bestmann et al., 2008; Hadar et al., 2012; Hadar et al., 2015; Kiers et al., 1997). When TMS is applied over the motor cortex, electrical responses called motor evoked potentials (MEPs), the amplitudes of which scale with the level of corticospinal excitability, can be observed in the muscle corresponding to the stimulated brain area (Barker et al., 1985; Merton & Morton, 1980; Merton et al., 1982). Like accumulation signals, MEP amplitudes recorded in the responding muscle have been shown to increase over the course of perceptual decisions before reaching a threshold-like maximum at the time of response (Michelet et al., 2010).

Importantly, Hadar et al. (2015) used a Gaussian smoothing kernel to generate a continuous MEP signal to track corticospinal excitability during a decision-making task, and suggested that this signal resembles a neural correlate of the decision variable. They found that effector-specific motoric activation built up during the decision-making process, and reported marked similarities between predictions made by a sequential sampling model and the MEP signal, supporting its validity as a correlate of decision-making. Specifically, they found that motoric activation was longer in hard compared to easy decisions. This is based on the notion that, if the MEP signal is purely motor-related, and the response preparation and execution follows the decision-making process serially (Donders, 1969; Sternberg, 1969), the stimulus-locked signal should show a difference in amplitude between the responding muscle and the non-responding muscle earlier in easy than in hard trials (due to longer decision-making processes in hard trials), while the response-locked signal should show this difference at the same latency regardless of task difficulty. Instead however, the findings were reversed relative to this prediction, with hard decisions onsetting earlier in the response-locked but not the stimulus-locked signal (i.e. the latency at which the responding muscle first displayed higher amplitudes than the non-responding muscle was similar across difficulty conditions in the stimulus-locked signal, but different in the response-locked signal, with hard trials displaying the divergence for longer). This indicated that the decision-making process began at a similar time but took longer in hard than in easy conditions (Hadar et al., 2015). Although these findings suggest that the MEP

signal is a promising candidate as a neural substrate of the decision variable, this signal has, to our knowledge, only been tested in the context of a difficulty manipulation and has not been used to explore the SAT.

Experiment 2 therefore set out to test the MEP signal under SAT instructions. Like in Experiment 1, we asked participants to complete a random dot motion task with varying difficulties and SAT instructions while recording their MEPs. Again, we used two models, a standard model with a variation in threshold and a rescaled model implementing a global change, to account for the behavioural data. We compared their accumulation profiles to the MEP signal in order to explore the neural mechanisms underlying the SAT.

## **2.2.1. Methods**

### **2.2.1.1. Participants**

An opportunity sample of 22 participants (nine males), primarily students and staff at City, University of London were recruited for the TMS study. Four participants were unable to successfully complete the practice task (like in Experiment 1, an unsuccessful performance was defined as reaching a calibrated coherence level of  $> 90\%$  for both 'easy' and 'hard' conditions; see section 2.1.1.2.2)<sup>4</sup>, and did not complete the experiment. The remaining 18 participants (11 female), with a mean age of 29.82 ( $SD = 8.38$ ), each took part in three sessions, each lasting between 2 and 2.5 hours, with the exception of one participant who withdrew from the study after two sessions. Three of the participants were researchers in the current project. All other participants were paid £8 per hour and an additional reward for task performance (up to £4 per session). In line with ethics procedures at City, University of London each participant received an email describing the potential risks associated with TMS at least 24 hours prior to the experiment, and completed a medical screening questionnaire to ensure their safety.

---

<sup>4</sup> The remaining participants reached average calibrated coherence levels of 23.81% ( $SD = 19.08$ ) in the 'hard' condition and 65.41% ( $SD = 30.91$ ) in the 'easy' condition.

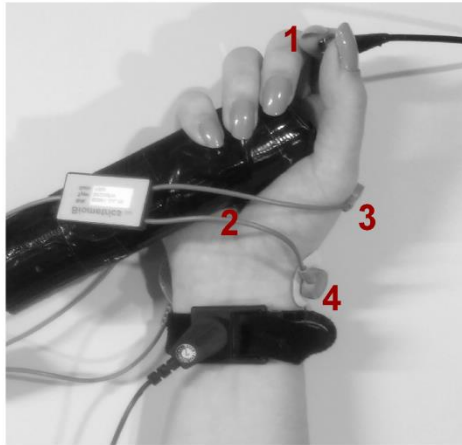
### **2.2.1.2. Stimuli and Procedure**

In this experiment, we used a random dot motion task, identical to the one described in Experiment 1 (see section 2.1.1.2). However, instead of holding a response button in each hand in order to indicate their decision, participants held two digital response buttons in their right hand. One button was placed between the thumb and index finger and required a 'pinch' response, contracting the first dorsal interosseous (FDI) muscle. The second button was placed on a plastic cylinder in the palm of the hand and required a 'grasp' response, contracting the abductor digiti minimi (ADM) muscle (see Figure 2.7). The pinch and grasp buttons indicated 'up' and 'down' responses respectively.

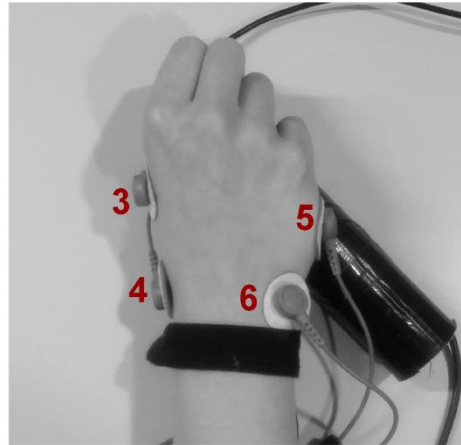
In each session, a total of 432 planned trials were completed. To ensure the required frequency of TMS pulses ( $< .2$  Hz), TMS-free trials were added during the session, leading to an average of 500 trials per session (see section 2.2.1.3).

### **2.2.1.3. Stimulation and Recording**

Participants' muscle activity was recorded using surface electromyography (EMG), sampled at 1000 Hz via a 13 bit A/D Biometrics Datalink system (version 7.5, Biometrics Ltd., Ladysmith, VA, U.S.A., 2008). We placed 22 mm x 28 mm surface Ag/AgCL electrodes on the skin above the FDI and the ADM of the right hand, as they contribute to the 'pinch' and 'grasp' responses respectively. Reference electrodes were placed at distances of approximately 2 cm to each of the two active electrodes (see Figure 2.7). Participants were instructed to relax their hand muscles in between responses, and the EMG signals were passed to two speakers to provide auditory feedback, informing participants of any unwanted muscle activation.



- 1 'Pinch' response button
- 2 'Grasp' response button
- 3 Active electrode: FDI



- 4 Reference electrode: FDI
- 5 Active electrode: ADM
- 6 Reference electrode: ADM

Figure 2.7: EMG recording setup: Left: palm facing up; Right: palm facing down. Participants held a 'pinch' response button between their thumb and index finger (1), as well as a response button placed on a plastic cylinder in the palm of their hand, requiring a 'grasp' response (2). To record the muscle activity associated with button presses, EMG electrodes were placed over the FDI (3) and ADM (5). Reference electrodes were placed approximately 2 cm away from the active electrodes (4 & 6).

During the experiment, single-pulse TMS was applied using a MagstimRapid<sup>2</sup> biphasic stimulator (Magstim Co. Ltd., Whitland, UK). To induce MEPs in both the ADM and the FDI of the right hand, a figure-of-eight coil was positioned on the scalp over the left primary motor cortex. The exact location was adjusted for each participant individually and the stimulation intensity was set at approximately 110% of the resting motor threshold. The resting motor threshold was defined as the minimal intensity necessary to elicit an MEP with a peak-to-peak amplitude of approximately 50  $\mu$ V in 50% of stimulations.

TMS pulses were planned in 66% of trials, but cancelled if a response had already been detected by the time of planned stimulation. In order to ensure a good distribution of TMS pulses over the course of the reaction time, TMS trials were divided into four equally sized, equiprobable time bins between 5 ms and 500 ms relative to the onset of the coherent motion in the 'speed' condition, and between 5 ms and 600 ms in the 'accuracy' condition. Within a given bin, the exact stimulation time was drawn uniform randomly. Since the experiment followed a single-pulse TMS protocol, the stimulation pulses were required to occur at a maximal frequency of .2 Hz. If, by chance, a planned pulse followed a

previous one after less than 5000 ms, the task was adjusted in several ways. If the timespan between the previous and the planned pulse was less than 5000 ms but more than 4000 ms, the inter-trial interval was increased in order to decrease the pulse frequency to  $< .2$  Hz. For scheduled intervals of less than 4000 ms, the planned trial was replaced with the next planned stimulation free trial. If no stimulation free trial remained, random stimulation free trials were generated in order to increase the interval between TMS pulses. Due to this method, an average of 68.67 ( $SD = 15.79$ ) trials were added per session.

#### **2.2.1.4. EMG/MEP Pre-processing**

In order to eliminate potential differences in the time required to execute 'pinch' and 'grasp' responses, we recorded the onset of movement (i.e. the onset of visible muscular activity in the EMG recording) as a measure of response time (EMG RT). To this end, EMG data from both channels, aligned to the onset of the coherent motion (stimulus onset) were displayed for each trial and visually inspected to manually select the onset of response-related EMG bursts. Visual inspection provided no information about the experimental condition of a given trial. In TMS trials, MEP amplitudes in both channels (FDI and ADM) of the right hand were defined as the difference between the minimal and maximal EMG values in a time window of 10 to 40 ms relative to stimulation time. An algorithm was used to detect EMG activity prior to the stimulation, in order to discard any trials in which there was activity greater than 50  $\mu$ V peak to peak in a period of 200 ms preceding the stimulation. These trials, as well as trials in which there was partial activation in more than one channel, or trials in which a clear EMG onset could not be detected, were excluded from further analysis (23.39% of trials). Additionally, trials with very fast ( $< 100$  ms) or very slow ( $> 1800$  ms) response onsets (5.12% of trials), trials in which no MEP was visible or in which the MEP amplitude could not be accurately detected due to saturation (1.05%), and trials in which the response preceded the planned TMS pulse (6.09%) were excluded. In total, 35.65% of all trials were discarded, with a total of 17,067 trials remaining, including 6535 usable TMS trials (57.15% of all planned TMS trials were excluded).

### 2.2.1.5. MEP Smoothing

For each condition, the remaining MEPs from correct trials were pooled across sessions and participants. To do this, MEP amplitudes were z-scored separately for each session, participant, and muscle, in order to normalise the magnitudes of evoked responses. Additionally, TMS latencies as well as EMG RTs were expressed as a percentage of their median EMG RT (since TMS pulses can affect the response, only EMG RTs of non-TMS trials were used to generate the median EMG RT).

The MEPs of each condition were then sorted in time and aligned once to the stimulus and once to the response, and smoothed using a Gaussian kernel:

$$\hat{Y}(t) = \frac{\sum_{i=1}^N e^{-\frac{(t-t_i)^2}{2\sigma^2}} Y_i}{\sum_{i=1}^N e^{-\frac{(t-t_i)^2}{2\sigma^2}}}, \quad (2.3.)$$

Where  $N$  is the number of MEPs, each of which being associated with a magnitude  $Y_i$  and a normalised time  $t_i$ . The smoothed signal was calculated in time steps of 1% median EMG RT, using a smoothing kernel with a full-width half maximum of 5% median EMG RT.

Smoothed signals were generated for stimulus and response-locked data, for each condition separately. Additionally, a smoothed MEP signal was generated for each condition for the difference between the MEP amplitudes associated with the responding and the non-responding muscle, as this signal cancels any non-specific spinal influences in the MEP data (see Figure 2.8). Note that since only correct trials were used, the responding muscle always refers to the muscle making the correct response.

### 2.2.1.6. Statistical Analysis

Two sets of statistical analyses were run on the MEP signal to assess its potential role as a correlate of the decision variable. Specifically, we tested slope and amplitude differences in the MEP signal between different conditions. Using a permutation approach, we compared 'easy' and 'hard' trials (per SAT instruction) as well as 'speed' and 'accuracy' trials (per difficulty level). In each of 1999 iterations, we resampled MEP difference values (responding minus

non-responding muscle) across conditions without replacement and randomly re-assigned them to new 'easy' and 'hard', as well as 'speed' and 'accuracy' conditions, and smoothed them to create a new set of waveforms with 90% bootstrap BCa confidence intervals for each condition. We then measured the slope difference by fitting a straight line to a time interval from 50% to 90% median EMG RT in the stimulus-locked, and -50% to -10% in the response-locked signal of each condition and taking the difference. Adapting established cluster permutation approaches for brain-imaging statistical inference (Blair & Karniski, 1993; Groppe, Urbach, & Kutas, 2011; Nichols & Holmes, 2001), we also measured the amplitude differences between conditions by summing across (i.e. forming a cluster statistic for) the adjacent MEP difference values at which the confidence interval between the two conditions to be compared (either 'easy' vs 'hard' or 'speed' vs 'accuracy') did not overlap.

This resulted in a permutation null distribution of slope differences and an equivalent distribution of cluster-thresholded amplitude differences (expressed in sums of MEP difference values), against which we compared the slope difference and amplitude differences (measured in the same way) of the original waveforms. If the original values were smaller or larger than 97.5% of the values in the relevant null distribution, the difference was considered significant at an alpha level of .05. This analysis was conducted separately for 'easy' compared to 'hard' data (once per SAT instruction), for 'speed' compared to 'accuracy' data (once per difficulty level), and for stimulus-locked and response-locked data.

#### **2.2.1.7. Model**

We used three different race models to fit the behavioural data. Since TMS pulses can affect the response, only stimulation-free trials were used to analyse behavioural data. Unless otherwise specified, the same procedure as described in Experiment 1 was used (see section 2.1.1.5). The models were fitted to normalised EMG RTs on a group level by pooling across participants. Modelled EMG RTs were simulated in 1% median RT based on equations (2.1.) and (2.2.).

The best-fitting model was rescaled to simulate a global gain modulation and both the standard and the rescaled model were used to simulate accumulation profiles. For a direct comparison between the simulated accumulation paths and the neurometric signal (MEP signal reflecting the difference in amplitude associated with responding and non-responding muscles), the simulated accumulation was subjected to similar processing as the MEP signal. Based on the estimated parameters, we simulated 20,000 accumulation paths for each condition and each model (standard and rescaled). Simulated MEP differences were computed by subtracting the amplitudes of the incorrect accumulator at simulated MEP latencies, which were generated in the same way as stimulation latencies during the data collection (see section 2.2.1.3), from the amplitudes of the correct accumulator at the same time points. Like in the empirical data set, simulated MEP differences were discarded if the decision formation preceded the simulated latency. To generate a continuous signal, these simulated data points were smoothed in the same way as the empirical MEP values (see section 2.2.1.5). This procedure is displayed in Figure 2.8.

Since in this experiment, all analyses are based on EMG RT, rather than the time of a button press, we assumed that virtually all of the estimated non-decision time described sensory processes. We therefore started the accumulation profile after a sensory delay given by  $T_{er}^5$ . As in Experiment 1 (see section 2.1.1.5.3), the arbitrary amplitude of the simulated profile was matched to the amplitude of the MEP signal by multiplying its scale by a parameter which was estimated using the same differential evolution algorithm as described above.

---

<sup>5</sup> Although a very small proportion of the non-decision time may be categorised as motor processing time to account for the brief interval in which the motor signal travels through the corticospinal tract, we estimated that this interval lasts only approximately 30 ms (based on timings of TMS pulses and MEPs), and argue that this is negligible.

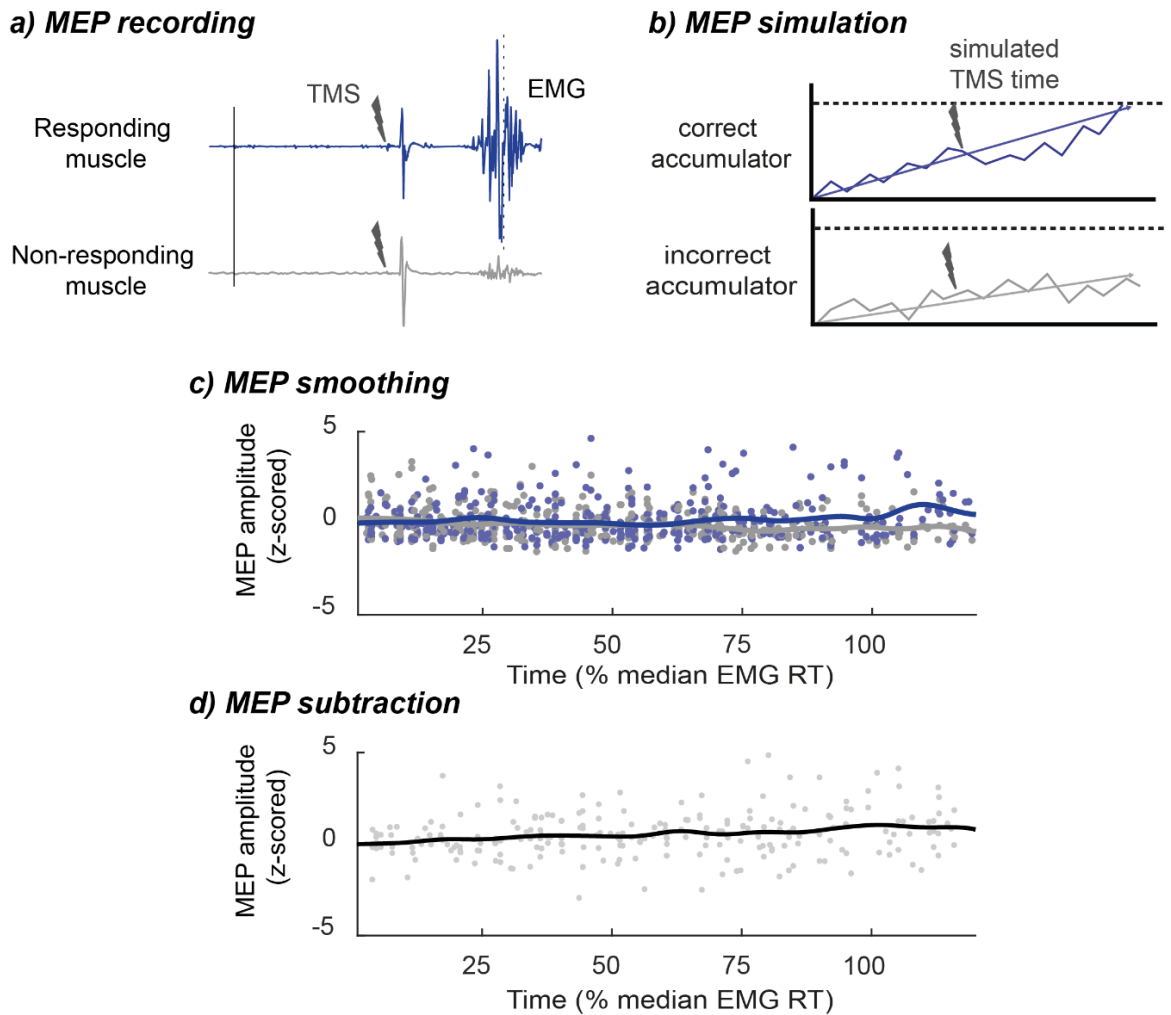


Figure 2.8: MEP processing and simulation: MEP amplitudes are recorded from both responding and non-responding muscles (a). The amplitudes are then z-scored per muscle, participant, and session, pooled, and sorted by latency (normalised by individual median EMG RT). A continuous signal is then created for each muscle, using a Gaussian smoothing kernel (c). To remove non-specific spinal signals, the same smoothing is applied to the difference between simultaneously recorded MEPs (responding minus non-responding); d). To create model predictions which are comparable to the continuous MEP signal, accumulation values from both the correct accumulator (corresponding to the responding muscle) and the incorrect accumulator (corresponding to the non-responding muscle) are sampled at simulated TMS times (b), and processed in the same way as recorded MEP amplitudes (c & d).

#### 2.2.1.7.1. Model Comparison

Like in Experiment 1, we then compared the standard and rescaled models based on the similarity of their respective accumulation profiles to the neural signal using the same bootstrap procedure as described in section 2.1.1.5.4. In each iteration, RTs were resampled with replacement within each condition and a new set of parameters for the standard race model was estimated and then rescaled. Accumulation profiles were then generated for the two new sets of parameters (standard and rescaled) and compared to the MEP signals which

were re-computed based on similarly resampled MEP differences (MEP signals were generated in the same way as described in section 2.2.1.5). Note that, while in Experiment 1, the model fit and CPP of each iteration was based on the same resampled trials, this was not the case here. Since only TMS trials were used to generate the MEP signal, and only stimulation free trials were included in the model fit, both sets of trials were resampled independently during the bootstrap procedure.

In each iteration, mean squared errors were generated for each prediction (standard and rescaled) relative to the MEP signal (note that the amplitude of the predictions was scaled to fit the MEP signal in the same way as described in section 2.1.1.5.3). The difference in mean squared errors between the standard and the rescaled model in each iteration was then used to form a bootstrap distribution, and, in combination with the mean squared error difference between the models of the original data, the BCa confidence interval was estimated. The null hypothesis that both the standard and the rescaled model resemble the MEP signal to the same extent was rejected if the BCa confidence interval did not include 0.

## **2.2.2. Results**

### **2.2.2.1. Behavioural Results**

Like in Experiment 1, trials remaining after EMG pre-processing were collapsed over 'up' and 'down' trials (see Figure 2.9). A 2 x 2 ANOVA, with the factors 'Instruction' ('speed'/'accuracy') and 'Difficulty' ('easy'/'hard') was used in order to explore behavioural differences in correct reaction times. There was a significant main effect of 'Instruction',  $F(1, 17) = 26.90$ ,  $p < .001$ ,  $\eta_p^2 = .61$ , with faster responses in the 'speed' ( $M = 406$  ms) than in the 'accuracy' ( $M = 469$  ms) condition. There was also a significant main effect of 'Difficulty',  $F(1, 17) = 62.14$ ,  $p < .001$ ,  $\eta_p^2 = .79$ , with faster responses in the 'easy' ( $M = 367.75$  ms) than in the 'hard' ( $M = 507$  ms) condition. Additionally, there was a significant interaction effect,  $F(1, 17) = 10.80$ ,  $p = .004$ ,  $\eta_p^2 = .39$ . Follow-up t-tests, to explore this interaction, revealed that the difference between 'easy' and 'hard'

RTs was larger in the ‘accuracy’ condition,  $t(17) = 7.87$ ,  $p < .001$ , than in the ‘speed’ condition,  $t(17) = 6.83$ ,  $p < .001$ . All reported effects are based on EMG RTs (time of EMG onset), but results based on response button RTs were not qualitatively different (main effect of ‘Instruction’:  $p < .001$ , main effect of ‘Difficulty’:  $p < .001$ , interaction effect:  $p = .011$ ).

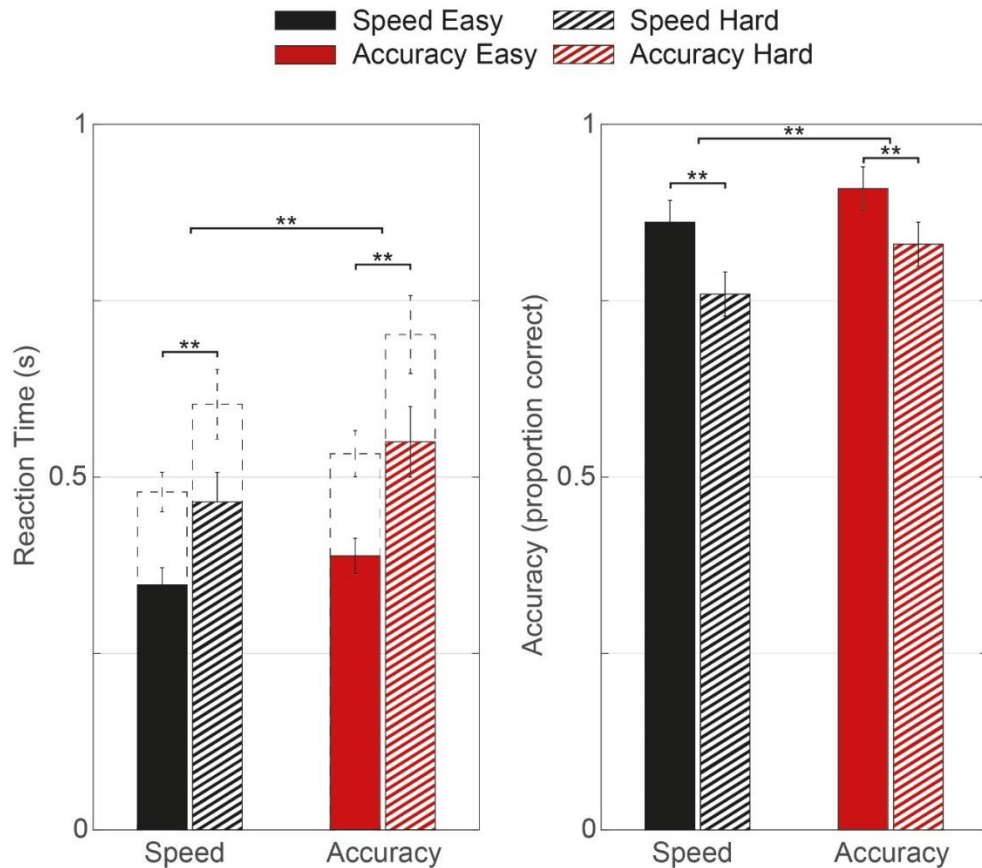


Figure 2.9: Behavioural results: reaction time (left) and accuracy scores (right) for each condition. Left panel shows both EMG RT (bars) and button RT (dashed lines). Error bars indicate 95% Confidence Interval. \*\* indicates  $p < .001$ .

In order to analyse the non-normally distributed accuracy data, we used a generalised linear mixed model (see section 2.1.2.1). Both ‘Instruction’ and ‘Difficulty’, and the ‘Instruction \* Difficulty’ interaction were entered as fixed effects, and both manipulations and their interaction within each participant and session were included as random effects (Wilkinson notation:  $\text{Accuracy} \sim 1 + \text{Instruction} * \text{Difficulty} + (1 + \text{Instruction} * \text{Difficulty} | \text{Participant}) + (1 + \text{Instruction} * \text{Difficulty} | \text{Session})$ )<sup>6</sup>. The model revealed that ‘Instruction’ was a significant predictor,  $t(208) = 4.81$ ,  $p < .001$ .

<sup>6</sup> The dispersion parameter of the model,  $\phi = 1.42$ , was calculated by dividing the sum of squared Pearson residuals by the residual degrees of freedom (Venables & Ripley, 2002).

.001, with 'accuracy' instructions ( $M = 87\%$ ) associated with higher accuracy scores than 'speed' instructions ( $M = 81\%$ ). Additionally, 'Difficulty' was a significant predictor,  $t(208) = 4.57$ ,  $p < .001$ , with 'easy' trials ( $M = 88\%$ ) associated with higher accuracy scores than 'hard' trials ( $M = 79\%$ ). The 'Instruction \* Difficulty' interaction was not a significant predictor of accuracy,  $t(208) = 1.66$ ,  $p = .098$ .

#### **2.2.2.2. MEP Results**

MEP signals are displayed in Figure 2.10, which shows that the MEP signal associated with the responding (correct) muscle built up over the course of the decision in each of the conditions. In line with the hypothesis that these signals reflect decision-related accumulation processes, we hypothesised that these build-up profiles should differ across conditions. In particular, we expected that difficulty would have an impact on the slope of the build-up of the responding MEP (relative to the non-responding MEP).

We tested the slope and amplitude of the MEP signal reflecting the difference between activation in responding and non-responding muscles. In line with our hypotheses, we found that, in the stimulus-locked MEP signal, the build-up occurred at a higher slope in 'easy' compared to 'hard' trials ( $p < .05$  in both the 'speed' and the 'accuracy' condition). No difference was observed in the response-locked signal ( $p > .05$ ). We also found a significant difference in MEP amplitude between 'easy' and 'hard' conditions, with the stimulus-locked signal displaying higher amplitudes in the 'easy' than in the 'hard' condition, visible from 74% and 81% median EMG RT in the 'speed' and 'accuracy' conditions respectively ( $p < .05$ ). Again, this difference was not observed in the response-locked signal. Additionally, we found no significant differences between 'speed' and 'accuracy' conditions in either slope or amplitude of either the stimulus or the response-locked MEP signal (all  $p > .1$ ).

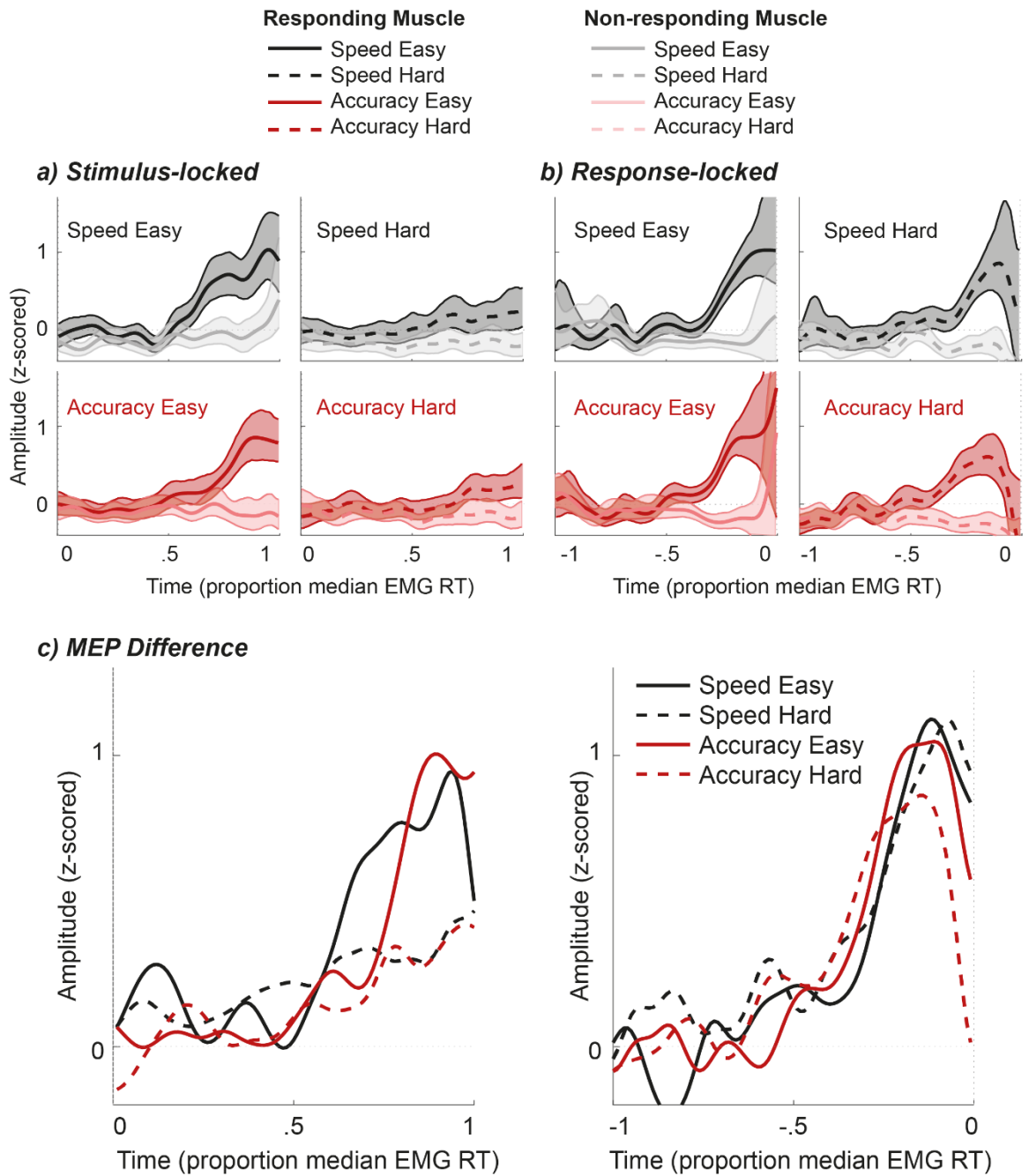


Figure 2.10: MEP results: a) stimulus-locked MEP signals for ‘easy’ (left) and ‘hard’ (right), as well as ‘speed’ (top) and ‘accuracy’ (bottom) trials. Each panel shows both the MEP signal associated with the responding muscle (dark) and the non-responding muscle (light). Shaded areas indicate 95% confidence interval. b) response-locked MEP signals associated with the responding (dark) and non-responding (light) muscle for each condition separately. Shaded areas indicate 95% confidence interval. c) stimulus-locked (left) and response-locked (right) MEP signals reflecting the difference between the MEPs associated with the responding and non-responding muscles for each condition.

### 2.2.2.3. Model Results

We fitted three race models to our data and compared their fit using BIC values. Just like in Experiment 1, we found that Model 2, in which drift rates varied across difficulty levels and both thresholds and starting points varied across

SAT instructions, provided the best account of the data (see Table 2.1). The estimated parameter values, as well as the rescaled parameter values, are displayed in Table 2.3. Again, like in Experiment 1, the estimated parameters of the standard model indicate higher thresholds and lower starting point variability in ‘accuracy’ compared to ‘speed’ conditions, and higher drift rates in ‘easy’ compared to ‘hard’ decisions. The rescaled model on the other hand, although mathematically equivalent (see Figure 2.11) indicates the same threshold across SAT instructions.

Table 2.3: Estimated parameter values for the chosen model (Model 2) and its rescaled version: note that the response threshold  $A$  in the ‘accuracy’ condition was set to 1 as a scaling parameter.

Parameters	Standard Model: parameter values per SAT Instruction		Rescaled Model: parameter values per SAT Instruction		
	<i>accuracy</i>	<i>speed</i>	<i>accuracy</i>	<i>speed</i>	
Starting point variability ( $S_z$ )	0.447	0.523	0.447	0.586	
Response threshold ( $A$ )	1	0.893	1		
Non-decision time ( $T_{er}$ )	0.382		0.382		
Non-decision time variability ( $S_{Ter}$ )	0.374		0.374		
Diffusion constant ( $\sigma^2$ )	0.499		0.499	0.558	
Drift rate ( $v$ )	correct	easy	1.28	1.28	1.433
		hard	0.634	0.634	0.710
	incorrect	easy	0.098	0.098	0.109
		hard	0.004	0.004	0.005

The quality of the model fit is shown in Figure 2.11. The RT distribution of both the empirical (circles) and the simulated (lines and crosses) data are summarised by five quantile estimates for each condition separately. The overlap between empirical and modelled quantiles indicates that the model fitted the data well. The mean difference between predicted and recorded RT quantiles was approximately 3.4% median EMG RT for correct responses, confirming that the model was able to account for the RT data.

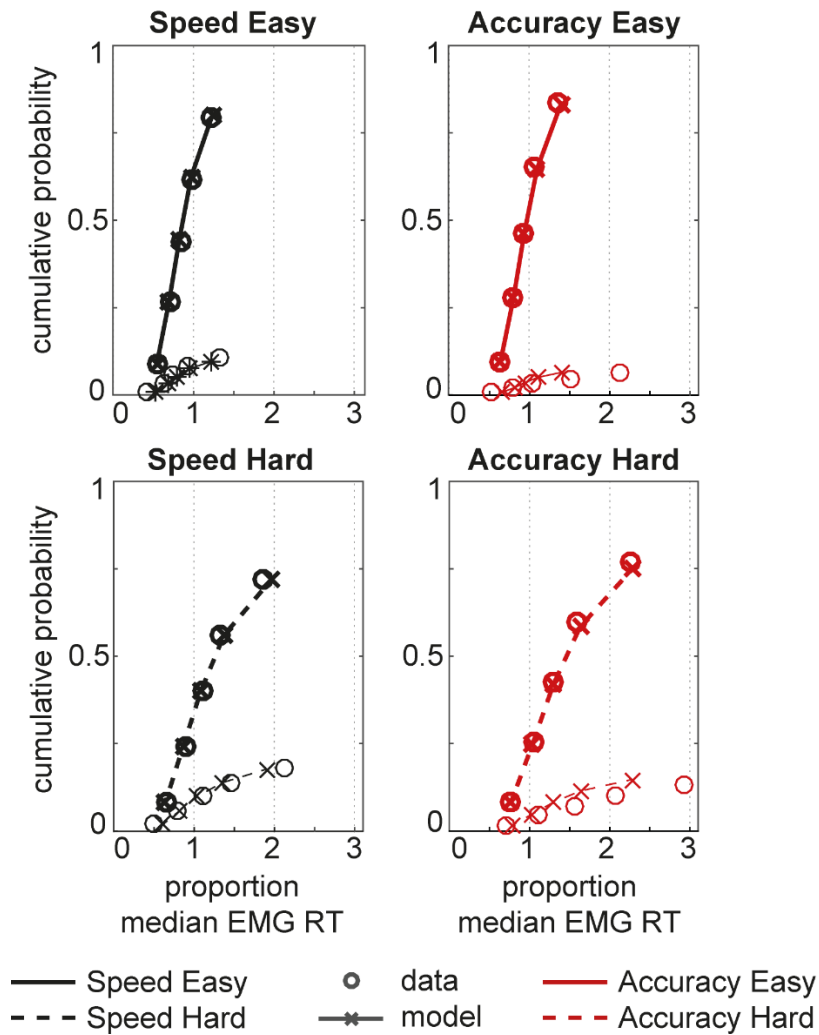


Figure 2.11: Model fit: quantiles estimated from behavioural data (circles) and Model 2 simulations (crosses and lines) for easy (top) and hard (bottom) decisions. For each condition, correct (thick) and incorrect (thin) quantiles are displayed separately. Note that the model fit is identical for the standard and the rescaled race model.

The estimated parameters were then used to simulate accumulation profiles for each condition, once for the standard model and once for the rescaled model. The resulting profiles are presented in Figure 2.12 b) and c). The accumulation profiles show similar patterns as those described in Experiment 1. In both the standard and the rescaled model (as well as in the MEP signal), ‘hard’ profiles show a slower build-up and lower amplitude than ‘easy’ profiles. The main difference between the two sets of predictions, as the rescaling would suggest, is the amplitude of the SAT conditions, with ‘accuracy’ profiles showing higher amplitudes in both stimulus-locked and response-locked profiles in the standard, but not in the rescaled model. This makes the rescaled model visibly more similar to the MEP signal than the standard model.

This similarity was confirmed by a bootstrap procedure which demonstrated that the mean squared error between the model prediction and the MEP signal was lower for the rescaled compared to the standard model ( $p < .05$ ).

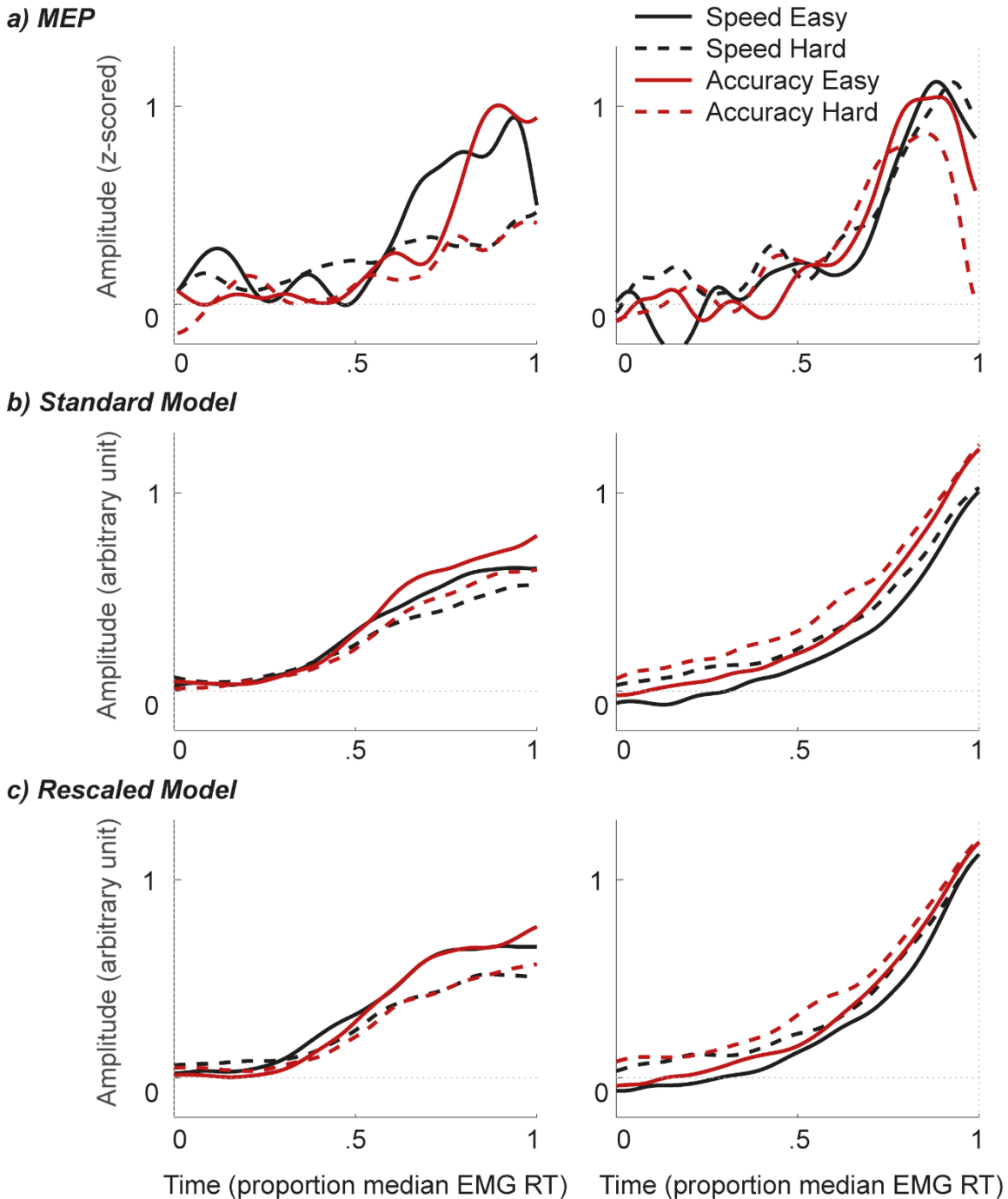


Figure 2.12: Decision variable (empirical and simulated): a) stimulus-locked (left) and response-locked (right) MEP signal (difference between MEPs associated with responding and non-responding muscles) for each condition. b) accumulation profile (difference between accumulation profiles predicted by the correct and incorrect accumulator) per condition as predicted by the standard race model. c) accumulation profile (difference between accumulation profiles predicted by the correct and incorrect accumulator) per condition as predicted by the rescaled race model.

### 2.2.3. Discussion Experiment 2

In Experiment 2, we set out to test the effects of difficulty ('easy', 'hard') and SAT instructions ('speed', 'accuracy') on an MEP signal and use the resulting waveforms to evaluate two models with different implementations of the SAT. Overall, we replicated the findings reported in Experiment 1. We found that faster responses were associated with 'easy' and 'speed' decisions, and more accurate responses were associated with 'easy' and 'accuracy' trials.

Importantly, we found that the MEP signal representing the difference between the responding and the non-responding muscle built up over the course of the decision, and peaked at the time of response, supporting previous findings which suggested this signal as a neural correlate of decision-making (Hadar et al., 2015). We further found that the rate at which this build-up occurred depended on the difficulty of the decision, with easier decisions associated with higher slopes than hard decisions. This pattern was observed in the stimulus-locked, but not the response-locked data. Although slope differences might be expected in both stimulus and response-locked data, due to the different alignment of the trials, they are typically more visible in the stimulus-locked data, while amplitude differences are more visible in the response-locked data. Our findings suggest that 'easy' and 'hard' trials build up at different rates but peak at similar amplitudes. These findings are consistent with evidence-dependent accumulation-to-bound dynamics and support the role of the MEP signal as a correlate of the decision variable. However, like in Experiment 1, we found no difference in slope or amplitude between 'speed' and 'accuracy' conditions.

We used the same two models as in Experiment 1 to describe the data, one with a threshold variation to explain the SAT, and one rescaled model which assumes a global variation in activity. Again, we found that the standard model predicted amplitude differences between 'speed' and 'accuracy' conditions, not observed in the MEP signal. The accumulation profile predicted by the rescaled model on the other hand, was similar to the pattern observed in the MEP signal.

Experiment 2 therefore not only supported the MEP signal as a neural correlate of decision-making, but also replicated the findings reported in Experiment 1. These findings suggest that the SAT is implemented by a global change in activity, rather than a specific modulation of the decision threshold.

## **2.3. General Discussion**

In this study, we set out to explore the effects of the SAT, as well as difficulty, on decision-making, using both human neural data and behavioural modelling. In two separate experiments, we recorded participants' EEG activity and MEP amplitudes while they completed a binary motion discrimination task with two difficulty levels and under the instructions to either focus on the speed of the decision or on its accuracy.

In both experiments, the behavioural data showed the expected patterns, with easy decisions leading to faster, more accurate responses than hard trials (Kelly & O'Connell, 2013; Roitman & Shadlen, 2002). Additionally, in line with previous research (Heitz, 2014; Murphy et al., 2016), we found that decisions made under 'speed' instructions were associated with faster and more error-prone responses than those under 'accuracy' instructions.

Both manipulations (difficulty and SAT instructions) have previously been shown to affect behavioural decision-making in these ways and, importantly, have each been explained in the context of sequential sampling models by variations in a single parameter. The manipulation of difficulty in particular has been researched extensively and explained by the drift rate parameter, with easier decisions associated with higher drift rates (i.e. faster build-up rates) than hard decisions (Donkin et al., 2009; Mulder et al., 2014; Ratcliff & McKoon, 2008; Ratcliff & Rouder, 1998). This suggested slope difference has been supported by neural evidence, showing that neurometric signals which have previously been found to reflect decision-related accumulation processes display steeper slopes in easy compared to hard decisions (Gold & Shadlen, 2000; Palmer et al., 2005; Roitman & Shadlen, 2002). This pattern has also

been observed in the CPP (Kelly & O'Connell, 2013; O'Connell et al., 2012), and in continuous MEP signals (Hadar et al., 2015). The current study supported these findings. We found that easy decisions were associated with higher build-up rates than hard decisions in both the CPP and the MEP signal, supporting the notion that these signals represent neural correlates of the decision variable.

While the impact of difficulty on the slope of the accumulation process has been demonstrated extensively in both sequential sampling models and neural correlates of the accumulation process (Donkin et al., 2009; Ho et al., 2009; Kelly & O'Connell, 2013; Mulder et al., 2014; Ratcliff & McKoon, 2008; Roitman & Shadlen, 2002), the impact of the SAT is less clear. Originally, sequential sampling models explained the behavioural differences caused by this trade-off by adjusting the threshold parameter, with decisions under speed stress being associated with a lower threshold (i.e. decision formation with less evidence), leading to fast but more error-prone decisions (Bogacz et al., 2006; Brown & Heathcote, 2008; Smith & Ratcliff, 2004; Usher & McClelland, 2001). However, more recently, this mechanism has been questioned by research exploring neural correlates of decision-making. We would expect a threshold difference between the conditions to lead to an amplitude difference in any neural correlate of the decision variable, with decisions under speed stress displaying a lower peak amplitude. However, a number of studies have failed to demonstrate this difference, and instead found more widespread changes across SAT conditions (Hanks et al., 2014; Heitz & Schall, 2012, 2013).

In line with these more recent findings, the difference in amplitude between SAT conditions was not observed in either of the data sets in this study. In fact, we found no evidence for any difference between 'speed' and 'accuracy' conditions in either the CPP or the MEP signal, despite large behavioural differences between the conditions. It could be argued that in the stimulus-locked signal, any amplitude difference induced by threshold differences would be reduced or even cancelled out by the increase in amplitude for 'speed' trials due to their shorter and less variable RTs (given that the amplitude of a single trial peaks at the same value at each response, averaging over waveforms with similar RTs

will lead to a higher average peak amplitude than averaging over trials with more variable RTs). However, this effect should be absent in the response-locked signal, where each profile is time-locked to the peak, and any threshold differences should be clearly visible. In our data, we found no differences in either the stimulus or the response-locked profiles, contradicting the notion of a difference in the amount of evidence accumulated across SAT conditions.

In order to directly compare the EEG and MEP data to accumulation profiles predicted by sequential sampling models, we fitted a race model to the behavioural data of each of the experiments. We tested three models, in each of which we let the drift rate vary across difficulty levels, and, in line with original assumptions of the underlying mechanisms of the SAT, we let the threshold vary across SAT conditions. In addition to these parameter variations, we found that the best model included a variation of starting point variability across SAT conditions in both experiments. This starting point difference, with higher starting points in 'speed' than in 'accuracy' conditions further exaggerated the difference in baseline-threshold distance between the conditions. In line with previous findings, the model with slope differences across difficulty conditions and differences in the baseline-threshold distance across SAT conditions accounted well for the behavioural data (Brown & Heathcote, 2008; Smith & Ratcliff, 2004). Contrary to the patterns observed in the CPP and MEP data, the resulting simulated accumulation profiles showed higher amplitudes for 'accuracy' compared to 'speed' profiles in both stimulus-locked and response-locked simulations of both experiments.

Since similar discrepancies between the notion of a difference in baseline-threshold distance to account for the SAT and neural correlates of the decision variable have been reported previously (Hanks et al., 2014; Heitz & Schall, 2013; Murphy et al., 2016), we implemented a second type of model to simulate accumulation profiles and explain the SAT in a slightly different way. In line with a previously suggested alternative explanation to the difference in the baseline-threshold difference, we suggest that the difference between 'speed' and 'accuracy' conditions is induced by a more global gain modulation (Heitz & Schall, 2012; Lo et al., 2015; Murphy et al., 2016; Perri et al., 2014; Thura &

Cisek, 2016). To implement this global change in activity, we ‘rescaled’ the standard race model and adjusted all parameters so that the thresholds for ‘speed’ and ‘accuracy’ conditions were equal, transferring the estimated difference between thresholds onto all other parameters (apart from the non-decision time parameters), while remaining mathematically equivalent to the estimated parameters of the standard model (see section 2.1.1.5.2.). This resulted in a model which provides the same fit to the RT data as the original model, but assumes different underlying mechanisms, with changes between SAT conditions not explained by a threshold difference, but by differences between virtually all other parameters, including drift rate and noise parameters, modelling a global shift in decision-related brain activity.

Unlike the predictions made by the standard model, simulated accumulation profiles of this rescaled model displayed qualitatively similar patterns to those observed in both the CPP and the MEP signals. The stimulus-locked profiles of all four signals (CPP, MEP signal, and the rescaled model prediction for each data set) displayed a slope difference between ‘easy’ and ‘hard’ trials and little difference between ‘speed’ and ‘accuracy’ trials. In the response-locked model simulations, the amplitude differences between SAT conditions are also reduced compared to the predictions of the standard model, showing a closer resemblance to the neural signals. Statistical comparisons confirmed the greater similarity between the accumulation profiles of the rescaled models and the CPP and the MEP signals, demonstrating that the simulations based on the rescaled models correspond to the neural signals better than the standard model predictions<sup>7</sup>. These findings support our hypothesis that differences induced by SAT instructions may be explained by a global modulation of activity, rather than by a shift in a single specific mechanism.

An alternative account for the SAT which does not assume a global modulation suggests that an urgency signal is added to the accumulation of evidence,

---

<sup>7</sup> However, note that the statistical comparison used here did not involve summary statistics for each participant and therefore generated findings which are generalisable only to the population from which we sampled. Our inferences therefore only apply to the general population to the extent that the observed processes in our sample are shared by the general population.

which pushes the accumulation towards the threshold independent of sensory evidence and may do so to a greater extent in decisions under speed stress (Cisek et al., 2009; Hawkins et al., 2015; Thura et al., 2012). This addition of a stronger urgency signal in speeded decisions is not dissimilar to our suggestion of a rescaled accumulation process, as the largest impact of the rescaling on the accumulation profile arguably stems from the increase in the ‘speed’ drift rate. This implies that, though different conceptually, both approaches avoid a difference in threshold, primarily by adjusting the slope of the accumulation across SAT conditions and may therefore make similar predictions. However, the implementation of an urgency signal often requires the addition of several parameters to the model to account for the same data. Since large numbers of parameters are undesirable, primarily due to the rising risk of overfitting with increasing numbers of parameters, we suggest that the rescaled model introduced here is a more appropriate account of the SAT. Additionally, it is important to note that the concept of urgency is an alternative to the standard model which used threshold variations to explain the SAT. The rescaled model suggested here on the other hand, is mathematically equivalent to the original model which has been confirmed to account for behavioural data in a large number of studies, but assumes different underlying mechanisms without affecting its robust fit. Nevertheless, the notion of an urgency signal and the rescaling suggested here differ primarily conceptually as they assume different neural mechanisms, but are likely to provide similar accounts of the data.

Although we argue that the simulated accumulation profiles of the rescaled models closely resemble both the MEP signal and the CPP profiles, supporting the notion of a global modulation of activity as the underlying mechanism explaining the SAT, there are nevertheless small differences between the empirical and simulated profiles. There are a number of reasons for these differences. Firstly, it is important to note that any model is a simplified approximation of a neural mechanism and is unlikely to perfectly simulate any given process. This is particularly the case in neural signals which inherently have a low signal-to-noise ratio. An ERP such as the CPP is based on the recording of the sum of all brain activity in the proximity of a given electrode, and although the data are processed and averaged to remove as much noise

as possible, a proportion of decision-unrelated activity is likely to remain in the data. The quality of the signal is also an issue for the generation of the MEP signal. Since we can only sample MEPs from a single time point during each trial and discard a large proportion of trials during the pre-processing stages, it is difficult to produce enough data to compare the resulting MEP signals with model predictions, which can be based on any number of simulations. However, it is important to note that these limitations associated with the quality of the signal are typical for experiments of this nature (Hadar et al., 2015; O'Connell et al., 2012), and we used large numbers of trials in both experiments in order to produce interpretable neural signals.

Additionally, the relevance as a decision-related signal of both the CPP and in particular the MEP signal has been supported by only a limited number of studies. Our interpretation could therefore be criticised as we are suggesting an alteration of a well-established model by rescaling its parameters based on a less researched neural signal. However, we came to our conclusions primarily for two reasons. Firstly, we obtained converging evidence from two fundamentally different signals, as both a parietal ERP and a signal of corticospinal excitability displayed qualitatively similar findings. Additionally, both signals displayed the previously reported modulations for the difficulty manipulation, supporting their roles as decision-related signals. Secondly, previous research using more established neural correlates of the decision variable in non-human primates has shown similar findings, with no threshold difference between SAT conditions and has instead found several widespread changes in activity (Hanks et al., 2014; Heitz & Schall, 2012, 2013).

Overall, the current study explored the impact of the SAT on two neural correlates of the decision variable, one parietal ERP and one MEP signal reflecting corticospinal excitability. Although a race model accounted well for the behavioural data by varying the threshold across SAT conditions, neither of the neural signals displayed the associated amplitude differences. We showed that the SAT can instead be explained by a rescaled model which transfers the threshold differences onto all other parameters, thereby modelling a global

modulation of activity between conditions under 'speed' and 'accuracy' instructions.

### **3. Testing Different Neural Correlates of the Decision Variable**

Perceptual decision-making has been the focus of a large body of research for several decades, receiving attention from a number of fields, including cognitive psychology (Ratcliff, 1978) and neuroscience (Gold & Shadlen, 2007). There is now a consensus that the way in which we make these quick sensorimotor choices can be explained by a family of computational models labelled sequential sampling models. These models assume that, in order to make a decision, we continuously accumulate sensory evidence towards a fixed decision boundary, and execute the appropriate response when the boundary is reached (Brown & Heathcote, 2008; Ratcliff & McKoon, 2008; Usher & McClelland, 2001). Although there are a number of models within this framework which differ in a range of aspects, such as the number of accumulators (Brown & Heathcote, 2008; Ratcliff & McKoon, 2008; Smith & Ratcliff, 2004), and the assumption of leakage (Brown & Heathcote, 2008; Usher & McClelland, 2001), all sequential sampling models share the assumption of an accumulation-to-bound process and therefore share a number of predictions.

Increasingly, this mathematical modelling of behavioural data is combined with neuroimaging approaches to provide converging evidence for sequential sampling processes. Although sequential sampling models were originally designed to account for behavioural decision-making data and made no claims regarding the neural underpinnings of decision-making, a number of neural signals have now been found to display the accumulation-to-bound profile predicted by these models (Donner et al., 2009; Gold & Shadlen, 2000; Platt & Glimcher, 1999). This suggests that sequential sampling models not only explain reaction time (RT) data, but may also predict neural processes reflecting the accumulation of evidence for decision-making. Therefore, to gain further insight into how we make decisions, recent research has been dedicated to exploring the potential neural correlates of the decision variable, i.e. the accumulation-to-bound dynamics of decision-making.

Particular progress regarding neural correlates of decision-making comes from research with non-human primates. Single-cell recordings, which are rarely used in humans, allow us to measure brain activity with great spatial resolution, as well as a very high temporal resolution, crucial in order to track how activity evolves over the course of short perceptual decisions. In a typical study, monkeys are presented with a binary perceptual decision task and indicate their decisions using saccades, while the firing rates of neurons involved in the oculomotor decision are recorded (Gold & Shadlen, 2000; Shadlen & Newsome, 1996, 2001). In this context, it has been shown that firing rates of neurons in the lateral intraparietal area (LIP) show characteristics of a neural substrate of decision-making, building up in a ramp-like fashion over the course of a decision, before reaching a stereotyped level at response time. The slope of the build-up depends on the strength of the sensory evidence, with stronger evidence leading to a steeper rise, and predicts the monkey's decision time (Roitman & Shadlen, 2002). Similarly, activity in the frontal eye field (Gold & Shadlen, 2000; Thompson, Bichot, & Schall, 1997) and superior colliculus (Horwitz, Batista, & Newsome, 2004; Paré & Wurtz, 2001) have been shown to display characteristics of accumulation-to-bound signals associated with sequential sampling models.

While a large amount of research has been dedicated to identifying neural correlates of the decision variable in monkeys, and there is now convincing evidence that single-cell firing rates, particularly in the LIP, display the same profile that is predicted by sequential sampling models (Huk & Shadlen, 2005; Paré & Wurtz, 2001; Platt & Glimcher, 1999; Shadlen & Newsome, 1996, 2001), research in human decision-making has been progressing more slowly.

Neuroimaging research of human perceptual decision-making has often made use of functional magnetic resonance imaging (fMRI), which has led to some insights into which brain areas are primarily involved in decision-making, such as the dorsolateral prefrontal cortex (Heekeren et al., 2004), the posterior parietal cortex (Tosoni et al., 2008), and the intraparietal sulcus (Kayser, Buchsbaum, Erickson, & Esposito, 2010). However, due to their low temporal

resolution, fMRI techniques do not lend themselves to the tracking of a dynamic signal within the course of a decision which takes no longer than 1000 ms. Magnetoencephalographic (MEG) and electroencephalographic (EEG) approaches on the other hand, have a high temporal resolution, and although they give little insight into the structural underpinnings of decision-making, are an appropriate method to identify neural substrates of the decision variable in the human brain.

A range of studies have made use of these techniques to identify decision-related signals. For example, in a series of studies, Philiastides and colleagues recorded EEG while participants performed a face-car discrimination task and used a machine learning approach to identify signals which were able to discriminate between the two stimulus categories (Philiastides et al., 2006; Philiastides & Sajda, 2006). However, this putatively decision-related signal, disappeared when the task switched from a face-car discrimination to a colour discrimination, questioning its role as a general-purpose decision variable. The component was later interpreted as a post-sensory signal feeding into the accumulation process (Philiastides et al., 2006; Ratcliff et al., 2009). In a similar study Philiastides, Heekeren, and Sajda (2014) identified an EEG signal which, like a decision variable, builds up over the course of the decision, at a rate that depends on the signal strength. However, the findings did not suggest that the build-ups which differed with the amount of sensory evidence converged to a stereotyped level to suggest the reaching of a decision boundary.

Van Vugt et al. (2012) used a regressor-based EEG approach which allowed them to search for a correlate of the accumulation profile predicted by a sequential sampling model while participants performed a random dot motion task. With this approach, they were able to identify oscillatory theta band (4-9 Hz) power over the parietal lobe as a neural correlate of the accumulation process. A similar approach was used by Wyart et al. (2012), who presented participants with a series of Gabor patterns and asked them to report the average tilt of the patterns. They found that the encoding of evidence fluctuated in accordance with delta band (1-3 Hz) oscillations.

A different approach to tracking decision-related M/EEG activity, which is comparable to the tracking of oculomotor neurons in monkeys, focuses on signals which are known to be indicators of motor preparation. Traditional theories of decision-making assume serial processing, in which sensory encoding, decision formation, and motor execution are separate stages, and response selection only occurs after the decision is made (Donders, 1969; Sternberg, 1969). However, more recent evidence does not support this assumption, indicating instead that motor preparation occurs throughout the decision-making process (Coles et al., 1985; Gluth et al., 2013; Hadar et al., 2012; Selen, Shadlen, & Wolpert, 2012). Therefore, researchers have measured effector-specific motor signals to track the decision variable, assuming that the evidence accumulation process is constantly fed forward into motor areas, so that, as evidence for a given alternative accumulates to a certain level, the response associated with the alternative is prepared to the same extent.

One signal which is known to be related to motor preparation and has been used to track evidence accumulation is the lateralised readiness potential (LRP). The LRP is the lateralised portion of a slow, negative potential over frontal and central electrodes which precedes voluntary movements of distal limbs, called the readiness potential (RP, or Bereitschaftspotential; Kornhuber & Deecke, 1965; Vaughan, Costa, & Ritter, 1968). Crucially, this negativity is larger in the hemisphere contralateral to the movement, and has been shown to arise from the supplementary motor area (Ikeda & Shibasaki, 1992; Lang et al., 1991). To measure the LRP, a typical study requires participants to respond to stimuli with a hand movement on the left or the right side, while EEG activity is recorded from electrodes over the left and right motor cortex (usually C3 and C4). The resulting EEG signals are then locked to a given event (either stimulus onset or response), averaged across trials, and the activity recorded from the ipsilateral hemisphere is subtracted from activity of the contralateral hemisphere, to generate the LRP waveform.

A number of studies have linked the LRP to decision-making, showing differences in the waveform with varying speed/accuracy decision strategies

(Rinkenauer et al., 2004) and decision bias (Noorbaloochi et al., 2015), or linking it to mechanisms of response caution (van Vugt et al., 2014). However, there is also some evidence to suggest that the LRP is a neural correlate of the decision variable itself. Polanía et al. (2014) found that the LRP waveform closely followed the accumulation profile predicted by sequential sampling models in both perceptual and value-based decisions. Kelly and O'Connell (2013) also investigated the role of the LRP in decision-making and found that it builds up over the course of the decision (although with negative polarity) and that its slope depends on the difficulty of the decision. However, these authors noted that although the LRP shows characteristics of the decision variable, it temporally lags behind a centroparietal component, which they identified to be the true neural correlate of the decision variable (see below). Similarly, Dmochowski and Norcia (2015) found that the LRP captures some, but not all characteristics of a decision variable, as it does not allow for a discrimination between fast and slow responses as well as other decision-related components. Similar findings have been reported for the RP (Gluth et al., 2013; Schurger, Sitt, & Dehaene, 2012).

Another motor-related EEG signal which has commonly been used to study perceptual decision-making is the power of beta-band oscillations. It has been shown that oscillations in this frequency (typically between 15 and 30 Hz) display a clear desynchronisation over the premotor cortex, contralateral to a manual response when the response is prepared (Doyle et al., 2005; Jasper & Penfield, 1949; Pfurtscheller, 1981; Zaepffel et al., 2013). While there is some methodological variation in the way event-related desynchronisation (ERD) profiles in the beta band are generated, and in particular which frequency range is chosen, a typical study requires participants to make one of two possible hand movements (left/right) and records EEG activity from electrodes over the contralateral motor cortex. One way in which to assess beta band activity is the band power method, in which the EEG signal is band-pass filtered, to remove all frequencies that do not fall within the chosen beta range. The resulting signal is then locked to a given event (e.g. stimulus onset) and squared to obtain power samples, as well as averaged over trials (Pfurtscheller & Lopes, 1999). Like the LRP, the decrease in beta power is interpreted as a response

preparation signal and, assuming that processing is not serial and motor preparation closely follows evidence accumulation, may therefore be used to track the decision-making process.

A number of studies have explored the role of beta ERD in decision-making. It has been found that desynchronisation increases as decision uncertainty reduces (Tzagarakis et al., 2010), and that the latency of the desynchronisation is shorter in easy compared to hard decisions, suggesting that the duration of motor preparation increases with the duration of the decision formation (Kaiser, Lennert, & Lutzenberger, 2007). In line with this finding, Donner et al. (2009) suggested that oscillations in the beta frequency may be a neural correlate of the decision variable. Using MEG during a human random dot motion task, it was found that beta power corresponds to the integral of the sensory evidence provided by the visual cortical area MT, and displays integration-to-bound dynamics (Donner et al., 2009; Siegel, Engel, & Donner, 2011). This was also supported by EEG studies which found that oscillations in the beta band show the same accumulation-like profile as expected for a decision variable (i.e. a ramp-like profile during a perceptual decision) and reach a stereotyped peak before the hand movement that indicates the decision (Kubanek et al., 2013; O'Connell et al., 2012). Additionally, unlike sensory signals which show a more linear change with increasing stimulus strength, the slope of the change in beta power was found to increase over time, indicating that it reflects the temporal integration of evidence (O'Connell et al., 2012). De Lange et al. (2013) used effector-specific activity in the beta band to explore the effects of prior expectations and found that decision bias results in a baseline shift in lateralised beta ERD. Since sequential sampling models predict a shift in the starting point of the accumulation process to account for biased decisions, this finding is in line with the claim that beta ERD may reflect the decision variable.

However, O'Connell et al. (2012) also noted that accumulation-like characteristics in beta ERD were only present in decisions involving hand movements. Similarly, if a decision is made without advanced knowledge of the stimulus-response mapping, no change in motor-related beta activity can be observed during the decision (Twomey et al., 2016).

This dependence on the response may seem to be an obvious limitation of motor-related signals as a read-out of accumulation. Since both the LRP and beta ERD are primarily correlates of hand-movement preparation, they are not expected to show accumulation-like profiles during decisions which do not require these responses, or decisions which are made without knowing which response is associated with each alternative. This finding demonstrates that what can be observed in these motor-related signals during decisions with known stimulus-hand mappings (e.g. Donner et al., 2009) is not a decision-making process, but is instead likely to occur down-stream from decision areas (Wyart et al., 2012). Nevertheless, response-preparation signals may still give insight into the accumulation process as evidence suggests that the decision state flows continuously to the motor areas (Donner et al., 2009; O'Connell et al., 2012). Note also that some of the most useful neural correlates of the decision variable in non-human primates track firing rates in oculomotor neurons during saccadic decisions, which are arguably equivalent to lateralised motor preparation signals in human decision-making requiring hand movements (Gold & Shadlen, 2000, 2003).

A different EEG signal which does not have the same limitations as motor-related activity was proposed by O'Connell et al. (2012). In a series of experiments, they recorded human EEG during a visual target-detection task, and identified the centroparietal positivity (CPP) as an accumulation-to-bound signal. The CPP is a large, positive ERP component recorded over centroparietal regions, which displays a number of characteristics of the decision variable. It shows a ramp-like increase over the course of the decision formation and peaks at a stereotyped level immediately prior to the response. By varying the difficulty of the gradual detection task both between and within trials, it was also demonstrated that the slope of the decision-related build-up is sensitive to the strength of the evidence, with easier decisions (stronger evidence) leading to steeper build-up rates, and changes in difficulty within a decision leading to changes in slope within the build-up.

Importantly, O'Connell et al. (2012) were able to dissociate the CPP from signals of both sensory encoding and motor processing. In a task in which the evidence increased over time, it was shown that, unlike correlates of sensory processing which display a linear build-up as stimulus strength increases, the CPP builds up at a rate which increases over the course of the decision, indexing the temporal integration of sensory evidence. Additionally, the build-up seen in sensory-related signals was shown to remain the same regardless of whether the sensory information was task-relevant or not, while the CPP only displayed a build-up when the sensory input was attended to make a decision. Further, the CPP was shown to display the same accumulation-to bound profile, regardless of whether or not the response required hand movements. In a follow-up study, it was also shown that, unlike motor signals, the CPP does not depend on foreknowledge of the stimulus-response mapping (Twomey et al., 2016). These findings suggest that the CPP provides a read-out of the decision-related accumulation of evidence. This notion was also supported by the finding that it is unaffected by modality, as auditory decisions were associated with the same CPP profiles as decisions based on visual evidence (O'Connell et al., 2012; Twomey et al., 2015).

However, as reported in Chapter 2, we were not able to demonstrate a difference in CPP waveforms between decisions that are made under speed stress (i.e. quick and error-prone decisions), and decisions which are made following instructions to be as accurate as possible (i.e. slow, accurate decisions). Sequential sampling models typically account for the behavioural differences of the speed-accuracy trade-off by adjusting the response caution parameter (Brown & Heathcote, 2008; Heitz, 2014; Ratcliff & McKoon, 2008). This threshold difference between 'speed' and 'accuracy' trials should be visible in the profile of a neural substrate of the decision variable as a difference in amplitude. We were not able to support this hypothesis in Chapter 2. Although this finding can be accommodated by sequential sampling models and may not question the role of the CPP as a neural substrate of the decision variable but rather be used to inform the neural implementation of sequential sampling models (see Chapter 2), it does raise questions about the CPP and its role.

Another limitation of the CPP was raised by Urai and Pfeffer (2014). They note that unlike motor-related signals of decision-making, the CPP is not able to predict the specific choice a participant is making. The CPP is not effector-specific and instead, builds up to a threshold in the same way for any response, while more established accumulation signals recorded in non-human primates display choice-selectivity (e.g. Shadlen & Newsome, 2001). This lack of selectivity led to the suggestion that the CPP may in fact display a build-up of choice confidence, rather than evidence accumulation (Urai & Pfeffer, 2014). Note however, that the comparatively poor spatial resolution of EEG allows for a discrimination between choices in motor signals due to the clear lateralisation of the motor cortices (i.e. right/left-hand responses can be tracked over the left/right hemisphere), but does not allow for a discrimination between neighbouring neural populations. It is therefore possible that evidence for different alternatives is in fact accumulated in separate neural populations, but that what is recorded on the scalp is a summation of activity.

In the light of this research, it becomes apparent that many questions regarding neural substrates of decision-making in the human brain, and in particular the CPP, are yet to be answered conclusively. In this study, we therefore set out to explore potential accumulation-to-bound signals in the human EEG. To do this, we explored decisions with differing levels of difficulty. We chose the difficulty manipulation not only because it is one of the most commonly used manipulations in the field of perceptual decision-making (de Lafuente, Jazayeri, & Shadlen, 2015; Ho et al., 2009; Ratcliff & McKoon, 2008; Roitman & Shadlen, 2002), but also because it is one of the only manipulations that has only one possible implementation in sequential sampling models. The behavioural effects of many standard manipulations in decision-making research can be explained by sequential sampling models in a number of different ways. This is not the case for the manipulation of difficulty. Difficulty has strong effects on the behavioural data, but, to our knowledge, these changes are explained by a difference in drift rate (i.e. the rate at which evidence is accumulated) in virtually all approaches using sequential sampling models (Donkin et al., 2009; Mulder et al., 2014; Ratcliff & McKoon, 2008; Ratcliff & Rouder, 1998; Voss, Rothermund, & Voss, 2004; but see Goldfarb, Leonard, Simen, Caicedo-Nunez,

& Holmes, 2014; Teodorescu & Usher, 2013). The drift rate uniquely accounts for behavioural differences induced by difficulty changes as it is the only parameter which simultaneously influences accuracy and RT in opposing directions (i.e. as drift rate increases, accuracy increases while RT decreases; see Figure 3.1). Since there is a consensus that the drift rate of the accumulation process, at least in part, accounts for behavioural differences due to different levels of difficulty, we assume that any neural correlate of the decision variable should display a different profile in easy and hard decisions. Specifically, we expect a higher slope in the build-up associated with easy decisions than with hard decisions (Kelly & O'Connell, 2013; Roitman & Shadlen, 2002). In this study, we made use of the data collected in Chapter 2 (Experiment 1) and tested whether this assumption holds true in the most commonly suggested decision-related human EEG signals, namely the CPP, the LRP, and beta ERD.

Additionally, we used a bottom-up approach to identify other potential signals which may display differences between easy and hard decisions and reflect accumulation. Bottom-up approaches which aim to identify signals which display characteristics of the decision variable have been used before, for example by van Vugt et al. (2012), who used a regressor-based analysis. This method has the advantage of being able to identify signals with specific characteristics, but identifies such signals regardless of their recording sites, which can make their interpretation difficult. Here, we therefore chose a method which, to our knowledge, has not previously been used to identify decision variable signals, namely cluster-based permutation tests (Maris & Oostenveld, 2007). This method identifies differences between conditions in the whole brain rather than just specific waveforms, and can be applied here since we have clear predictions about the effects of difficulty on an accumulation signal. Importantly, this method uses biophysically motivated constraints, which not only increase its sensitivity, but also make it more interpretable. By combining this approach with the exploration of established EEG signals, we aimed to identify the most suitable neural correlate of the decision variable.

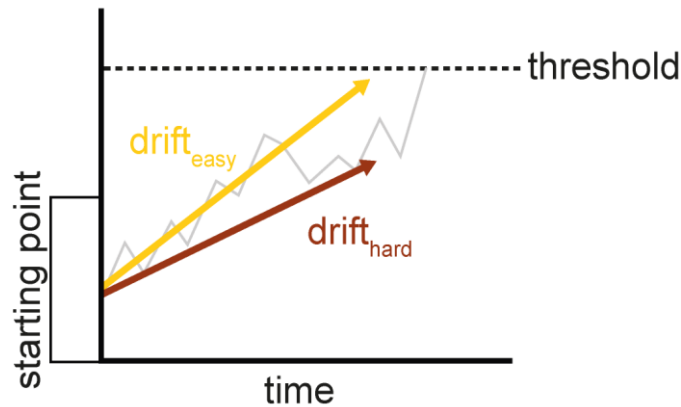


Figure 3.1: Simplified illustration of an accumulation process in a sequential sampling model framework: evidence accumulates from a starting point towards the threshold. The slope of the accumulation is defined by the drift rate, which varies with task difficulty. The easier the decision, the higher the slope of the accumulation.

## 3.1. Methods

Since this study uses data collected in Chapter 2, the data collection methods are only described briefly (please see Chapter 2 for more details).

### 3.1.1. Participants

A total of 26 participants (nine males) were recruited using poster advertisements and word of mouth. Three participants were excluded from the experiment as they were unable to perform the task as required by criteria established prior to the experiment (see Chapter 2, section 2.1.1.2.2). The remaining sample was made up of 23 participants (eight males) with a mean age of 29.39 ( $SD = 7.47$ ). Each participant took part in a two-hour session, completing 800 trials, and was paid £8 per hour, as well as an additional performance-based reward of up to £4. All procedures were approved by the City, University of London Psychology Department Ethical Committee.

### 3.1.2. Stimuli and Procedure

Participants were asked to complete a random dot motion task, in which they viewed an array of moving dots, a proportion of which moved coherently either up or down, while the rest of the dots moved in random directions. Participants were asked to indicate the direction of the coherent motion. The difficulty of the

task was determined by the coherence level, i.e. the ratio between coherently and randomly moving dots. Each participant was presented with 'easy' and 'hard' trials, the coherence levels of which were calibrated individually using the QUEST staircase procedure, implemented in Psychtoolbox (Watson & Pelli, 1983). The QUEST procedure estimated the coherence levels at which a given participant was able to respond correctly in 75% of trials for the 'hard' condition, and 95% for the 'easy' condition. Overall, the appropriate difficulty levels estimated for the final sample resulted in a mean of 30.63% ( $SD = 18.69$ ) coherence for 'hard', and 67.67% ( $SD = 28.23$ ) for 'easy' trials. 'Easy' and 'hard' trials, as well as trials with upward and downward motion were randomly intermixed. The original experiment also included a manipulation of speed and accuracy instructions (see Chapter 2, section 2.1.1.2.3). However, this manipulation is ignored here and all analyses are performed to compare only difficulty conditions, collapsed over speed and accuracy conditions.

The trial procedure is displayed in Figure 3.2. To start each trial, participants were presented with a fixation cross for 500 ms (plus a jitter of up to 1000 ms, drawn from a uniform distribution). Then, 100% of the dots moved randomly for 1000 ms (plus a jitter of up to 1500 ms, drawn from a gamma distribution with shape parameter 1 and scaling parameter 150). This period of random motion was introduced as the onset of the moving dots is likely to produce a visual evoked potential (VEP). By allowing this VEP to occur before the onset of coherent motion, we were able to clearly track decision-related potentials from the onset of the accumulation process (i.e. the onset of coherent motion). The random motion was followed by the onset of coherent motion, when a proportion of dots started moving coherently either up or down, for up to 2000 ms, or until the response. Feedback was provided after each trial. All stimuli were written in Matlab (The Mathworks, Natick, U.S.A.), using the Psychtoolbox extension (Brainard, 1997; Kleiner et al., 2007; Pelli, 1997) and run on a PC.

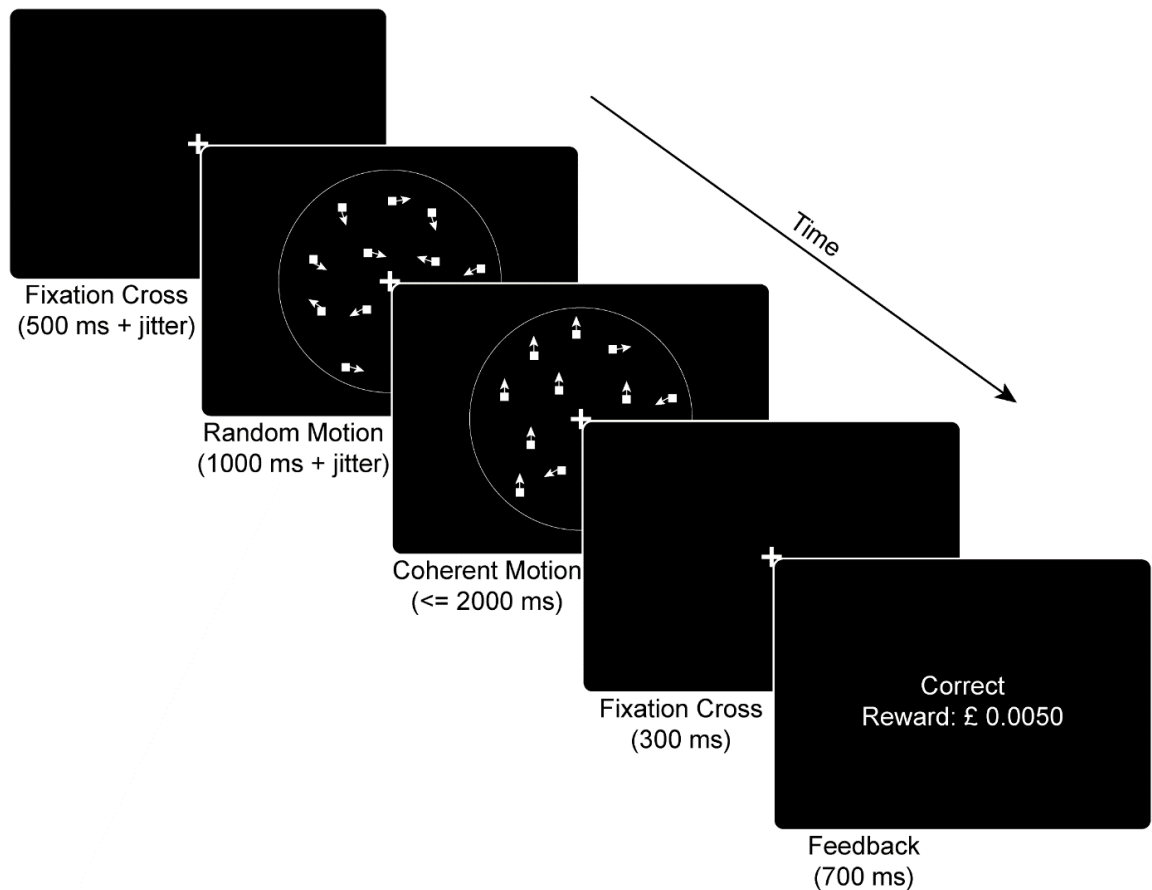


Figure 3.2: Random dot motion task trial procedure: in each trial, a fixation cross was followed by a period of random motion (coherence: 0%). Then, the coherent motion (up/down) was presented according to each participant's difficulty level (here: coherence: 70%, direction: up). The coherent motion continued for 2000 ms or until a response was given. Feedback was provided after each trial. Note that the size and number of dots have been adjusted for illustration.

### 3.1.3. EEG Recording and Analysis

Continuous EEG was recorded using 64 active electrodes, placed equidistantly on the scalp (EasyCap, M10 Montage) and referenced to the right mastoid. Using a BrainAmp amplifier (BrainProducts), data were recorded at a sampling rate of 1000 Hz and band-pass filtered from 0.016 – 1000 Hz. The data were then pre-processed using custom scripts in Matlab (The Mathworks, Natick, U.S.A.), drawing on functions from the EEGLAB toolbox (Delorme & Makeig, 2004).

EEG data were re-referenced to the average reference and filtered at 0.1 (low cut-off) and 45 Hz (high cut-off), using a Hamming windowed finite impulse response filter. To improve the signal-to-noise ratio, we initially visually

inspected the data to remove large muscle artifacts before applying independent component analysis to remove eye blink components. Any remaining artifacts were removed manually during a second visual inspection. Afterwards, spherical spline interpolation was used to reconstruct noisy channels, which were identified and rejected during the first visual inspection.

### **3.1.3.1. Event-related Potentials**

To generate ERP waveforms, matched stimulus-locked (-200 to 2000 ms relative to the onset of coherent motion) and response-locked (-1000 to 100 ms relative to button press) epochs were extracted from the continuous data. All epochs were baselined to the average over a 200 ms period preceding the onset of coherent motion. Epochs were then separated into 'easy' and 'hard' conditions. Since we assume equivalent decision processes for trials with upward and downward motion, we collapsed trials over motion direction. However, since trials with upward and downward motion were associated with right and left-hand responses, leading to stronger changes in the left and right hemisphere respectively, simply averaging over both motion directions would distort the lateralisation of motor processes. Therefore, the topography of all trials with a right-hand response (correct 'up' trials and incorrect 'down' trials) was mirrored along the midline, so that all contralateral activity was projected onto the right hemisphere (i.e. activity recorded in electrodes on the left hemisphere was now associated with electrodes on the right hemisphere). Finally, in line with previously suggested procedures (Kelly & O'Connell, 2013; O'Connell et al., 2012), the data were converted to current source density (CSD) estimates to increase spatial selectivity. The CSD transformation was applied using the CSD toolbox, which uses a spherical spline algorithm, with the spline interpolation constant  $m$  set to its default value ( $m = 4$ ; Kayser & Tenke, 2006).

#### **3.1.3.1.1. Centroparietal Positivity (CPP)**

To generate the CPP waveform, centroparietal electrodes were chosen for each participant individually by inspecting the averaged ERP topography and identifying the electrode associated with the maximum amplitude (chosen

electrodes: 1, 5, or 14, roughly equivalent to electrodes Cz, CPz, and Pz in the 10-20 system; see Figure 3.4 a). The activity in the selected electrodes was averaged over correct trials and participants for each difficulty condition and for stimulus and response-locked signals separately.

#### 3.1.3.1.2. *Lateralised Readiness Potential (LRP)*

Similarly, ERP topographies, as well as waveforms at different electrodes were visually inspected to identify appropriate frontocentral electrodes for the LRP waveform per participant (chosen contralateral electrodes: 18 or 31, ipsilateral electrodes: 10 or 22, roughly equivalent to electrodes FC3, C5, FC4, C6 in the 10-20 system)<sup>8</sup>. Activity recorded from the chosen ipsilateral electrode was subtracted from the recordings from the corresponding contralateral electrode. The resulting activity was averaged over correct trials and participants to generate the LRP waveform.

#### 3.1.3.2. **Time-Frequency Analysis**

To estimate the time-varying spectral content of the data, longer epochs than those required for the ERP analysis were extracted (-2000 to 2000 ms relative to the onset of coherent motion for stimulus-locked, and -2000 to 1000 ms relative to the response for response-locked data). Segments were separated into 'easy' and 'hard' conditions, collapsed over 'up' and 'down' trials, mirrored, and CSD-transformed in the same way as described above for the ERP analysis. Error trials were discarded from the analysis. The time-frequency analysis was performed using the wavelet decomposition method, in which the data is convolved with a Morlet wavelet. We used wavelets with four cycles on a single trial basis before averaging the resulting transforms. Frequencies from 2 to 40 Hz were analysed in steps of 1 Hz. The resulting time-frequency representation (TFR) was normalised by dividing the power in each frequency by its mean during a baseline interval of -500 to -100 ms relative to the onset of coherent motion.

---

<sup>8</sup> Note that we repeated all analyses based on an LRP which was generated using the standard electrodes 17 and 11 (roughly equivalent to C3 and C4 in the 10-20 system) and found qualitatively identical results.

### 3.1.3.2.1. *Event-Related Beta Desynchronisation*

In order to explore event-related desynchronisation, we visually inspected each participant's time-frequency plot and identified the 15 to 25 Hz frequency range to be suitable for all participants. We used the band-power method (Pfurtscheller & Lopes, 1999) to analyse the time-varying power of this beta band. Each participant's temporospatial signal was filtered between 15 and 25 Hz, using a Butterworth band-pass filter (order = 4). The resulting signal was squared, averaged, and then smoothed using a moving average with a 50 ms window. Lastly, the power was expressed in percentage of change from the baseline interval of -200 to 0 ms relative to the onset of the coherent motion, by subtracting the mean baseline power from the waveform, dividing the resulting signal by the mean baseline power and multiplying it by 100. In line with standard procedures (Doyle et al., 2005; O'Connell et al., 2012; Pfurtscheller, 1981), we chose electrode 17 (roughly equivalent to C3 in the 10-20 system) to test contralateral beta power. In order to test lateralised beta ERD, we subtracted signals recorded from the ipsilateral electrode 11 (roughly equivalent to C4 in the 10-20 system), from activity in electrode 17.

### 3.1.3.3. **Statistical Analysis**

In order to test for characteristics of the decision variable in the generated ERP and ERD waveforms, we compared the slope of the build-up between 'easy' and 'hard' conditions. To do so, we fitted a straight line and measured its slope for each participant's signal. In line with Kelly and O'Connell (2013), the chosen time intervals to which we fitted a line were 200 to 350 ms for the stimulus-locked CPP, -250 to -100 ms for the response-locked CPP, 300 to 450 ms for the stimulus-locked LRP and ERD, and -300 to -150 ms for the response-locked LRP and ERD.

Additionally, we analysed the impact of difficulty on the amplitude of the waveform. Using t-tests, we compared the values in 'easy' and 'hard' ERPs and ERDs in each time sample between 0 and 1000 ms for the stimulus-locked, and -1000 to 0 ms in the response-locked signal. The results were controlled for

multiple comparisons using the false discovery rate (FDR) approach (Benjamini & Hochberg, 1995). In this procedure, the uncorrected  $p$ -values are sorted from lowest to highest ( $p_i$  refers to the  $i$ th lowest value out of  $m$  total  $p$ -values). The largest  $i$  for which  $p_i < \left(\frac{i}{m}\right) \alpha$  is identified and all  $p$ -values associated with  $i$ s smaller or equal to the identified  $i$  are considered significant.

#### **3.1.3.4. Exploratory Approach**

Since there is no single signal in the human EEG which has been conclusively proven to be a correlate of decision-related evidence accumulation, we set out to not only test those signals which have previously been suggested to play this role, but also to explore the data using a bottom-up approach. Since sequential sampling models make strong predictions about differences in accumulation due to different difficulty levels, we used a data-driven method to search the data for differences between signals associated with 'easy' decisions and those associated with 'hard' decisions. To this end, we employed a non-parametric cluster permutation approach to evaluate both ERP data (temporal and spatial dimensions) and TFR data (temporal, spatial, and spectral dimensions; Maris & Oostenveld, 2007). This method not only allows for a less conservative solution to the multiple comparison problem than, for example, Bonferroni corrections, but is also built on biological concepts and makes use of the assumption that, if a difference between conditions is meaningful, it ought to be visible across a multidimensional cluster (i.e. across time and space, or across time, space, and frequency if TFR data are used).

Following this method, we first generated dependent-measures  $t$ -statistics for the comparison between 'easy' and 'hard' trials for each of the samples (one sample corresponds to one time-electrode pair for ERP comparisons and one time-electrode-frequency pair for TFR comparisons), to identify all samples at which a given cut-off (defined here as  $p < .05$ ) was exceeded. These  $t$ -tests were run across all electrodes, and all time points in the time interval of 0 to 1000 ms relative to the onset of coherent motion in the stimulus-locked data, as well as for each frequency between 2 and 40 Hz for TFR comparisons. If

neighbouring samples exceeded the threshold and shared the same sign, they were grouped into a cluster. The cluster statistic is defined as the sum of all  $t$ -values in a cluster. Each cluster is then assigned a  $p$ -value by comparing it against the permutation distribution of the maximum cluster-level statistic. The permutation distribution is approximated using a Monte-Carlo estimate after performing 500 random partitions of the data (i.e. data is shuffled across conditions and randomly assigned into two new conditions) and re-calculating the statistic of interest on the shuffled data.

The analysis was run in Matlab (The Mathworks, Natick, U.S.A.), using custom scripts drawing on functions of the fieldtrip extension (Oostenveld, Fries, Maris, & Schoffelen, 2011). Cluster permutation tests were only performed on stimulus-locked data, as we expected a neural correlate of the decision variable to display differences between 'easy' and 'hard' trials in the stimulus-locked, but not in the response-locked amplitude, as according to sequential sampling models, response-locked signals should converge to a common bound. Although slope differences are expected in both the stimulus and the response-locked data, these differences are often less visible in response-locked data, and do not necessarily translate into a clear difference in amplitude. To explore any clusters identified in the stimulus-locked signal in the response-locked data, we generated the response-locked signal of the electrodes (and frequencies for TFR clusters) defined by the cluster and performed the same FDR controlled  $t$ -tests as defined above to evaluate the signal.

## **3.2. Results**

### **3.2.1. Behavioural Results**

In order to test the effects of the difficulty manipulation on the behavioural data, data were collapsed over 'up' and 'down' trials. Trials with very short ( $< 180$  ms) and very long ( $\geq 2000$  ms) RTs were excluded from the analysis (6.08% of trials). The remaining data are displayed in Figure 3.3. A paired-samples  $t$ -test revealed that response times in correct trials were significantly different

between difficulty levels,  $t(22) = 11.19$ ,  $p < .001$ ,  $d = 2.33$ , with ‘easy’ decisions being associated with shorter RTs ( $M = 533$  ms) than ‘hard’ decisions ( $M = 679$  ms).

To explore this effect in the accuracy data, a generalised linear mixed-effects model with a logistic link function and binomial data model was used, which, unlike a t-test, appropriately models the non-normal distribution of the data. Using the ‘fitglm’ function in Matlab (The Mathworks, Natick, U.S.A.), parameter estimates were based on a maximum likelihood method using the Laplace approximation. In this model, ‘Difficulty’ was included as a fixed effect and ‘Participant’ was included as a random effect (Wilkinson notation:  $\text{Accuracy} \sim 1 + \text{Difficulty} + (1 + \text{Difficulty} | \text{Participant})$ )<sup>9</sup>. It was found that ‘Difficulty’ was a significant predictor,  $t(44) = 4.69$ ,  $p < .001$ , with higher accuracies observed in easy ( $M = 86\%$ ) compared to hard trials ( $M = 79\%$ ).

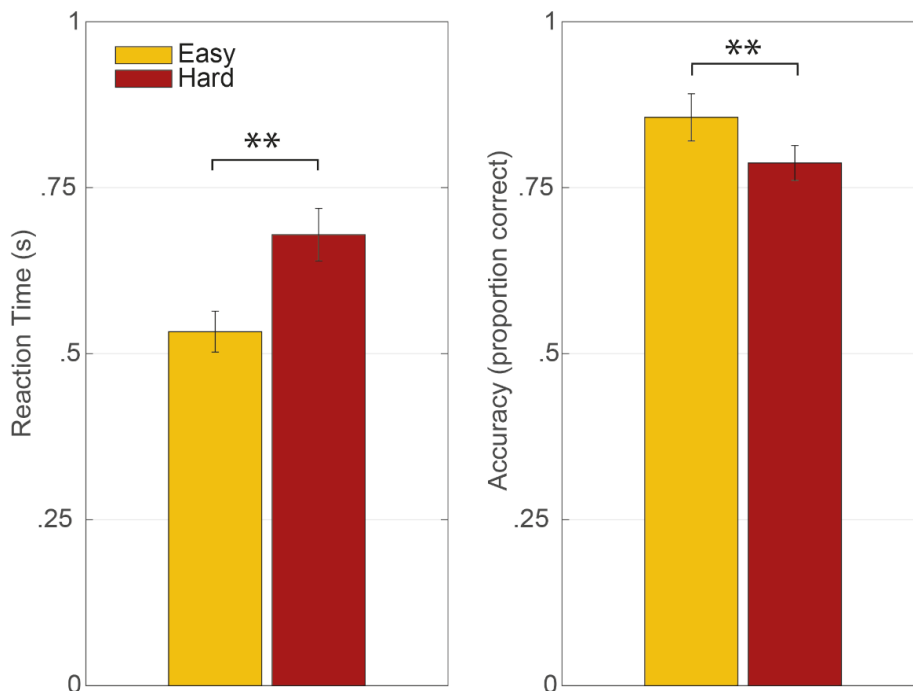


Figure 3.3: Behavioural results: reaction time in seconds (left) and accuracy in proportion correct (right). Error bars indicate 95% confidence interval. \*\* indicates  $p < .001$ .

<sup>9</sup> The dispersion parameter of the model,  $\phi = .80$ , was calculated by dividing the sum of squared Pearson residuals by the residual degrees of freedom (Venables & Ripley, 2002).

## 3.2.2. Neural Results

### 3.2.2.1. Centroparietal Positivity (CPP)

We generated the CPP (see Figure 3.4 a) and conducted a t-test to investigate the difference in slope between signals associated with ‘easy’ and ‘hard’ decisions. In the CPP waveform, we found a significant difference in slopes in both stimulus-locked,  $t(22) = 3.67, p = .001, d = .77$ , and response-locked  $t(22) = 3.60, p = .002, d = .75$ , waveforms. In accordance with sequential sampling models which assume a higher drift rate (i.e. a steeper slope of accumulation) in ‘easy’ compared to ‘hard’ choices, we found that slopes in trials with high motion coherence ( $M_{stimulus-lock} = .07, M_{response-lock} = .06$ ) were significantly higher than those in trials with lower motion coherence ( $M_{stimulus-lock} = .06, M_{response-lock} = .04$ ).

Additionally, an FDR-corrected series of t-tests revealed statistically significantly higher amplitudes in ‘easy’ compared to ‘hard’ trials in all time samples between 265 and 632 ms in the stimulus-locked CPP (corrected  $p < .05$ ). The response-locked CPP showed no significant difference in amplitude between ‘easy’ and ‘hard’ trials after FDR correction (see Figure 3.4 a).

### 3.2.2.2. Lateralised Readiness Potential (LRP)

Further, we generated the LRP waveform (see Figure 3.4 b) and found a significant difference in slopes between difficulty conditions in the stimulus-locked data,  $t(22) = -5.00, p < .001, d = -1.04$ , with a steeper slope associated with ‘easy’ ( $M_{stimulus-lock} = -.07$ ) compared to ‘hard’ ( $M_{stimulus-lock} = -.04$ ) trials. However, there was no significant difference in slope in the response-locked LRP  $t(22) = -.31, p = .076, d = -.06$  ( $M_{response-lock} = -.03$  for both difficulty levels).

FDR-corrected t-tests showed significant differences in the stimulus-locked LRP, with higher amplitudes in ‘easy’ compared to ‘hard’ trials, between 8 and 12 ms relative to stimulus onset (corrected  $p < .049$ ), as well as in 212 out of 278 time samples between 318 and 596 ms relative to stimulus onset (corrected

$p < .05$ ). There was no significant difference in amplitude between the difficulties in the response-locked LRP (corrected  $p > .58$ ; see Figure 3.4 b).

### 3.2.2.3. Event-Related Beta Desynchronisation

For contralateral beta power (see Figure 3.4 c), we first tested differences between difficulty levels. We found that the slope of the ERD did not differ significantly between 'easy' ( $M_{stimulus-lock} = -.05$ ,  $M_{response-lock} = -.03$ ) and 'hard' ( $M_{stimulus-lock} = -.04$ ,  $M_{response-lock} = -.04$ ) conditions in either the stimulus-locked,  $t(22) = .42$ ,  $p = .68$ ,  $d = .09$ , or the response-locked data,  $t(22) = .38$ ,  $p = .71$ ,  $d = .08$ . We further tested the amplitude difference between 'easy' and 'hard' conditions throughout the decision-making process. After FDR correction for multiple comparisons, we found no difference in either the stimulus-locked (corrected  $p > .07$ ), or the response-locked data (corrected  $p > .9$ ).

We then performed the same test on the lateralised spectral power in the beta frequency (see Figure 3.4 d). Again, we found no significant difference in slope between the 'easy' ( $M_{stimulus-lock} = -.02$ ,  $M_{response-lock} = -.003$ ) and the 'hard' ( $M_{stimulus-lock} = -.02$ ,  $M_{response-lock} = -.005$ ) conditions in either the stimulus-locked,  $t(22) = -1.06$ ,  $p = .30$ ,  $d = -.22$ , or the response-locked data,  $t(22) = .09$ ,  $p = .93$ ,  $d = .02$ . Similarly, we found no significant differences between 'easy' and 'hard' waveforms in amplitude in either the stimulus-locked (corrected  $p > .38$ ) or the response-locked data (corrected  $p > .26$ ).

Overall, these findings are explained by the fact that we did not observe any desynchronisation in the lateralised part of beta ERD. To quantify this lack of lateralisation, we used t-tests to test the null hypothesis that each time sample (like all other analyses, time samples were taken at an interval of 0 to 1000 ms relative to stimulus onset and -1000 to 0 ms relative to response) of each condition stems from a distribution with a mean of zero, and corrected for multiple comparisons using FDR corrections. We found no time sample at which the null hypothesis was rejected (minimum corrected  $p$ -value across stimulus and response-locked data .06). This indicates that the same patterns were recorded on both contralateral and ipsilateral sites, and that the

desynchronisation observed in the contralateral signal was not effector-specific, but merely reflected a more general motor preparation.

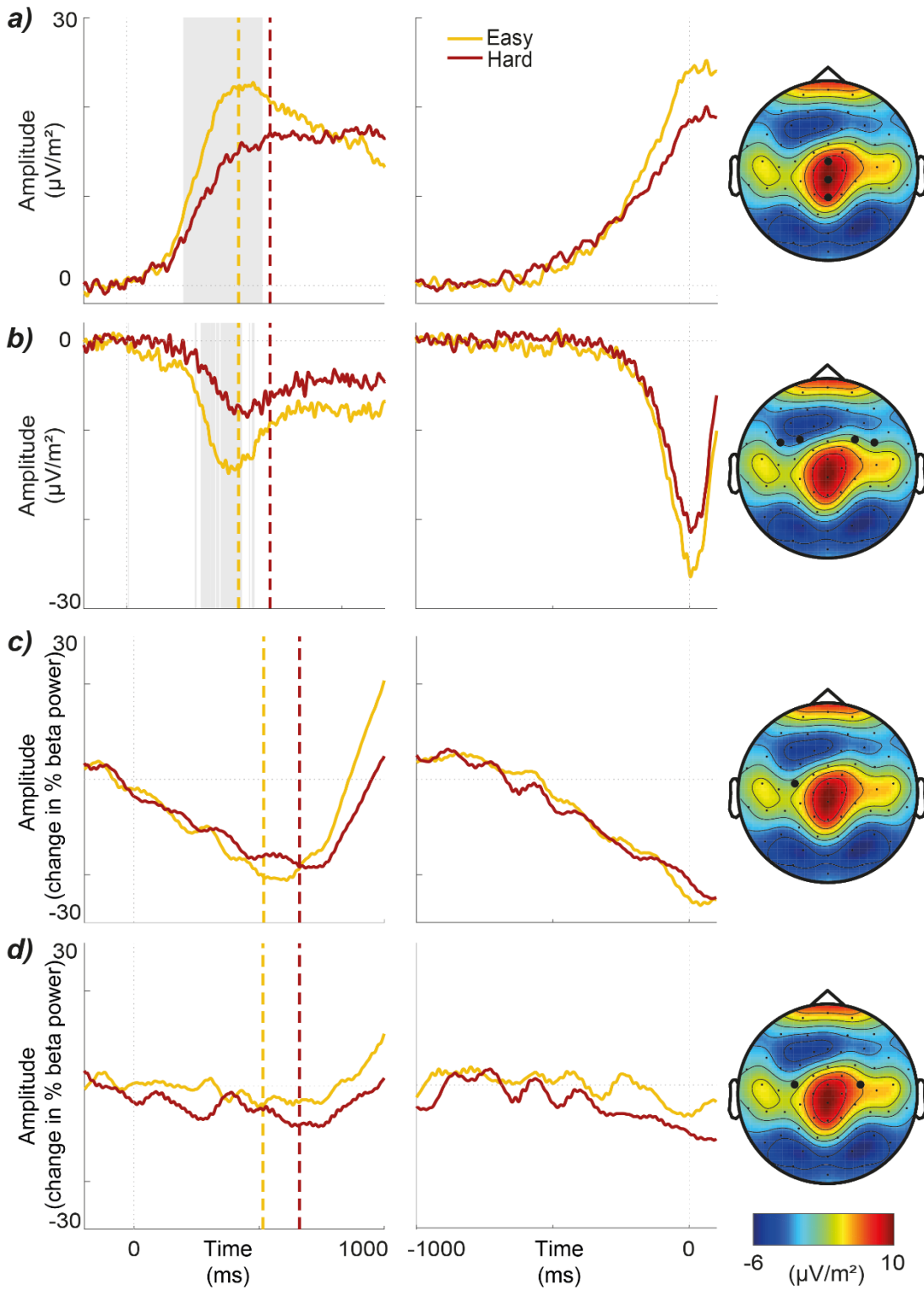


Figure 3.4: Neural results: from left to right: stimulus-locked, and response-locked waveforms, and ERP topographies. Topoplots show the mean ERP activity between 0 and 1000 ms relative to the onset of coherent motion. The electrodes used to generate each waveform are highlighted. Shaded grey areas in the waveform panels indicate a significant difference in amplitude between 'easy' and 'hard' trials. Vertical dashed lines indicate mean RT (note that these mean RTs only include RTs from trials which were

*ultimately included to generate the waveform and therefore differ slightly from RTs displayed in Figure 3.3, as well as between ERP and spectral data). a) CPP; b) LRP; c) Beta ERD; d) lateralised Beta ERD.*

#### **3.2.2.4. Exploratory Approach**

We further compared ‘easy’ and ‘hard’ decisions using a more exploratory analysis for both ERP and TFR data (Maris & Oostenveld, 2007). In the ERP data, a non-parametric cluster permutation test showed that there was a significant difference between the ERPs associated with ‘easy’ and ‘hard’ decisions. It revealed the presence of a cluster ( $p = .002$ ) between 228 and 1000 ms relative to the onset of coherent motion, in which the waveform associated with ‘easy’ trials built up faster and higher than the one associated with ‘hard’ trials. This cluster included a large range of electrodes, primarily over centroparietal regions (see Figure 3.5). We applied this cluster to response-locked data by averaging over the ERPs of the identified electrodes. FDR-corrected t-tests showed that ‘easy’ ERPs built up higher than ‘hard’ ERPs in 238 out of 240 time samples between -239 and 0 ms relative to the response (corrected  $p < .05$ ).

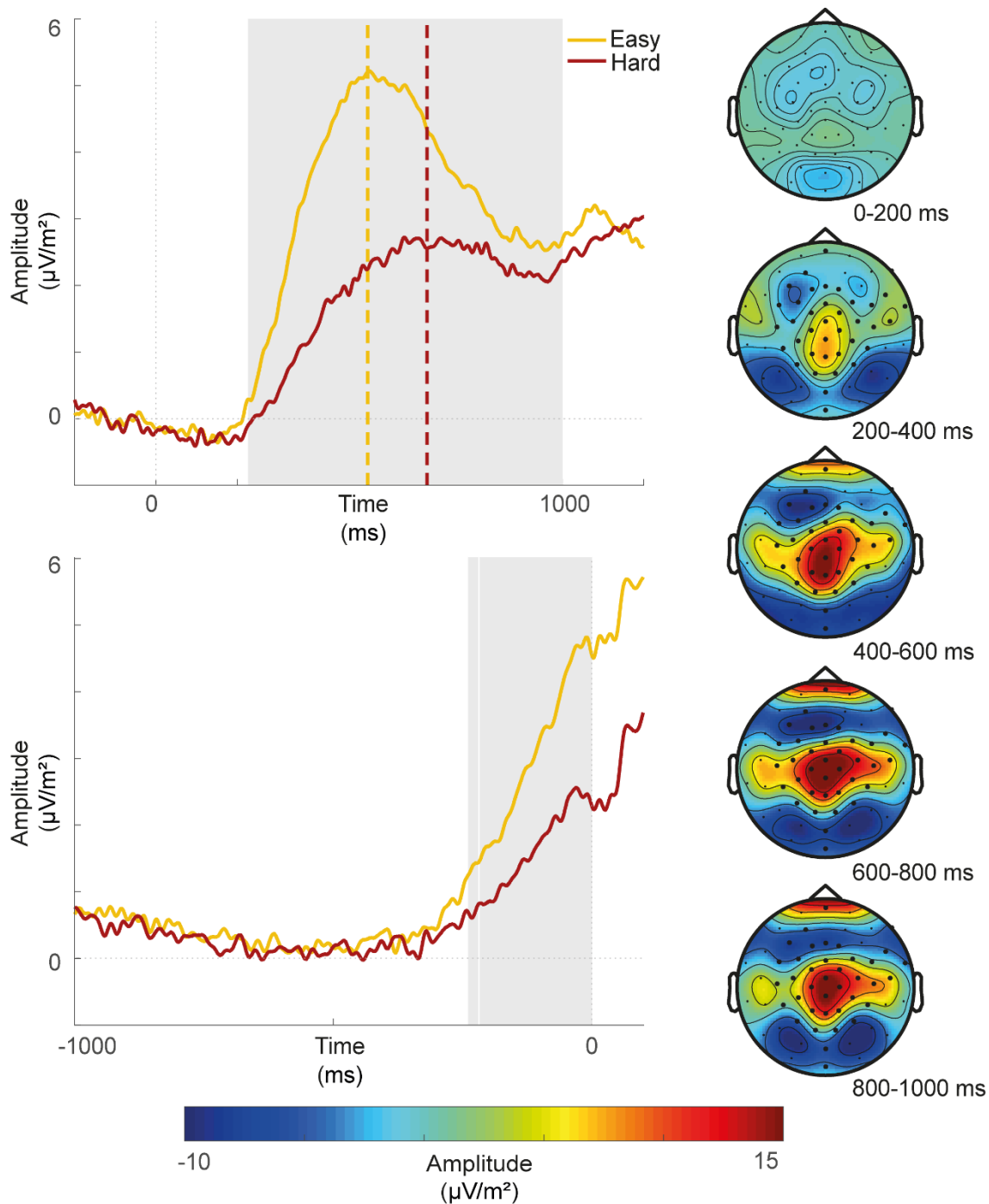


Figure 3.5: ERP cluster: Left: ERPs averaged over the identified electrodes (see topography) for stimulus-locked (top) and response-locked (bottom) data (note that the cluster permutation test was only performed on stimulus-locked data). Vertical dashed lines indicate mean RT (like in Figure 3.4, mean RT is based only on trials used to generate the waveform and slightly differs from behavioural data displayed in Figure 3.3). Shaded grey areas indicate a significant difference between 'easy' and 'hard' conditions. In the stimulus-locked data, this is based on the time samples identified in the cluster, while in the response-locked data, significance is based on a number of FDR-controlled  $t$ -tests. Right: ERP topography over time. Electrodes identified by the cluster are highlighted.

A second cluster-based permutation test was used to identify differences between 'easy' and 'hard' decisions in TFR data. Again, the test showed that there was a significant difference in the TFR data between the two difficulty levels and revealed the presence of two clusters (both  $p = .002$ ). One cluster was found between 700 and 1000 ms. Since this is a time interval in which most decisions have already been completed, we assumed that this cluster is not decision-related and discarded it from further investigation. The second cluster revealed higher power in delta and theta frequencies (2 to 7 Hz) in 'easy' compared to 'hard' trials, between 170 and 640 ms. This cluster was observed in a large range of mainly frontal and parietal electrodes (see Figure 3.6). We applied this cluster to response-locked TFR data by averaging over the frequencies and electrodes identified. FDR-corrected t-tests on this data revealed that 'easy' trials built up significantly higher than 'hard' trials during the interval of -280 to 0 ms relative to response (corrected  $p < .042$ ).

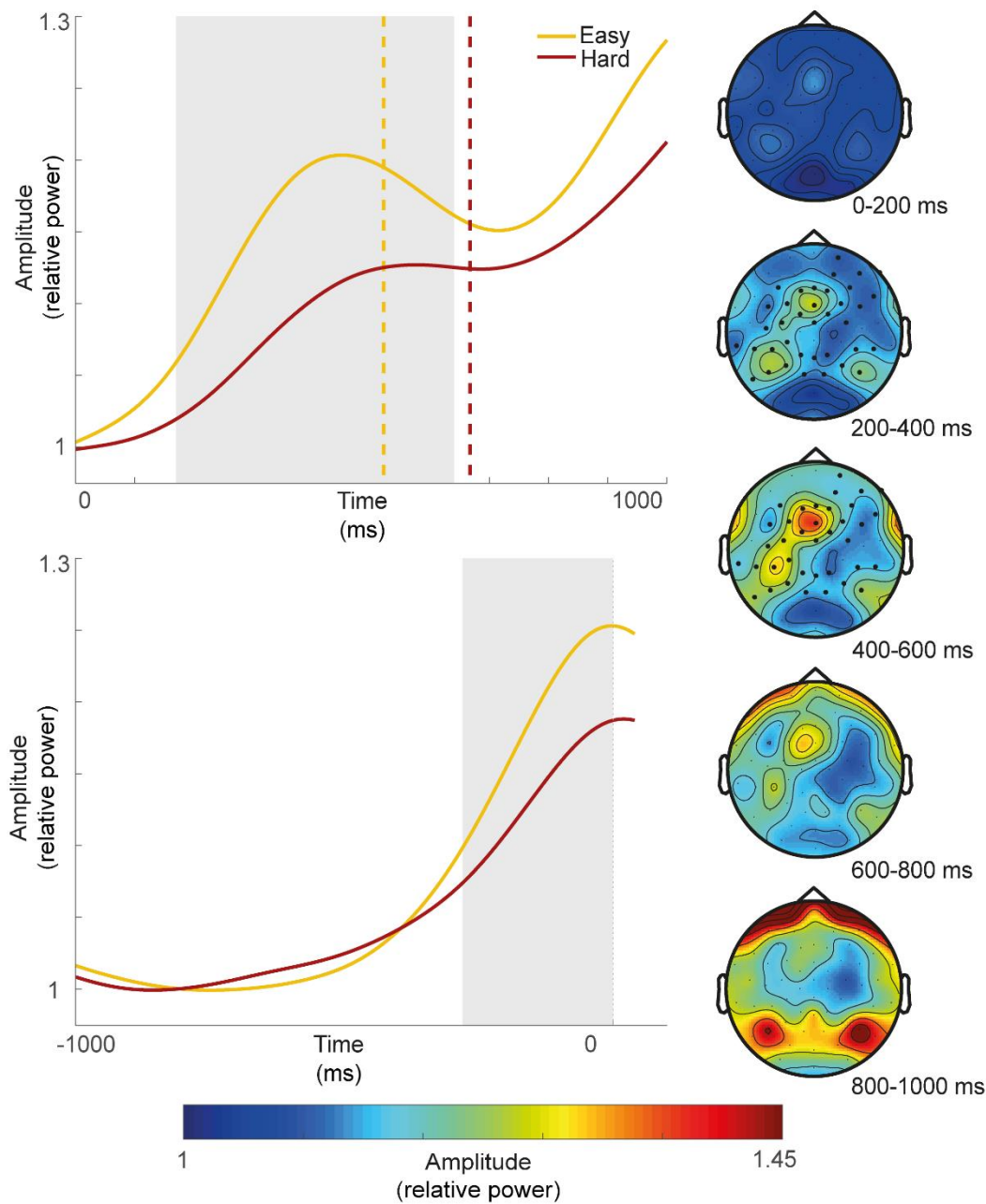


Figure 3.6: TFR cluster: Left: Spectral power averaged over the identified frequency range (2 to 7 Hz) and electrodes (see topography) for stimulus-locked (top) and response-locked (bottom) data (note that the cluster permutation test was only performed on stimulus-locked data). Vertical dashed lines indicate mean RT (like in Figure 3.4, mean RT is based only on trials used to generate the waveform and differs slightly from behavioural data displayed in Figure 3.3). Shaded grey areas indicate a significant difference between 'easy' and 'hard' conditions. In the stimulus-locked data, this is based on the time samples identified in the cluster, while in the response-locked data, significance is based on a number of FDR-controlled t-tests. Right: Topography of spectral power in the identified frequency band (2 to 7 Hz) over time. Electrodes identified by the cluster are highlighted.

### 3.3. Discussion

In this study, we set out to test different potential neural correlates of the decision variable in the human EEG. We tested the impact of a difficulty manipulation on a number of signals which have previously been suggested to display accumulation-to-bound characteristics, namely the CPP (Kelly & O'Connell, 2013; O'Connell et al., 2012), the LRP (Kelly & O'Connell, 2013; Polanía et al., 2014), and beta ERD (Donner et al., 2009; Siegel et al., 2011). Additionally, we used an exploratory approach to identify other potential difficulty-related differences.

We chose the manipulation of difficulty as it has strong effects on behavioural data, which have been studied extensively in the sequential sampling model literature and are universally accounted for by a variation in just one parameter, namely the variation of drift rate, which makes strong predictions about the profile of the accumulation process (Brown & Heathcote, 2008; Mulder et al., 2014; Ratcliff & McKoon, 2008; Voss, Nagler, & Lerche, 2013). Using two levels of difficulty ('easy', 'hard'), we expected strong behavioural differences, with 'easy' decisions leading to shorter, and more accurate decisions than 'hard' decisions. The results support this hypothesis, showing that the 'easy' condition was associated with fewer errors and RTs which were on average approximately 150 ms shorter.

Importantly, we further expected that a signal which reflects the decision variable would mirror these differences. An accumulation signal therefore has to not only build up over time and peak at the time of response, but also differ in slope between the conditions, with higher slopes (i.e. higher drift rates) in 'easy' compared to 'hard' decisions. Note that, due to the nature of EEG, we expect this difference in slope to be associated with a difference in amplitude in the stimulus-locked, but not in the response-locked data. We predict that the difference in difficulty is accounted for by a variation of only the drift rate (i.e. slope), while all other parameters are equal across conditions. This implies that the distance between the starting point of accumulation and the decision

threshold (i.e. the amplitude of the peak of each accumulation process) does not differ (given that the accumulation terminates immediately after reaching the threshold, but see below). However, in stimulus-locked EEG signals, the amplitude of the average peak is dependent on the variability of its latency across trials. Since ‘hard’ decisions are associated with longer, more variable RTs, the stimulus-locked average peak is necessarily smaller. This difference in amplitude should however disappear in the response-locked data, where, assuming a true decision variable signal, the signal is locked to the peak, removing any effects of variability in latency. In the following, we briefly re-introduced each of the suggested signals and addressed to which extent they meet these slope and amplitude expectations.

### **3.3.1. Centroparietal Positivity (CPP)**

The CPP is a centroparietal ERP component, which has been shown to display accumulation-like profiles, independently of sensory or motor processes (O’Connell et al., 2012). It has been found to display the same build-up over the course of the decision and peak at the response for both visual and auditory decisions, as well as for decisions with and without motor responses. However, its role has been questioned as it is not effector-specific, which means that it cannot predict which decision is being made (Urai & Pfeffer, 2014). The slope of the CPP has previously been shown to scale with task difficulty (Kelly & O’Connell, 2013; O’Connell et al., 2012).

In the current study, we were able to confirm this finding. As predicted for a decision variable signal, the CPP displayed the expected gradual build-up over the course of the decision, the peak of which co-occurred with the response (see Figure 3.4 a). In line with Kelly and O’Connell (2013), we found that the slope of the build-up was higher for ‘easy’ compared to ‘hard’ decisions, in both the stimulus-locked and the response-locked data. This suggests that ‘easy’ decisions are associated with a faster integration of evidence and a steeper accumulation, supporting the role of the CPP as a neural substrate of decision-making.

We further compared the amplitude of 'easy' and 'hard' trials and found that, in the stimulus-locked ERP, 'easy' trials had a larger amplitude for the majority of the decision-making process. Sequential sampling models do not predict a difference in peak amplitude, which is arguably equivalent to a difference in decision threshold and/or starting point. However, a difference in slope can, over time, lead to a separation of the signal amplitudes. Additionally, as described above, a difference in amplitude is likely to be caused by differences in RT variability between the difficulty conditions. If we assume that the build-up peaks at a stereotyped level at response, averaging waveforms over trials and participants will lead to higher means when said peaks are less variable in time. Therefore, a difference in amplitude in the stimulus-locked ERP signal is not necessarily indicative of a difference in accumulation amplitude. The response-locked ERP signal on the other hand, provides a truer reflection of the ERP amplitude at response. As predicted for a decision variable signal, there was no significant difference in amplitude between 'easy' and 'hard' conditions in the response-locked ERP.

However, although the difference was not significant, visual inspection of the waveform and uncorrected  $p$ -values contradict previous CPP studies, which found that the amplitudes of response-locked peaks of ERPs associated with different difficulties were virtually identical (Kelly & O'Connell, 2013; O'Connell et al., 2012). We suggest two explanations for this difference. Firstly, it is important to note that accumulation may continue after the threshold is reached. Once enough evidence is accumulated and the boundary is reached, a decision is made and the response is initiated. However, the stimulus only turns off when the button is pressed. This implies that there is a brief time interval between the reaching of the threshold and the press of the response button in which evidence is still being observed and potentially accumulated. Since accumulation is shown to be faster for 'easy' than for 'hard' decisions, this means that, given the same time interval, 'easy' decisions will accumulate to a higher amplitude. Since the response-locked signal is locked to the press of the button, not the reaching of the threshold, we expect a small difference and are, in fact, surprised by Kelly and O'Connell's (2013) finding of virtually identical

amplitudes, which may be specific to their experimental setup. A second, not mutually exclusive, explanation for the small difference seen in the amplitude between conditions at response, was brought up by Philiastides et al. (2014). They suggested that the distributed nature of EEG recordings in combination with the spatial averaging due to volume conduction make it highly unlikely that we would observe different accumulation signals converging to the same boundary, as observed in single-unit recordings.

Overall, the CPP displayed all of the characteristics of a decision variable outlined above. We observed a gradual build-up which peaks at the response, and is influenced by task difficulty, with 'easy' decisions leading to steeper build-up rates. Therefore, we conclude that the CPP is a potential neural substrate of the decision variable.

### **3.3.2. Lateralised Readiness Potential (LRP)**

The LRP is a motor-related ERP component associated with the lateralised part of motor preparation and is generated by subtracting ipsilateral motor cortex activity from contralateral signals. It has been suggested to correlate with decision-related accumulation (Kelly & O'Connell, 2013; Polanía et al., 2014). However, as an effector-specific motor preparation signal, it can only track accumulation for decisions associated with particular motor (usually left/right-hand) responses. The LRP has been tested in the context of difficulty manipulations and it has been shown that, similar to the CPP's, its slope is steeper (although negative) with easier decisions (Kelly & O'Connell, 2013).

In the current study, we replicate this finding only in part. We observed a significant difference in slope in the stimulus-locked signal, with higher slopes for 'easy' compared to 'hard' decisions. There was no difference in slope in the response-locked signal. This finding questions the role of the LRP as a decision variable signal, as sequential sampling models predict difficulty-related differences in slope throughout the decision-making process. However, it is

important to note that difficulty-induced slope differences are typically observed in stimulus-locked data and less visible in response-locked data.

Additionally, we tested the effects of difficulty on the amplitude of the LRP. Here, the results are similar to the CPP's. Like for the CPP, although over a shorter time period and with more variable t-values, we found differences in amplitude in the stimulus-locked data, with 'easy' decisions showing a higher amplitude than 'hard' decisions. There was no difference in amplitude between 'easy' and 'hard' conditions in the response-locked signals. Overall, the amplitude of the LRP, although somewhat noisier, is qualitatively similar to the CPP amplitudes reported above, supporting the similarities between the LRP and an accumulation signal.

Overall, the statistical findings as well as the shapes of the LRP waveforms appear very similar to those found for the CPP. However, the results are less clear, and there was no significant difference in slope between 'easy' and 'hard' trials in the response-locked data. We conclude that, although we do not rule out the possibility of the LRP displaying an accumulation-to-bound-like profile, the slight ambiguity of the findings as well as its response-dependent nature make the LRP a less appropriate neural correlate of the decision variable than the CPP.

### **3.3.3. Event-related Beta Desynchronisation**

Event-related desynchronisation in the beta frequency band is, similarly to the LRP, a signal which has been linked to the preparation of hand movements (Jasper & Penfield, 1949; Pfurtscheller, 1981; Zaepffel et al., 2013). Although studies vary in the methods used to generate the beta waveform, changes in beta power have been suggested to display characteristics of decision-related accumulation both recorded from electrodes over the contralateral motor cortex (O'Connell et al., 2012), and lateralised by subtracting ipsilateral activity from the contralateral signal (Donner et al., 2009). However, both signals are, like the LRP, dependent on motor responses. Beta power has been tested under

different difficulty manipulations previously, but the findings have been mixed. De Lange et al. (2013) found that difficulty had an impact on the slope of beta power in the response-locked signal, but not in the stimulus-locked signal, while Twomey et al. (2016) found no difficulty-induced difference in the slope of beta power.

In the current study, we found no evidence for a slope difference between 'easy' and 'hard' conditions in either the stimulus-locked or the response-locked spectral power in the beta-band, recorded contralateral to the response. We also found no slope difference in the lateralised beta power (but see below). Additionally, there was no difference in contralateral beta power amplitude between 'easy' and 'hard' conditions in either the stimulus-locked or the response-locked data. Again, no amplitude difference was observed in the lateralised part of the beta power.

In fact, we did not observe any lateralised desynchronisation in beta power. Subtracting ipsilateral activity from contralateral signals removed any change in power over time, indicating that desynchronisation recorded over the contralateral hemisphere reflects a general motor preparation, rather than an effector-specific build-up. The fact that previous research demonstrated lateralised beta desynchronisation while we only observed a general effector-non-specific desynchronisation, may be explained by our comparatively short RTs. The typical approach to explore motor-related activity in the beta frequency makes use of delayed response paradigms, in which participants select a response based on a presented stimulus, and wait for a response cue before making the appropriate movement (Kaiser, Birbaumer, & Lutzenberger, 2001; Kühn et al., 2004; Zaepffel et al., 2013). This gives participants more time (often several seconds) to prepare the response, which may be necessary to observe a clear lateralisation. Although this lateralisation has been observed in perceptual decision-making and reaction time tasks before, these studies tend to report much longer RTs than the ones we observed (de Lange et al., 2013; Twomey et al., 2016). Therefore, the duration of the motor preparation period in our experiment may be too short to observe a lateralisation of beta ERD.

Since we did not observe a lateralisation of desynchronisation in the beta frequency, we cannot comment on its characteristics as a neural correlate of a decision variable. However, it is in the nature of perceptual decisions to be quick, and sequential sampling models are designed to apply to fast decisions with RTs less than approximately 1000 ms. Therefore, the use of a neural correlate of the decision variable which can only be tracked for slow decisions is questionable.

Overall, we found no evidence to suggest that changes in spectral power in the beta band show characteristics of the decision variable. Contralateral beta power showed no modulation in amplitude or slope with varying levels of difficulty, and we were unable to generate lateralised beta ERD. Although these findings do not rule out the possibility that beta power may display characteristics of accumulation in other experimental setups, we observed no evidence to support this role in our paradigm.

### **3.3.4. Exploratory Approach**

Lastly, we employed a more exploratory approach in the form of a non-parametric cluster permutation test, in order to identify any signals which differ between 'easy' and 'hard' decisions and may reflect decision-related accumulation. In the first test, we explored temporospatial data and identified a cluster between approximately 200 ms and 1000 ms relative to the onset of coherent motion, in which both the 'easy' and the 'hard' waveform displayed a gradual build-up over the course of the decision, with 'easy' trials building up faster and higher than 'hard' trials. This cluster contained a large number of electrodes, most of which were centred around centroparietal regions. Based on the similarity in waveform and topography, it may be speculated that this cluster does in fact, at least in part, show the CPP, further supporting its role as a potential neural correlate of the decision variable. However, applying this cluster to response-locked data showed a significant difference in amplitude between 'easy' and 'hard' trials, with 'easy' trials building up to a higher peak at response. Although, as outlined above, we might expect a slight difference

between difficulty levels at response time, a large, significant difference is somewhat unexpected given that we assume the same baseline-to-threshold difference to underlie both types of decisions. Nevertheless, it is important to note the similarities between the ERP cluster and the CPP.

In the second analysis, we tested time-frequency data to identify any clusters across temporal, spatial, and spectral dimensions. The test revealed one relevant cluster in the delta/theta frequency band. Again, power in these frequencies (2 to 7 Hz) displayed a gradual build-up over the course of the decision, which was steeper and higher for 'easy' compared to 'hard' decisions. This difference was seen between approximately 200 and 650 ms, and across a range of mainly parietal and frontal electrodes. This is particularly interesting as this frequency range has been associated with accumulation previously (van Vugt et al., 2012; Wyart et al., 2012). In particular, van Vugt et al. (2012) found theta power (4 to 9 Hz) to be correlated with evidence accumulation. However, applying the cluster to response-locked TFR data showed significantly higher amplitudes in 'easy' than 'hard' trials. As in the ERP cluster, this difference questions the validity of the signal as a potential neural correlate of the decision variable. Although it does not rule out the possibility that these oscillations do in fact reflect evidence accumulation, it is clear that more research is needed in order to comment on their role as a neural correlate of decision-making.

### **3.3.5. Summary**

Overall, we tested a number of potentially decision-related signals by comparing their profiles for easy and hard decisions. Since sequential sampling models make clear predictions about accumulation to account for behavioural differences due to task difficulty, we expected a neural correlate of the decision variable to display a higher build-up rate in easy compared to hard decisions. We found no evidence for this in event-related beta desynchronisation. The LRP displayed mixed results with slope differences visible in the stimulus-locked, but not in the response-locked data, although it seems to mirror the overall shape of the CPP.

However, both beta ERD and LRP are motor-related signals, which, although roughly equivalent to more established decision-related signals in monkeys' oculomotor firing rates, is arguably a disadvantage as they can only be observed when a decision is associated with a specific hand movement. The CPP on the other hand, has been shown to be independent of the decision-response mapping (O'Connell et al., 2012). Here, we were able to further support the role of the CPP as a neural correlate of accumulation as it showed the expected differences in slope and amplitude, with easy decisions leading to steeper accumulation. Exploratory analyses of the ERP data added further support to centroparietal signals. Additionally, exploratory tests of the TFR data identified power in delta/theta bands as a potentially decision-related signal. However, more research is needed to comment on its role in accumulation.

In summary, we were not able to provide any conclusive evidence for either LRP or beta ERD to correlate with decision-related accumulation, and the evidence for motor-related signals remains mixed. However, we showed that the CPP displays the expected characteristics of the decision variable, with decision difficulty influencing the slope of the signal, supporting the notion that the CPP is a neural substrate of decision-making.

## **4. Testing the CPP as a Decision Variable Signal by Manipulating Evidence Dynamics and Biases**

Our ability to make perceptual decisions and quickly respond to sensory stimuli is a crucial aspect of human cognition, and a vast body of literature has been dedicated to the question of how we make these decisions. Although many questions are yet to be answered, there is a consensus that the way we make perceptual decisions can be described by sequential sampling models (Brown & Heathcote, 2008; Ratcliff & McKoon, 2008; Usher & McClelland, 2001). Sequential sampling models are a group of computational models which assume that, to make a decision, we accumulate sensory evidence over time, until a set decision boundary is reached, at which point we initiate the corresponding motor response.

There are several different models within this framework, which differ in a number of aspects, such as the number of accumulators, or the assumption of inhibition and leakage (Ratcliff & McKoon, 2008; Usher & McClelland, 2001), but all sequential sampling models share the fundamental assumption of accumulation-to-bound decision-making. Although sequential sampling models were developed to explain behavioural data, i.e. reaction time (RT) and accuracy data, and have done so successfully in a large variety of paradigms (Huk & Shadlen, 2005; Milosavljevic et al., 2010; Ratcliff, 2002; Ratcliff, Thapar, College, & Mckoon, 1992), more recently, several neural signals have been suggested to reflect the accumulation process described by these models.

Research in non-human primates has identified firing rates of neurons in the lateral intraparietal area (LIP), frontal eye field (FEF), and superior colliculus (SC) as potential neural substrates of a decision variable, i.e. an accumulation-to-bound profile as suggested by sequential sampling models (Gold & Shadlen, 2000, 2003; Horwitz et al., 2004; Huk & Shadlen, 2005; Roitman & Shadlen, 2002; Shadlen & Newsome, 1996, 2001; Thompson et al., 1997). Firing rates in neurons in these areas have been shown to undergo ramp-like changes over

the course of the decision, the slope of which depends on the strength of sensory evidence, and to peak at the time of response.

While neurophysiological findings in non-human primates have been advancing quickly, the identification of a neural substrate of the decision variable in the human brain has been more difficult, primarily due to restrictions of the neuroimaging techniques available. A number of studies have used functional magnetic resonance imaging (fMRI) in order to shed light on human decision-making (Heekeren et al., 2004; Kayser et al., 2010; Mulder et al., 2014; Tosoni et al., 2008). This technique has the advantage of a high spatial resolution in combination with system-level perspective, allowing it to identify whole networks. However, while fMRI designs can successfully identify areas involved in the decision-making process, the technique's low temporal resolution does not lend itself to directly tracking the fast and dynamic build-up associated with a decision variable.

Electroencephalography (EEG) and magnetoencephalography (MEG) on the other hand, have a very high temporal resolution and are therefore favourable in the identification of a neural substrate of the decision variable in the human brain. In fact, there are a number of M/EEG studies which have explored electrical brain activity during perceptual decision-making and a variety of different signals have been suggested as potentially decision-related, ranging from event-related potential (ERP) components (Philiastides et al., 2006; Philiastides & Sajda, 2006; Ratcliff et al., 2009) to changes in theta band power (van Vugt et al., 2012), and motor-related lateralised desynchronisation in beta power (Donner et al., 2009; Siegel et al., 2011).

A particularly promising approach was introduced by O'Connell et al. (2012). In a series of experiments, they identified the centroparietal positivity (CPP) as an ERP component that displays an accumulation-to-bound profile and described it as a decision variable signal. It was demonstrated that the CPP shows all properties of a decision variable that have previously been established in single-cell recordings in monkeys. It displays a build-up over the course of the decision, reflecting a cumulative function of sensory evidence. Further, this

waveform builds up at a rate which varies with the quality of the sensory evidence, and its crossing of a stereotyped level was shown to predict reaction time (Kelly & O'Connell, 2013; O'Connell et al., 2012).

Importantly, it was shown that the CPP is independent of sensory and motor signals. In a series of experiments, a rapidly flickering, continuous target detection task with a gradual target onset was used, allowing the authors to track steady-state visual evoked responses (SSVEPs) while avoiding visual evoked potentials at the onset of the stimulus, leading to clear view on decision-related signals. By adjusting the task in these ways, O'Connell et al. (2012) were able to track three different signals during the decision-making process: the SSVEPs as a readout of sensory input, the CPP as a decision variable, and contralateral beta power as a motor signal. Importantly, they were able to fully dissociate these signals, showing that only the CPP is a valid decision-making signal, and demonstrating that it is independent of decision-unrelated sensory input or motor responses. In fact, in a later study which directly compared the CPP with motor-related beta power, it was shown that while both signals build up over the course of the decision, the CPP drops back to baseline levels after a given boundary is reached, while beta activity persisted until a delayed response. Importantly, the study also demonstrated that without foreknowledge of the stimulus-effector mapping, beta activity is eliminated while the CPP remains unchanged, further supporting the role of the CPP as an abstract decision signal, dissociated from response specific signals (Twomey et al., 2016). Interestingly, the CPP was also observed in an auditory decision-making task, leading the authors to suggest that it is a supramodal decision variable signal (O'Connell et al., 2012).

However, studies validating the CPP's role as a decision variable remain scarce. In particular, its relation to sequential sampling models is not well-established. Although the CPP has undergone several statistical tests to analyse whether it shows the conceptual characteristics of a decision variable, few attempts have been made to directly compare its profile to model predictions. Kelly and O'Connell (2013) used a sequential sampling model labelled the Diffusion model (Ratcliff & McKoon, 2008) to account for

behavioural decision-making data, and found that, in an experiment with different levels of difficulty, RT data was accounted for by a model with a varying drift rate parameter. This means that just like the CPP, which shows an increased slope with decreased task difficulty, the model fits also indicate a varying slope (i.e. varying drift rate) across difficulty conditions. However, no further parallels between the model and the EEG data were drawn. Twomey et al. (2015) fitted the same model, a Diffusion model with varying drift rates for varying difficulty levels, to a separate data set, but added a further step to their analysis to allow for a comparison between the model and the CPP. After fitting the Diffusion model, Twomey and colleagues used the resulting parameters to simulate the mean accumulation, as predicted by the model. They found that the simulated accumulation profile and the CPP shared key characteristics, as in both profiles, the slope varied with task difficulty, and a stereotyped level was reached before the response. This finding is important as it goes beyond comparing a potential neural substrate of decision-making against a set of conceptual characteristics and instead allows for a direct comparison of the entire accumulation profile. This is particularly crucial as with increasing complexity of sequential sampling models (e.g. by introducing inhibition or leakage; Usher & McClelland, 2001), it becomes virtually impossible to make conceptual predictions about how accumulation profiles may change as a function of different manipulations.

The current study therefore set out to further explore the CPP in the light of sequential sampling models. As outlined above, to date, the CPP has only been tested in the context of a limited number of manipulations, with most studies focusing on task difficulty (Kelly & O'Connell, 2013; Twomey et al., 2015), and only the manipulation of decision difficulty has been compared to simulations based on sequential sampling model fits. We therefore aimed to build on Twomey et al.'s (2015) approach to compare the CPP profile to model predictions under a variety of manipulations affecting the accumulation profile.

To this end, we used two sets of manipulations which affect decision-making, namely decision biases, which, to our knowledge, have not been previously tested using the CPP, and non-stationary evidence, and fitted a sequential

sampling model to the resulting RT data. We then used the estimated parameter values to simulate the accumulation profiles as predicted by the model and compared them to the CPP, which was recorded during the decision-making process. To do so, we chose an accumulator model to fit the behavioural data (Brown & Heathcote, 2008; Heathcote & Love, 2012). There are two main groups of sequential sampling models, namely accumulator models with an absolute stopping rule and random walk models with a relative stopping rule (Smith & Ratcliff, 2004). Random walk models assume that all evidence within a binary choice is integrated in a single accumulator. This accumulator has a decision boundary to either side of the starting point, each associated with a given response alternative, and the accumulation profile has a positive or negative mean slope (drift rate), depending on which alternative is receiving more evidence. Although random walk models have been shown to provide good fits to behavioural data in a number of paradigms (Ratcliff et al., 2004; Ratcliff, Perea, Colangelo, & Buchanan, 2004; Thapar, Ratcliff, & McKoon, 2003), they have also received criticism as they are challenging to generalise to choices with more than two alternatives, and, importantly, are motivated more by mathematical optimality than neurobiological plausibility (Ratcliff et al., 2016; Usher & McClelland, 2001). Accumulator models, on the other hand, assume that evidence for each response alternative is integrated in separate accumulators, which race to reach a common threshold. It is conceivable that processes similar to these occur in the brain, with each accumulator being associated with a neural population, integrating information fed forward by sensory areas.

Since we aim to compare model predictions to neural signals, we chose an accumulator model as a neurophysiologically plausible way to model our data. Specifically, we chose a race model, which, on one hand, requires a minimal number of assumptions (as compared to models which, for example, assume leakage over time; Usher & McClelland, 2001), while on the other hand, remaining biologically plausible (as compared to simplified models which, for example, assume integration without noise; Brown & Heathcote, 2008). Given the nature of EEG, which records the sum of all underlying electrical activity

from the scalp, we assume that the CPP is best predicted by the summed activity of all accumulators in a race model<sup>10</sup>.

We fitted this model to behavioural data from two experiments and predicted the associated accumulation profile using the estimated parameters. The predicted accumulation was then used to evaluate the associated CPP waveform.

This approach of directly comparing the CPP with the model prediction drawn from the behavioural decision-making data allowed us to evaluate the role of the CPP as a neural correlate of the decision variable.

## **4.1. Experiment 1: Non-stationary Evidence**

The first experiment set out to explore the effects of non-stationary evidence on the CPP. Most research in the field of perceptual decision-making has focused on binary choices with stationary evidence, where a choice is based on fixed information which remains virtually unchanged in quality and intensity throughout the decision-making process (Gold & Shadlen, 2000; Kelly & O’Connell, 2013; Ratcliff & McKoon, 2008; Ratcliff et al., 2010). While these comparatively simple decisions are associated with a range of practical advantages and have led to numerous insights into decision-making, decisions we make every day typically occur in a dynamic environment, in which sensory evidence is continuously changing. Recently, studies have drawn attention to the fact that a comprehensive model of decision-making has to be able to account for decisions with non-stationary evidence.

Researchers have hence started to use decisions in response to non-stationary evidence in order to distinguish between different sequential sampling models

---

<sup>10</sup> In the course of our research, we explored various models with a view to a model comparison. However, this work is ongoing. We therefore chose the model we deemed most suitable, i.e. the race model, as a representative of sequential sampling models overall and will discuss our findings in the context of this framework, rather than a specific model (but see section 4.3).

(Nunes & Gurney, 2016; Tsetsos et al., 2011; Zhou, Wong-Lin, & Philip, 2009), which often offer indistinguishable accounts of data from traditional decision-making paradigms (Brown & Heathcote, 2008; Ratcliff & Smith, 2004; Teodorescu & Usher, 2013). For example, Tsetsos et al. (2011) used a paradigm in which the evidence for a given alternative changed dynamically throughout a trial to compare accumulator (Brown & Heathcote, 2008; Usher & McClelland, 2001) and random-walk models (Ratcliff & McKoon, 2008), supporting the accumulator model as a suitable account of the data.

Similarly, Holmes, Trueblood, and Heathcote (2016) used dynamically changing evidence to explore different models. Participants were asked to discriminate between left and right motion in a random dot motion task, in which, halfway through the decision-making process, the motion direction switched. Findings showed that switch effects were only seen in trials with long RTs, suggesting that participants react to the switch in motion, but do so with a delay. In order to explore the underlying mechanisms of these behavioural findings, a number of variations of a simplified accumulator model labelled the linear ballistic accumulator (LBA) model, incorporating different assumptions regarding the implications of the switch in evidence, were compared. It was found that a version of the LBA, labelled 'piecewise LBA', provided the best account of the data. It was shown that the difference in accumulation rates between two accumulators (one for each alternative) was larger after the motion switch than before, indicating that the discrimination between motion directions improved after the switch. This was a surprising finding, as the switch in evidence led to motion in the opposite direction but equal in magnitude. The model also confirmed the presence of a delay between the switch in evidence and its integration, and found no evidence for increased response caution.

Dynamically changing evidence also has implications for any neural signals which claim to reflect the accumulation of evidence towards a threshold. For a signal to be validated as a decision variable signal, a modification of sensory evidence must not only lead to a change in the signal's profile to show that the signal is decision-related, but also continue to affect the signal for a prolonged period of time, to demonstrate that the signal is not a mere reflection of sensory

encoding. To date, there is little research to test the range of neural signals which have been suggested to reflect the decision variable under these conditions.

An exception is the firing rate of LIP neurons in non-human primates. Huk and Shadlen (2005) recorded single-cell activity while monkeys performed a saccadic random dot motion task. In two thirds of the trials, 100 ms pulses of motion in either the same or the opposite direction of the overall trial motion were added. It was demonstrated that these added motion pulses had persistent effects not only on the behavioural choices, but also on LIP activity, which increased/decreased with positive/negative motion pulses and remained altered for several hundreds of milliseconds. The authors concluded that LIP neuronal firing rates represent the temporal integration of motion evidence.

There is also some evidence to suggest that dynamic evidence influences the profile of neural correlates of decision-making in the human EEG, such as motor-related beta band power and the CPP (O'Connell et al., 2012). In a detection task, participants were presented with stimuli which gradually decreased in contrast and instructed to respond when the fading was perceived. When this gradual decrease was interrupted by a 450 ms increase towards the baseline, before continuing the reduction of contrast, participants demonstrated longer RTs, but no difference in accuracy (note that a free response task with no pressure to respond under uncertainty was used). Importantly, the CPP (and, to a lesser extent, beta power) was shown to be sensitive to this manipulation, as following the perturbation, the stereotypical build-up was interrupted and plateaued for several hundreds of milliseconds before continuing, further supporting its role as a decision variable.

However, the data were not fitted using a sequential sampling model and no comparisons were made between potential accumulation profile simulations and the recorded CPP waveform. Although it is conceptually reasonable to assume that sequential sampling models would predict a dip in accumulation, similar to the one observed in the CPP, the complexity of these models makes it difficult to predict the timescale and shape of this perturbation. We therefore argue that

it is necessary to compare the CPP profile directly to simulations of sequential sampling in order to evaluate its role as a neural substrate of decision-making.

To this end, we presented participants with a random dot motion task which required them to discriminate between motion to the left and right, while recording their EEG. Since difficulty is a more established manipulation (see Chapter 3), the task involved an ‘easy’ and a ‘hard’ condition. In one third of the trials, the motion remained unchanged throughout the trial (‘continuous’ condition), while in another third of the trials, the motion was interrupted by motion in the opposite direction for 200 ms before continuing in the original direction (‘reverse’ condition). Additionally, we added a third condition in which the motion in a given direction was interrupted by random motion without any directional evidence (‘stop’ condition). We hypothesised that these different perturbations would lead to different CPP waveforms, and that using sequential sampling models to simulate accumulation profiles would allow us to compare the signal patterns and thereby evaluate the role of the CPP as a decision-variable signal. Specifically, we expected that a ‘stop’ in evidence would also lead to a stop in the build-up of the accumulation profile, and thereby a plateau in any neural signal which reflects the decision variable, which is clearly distinguishable from accumulation in ‘continuous’ trials. Although the prediction regarding the impact of a reversal of evidence on the accumulation profile is less clear, we hypothesised that it would differ from the profile observed in the ‘stop’ condition. Since the true accumulation profiles of each condition are difficult to predict conceptually, we use a race model to directly compare modelled accumulation profiles with observed EEG patterns in order to evaluate the potential role of the CPP as a neural correlate of the decision variable.

### **4.1.1. Methods**

#### **4.1.1.1. Participants**

For this study, a total of 21 participants (eight males) with a mean age of 27.33 ( $SD = 8.66$ ) were recruited. To ensure a reasonable and distinguishable task performance at two different difficulty levels, each participant completed a

staircase procedure to establish the appropriate level of difficulty, i.e. level of coherence, for 'easy' and 'hard' trials (see section 4.1.1.2). In line with criteria defined prior to data collection, participants were excluded from the experiment if the calibrated level of coherence exceeded 98% for the 'easy' condition.

Based on this criterion, one participant did not continue to the main experiment, leading to a sample of 20 participants (seven males) with a mean age of 27.55 ( $SD = 8.83$ ). Each remaining participant took part in a single two-hour session.

Participants were recruited using poster advertisements and word of mouth.

Two of the participants were researchers in the current study. All other participants were paid £8 per hour. The experiment was approved by the City, University of London Psychology Department Ethics Committee.

#### **4.1.1.2. Stimuli and Procedure**

Participants were asked to complete a random dot motion task. The task was written in Matlab (The Mathworks, Natick, U.S.A.), making use of Psychtoolbox functions (Brainard, 1997; Kleiner et al., 2007; Pelli, 1997). In this task, an array of white dots was presented on a black screen. A proportion of dots moved coherently either to the left or to the right, while the rest of the dots moved in random directions. Participants were instructed to indicate the perceived motion direction by pressing a button in their right/left hand for movement to the right/left. For this, digital response buttons interfaced via a 16 bit A/D card (National Instruments X-series PCIe-6323, sample rate 100,000 Hz) were held between the thumb and index finger of each hand. Participants were seated 100 cm away from a cathode ray tube screen (size: 41 x 30 cm), operating at a refresh rate of 85 Hz and a resolution of 1240 x 786. A total of 300 dots, 0.04 x 0.04 degrees visual angle (dva) in size, were presented within a 5 dva circular aperture. All dot movement occurred at a speed of 3.3 dva per second. The proportion of dots determining the motion direction moved either to the left or to the right, depending on the trial, while the rest of the dots moved in a direction which was randomly selected for each dot and each frame. The position of all dots was randomised every five frames. Each trial began with a central fixation cross (size: 0.33 x 0.33 dva) for 500 ms (plus a jitter of up to 1000 ms, drawn from a uniform distribution), followed by a period of random motion (1000 ms

plus a jitter of up to 1500 ms, drawn from a gamma distribution with shape parameter 1 and scaling parameter 150<sup>11</sup>). Since the onset of moving dots on the screen is likely to produce a visual evoked potential which would interfere with the recording of the CPP, this period of random motion was introduced to allow for the evoked potential to occur before the onset of the decision-making process. The random motion was followed by the onset of coherent motion (left/right) which continued for up to 2000 ms or until the response (see Figure 4.1).

Participants completed a minimum of 100 practice trials at high levels of coherence (i.e. > 80% of dots moving in one direction) to familiarise themselves with the task. In order to calibrate suitable levels of difficulty for 'easy' and 'hard' trials for each participant individually, a further 100 trials were completed in which the QUEST (Watson & Pelli, 1983) staircase procedure, implemented in Psychtoolbox, estimated the coherence level at which each participant responded correctly in 80% of trials. This coherence level was then used for the 'hard' condition. The 'easy' coherence level was set as 150% of the 'hard' coherence level. Participants had 1300 ms to respond, and no feedback was provided during staircase trials. Overall, the appropriate difficulty levels estimated for the remaining participants resulted in a mean of 27.70% ( $SD = 14.74$ ) coherence for 'hard', and 40.15% ( $SD = 22.15$ ) for 'easy' trials.

After the staircase procedure, participants were asked to complete a further 100 practice trials which included all conditions of the main experiment, including the different difficulties and evidence interruptions (see below). During this training, participants were given feedback in the form of their mean accuracy and RT every 10 trials. Participants were instructed to aim for a mean accuracy of at least 80% and a mean RT of less than 1000 ms.

In the main experiment, in addition to the manipulation of difficulty, we also manipulated the continuity of the evidence by introducing three motion

---

<sup>11</sup> A gamma distributed fore period with a shape parameter of 1 was chosen as it is associated with a uniform hazard function (Luce, 1986).

conditions (see Figure 4.1). One third of the trials, like the practice and staircase trials, were 'continuous' trials, i.e. the coherent motion began after a period of random motion and remained throughout the trial. In the 'stop' condition, the coherent motion was interrupted 200 ms after motion onset and replaced by a 200 ms period of random motion, before being reinstated. Similarly, in the 'reverse' condition, the coherent motion was interrupted for the same time, but replaced by coherent motion in the opposite direction (see Figure 4.1). Informal questioning of participants indicated that these interruptions were not perceived consciously. During the main task, the interruption condition ('continuous', 'stop', or 'reverse'), motion direction (left or right) and coherence level ('easy' or 'hard') varied randomly from trial to trial. Each participant completed 16 blocks of 60 trials. After each block, participants were given feedback in the form of their mean accuracy and RT. No feedback was provided for individual trials.

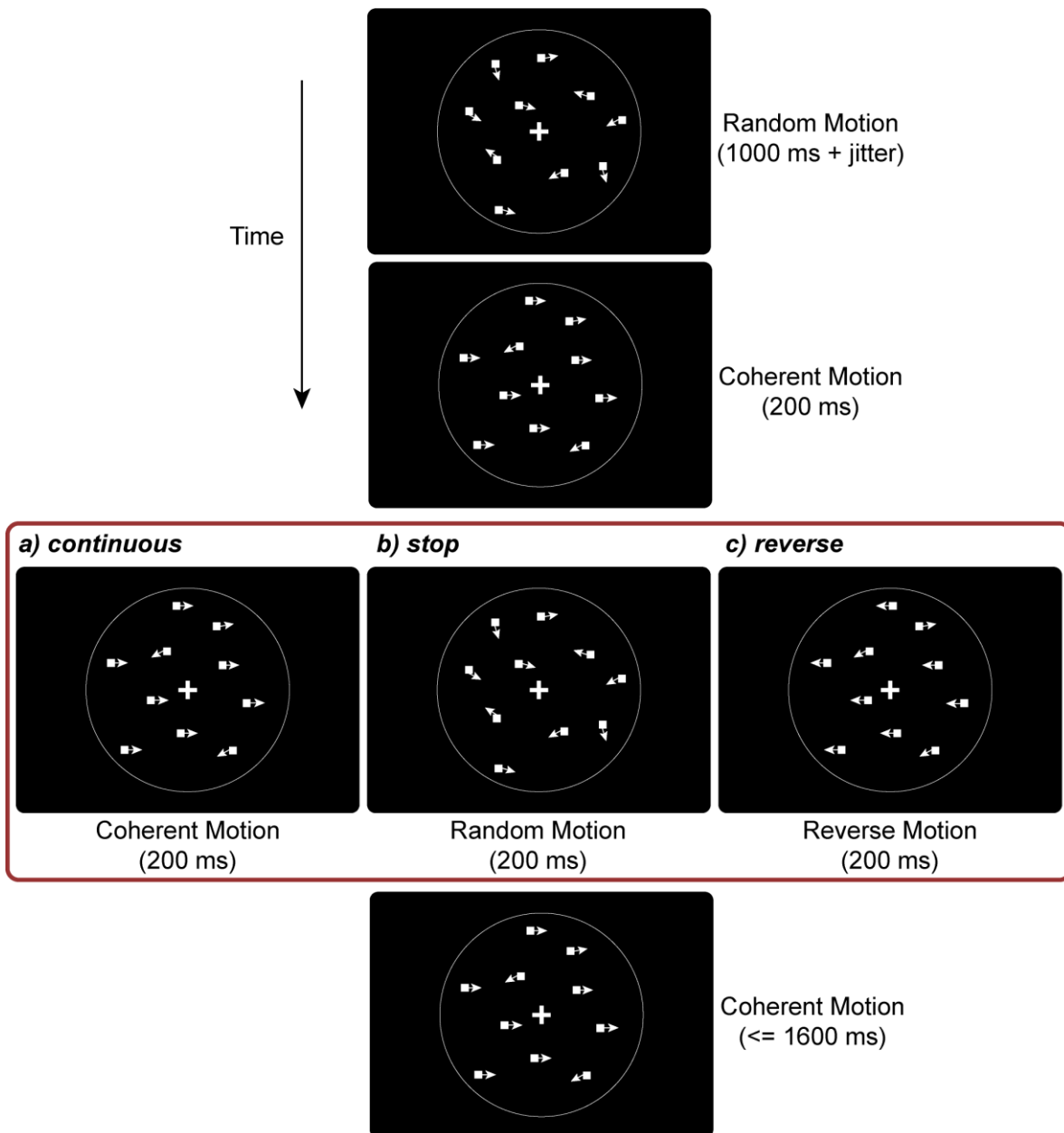


Figure 4.1: Experiment 1 random dot motion task trial procedure: each trial began with a period of random motion, followed by coherent motion (here: direction: right; coherence: 70%, i.e. 70% of dots move to the right, while 30% of the dots move in random directions). a) In the 'continuous' condition, the motion continued unchanged; b) in the 'stop' condition, the coherent motion was interrupted after 200 ms, and replaced with random motion (coherence: 0%) for a further 200 ms, before continuing in the original direction; c) in the 'reverse' condition, the coherent motion was interrupted after 200 ms and replaced by motion of equal strength in the opposite direction (here: direction: left; coherence: 70%) for a further 200 ms, before continuing in the original direction. Note that the size and number of dots have been adjusted for illustration.

#### 4.1.1.3. EEG Recording and Pre-processing

During the task, we recorded participants' EEG using 64 active electrodes, placed equidistantly on the scalp (EasyCap, M10 Montage) and referenced to the right mastoid. Data were recorded through a BrainAmp amplifier

(BrainProducts) and band-pass filtered from 0.016 to 1000 Hz (sampling rate: 1000 Hz).

The data were pre-processed in Matlab (The Mathworks, Natick, U.S.A.), using custom scripts and implementing functions from the EEGLAB toolbox (Delorme & Makeig, 2004). Data were re-referenced to the average reference and band-pass filtered from 0.1 (low cut-off) to 45 Hz (high cut-off), using a Hamming windowed finite impulse response filter. We then visually inspected the data to remove noisy channels and reject large artifacts, before applying independent component analysis to correct for eye blinks. Afterwards, the data was visually inspected a second time in order to manually remove any remaining noise. Lastly, we used spherical spline interpolation to reconstruct any channels that were previously removed. In line with the procedures used in previous CPP studies (Kelly & O'Connell, 2013; O'Connell et al., 2012), the data were converted to current source density (CSD) estimates to increase spatial selectivity. The CSD transformation was applied using the CSD toolbox, which uses a spherical spline algorithm, with the spline interpolation constant  $m$  set to its default value ( $m = 4$ ; Kayser & Tenke, 2006).

#### 4.1.1.3.1. *ERP Analysis*

For the ERP analysis, we extracted both stimulus-locked (-200 to 2000 ms, relative to motion onset) and response-locked (-1000 to 100 ms, relative to the button press) epochs. All epochs were baseline corrected to the average over a 200 ms period preceding the motion onset. Since we assumed no difference in decision-making depending on the direction of motion, we collapsed over 'left' and 'right' decisions. However, simply averaging over right/left-hand responses would remove any visible lateralisation of activity. Therefore, activity recorded in trials in which a right-hand response was given was mirrored along the midline, so that all contralateral activity was projected onto the right hemisphere (i.e. activity recorded in electrodes on the left hemisphere is now associated with electrodes on the right hemisphere). Although this step was not strictly necessary to analyse the CPP, which is recorded from the midline, this mirroring allows for a better visualisation of activation across the scalp.

The appropriate electrode to generate the CPP waveform was chosen individually, by visually inspecting each participant's averaged ERP topography to identify the centroparietal region of maximum amplitude (chosen electrodes: 1, 5, or 14, roughly equivalent to electrodes Cz, CPz, and Pz in the 10-20 system; see Figure 4.5). The activity in the selected electrodes was averaged for each condition and for stimulus and response-locked signals separately. Lastly, error trials were removed from the ERPs.

#### **4.1.1.4. Statistical Analysis**

In order to test the effects of the difficulty and interruption manipulations on the ERP, we explored both the slopes and the amplitudes of the waveforms. First, we compared the slopes between the different conditions by fitting a straight line to the CPP for each participant and each condition and measuring its slope. The resulting slopes were then compared in an 'Interruption' ('continuous', 'stop', 'reverse') x 'Difficulty' ('easy', 'hard') repeated-measures ANOVA.

We compared slopes during two different time intervals in the stimulus-locked data: an early interval between 100 and 300 ms and a late interval between 300 and 500 ms relative to the onset of coherent motion. Given the interruption interval of 200 to 400 ms and the assumption of a small lag between stimulus presentation and accumulation, we assume that the early interval reflects accumulation mainly before the interruption and the late interval reflects accumulation mainly during the interruption. In the response-locked data, it is not possible to make the distinction between interruption intervals, so we only explored one time interval and followed Kelly and O'Connell's (2013) recommendation of a -250 ms to -100 ms interval.

Additionally, we analysed the impact of difficulty and interruption on the amplitude of the waveform. Between 0 and 1000 ms in the stimulus-locked data, and between -1000 to 0 ms in the response-locked data, we compared conditions using an 'Interruption' ('continuous', 'stop', 'reverse') x 'Difficulty' ('easy', 'hard') ANOVA at each time point. The results were controlled for

multiple comparisons using the false discovery rate (FDR) approach (Benjamini & Hochberg, 1995)<sup>12</sup>.

#### 4.1.1.5. Model Fit

To model the behavioural data, we used a race model which is, at least conceptually, one of the simplest sequential sampling models (Brown & Heathcote, 2008; Usher & McClelland, 2001; see Figure 4.2). In this model, evidence for each response alternative is integrated in an independent accumulator. In a binary choice like the one in our experiment, evidence is integrated in two accumulators, which race towards the decision threshold. The evidence strength at which accumulation starts is drawn from a uniform distribution between 0 and  $S_z$  (to represent bias). At each point in time, a given accumulator  $m$  accumulates the input evidence  $I_m$  supporting alternative 'M', as well as noise  $N$ , drawn from a normal distribution with mean 0 and standard deviation  $\sigma$ , so that the quantity accumulated at each time point is described by

$$dx_m = I_m + N(0, \sigma^2) \quad (4.1.)$$

To remain physiologically plausible, this accumulation process is restricted to positive values at each time step:

$$x_m(t + 1) = \max(0, x_m(t) + dx_m) \quad (4.2.)$$

Once either of the accumulators reaches the threshold  $A$ , the decision is made and the corresponding response is initiated. The time taken to reach the threshold, in addition to a non-decision time which represents any time taken for sensory and motor processes before and after the accumulation process respectively, defines the modelled RT. The non-decision time is drawn from a uniform distribution with width  $S_{Ter}$ , centred on  $T_{er}$ .

This results in a standard race model for binary choices with seven parameters: the starting point distribution parameter  $S_z$ , mean drift rates for the correct and

---

<sup>12</sup> In this procedure, the uncorrected  $p$ -values are sorted from lowest to highest ( $p_i$  refers to the  $i$ th lowest value out of  $m$  total  $p$ -values). The largest  $i$  for which  $p_i < \left(\frac{i}{m}\right) \alpha$  is identified and all  $p$ -values associated with  $i$ s smaller or equal to the identified  $i$  are considered significant.

incorrect accumulators,  $v_{correct}$  and  $v_{incorrect}$ , the threshold  $A$ , the non-decision time  $T_{er}$  and its distribution  $S_{T_{er}}$ , and the diffusion constant  $\sigma^2$ . However, one parameter is chosen as a scaling parameter and fixed to an arbitrary value (i.e. changing its value will lead to a change in the value of all parameters but not in their relation to each other and therefore will not affect the model fits) leading to a standard model with only six free parameters.

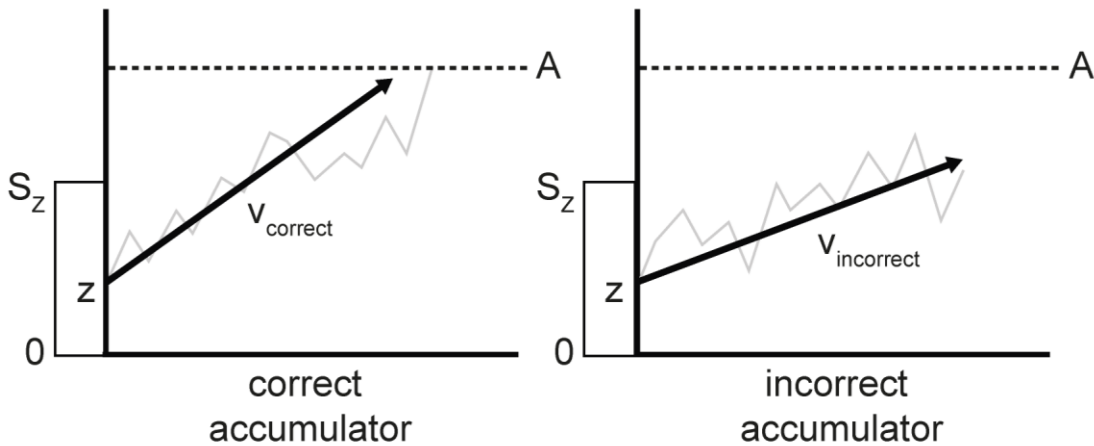


Figure 4.2: Race model: in a binary choice, there are two accumulators, each associated with one response alternative (correct/incorrect). In each accumulator, accumulation traces begin at a starting point drawn from a uniform distribution between 0 and  $S_z$  and race towards the threshold  $A$ . The accumulation profile of each accumulator is defined by the associated drift rate  $v$  and added noise, defined by the diffusion constant  $\sigma^2$ . The time taken for the first accumulator to reach the threshold, in addition to a non-decision time  $T_{er}$ , defines the response time.

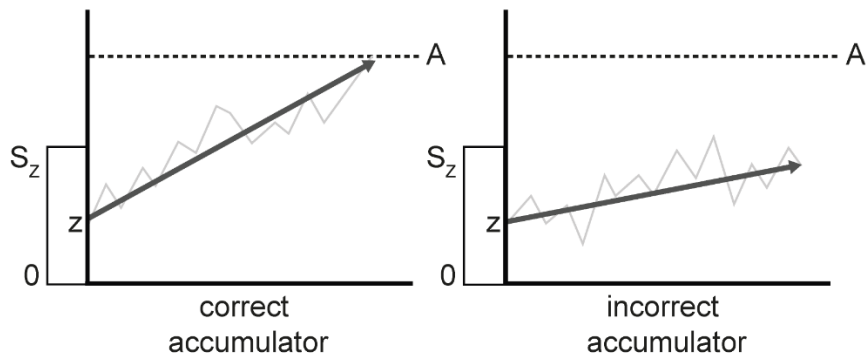
To apply this model to the current experiment, we tested two models, both of which assume that with dynamically changing evidence, only drift rates change during the interruption interval (200 to 400 ms relative to the decision onset; see Figure 4.3). In both models, the response threshold  $A$  was chosen as the scaling parameter and fixed to 1.

Model 1 consisted of a total of eight parameters and assumed that the given drift rates  $v_{correct}$  and  $v_{incorrect}$  begin to accumulate and continue throughout the trial in ‘continuous’ trials. In ‘stop’ trials, the evidence becomes random during the interruption interval and we assume that only noise is accumulated during this period, (i.e.  $v_{stop_{correct}} = v_{stop_{incorrect}} = v_{incorrect}$ ), before returning to the starting drift rates ( $v_{correct}$  and  $v_{incorrect}$ ). In the ‘reverse’ condition, the evidence changes direction during the interruption interval, but remains at its original strength, which may lead to a reversal of drift rates, i.e.  $v_{reverse_{correct}} = v_{incorrect}$ ,

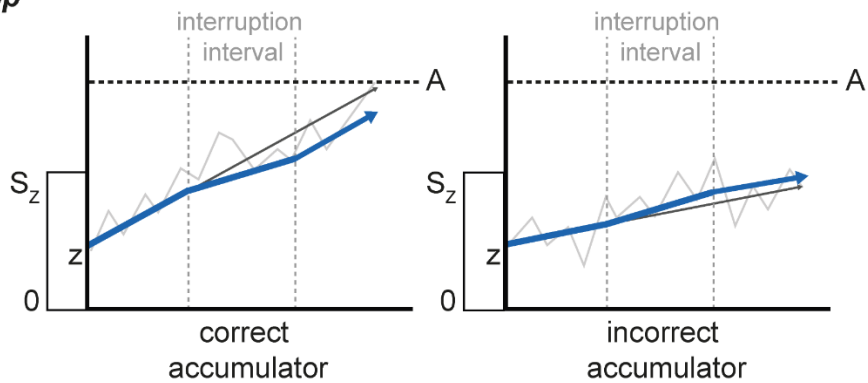
$v\text{-reverse}_{incorrect} = v_{correct}$ , before returning to the starting drift rates ( $v_{correct}$  and  $v_{incorrect}$ ). This describes a model with only four drift rates ( $v_{correct}$  and  $v_{incorrect}$  for both easy and hard decisions), as well as the parameters  $S_z$ ,  $T_{er}$ ,  $S_{Ter}$ , and  $\sigma^2$  which were fixed between conditions (see Table 4.1).

Model 2 did not assume a symmetrical change in drift rates with changing evidence as described above (see Figure 4.3). Instead, we estimated a new set of drift rates for the 'stop' and 'reverse' intervals, leading to a total of 12 drift rates (for each difficulty condition:  $v\text{-continuous}_{correct}$ ,  $v\text{-continuous}_{incorrect}$ ,  $v\text{-stop}_{correct}$ ,  $v\text{-stop}_{incorrect}$ ,  $v\text{-reverse}_{correct}$ ,  $v\text{-reverse}_{incorrect}$ ). All other parameters ( $S_z$ ,  $T_{er}$ ,  $S_{Ter}$ ,  $\sigma^2$ ) were fixed between conditions, resulting in a model with a total of 16 free parameters (see Table 4.1).

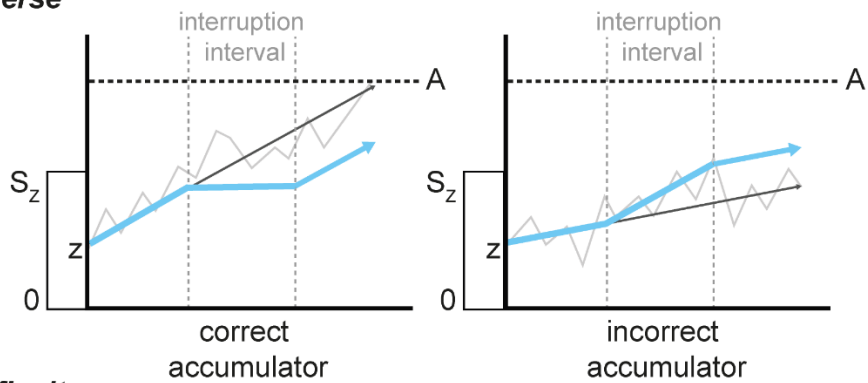
**a) continuous**



**b) stop**



**c) reverse**



**d) difficulty**

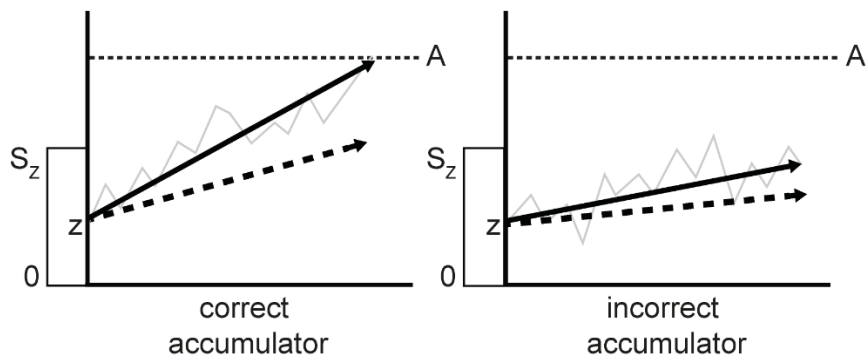


Figure 4.3: Race model applied to interruption and difficulty conditions: visualisation of the concepts used in Model 2 (Model 1 only differs in the slopes during the interruption periods). a) in the 'continuous' conditions, a single drift rate per accumulator is continuous throughout the trial; b) in the 'stop' condition, new drift rates are estimated for the interruption period, which will arguably lead to lower drift rates in the correct accumulator; c) in the 'reverse' condition, like in the 'stop' condition, new drift rates are estimated for the duration of the interruption, arguably leading to a decrease in the correct and an increase in the incorrect drift rate; d) the manipulation of difficulty is assumed to affect the slope of the accumulation throughout the trial, with 'easy' trials (solid lines) associated with higher drift rates than 'hard' ones (dashed

*lines). The effects of difficulty, although displayed separately here, affect all interruption conditions. Note that, since the drift rates during the interruption periods in both 'stop' (b) and 'reverse' (c) conditions are free to vary, their slopes are set to arbitrary values for illustration only and should not be directly compared based on this figure.*

In line with approaches employed in previous studies (Dmochowski & Norcia, 2015; Twomey et al., 2015), individual RTs were pooled across participants to determine the best-fitting model parameters at the group level to fit each model to our data. Trials with RTs faster than 180 ms or slower than 2000 ms (less than 3%) were discarded. Modelled RTs were simulated based on the equations described above and compared to RT data using Quantile Maximum Probability Estimation (Heathcote et al., 2002). Parameter values were adjusted using a differential evolution algorithm implemented in Matlab (The Mathworks, Natick, U.S.A.; Price et al., 2005).

We compared the goodness of fit of the two models by calculating the Bayesian information criterion (BIC, Schwarz, 1978) as well as the Akaike information criterion (AIC; Akaike, 1977). These measures take into account the likelihood of the model but also penalise a model for the number of parameters used in order to resolve the problem of overfitting. The model which best fitted the data according to these measures was then used to generate predictions of the accumulation profile.

#### **4.1.1.6. Model Prediction**

Since EEG recordings reflect the summation of neural activity in a given area, we assumed that, if the CPP is a neural correlate of the decision variable, it represents the sum of all evidence accumulation. Although a binary choice may recruit separate neural populations to accumulate evidence, these neural populations would likely be in close proximity. An ERP component recorded at the scalp over these neural populations measures the summation of electrical activity and therefore the sum of both accumulation processes. In order to compare the model prediction to the CPP, we therefore considered the sum of the correct and incorrect accumulation profiles of correct choices.

Based on the model equations described above, a total of 20,000 accumulation paths (in 10 ms time steps) were computed for each condition. To account for sensory processes, accumulation started after a sensory delay (fixed to 50% of  $T_{er}$ ). Evidence was then accumulated until the response threshold and continued to be accumulated for a short period after the boundary was reached to account for motor processes (50% of  $T_{er}$ ; note that we assume that accumulation continues until the offset of the stimulus, i.e. during the time to reach the threshold plus the time taken to make the motor response and stop the stimulus).

To match with EEG processing, the 'sum of accumulations' signal was baseline corrected by subtracting the first data point value from the whole trial. Finally, we averaged accumulation signals in each condition, once locked to the estimated onset of the decision process (stimulus-locked) and once locked to the response (response-locked). Since the stimulus-locked signal includes varying time spans of post-decision stages, and we can only speculate about the behaviour of the accumulator after the response, we removed simulated trials from averaging after the response (i.e. after the crossing of the threshold plus 50%  $T_{er}$ ).

To compare the EEG signal with these model predictions, we recomputed the CPP as an average over single-trial data pooled across participants, rather than a grand average. Additionally, to match the stimulus-locked CPP with the stimulus-locked model predictions, we removed trials from the average once they reached the associated RT. The resulting averages were then low-pass filtered with a cut-off of 5 Hz for better visualisation, and downsampled to match the 10 ms time steps used in the model predictions.

## 4.1.2. Results

### 4.1.2.1. Behavioural Results

Behavioural data were collapsed over 'left' and 'right' trials. All trials with very short (< 180 ms) or very long ( $\geq$  2000 ms) RTs were excluded from the analysis (2.99% of trials). The remaining data are displayed in Figure 4.4.

We conducted a repeated-measures ANOVA to explore the effects of the factors 'Interruption' ('continuous', 'stop', 'reverse') and 'Difficulty' ('easy', 'hard') on correct RTs. The results showed a significant main effect of 'Difficulty',  $F(1, 19) = 134.96$ ,  $p < .001$ ,  $\eta_p^2 = .88$ , with 'easy' trials ( $M = 769$  ms) associated with shorter RTs than 'hard' trials ( $M = 863$  ms). For the main effect of 'Interruption', Mauchley's test indicated that the assumption of sphericity had been violated,  $\chi^2(2) = 18.77$ ,  $p < .001$ . We therefore corrected the degrees of freedom using Greenhouse-Geisser estimates of sphericity ( $\epsilon = .61$ ). There was a significant main effect of 'Interruption',  $F(1.21, 23.07) = 63.45$ ,  $p < .001$ ,  $\eta_p^2 = .77$ . Since this factor has three levels, we used Fisher's Least Significant Difference (LSD) for pairwise comparisons, which revealed that all three levels of 'Interruption' were significantly different from each other with 'continuous' trials ( $M = 735$  ms) leading to shorter RTs than 'stop' ( $p = .001$ ) and 'reverse' ( $p < .001$ ) trials ( $M = 870$  ms), and 'stop' trials ( $M = 843$  ms) showing shorter RTs than 'reverse' trials ( $p = .005$ ). There was no significant interaction effect,  $F(2, 38) = 2.00$ ,  $p = .15$ ,  $\eta_p^2 = .10$ .

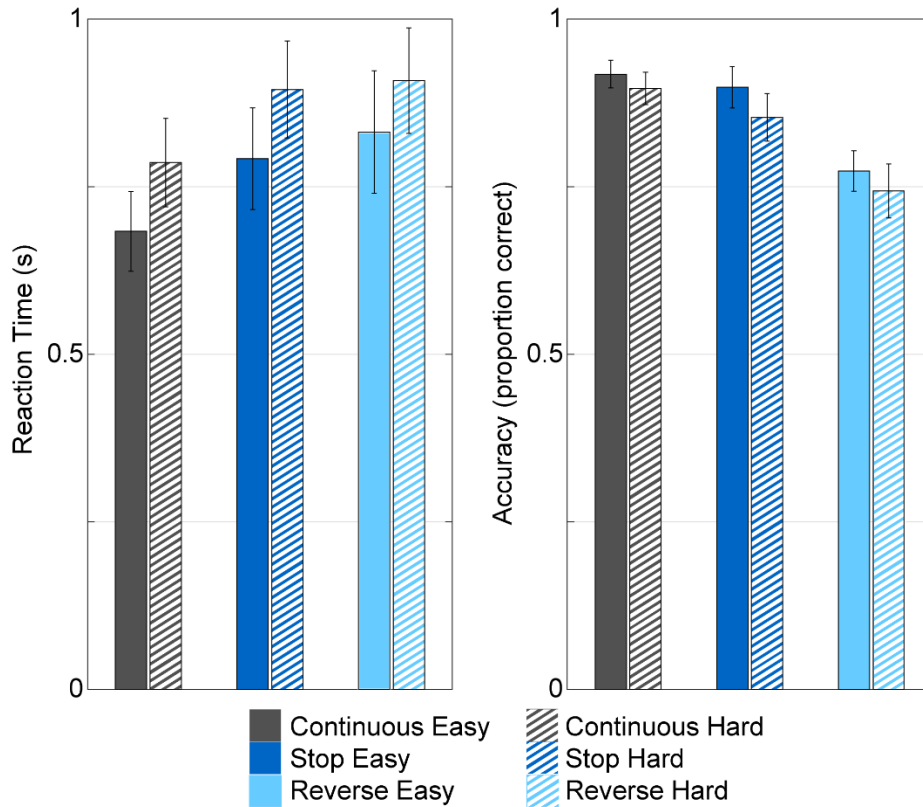


Figure 4.4: Behavioural results: reaction time (left) and accuracy (right) averages for all conditions. Error bars indicate 95% confidence intervals.

Since accuracy data do not meet the distributional assumptions necessary to conduct an ANOVA, we used a generalised linear mixed effects model to explore the effects of ‘Interruption’ and ‘Difficulty’ on participants’ accuracy. Using the ‘fitlme’ function in Matlab (The Mathworks, Natick, U.S.A.), we used a model with a logistic link function and binomial data model. Parameter estimates were based on a maximum likelihood method using Laplace approximation. In line with recommendations by Barr et al. (2014) we used a ‘maximal’ random effects structure, i.e. both manipulations, ‘Interruption’ and ‘Difficulty’, and the ‘Interruption \* Difficulty’ interaction were included as fixed effects, and both manipulations and their interactions within each participant were included as random effects (Wilkinson notation:  $Accuracy \sim 1 + Interruption * Difficulty + (1 + Interruption * Difficulty | Participant)$ <sup>13</sup>. The model showed that ‘Difficulty’ was a significant predictor,

<sup>13</sup> The dispersion parameter of the model,  $\phi = .61$ , was calculated by dividing the sum of squared Pearson residuals by the residual degrees of freedom (Venables & Ripley, 2002), and indicates that there was no issue with overdispersion.

$F(1, 114) = 7.19, p = .008$ , with 'easy' ( $M = 86\%$ ) conditions associated with higher accuracy scores than 'hard' ( $M = 83\%$ ) conditions. Additionally, 'Interruption' was a significant predictor,  $F(2, 114) = 108.88, p < .001$ . The 'Interruption \* Difficulty' interaction was not a significant predictor,  $F(2, 114) = 2.33, p = .10$ .

In order to explore the differences between all three levels of 'Interruption' ('continuous', 'stop', 'reverse'), we fitted the model a second time, but setting the reference level of 'Interruption' to 'stop', rather than 'continuous'. We found that both the 'continuous' ( $M = 91\%$ ) and the 'stop' ( $M = 88\%$ ) conditions were associated with higher accuracy scores than the 'reverse' ( $M = 76\%$ ) condition ( $p < .001$ ). However, there was no significant difference between the 'continuous' and the 'stop' conditions ( $p = .13$ ).

#### **4.1.2.2. ERP Results**

The resulting ERPs are displayed in Figure 4.5. The CPP displays a build-up over the course of the decision, which is disrupted by the interruption of evidence. To quantify this effect, we compared the slopes of the ERP before and during the interruption period.

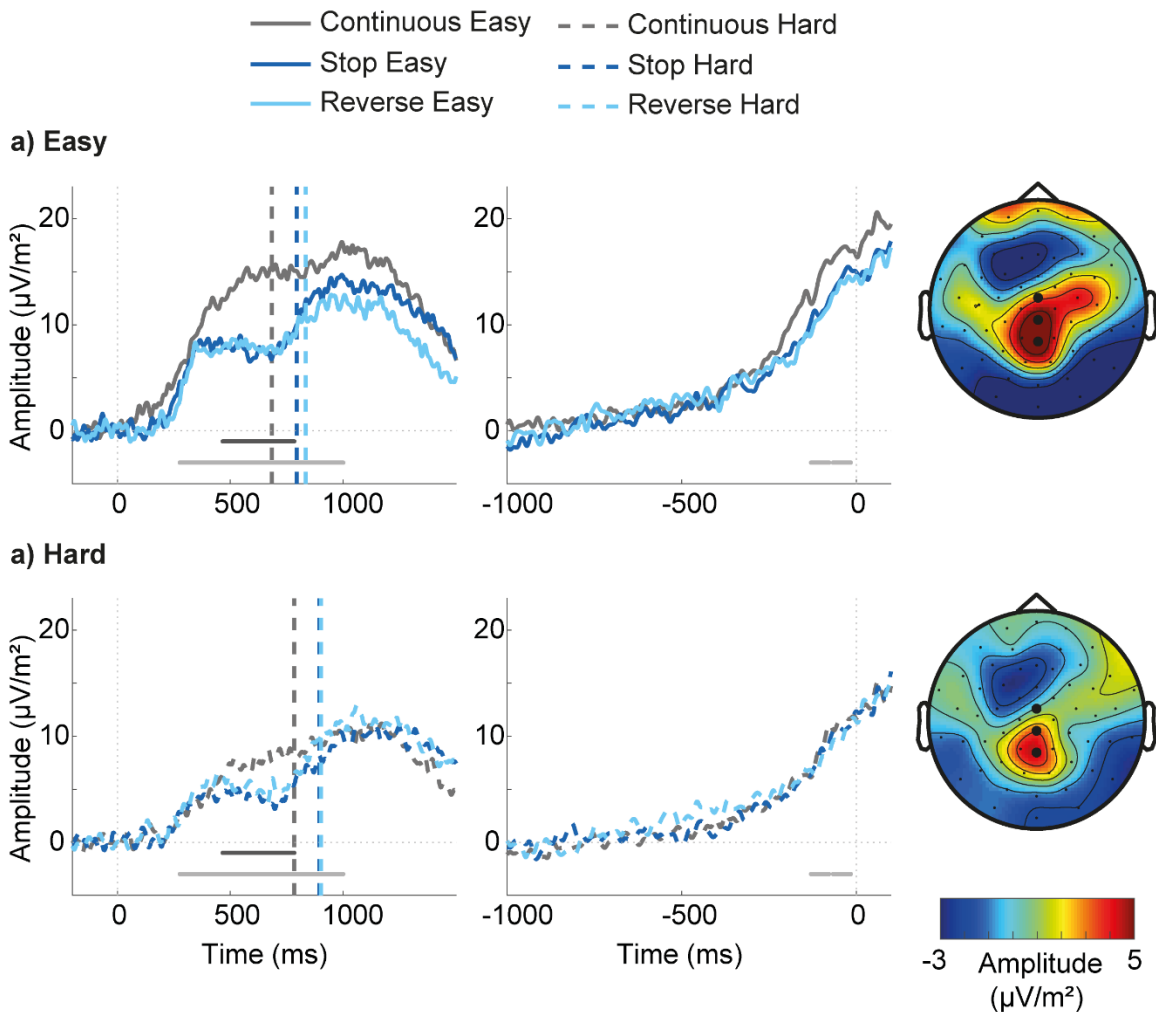


Figure 4.5: CPP results: CPP waveforms (left) and topographies (right) for easy (a), and hard (b) trials. From left to right: stimulus-locked waveform, response-locked waveform, and topography averaged over the stimulus-locked 0 to 1000 ms interval. Electrodes used to generate the waveform are highlighted in the topoplots. Vertical dashed lines in the stimulus-locked CPP represent mean RTs per condition. Note that the mean RTs here are computed only from trials which were included to generate the waveform and therefore differ slightly from those displayed in Figure 4.4. Grey dots at the bottom of the waveforms indicate significance based on FDR-controlled comparisons of amplitude: dark grey dots indicate a significant main effect of 'Interruption', while light grey ones indicate a significant main effect of 'Difficulty'.

An 'Interruption' x 'Difficulty' ANOVA investigating the slope of the CPP showed that in the stimulus-locked data, there was a significant main effect of 'Difficulty' in the pre-interruption interval,  $F(1, 19) = 12.93, p = .002, \eta_p^2 = .40$ , with 'easy' waveforms displaying a higher slope ( $M = .02$ ) than 'hard' waveforms ( $M = .01$ ). There was no main effect of 'Interruption',  $F(2, 38) = 1.01, p = .38, \eta_p^2 = .05$ . There was no interaction effect between 'Interruption' and 'Difficulty', ( $p = .82$ ).

Conversely, in the interruption interval, there was no significant main effect of 'Difficulty',  $F(1, 19) = .19, p = .67, \eta_p^2 = .01$  ( $M_{easy} = .02, M_{hard} = .01$ ), however, there was a significant main effect of 'Interruption',  $F(2, 38) = 9.52, p < .001, \eta_p^2$

= .33. We used Fisher's LSD post hoc tests to explore the main effect further. They revealed that the slope of the 'continuous' waveform ( $M = .03$ ) was significantly higher than the slopes of both the 'stop' ( $M = .01$ ) and the 'reverse' ( $M = .01$ ) waveforms,  $t(19) > 3.40$ ,  $p < .003$ . There was no significant difference in slope between the 'stop' and 'reverse' conditions,  $t(19) = .76$ ,  $p = .46$ . There was no significant interaction between 'Difficulty' and 'Interruption' in the interruption interval ( $p = .39$ ).

In the response-locked CPP, we found a significant main effect of 'Difficulty',  $F(1, 19) = 7.46$ ,  $p = .013$ ,  $\eta_p^2 = .28$ , with 'easy' waveforms associated with a higher slope ( $M = .04$ ) than 'hard' ones ( $M = .03$ ). There was no main effect of 'Interruption', and no interaction effect, ( $p > .14$ ).

We also compared the amplitudes of the waveforms associated with the different conditions by performing a series of FDR-controlled 'Interruption' ('continuous', 'stop', 'reverse') x 'Difficulty' ('easy', 'hard') ANOVAs. For brevity, we only report significant results which show a corrected  $p$ -value of  $< .05$  for at least 50 ms continuously. In the stimulus-locked CPP data, a main effect of 'Interruption' was observed between 466 and 783 ms (corrected  $p < .049$ ; see Figure 4.5). Fisher's LSD-corrected post hoc tests found that the 'continuous' waveform displayed a higher amplitude than both the 'stop' waveform (between 466 and 783 ms relative to the onset of coherent motion, corrected  $p < .02$ ) and the 'reverse' waveform (between 488 and 783 ms, corrected  $p < .046$ ). There was no significant difference in amplitude between 'stop' and 'reverse' conditions (corrected  $p > .26$ ).

Further, we found a significant main effect of 'Difficulty' in the time interval between 276 and 1000 ms relative to stimulus onset, with 'easy' waveforms reaching higher amplitudes than 'hard' waveforms (corrected  $p < .046$ ). There was no significant interaction between 'Interruption' and 'Difficulty' (corrected  $p > .34$ ).

In the response-locked CPP, we found no main effect of 'Interruption' (corrected  $p > .07$ ). There was a significant main effect of 'Difficulty' during 160 out of 229

time points between -229 and 0 ms relative to response, with ‘easy’ trials displaying a higher amplitude than ‘hard’ trials. There was no significant interaction effect (corrected  $p > .9$ ).

#### 4.1.2.3. Model Fit

We fitted two race models to the data, one of which assumes symmetric changes in drift rate with changing evidence (Model 1, 8 parameters), and one which fits a new drift rate to each evidence interruption (Model 2, 16 parameters). To compare the goodness of fit among the models, we calculated the BIC (Schwarz, 1978) of each model fit. The BIC takes into account the likelihood of the model but also penalises a model for the number of parameters used in order to resolve the problem of overfitting. The best (lowest) BIC was obtained for Model 2 (see Table 4.1). This implies that the additional drift rate parameters of Model 2 increased the quality of the fit enough to warrant the increased model complexity, and suggests that evidence is integrated at different rates throughout the trial. The same comparison using the AIC (Akaike, 1973) instead of the BIC supported the same conclusion (see Table 4.1).

Table 4.1: Model Comparison: BIC and AIC values for each model. Model 1 has higher (worse) BIC and AIC values, despite its comparatively small number of parameters (best BIC and AIC values in bold).

Model	Number of parameters	AIC	BIC	Parameters
Model 1	8	71,992	72,053	$v\text{-easy}_{correct}$ , $v\text{-easy}_{incorrect}$ , $v\text{-hard}_{correct}$ , $v\text{-hard}_{incorrect}$ , $S_z$ , $T_{er}$ , $S_{Ter}$ , $\sigma^2$
Model 2	16	<b>71,875</b>	<b>71,998</b>	$v\text{-easy-continuous}_{correct}$ , $v\text{-easy-continuous}_{incorrect}$ , $v\text{-easy-stop}_{correct}$ , $v\text{-easy-stop}_{incorrect}$ , $v\text{-easy-reverse}_{correct}$ , $v\text{-easy-reverse}_{incorrect}$ , $v\text{-hard-continuous}_{correct}$ , $v\text{-hard-continuous}_{incorrect}$ , $v\text{-hard-stop}_{correct}$ , $v\text{-hard-stop}_{incorrect}$ , $v\text{-hard-reverse}_{correct}$ , $v\text{-hard-reverse}_{incorrect}$ , $S_z$ , $T_{er}$ , $S_{Ter}$ , $\sigma^2$

Table 4.2: Estimated parameter values for the chosen model (Model 2): note that the response threshold  $A$  was set to 1 as a scaling parameter.

Model 2: Parameters	
Starting point variability ( $S_z$ )	0.7538
Response threshold ( $A$ )	1

Non-decision time ( $T_{er}$ )			0.2895		
Non-decision time variability ( $S_{Ter}$ )			0.266		
Diffusion constant ( $\sigma^2$ )			0.5011		
Drift rate ( $v$ )	'Continuous'	correct	easy	1.4355	
			hard	1.1571	
		incorrect	easy	0.02	
			hard	0.0135	
		'Stop'	correct	easy	0.4121
				hard	0.2447
	incorrect		easy	0.0471	
			hard	0.0163	
	'Reverse'		correct	easy	0.0369
				hard	0.0534
		incorrect	easy	0.7725	
			hard	0.9237	

The parameter estimates of the chosen race model are displayed in Table 4.2. We found that, as expected, drift rates in interrupted conditions were lower than 'continuous' drift rates. Additionally, the best-fitting drift rates in the incorrect accumulator of the 'reverse' condition (e.g.  $v\text{-easy-reverse}_{incorrect} = .77$ ) were much lower than the ones in the correct accumulator of the 'continuous' condition (e.g.  $v\text{-easy-continuous}_{correct} = 1.14$ ) despite the equally strong sensory evidence.

Figure 4.6 shows the quality of the model fit by displaying empirical (circles) and modelled (lines and crosses) RT distributions for correct (bold symbols) and incorrect (thin symbols) responses in each condition. Each distribution is summarised by five quantile estimates (from left to right: 10%, 30%, 50%, 70%, 90%), the RT (x-axis) and proportion of data (y-axis) of which are shown. The overlap between empirical and modelled quantiles indicates that the model fitted the data well. The mean difference between predicted and observed RTs at each quantile for correct responses was approximately 36 ms, confirming that the race model with varying drift rates can account for decision-making with non-stationary evidence.

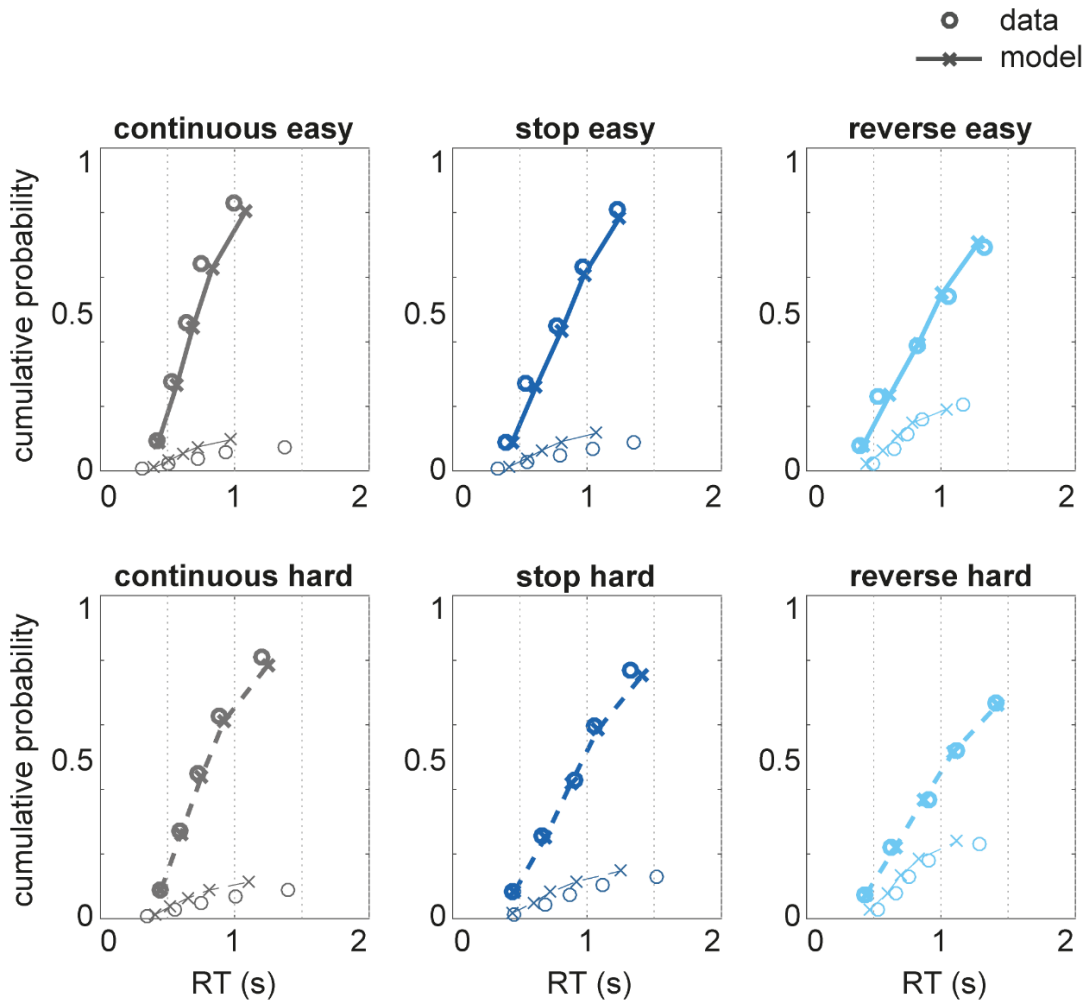


Figure 4.6: Model fit: quantiles estimated from behavioural data (circles) and race model (Model 2) simulations (crosses and lines) for easy (top) and hard (bottom) decisions. For each condition, correct (thick) and incorrect (thin) quantiles are displayed separately.

#### 4.1.2.4. Model Prediction

The parameters of the chosen model were then used to estimate the average accumulation profile for each condition. Figure 4.7 displays the resulting predictions (a) and the corresponding EEG data (b) for stimulus (left) and response-locked (right) data, as well as easy (top) and hard (bottom) data. Visual inspection shows that the EEG and predicted profiles are qualitatively very similar. With stimulus-locking, both profiles show an initial build-up which is slower (lower slope) in 'hard' (dashed lines) compared to 'easy' (solid lines) conditions, but similar across interruption conditions. Both profiles also show that the 'continuous' waveforms continue the build-up, while 'stop' and 'reverse' waveforms display a drop at approximately the same time, before continuing to build up. A further similarity between the model prediction and the EEG signal is the unexpected finding of an overlap of the 'stop easy' and 'reverse easy'

conditions during the interruption period. However, there are also small differences between modelled and observed accumulation, such as the difference between 'stop hard' and 'reverse hard' profiles predicted by the models, which is less pronounced in the EEG waveform. Additionally, the CPP displays a negative dip as a response to evidence interruption while the model prediction shows a much reduced, but still positive slope. The response-locked signal is overall very similar in both the EEG and the predicted profiles, as no differences between conditions are seen, with the exception of a small deviation of the 'continuous easy' waveform in the EEG signal.

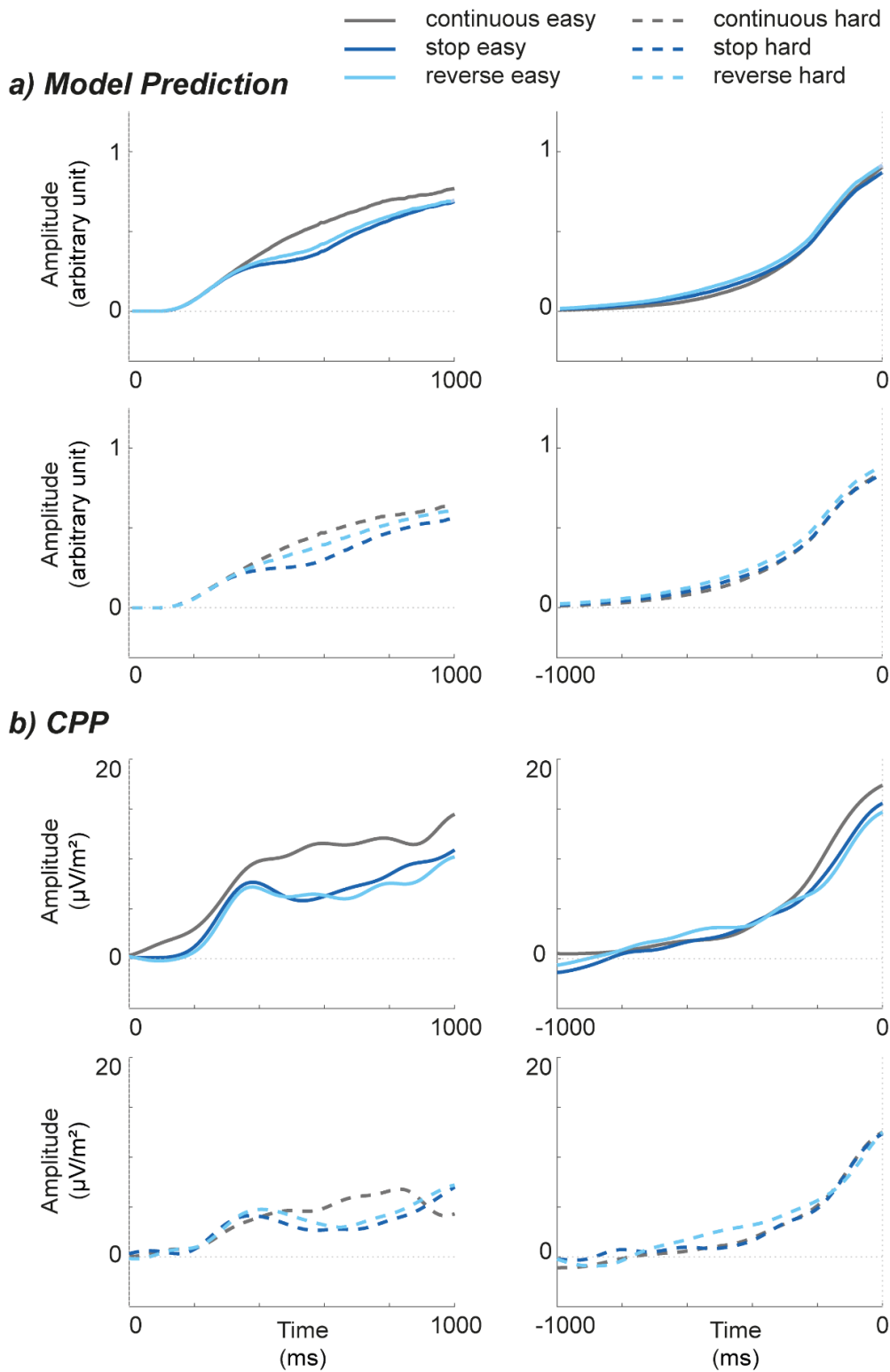


Figure 4.7: Decision variable (empirical and simulated): a) accumulation profile (correct and incorrect accumulator summed) per Interruption condition as predicted by the race model, for easy (top) and hard (bottom) trials, as well as stimulus (left) and response-locked (right) data. b) CPP waveform for easy (top) and hard (bottom) trials, as well as stimulus (left) and response-locked (right) data. The CPP here differs from the one displayed in Figure 4.5 as it is a pooled average and has been filtered and downsampled to match model predictions.

### 4.1.3. Discussion Experiment 1

In the first experiment, we set out to test the impact of non-stationary evidence on a potential neural substrate of the decision variable, the CPP. Since we assume that a change in evidence must necessarily induce a change in the accumulation profile, we hypothesised that, in order to support its role as a decision variable signal, the CPP waveform should also display a non-stationary build-up. To test this, we observed the CPP under three different ‘Interruption’ conditions: a ‘continuous’ condition in which the evidence continued at the same level of strength throughout the trial, a ‘stop’ condition in which the evidence was stopped and replaced by random noise for a brief interval, and a ‘reverse’ condition in which the evidence was reversed to support the opposite alternative for a brief period. We hypothesised that these three conditions would lead to three different profiles, with the continuous condition leading to the stereotypical, smooth build-up, while the stop and reverse profiles would deviate from this build-up to varying extents. We also added a more established manipulation of difficulty to the design and hypothesised that (as demonstrated in Chapter 3), this would affect the slope of the different accumulation profiles.

Behavioural results indicated that both the interruption conditions and the difficulty conditions had the expected effects on the RTs and accuracy scores. ‘Easy’ decisions were associated with faster, more accurate responses than ‘hard’ decisions. Similarly, ‘continuous’ trials led to faster and more accurate decisions than ‘reverse’ trials. ‘Stop’ trials were associated with shorter RTs and higher accuracy scores than ‘reverse’ trials and longer RTs than ‘continuous’ trials. These behavioural findings are in line with previous research, which has repeatedly shown that disruptions in evidence lead to an increase in RT (Holmes et al., 2016; Huk & Shadlen, 2005; O’Connell et al., 2012). Accuracy results in these studies have been less consistent, but these are arguably dependent on the procedures of each study. For example, O’Connell et al. (2012) used a target detection paradigm with no response deadline in which participants were unlikely to respond under uncertainty, and found no difference in accuracy caused by the non-stationary evidence. In the current study, on the other hand, we implemented a comparatively short (2000 ms) deadline, which is

likely to push participants into responding under increased uncertainty in interrupted trials. Overall, as expected, interrupted trials led to worse performances than continuous trials, with evidence reversal disrupting the decision more than a simple pause in the evidence.

Importantly, we expected that the manipulations of difficulty and interruption would not only affect the behavioural data, but also the accumulation profile. As described in detail in Chapter 3, the slope of the accumulation should vary with difficulty (Brown & Heathcote, 2008; Kelly & O'Connell, 2013; Ratcliff & McKoon, 2008; Ratcliff & Rouder, 1998). Furthermore, the interruption of evidence should lead to an interruption in the build-up of the accumulation. Specifically, we hypothesised that a 'stop' in evidence would also cause the accumulation to stop and plateau for the duration of the interruption interval. The impact of the 'reverse' condition on the accumulation profile is somewhat harder to predict as it is particularly dependent on the specifications of the model, as, for example, the assumption of inhibition may lead to a downward slope during the reversal interval, while a model that does not assume inhibition between accumulators would predict a mere decrease in the slope while remaining positive<sup>14</sup>. However, it is important to note that even the comparatively simple race model used here contains a large amount of interacting parameters, the results of which are difficult to predict conceptually.

The CPP waveform revealed patterns which largely supported our hypotheses. We found that task difficulty affected the slope of the CPP, with 'hard' decisions leading to lower build-up rates than 'easy' decisions. In the 'continuous' condition, we observed the stereotypical build-up over time which peaked at the time of response. Importantly, we found that both the 'stop' and the 'reverse' waveforms displayed a clear divergence from this pattern. While all three conditions ('continuous', 'stop', 'reverse') displayed the same build-up up in the pre-interruption period, we observed a clear disruption of the build-up in both

---

<sup>14</sup> Note that the intuitive prediction that the reversal of evidence would lead to a reversal in accumulation (i.e. a downward slope) even without the assumption of inhibition is only accurate with regards to the correct accumulator, but not the sum of both accumulators which is used here.

the 'stop' and 'reverse' profiles, which plateaued before continuing to build up, approximately 300 ms later. This finding of the perturbation in evidence translating into a perturbation in the CPP build-up is in line with our hypothesis and with previous research which found that the evolution of the CPP is sensitive to a brief interruption of evidence (O'Connell et al., 2012). However, contrary to our hypotheses, we observed no difference between 'stop' and 'reverse' CPP profiles, as both conditions displayed the same build-up and plateau behaviour (but see below).

An additional finding worth noting is the delay in the disruption of the CPP build-up compared to the timing of the evidence interruption. While the interruption of motion took place between 200 and 400 ms, the divergence in CPP amplitude between 'continuous' profiles and the two interrupted profiles was observed between approximately 470 and 780 ms. Although this delay was not tested specifically and the race model was able to account for the data without an additional delay parameter, we speculate that this temporal difference is larger than would be expected from a delay based on sensory processes alone. A similar delay between presentation and incorporation of the new information has been described by Holmes et al. (2016), although with a larger magnitude (approximately 450 ms). This finding further supports the role of the CPP as an accumulation signal, rather than a mere sensory signal, which would arguably display a faster reaction in response to the change in evidence. The CPP however, responds to the change slowly and is affected by the change for a longer period than the duration of the interruption interval, suggesting that it represents a higher-level integration of evidence.

Overall, the CPP profile showed the majority of the expected patterns. However, the hypotheses against which the CPP was compared were largely intuitive. In order to gauge the extent to which the observed profiles match true accumulation profiles, we fitted a sequential sampling model to our data. We found that a race model with separate drift rates for each difficulty and interruption condition was able to fit our RT data well. In line with Holmes et al. (2016) we found that a change in evidence was better explained by a new, independent drift rate, rather than a symmetric drift rate, even when the change

in evidence itself was symmetric (i.e. in the best model, the drift rates during the reversal of the motion direction did not equal the inverse of the initial drift rates). However, Holmes et al. (2016) found larger drift rates after evidence reversal, while we found that the incorrect drift rate during the 'reverse' period was lower than the correct drift rate prior to the interruption, even though the sensory evidence associated with both was equivalent. Our findings indicate that there might be an inhibitory mechanism, impeding the increase of the losing accumulator. Although we fitted a race model which explained the data well without an inhibition parameter, it may be useful to explore other models which assume inhibition, such as the leaky competing accumulator model (Usher & McClelland, 2001) in future work. The difference in findings between our study and that of Holmes et al. (2016) may be explained by the different task procedures as we used brief perturbations while the evidence in Holmes et al. (2016) remained reversed for the rest of the trial. It is conceivable that evidence which opposes the winning accumulator is inhibited at first, but, if it continues long enough, eventually catches up and is then, potentially to compensate for the delay, accumulated faster.

Importantly, we used the estimated parameters to simulate the accumulation profile associated with each condition and directly qualitatively compared the resulting patterns to the CPP. We found considerable overlap between the model predictions and the neural signal, even though these profiles were not fitted to one another directly. Both profiles showed the same slope differences between 'easy' and 'hard' trials. Additionally, neither the model prediction nor the CPP showed large differences between conditions in the response-locked data. The model predictions also showed the same gradual build-up in the 'continuous' condition and the interruption of the build-up in the 'stop' and 'reverse' conditions, as observed in the EEG signal. Interestingly, the model predictions also mimicked the CPP signal in the similarity between the 'stop' and 'reverse' waveforms. These patterns are particularly interesting as they oppose our prior hypotheses and show an overlap between neural data and evidence accumulation which might not have been predicted based on intuitive reasoning alone. Overall, these similarities support the role of the CPP as a neural substrate of decision-making.

## 4.2. Experiment 2: Decision Bias

In Experiment 2, we set out to explore a second manipulation, which, to our knowledge, has not been used previously to evaluate the CPP as a potential neural correlate of the decision variable. To this end, we tested the effects of decision biases on the CPP. The notion of a decision bias is a common topic in the perceptual decision-making literature, as it is a manipulation which is associated with strong behavioural effects, which can often be explained using sequential sampling models by varying just one parameter (Summerfield & de Lange, 2014). In a sequential sampling process, evidence is accumulated from a given starting point towards a threshold. With the introduction of a bias towards a given alternative, the starting point moves towards the threshold associated with that alternative, thereby decreasing the amount of evidence required to make the choice in favour of the biased alternative (Spaniol, Voss, Bowen, & Grady, 2011; Voss et al., 2013). Specifically, in accumulator models, which assume that there are two accumulators in a binary choice, each integrating evidence for a given alternative and racing towards a common threshold, biases can be implemented by increasing the starting point (i.e. decreasing the amount of evidence required to reach the threshold) in only one of the accumulators and/or decreasing the starting point of the remaining accumulator, making the biased choice more likely (Gao et al., 2011).

Other ways to implement bias effects in sequential sampling models have been suggested. For example, it has been proposed that a variation in drift rate, i.e. the slope of the accumulation, may account for biased decisions, with biases towards a specific alternative leading to increased slopes (Diederich & Busemeyer, 2006; Gao et al., 2011; Hanks, Mazurek, Kiani, Hopp, & Shadlen, 2011; Mulder et al., 2012). It has also been suggested that the way a model best accounts for biased decisions depends on the nature of the bias, as variations in starting point, and potentially in drift rate, may differ depending on whether a bias towards a given alternative is caused by its increased frequency or by the association of the alternative with an increased payoff (Diederich &

Busemeyer, 2006; Feng, Holmes, Rorie, & Newsome, 2009; Leite & Ratcliff, 2011; Mulder et al., 2012; Summerfield & de Lange, 2014).

However, an overwhelming amount of evidence suggests either that a difference in the starting point accounts for behavioural data from biased decisions (Bode et al., 2012; Gao et al., 2011; Mulder et al., 2012; Ratcliff et al., 2016; Spaniol et al., 2011; Summerfield & Koechlin, 2010), or a variation of this idea which claims that evidence accumulation is preceded by a process which evaluates a given bias and sets the starting point for accumulation (Diederich, 2008; Diederich & Busemeyer, 2006).

Biased decisions have also been explored using neural signals which have previously been proposed to reflect the accumulation profile described by sequential sampling models. Rorie, Gao, McClelland, and Newsome (2010) presented monkeys with a binary motion-discrimination task in which the reward for the two choices was either equal or unequal. It was found that the rewards primarily influenced LIP firing rates prior to the motion onset, with unbalanced payoffs leading to a baseline shift towards the rewarded threshold. These findings support the notion of a starting point difference in accumulation for biased decisions. No difference in the slope of the build-up in firing rate throughout the decision was observed. The same finding of a shift in baseline activity and unaltered slopes in LIP firing rates was supported when instead of unequal payoffs, directional cues were used in a motion discrimination task (Rao, DeAngelis, & Snyder, 2012). Similarly, it has been shown that firing rates in SC neurons, which show a build-up to threshold profile associated with a given choice, show a reduction in baseline activity with decreasing probability of this choice (Basso & Wurtz, 1998; Dorris & Munoz, 1998), further supporting the role of starting point activity in decision biases.

Evidence from neural correlates of evidence accumulation in humans remains somewhat scarce. fMRI studies have reported correlates of a biased decision variable in parietal and prefrontal regions (Chen et al., 2015; Mulder et al., 2012; Summerfield & Koechlin, 2010). EEG research on the other hand, has focused primarily on motor signals to track decision biases. Noorbaloochi et al.

(2015) recorded human EEG during a decision task with either biased or unbiased payoffs and explored the lateralised readiness potential (LRP) as a signal reflecting evidence accumulation. In line with findings from non-human primates, it was found that in biased decisions, the LRP amplitude was shifted towards the alternative associated with the higher payoff prior to the stimulus onset, suggesting a starting point difference. However, the behavioural data were best explained by a model with an additional accumulator which represents a fast guess process and races with the evidence accumulators, rather than by traditional models with starting point or drift rate variations to explain decision biases. On the other hand, de Lange et al. (2013) concluded that it is in fact a variability in starting point which accounts for bias-related activity. Using MEG, de Lange and colleagues found that motor-related activity in the beta frequency range displayed a pre-stimulus bias into the direction associated with the biased alternative. Together, these data suggest that biases push accumulation signals prior to the accumulation onset towards the threshold, without affecting the accumulation slope.

To our knowledge, the effects of decision biases have not yet been explored using the CPP. In order to test whether the CPP reflects a neural substrate of the decision variable, we set out to explore the CPP waveform under different bias conditions. We presented participants with a motion direction discrimination task after viewing cues which either provided information regarding the likely direction of the following motion or gave no directional information. Based on the literature summarised above, we hypothesised that the presence of a directional cue would lead to a starting point difference in accumulation. However, it is unclear how this difference would translate into the CPP. One possibility is that a starting point difference would lead to baseline difference in the CPP, which, since the generation of the CPP waveform requires a baseline correction, would appear in the CPP amplitude (e.g. an increase in baseline leads to a decrease in the baseline-to-boundary distance and a decrease in the absolute magnitude of the accumulation). However, if, as we assume, the CPP reflects the sum of the accumulators, it is possible that we would observe no difference in the waveforms, as the increased starting point in the cued accumulator might co-occur with a decreased starting point in the non-cued

accumulator, the sum of which might be zero. Fitting a sequential sampling model to the resulting behavioural data and directly comparing it to the recorded CPP waveform is therefore crucial to yield insights into the role of the CPP as an accumulation signal.

## **4.2.1. Methods**

### **4.2.1.1. Participants**

Twenty participants (five males), with a mean age of 30.15 ( $SD = 7.28$ ) were recruited. Exclusion criteria required participants to achieve an average accuracy score of 80% in the random dot motion task at a coherence level no greater than 90% (i.e. 90% of dots moving coherently; see 4.2.1.2). All 20 participants met this requirement. Each participant took part in a session lasting between 2 and 2.5 hours. Participants were recruited using either poster advertisements or emails targeted at participants from previous studies. Two of the participants were researchers in the current project. All other participants were paid £8 per hour. The experiment was approved by the City, University of London Psychology Department Ethics Committee.

### **4.2.1.2. Stimuli and Procedure**

Participants were asked to complete a random dot motion task. The basic task and setup were, unless otherwise stated, identical to the description in Experiment 1 (see section 4.1.1.2). All participants completed a minimum of 50 practice trials at a coherence level of 80% in order to familiarise themselves with the task. During the practice trials, feedback was provided after each trial ('correct'/'incorrect'). Afterwards, each participant completed 100 trials without feedback in order to establish an appropriate level of difficulty for the experiment. For this, we again used the QUEST staircase procedure targeting 80% correct. The resulting average level of coherence was 32.25% ( $SD = 27.92$ ).

For the main experiment, each participant completed 450 trials. The trial procedure is displayed in Figure 4.8. Each trial began with the display of a

fixation cross for 500 ms (plus a jitter of up to 200 ms drawn from a uniform distribution), followed by a cue (500 ms) that consisted of two arrows, one pointing to the left, and one pointing to the right. In one third of the trials, both arrows were white, indicating no specific direction ('uncued'), while in two thirds of the trials, one arrow was yellow, providing a cue towards a given direction. One half of these cued trials was cued to the left while the other half was cued to the right. If a directionally specific cue was given, the following dot motion was congruent with the cue 80% of the time ('congruent'), and incongruent in 20% of the trials ('incongruent'). In each trial, the cue was followed by random dot motion, i.e. a coherence level of 0%. After the random motion (like in Experiment 1: 500 ms + jitter up to 1000 ms, drawn from a gamma distribution with shape parameter 1 and scaling parameter 150), the coherent motion started (left/right) and lasted up to 1300 ms or until the response. No feedback was provided after each trial, but every 60 trials, participants took self-timed breaks during which they were provided with feedback in the form of mean accuracy scores and RTs over the last 60 trials.

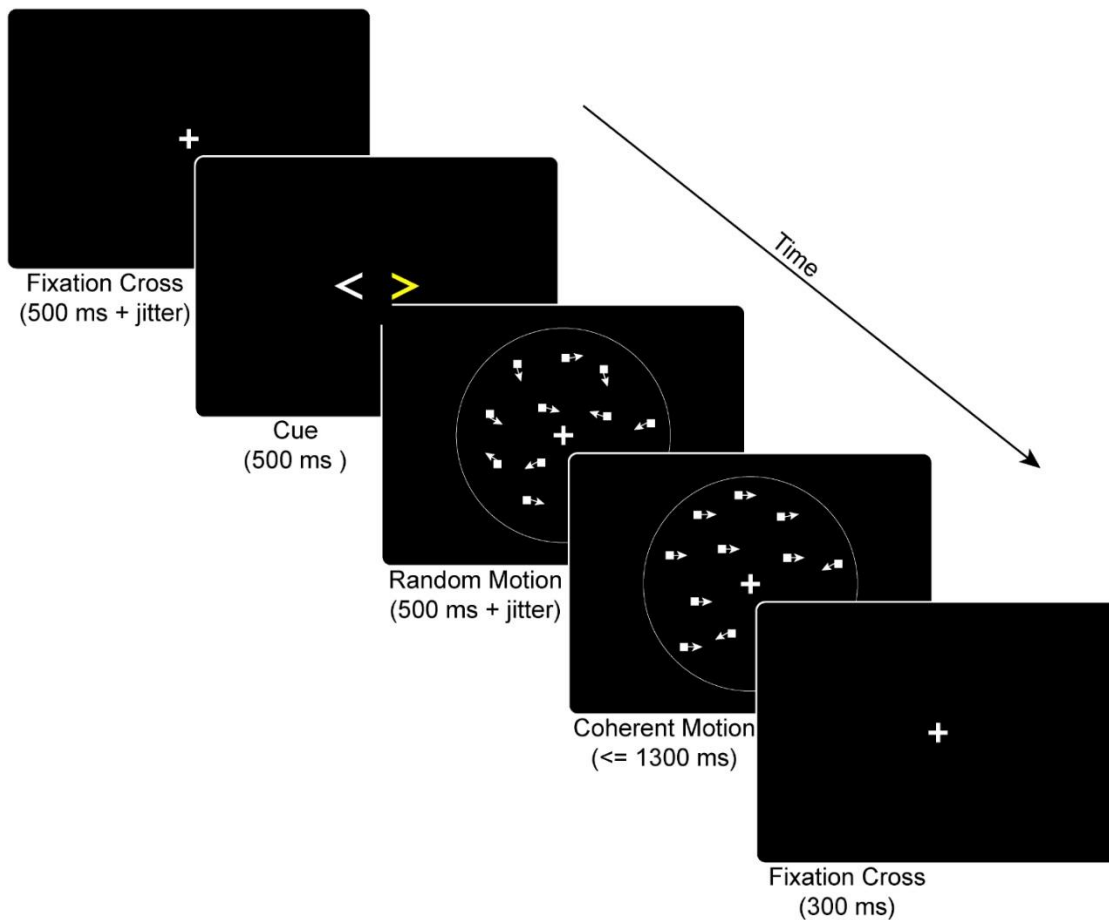


Figure 4.8: Random dot motion task trial procedure: in each trial, a fixation cross was followed by a cue consisting of two arrows. If both arrows were white ('uncued'), no directional information was given. If one of the arrows was yellow, this cue was correctly describing the direction of the upcoming motion in 80% of the trials ('congruent'), and was false in 20% of the trials ('incongruent'). Here, the right side is cued, and the coherent motion following the random motion is to the right ('congruent'). Note that the size and number of dots have been adjusted for illustration.

#### 4.2.1.2.1. EEG Recording and Pre-processing

Continuous EEG was recorded and pre-processed, using the same setup as described in Experiment 1.

#### 4.2.1.2.2. ERP Analysis

The CPP for each condition was generated in the same way as described in Experiment 1.

#### 4.2.1.3. Statistical Analysis

In order to analyse the impact of the different cue conditions on the ERP waveform, we compared both the slope and the amplitude between conditions.

Like in Experiment 1, we compared the build-up rate by fitting a straight line to the waveform for each participant and each condition and measuring its slope. The chosen time intervals to which we fitted a line were 200 to 350 ms for the stimulus-locked CPP, and -200 to -150 ms for the response-locked CPP (Kelly & O'Connell, 2013). The resulting slopes were then compared using a one-way ANOVA to compare 'congruent', 'incongruent', and 'uncued' waveforms.

Amplitudes were analysed in the same way as described in Experiment 1, by running a series of FDR-controlled one-way ANOVAs between 0 and 1000 ms in the stimulus and -1000 to 0 ms in the response-locked CPP.

#### **4.2.1.4. Model Fit**

The same race model as described in Experiment 1 was used to model these data. In this model, two accumulators integrate evidence, one for each alternative, and race towards a threshold.

In order to account for different bias conditions, we tested two different models, both of which varied only in starting point in order to account for different bias conditions (see Figure 4.9). In both models, the response threshold  $A$  was chosen as the scaling parameter and fixed to 1. Since the number of trials across conditions was not balanced (i.e. fewer trials in the 'incongruent' than the 'congruent' condition), adjusted, balanced trial numbers were used to estimate the parameters of each model, to avoid overfitting on the 'congruent' condition.

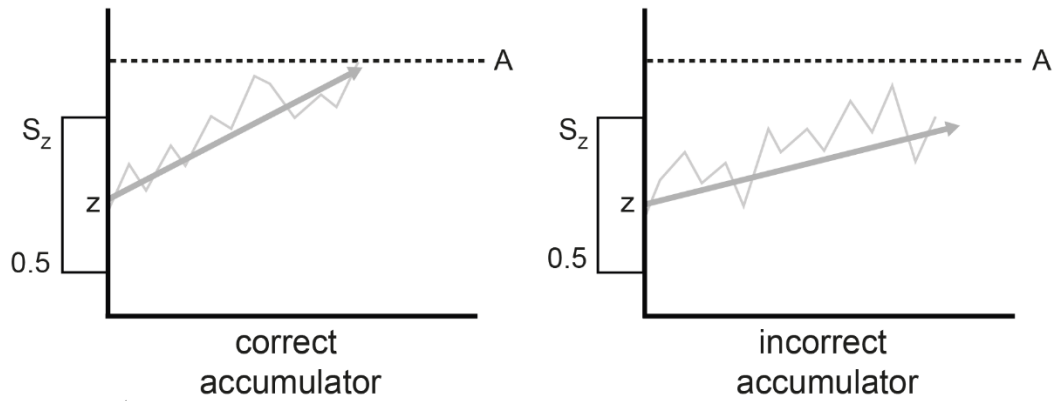
The first model (Model 1) assumed that starting points change symmetrically in response to cues. The starting point of the accumulation process in the standard race model is drawn from a uniform distribution with the upper limit of  $S_z$  and the lower limit of 0. To allow for a variation in starting point in either direction, we fixed the lower limit of the starting-point distribution to 0.5, and used an additional bias parameter to allow bias-related variation. In 'uncued' trials, the starting point distribution remained between 0.5 and  $S_z$  for both correct and incorrect accumulators. In contrast, in the 'congruent' condition, the starting point distribution for the correct accumulator (in line with the cue) was

defined by the range of  $[0.5 S_z] + bias$ , and the distribution for the incorrect accumulator (opposing the cue) was defined by the range  $[0.5 S_z] - bias$ . The opposite pattern was used in 'incongruent' trials, where incorrect starting point distributions (in line with the cue) ranged within  $[0.5 S_z] + bias$ , and correct distributions (opposing the cue) ranged within  $[0.5 S_z] - bias$ . All other parameters ( $S_z, V_{correct}, V_{incorrect}, T_{er}, S_{Ter}, \sigma^2$ ) were fixed between conditions, resulting in a model with a total of seven parameters (see Table 4.3 Table 4.1).

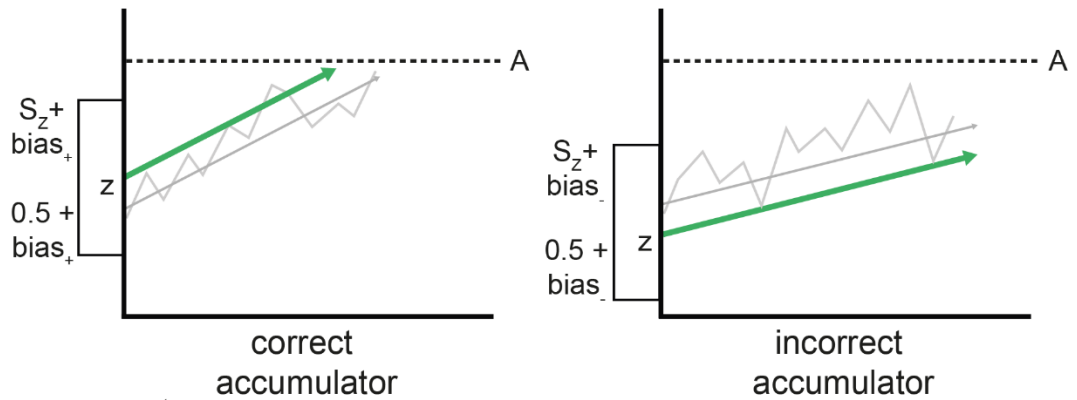
The second model (Model 2) also used starting point variations to account for differences induced by cue conditions. However, this model did not restrict these variations to be symmetric, instead using two bias parameters, one for positive biases, i.e. responses in line with the cue ( $bias_{positive}$ ), and one for negative biases, i.e. responses opposing the cue ( $bias_{negative}$ ). In the 'congruent' condition, the starting point distribution for the correct accumulator (in line with the cue) was defined by the range  $[0.5 S_z] + bias_{positive}$ , and the incorrect accumulator (opposing the cue) was defined as ranging within  $[0.5 S_z] + bias_{negative}$ . The opposite pattern was used in the 'incongruent condition, with bounds of  $[0.5 S_z] + bias_{negative}$  defining the starting point distribution of the correct accumulator (opposing the cue), and bounds of  $[0.5 S_z] + bias_{positive}$  defining the starting point distribution of the incorrect accumulator (in line with the cue). In the 'uncued' condition, the starting point distribution remained between 0.5 and  $S_z$ . All other parameters ( $S_z, V_{correct}, V_{incorrect}, T_{er}, S_{Ter}, \sigma^2$ ) were fixed between conditions, leading to a model with a total of eight parameters (see Table 4.3, Table 4.4).

Like in experiment 1, to fit the model to our data, individual RTs were pooled across participants to determine the best-fitting model parameters at the group level. Trials with RTs faster than 180 ms or slower than 1300 ms (less than 6%) were discarded. Modelled RTs were simulated based on the equations described in Experiment 1 (a total of 20,000 simulated responses), and compared to RT data using Quantile Maximum Probability Estimation (Heathcote et al., 2002). Model fits were compared using BIC and AIC and the best performing model was chosen to generate the appropriate accumulation profile and compare it to the EEG data.

**a) uncued**



**b) congruent**



**c) incongruent**

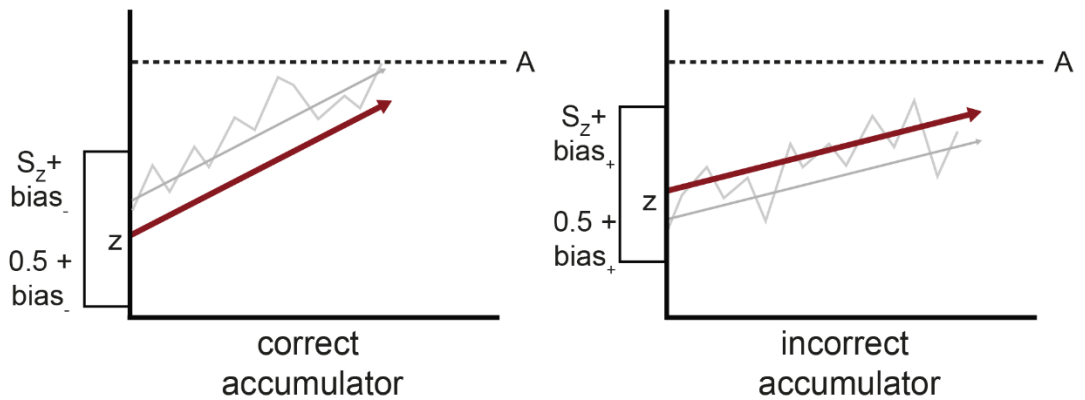


Figure 4.9: Race model applied to biased decisions: to allow for variation of the starting point in either direction, the default lower limit of the starting point distribution in unbiased decisions was raised from 0 to 0.5. a) in 'uncued' trials, no decision bias is expected and the lower limit of the starting point distribution remains at 0.5. b) in the 'congruent' condition, a bias towards the correct choice leads to an increase/decrease in the starting point values in correct/incorrect accumulators; c) in 'incongruent' trials, the opposite pattern is expected, as the cue in the incorrect direction leads to an increased/decreased starting point in the incorrect/correct accumulator. Note that  $bias_{positive}$  and  $bias_{negative}$  are displayed as  $bias_+$  and  $bias_-$  respectively. While the figure displays Model 2, Model 1 only differs by assuming that the increase/decrease in starting point is symmetrical.

#### 4.2.1.5. Model Prediction

To generate the model predictions and the EEG profile to compare it to, the same procedures as in Experiment 1 were followed.

### 4.2.2. Results

#### 4.2.2.1. Behavioural Results

To assess the impact of the cues on the behavioural data, we collapsed over 'left' and 'right' trials, and removed any trials with RTs less than 180 ms or greater than or equal to 1300 ms (approximately 5.34%) to exclude trials in which it is unlikely that the participant made a decision. The remaining data are displayed in Figure 4.10. We then performed a one way repeated-measures ANOVA to explore the effect of the 'Cue' ('congruent', 'incongruent', 'uncued') on correct RTs. There was a statistically significant difference between the groups,  $F(2, 38) = 42.72, p < .001, \eta_p^2 = .69$ . Fisher's LSD corrected follow-up t-tests revealed that all three groups differed significantly from each other, with 'congruent' RTs ( $M = 664$  ms) being faster than both 'uncued',  $t(19) = 6.21, p < .001$ , and 'incongruent',  $t(19) = 7.38, p < .001$ , RTs, and 'uncued' RTs ( $M = 705$  ms) being faster than 'incongruent' ones ( $M = 761$  ms),  $t(19) = 5.17, p < .001$ .

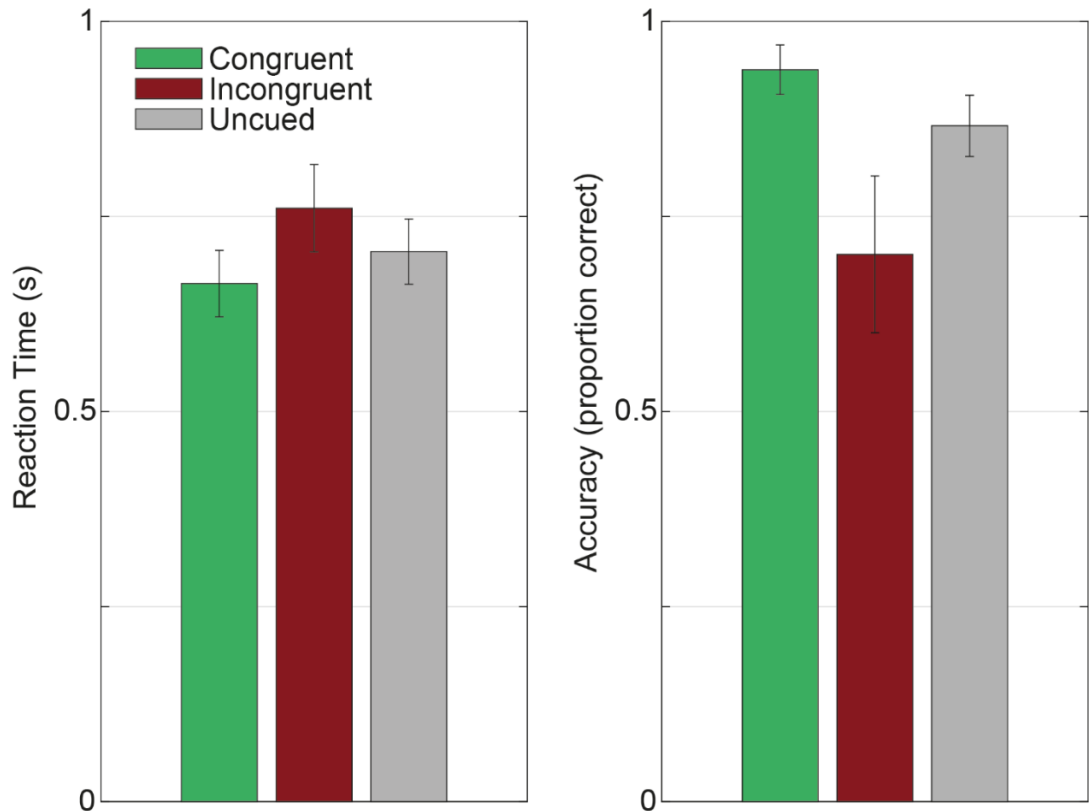


Figure 4.10: Behavioural results: reaction time (left) and accuracy (right) averages for ‘congruent’, ‘incongruent’, and ‘uncued’ trials.

Since accuracy data do not meet the distributional assumptions necessary to conduct an ANOVA, we used a generalised linear mixed effects model to explore the effects of ‘Cue’ on participants’ accuracy. Using the ‘fitglme’ function in Matlab (The Mathworks, Natick, U.S.A.), we used a model with a logistic link function and binomial data model. Parameter estimates were based on a maximum likelihood method using Laplace approximation. The manipulation ‘Cue’ was included as a fixed effect, and participants were included as a random effect (Wilkinson notation:  $\text{Accuracy} \sim 1 + \text{Cue} + (1 + \text{Cue} | \text{Participant})$ )<sup>15</sup>. The model revealed that ‘Cue’ was a significant predictor,  $F(1, 57) = 18.56, p < .001$ . In order to explore the differences between all three levels of ‘Cue’ (‘congruent’, ‘incongruent’, ‘uncued’), we fitted the model a second time, but setting the reference level of ‘Cue’ to ‘incongruent’, rather than ‘congruent’. We found that both the ‘congruent’ condition ( $M = 94\%$ ) and the

<sup>15</sup> The dispersion parameter of the model,  $\phi = .70$ , was calculated by dividing the sum of squared Pearson residuals by the residual degrees of freedom (Venables & Ripley, 2002), and indicates that there was no issue with overdispersion.

‘uncued’ ( $M = 87\%$ ) condition were associated with higher accuracy scores than the ‘incongruent’ ( $M = 71\%$ ) condition ( $p < .001$ ). Additionally, the ‘congruent’ condition was associated with higher accuracy scores than the ‘uncued’ condition ( $p < .001$ ).

#### 4.2.2.2. ERP Results

The CPP waveform for each condition is displayed in Figure 4.11. In both the stimulus-locked and the response-locked CPP, the waveform associated with ‘incongruent’ trials displays the highest amplitude, followed by the ‘uncued’ and ‘congruent’ waveforms. In order to quantify the impact of ‘Cue’ on the ERP waveform, we first compared the slopes of the different conditions. We observed no significant difference in slope in either the stimulus-locked,  $F(2, 38) = .39, p = .68, \eta_p^2 = .02$ , or the response-locked CPP,  $F(2, 38) = .40, p = .67, \eta_p^2 = .02$ .

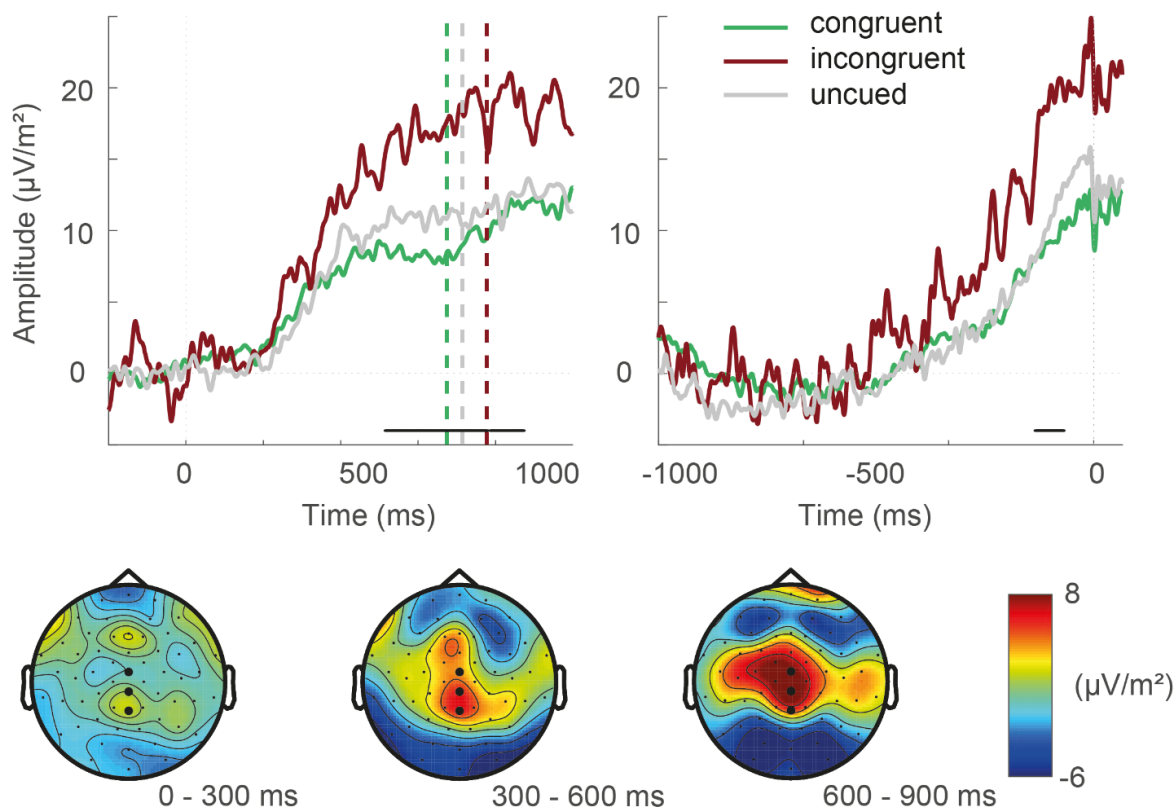


Figure 4.11: CPP results: Top: CPP waveform per condition for stimulus-locked (left) and response-locked (right) data. Vertical dashed lines in the stimulus-locked CPP indicate mean RTs per condition. Note that the mean RTs are based only on trials which were included in the generation of the waveform and differ slightly from the ones displayed in Figure 4.10. Black dots in the bottom of the waveform indicate time points at which FDR-controlled comparisons of amplitude showed a significant main effect of ‘Cue’ conditions. Bottom: ERP topographies averaged over three stimulus-locked time intervals show the evolution of the CPP. Electrodes used to generate the waveform are highlighted.

We also tested the variation of amplitudes in the CPP using a series of FDR-controlled one-way ('Cue': 'congruent'/'incongruent'/'uncued') ANOVAs. In the stimulus-locked CPP, we found a significant effect for 'Cue' in 345 out of 355 time points between 518 and 873 ms relative to the onset of coherent motion (corrected  $p < .049$ ). Follow-up t-tests revealed that 'incongruent' amplitudes were higher than both the 'congruent' (for the entire duration of the main effect, corrected  $p < .02$ ), and the 'uncued' ones (for 244 out of 321 time points between 542 and 863 ms relative to stimulus onset, corrected  $p < .05$ ). However, there was very little difference between 'congruent' and 'uncued' amplitudes (corrected  $p < .05$  only between 639 and 645 ms).

In the response-locked CPP, we found a significant main effect between -198 and -104 ms relative to the response (corrected  $p < .047$ ). Post hoc tests showed the same patterns as the stimulus-locked data, with higher amplitudes in 'incongruent' than 'congruent' trials (during the entire duration of the main effect, corrected  $p < .018$ ) and in incongruent than 'uncued' trials (during 76 out of 90 time samples between -198 and -108 ms, corrected  $p < .049$ ). There was no difference between 'congruent' and 'uncued' trials ( $p > .09$ ).

#### **4.2.2.3. Model Fit**

Based on the literature, two models assuming changes in starting point across bias conditions were fitted to the data. One model assumed that the increase/decrease in starting point for responses congruent/incongruent with the cue is symmetrical (Model 1, 7 parameters), while Model 2 let the bias parameter for increasing/decreasing starting points vary independently (Model 2, 8 parameters). The best (lowest) BIC was obtained for Model 2 (see Table 4.3). This implies that the additional bias parameter of Model 2 increased the quality of the fit enough to warrant the increased model complexity. The same comparison using AIC instead of BIC values supported the same conclusion (see Table 4.3). Therefore, Model 2 was chosen to generate accumulation profiles (note that Model 1 produced similar fits as well as similar predictions).

Table 4.3: Model Comparison: BIC and AIC values for each model. Model 1 has higher (worse) BIC and AIC values, despite its smaller number of parameters (best BIC and AIC values in bold).

Model	Number of parameters	AIC	BIC	Parameters
<b>Model 1</b>	7	30,675	30,723	<i>bias</i> , $V_{correct}$ , $V_{incorrect}$ , $S_z$ , $T_{er}$ , $S_{Ter}$ , $\sigma^2$
<b>Model 2</b>	8	<b>30,656</b>	<b>30,712</b>	$bias_{positive}$ , $bias_{negative}$ , $V_{correct}$ , $V_{incorrect}$ , $S_z$ , $T_{er}$ , $S_{Ter}$ , $\sigma^2$

Table 4.4: Estimated parameter values for the chosen model (Model 2): note that the response threshold  $A$  was set to 1 as a scaling parameter, and that all lower limits of the starting point distributions were generated with just two free bias parameters ( $0.5 + bias_{positive}/bias_{negative}$ ). Note that, due to the raised starting point in the uncued condition, these parameters are not directly comparable to the ones displayed in Experiment 1 (Table 4.2).

Model 2: Parameters			
Starting point variability ( $S_z$ )		0.2281	
Response threshold ( $A$ )		1	
Non-decision time ( $T_{er}$ )		0.0989	
Non-decision time variability ( $S_{Ter}$ )		0.0755	
Diffusion constant ( $\sigma^2$ )		0.1882	
Drift rate ( $v$ )		correct	0.5993
		incorrect	0.2724
Lower limit of the starting point distribution	'congruent'	correct	0.54
		incorrect	0.4378
	'incongruent'	correct	0.4378
		incorrect	0.54
'uncued'	correct	0.5	
	incorrect	0.5	

The parameter estimates of the chosen race model are displayed in Table 4.4. It shows that the positive bias was slightly smaller ( $bias_{positive} = .04$ ) than the negative bias ( $bias_{negative} = -.06$ ). Figure 4.12 shows the quality of the model fit by displaying empirical (circles) and modelled (lines and crosses) RT distributions for correct (bold symbols) and incorrect (thin symbols) responses in each condition. It was found that a race model with varying starting points can account for biased decision-making, with the mean difference between predicted and observed RT quantiles for correct responses being approximately 18 ms.

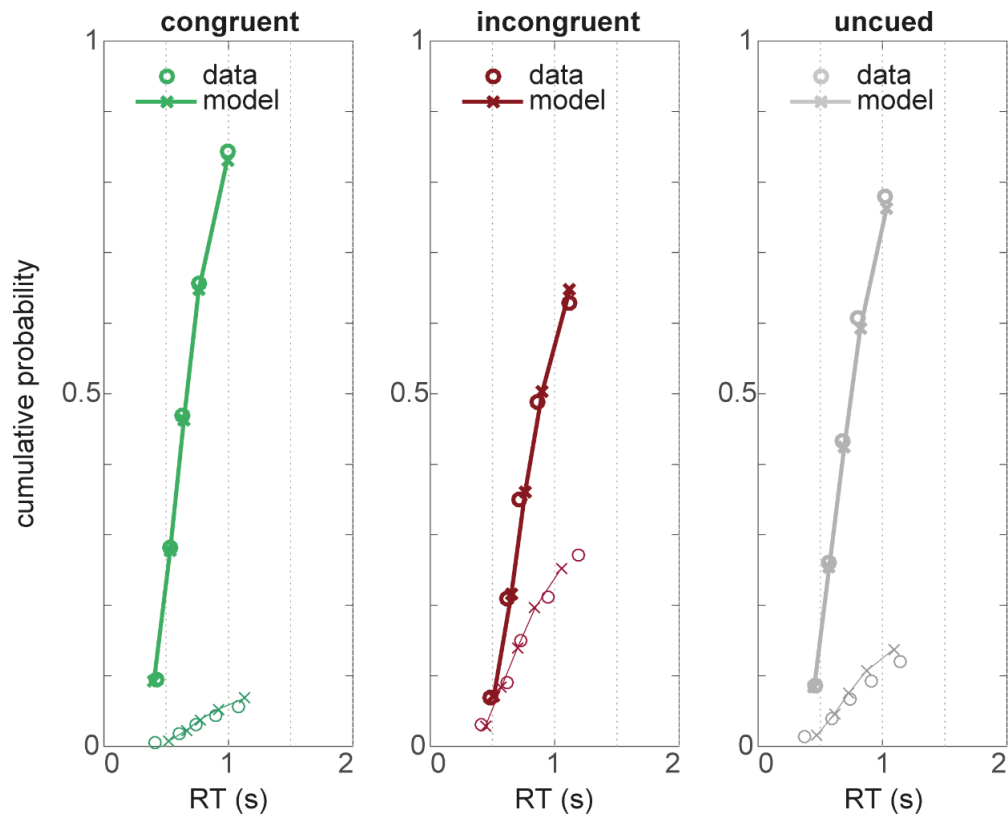


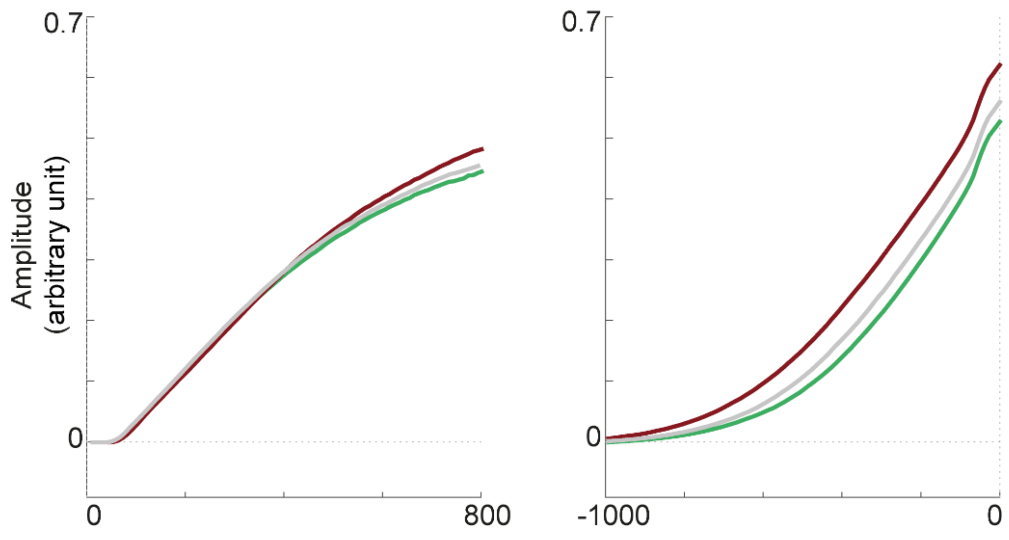
Figure 4.12: Model fit: quantiles estimated from behavioural data (circles) and race model simulations (crosses and lines) for each cue condition. Correct (thick) and incorrect (thin) quantiles are displayed separately.

#### 4.2.2.4. Model Prediction

The parameters of the chosen model (Model 2) were used to estimate the predicted accumulation profile for each condition. Figure 4.13 displays the resulting predictions (a) and the corresponding CPP (b) for stimulus (left) and response-locked (right) signals. Visual inspection shows great qualitative similarities between the model predictions and the EEG signals. Both signals show a stimulus-locked build-up which peaks at the time of response. Importantly, both the model prediction and the CPP display an amplitude difference, with ‘incongruent’ decisions being associated with the highest values, followed by ‘uncued’ decisions, and ‘congruent’ trials associated with the lowest amplitudes. This pattern is visible in both the stimulus-locked and the response-locked waveforms in both the prediction and the EEG signal. Additionally, there appears to be a larger difference in amplitude between the ‘incongruent’ and the remaining conditions, in both the stimulus and the

response-locked profiles. This pattern is particularly visible in the CPP data, but also, to a smaller extent, in the model prediction. However, the two signals are not identical. In particular, the amplitude differences in the EEG signal appear far more pronounced than the ones in the model predictions.

**a) Model Prediction**



**b) CPP**

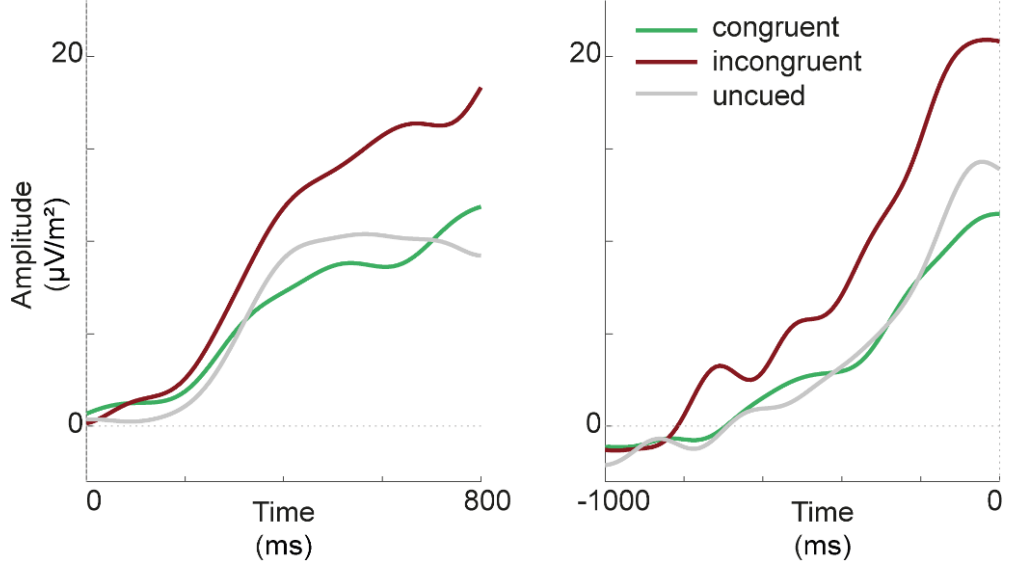


Figure 4.13: Decision variable (empirical and simulated): a) accumulation profile per cue condition as predicted by the race model, for stimulus (left) and response-locked (right) data. b) CPP waveform for stimulus (left) and response-locked (right) data. The CPP here differs from the one displayed in Figure 4.11 as it is a pooled average and has been filtered and downsampled to match model predictions.

### 4.2.3. Discussion Experiment 2

In Experiment 2, we tested how decision biases affect the CPP waveform and, like in Experiment 1, compared its profile to model predictions. To this end, we asked participants to complete a motion discrimination task in which cues prior to each trial either gave no information about the direction of the upcoming trial ('uncued'), or indicated the upcoming direction either correctly ('congruent') or incorrectly ('incongruent'). We found that these manipulations had the expected effects on the data. All conditions were significantly different from each other in both RT and accuracy, with 'congruent' trials associated with the fastest RTs and fewest errors, 'incongruent' trials associated with low accuracy rates and longer RTs, and 'uncued' trials falling mid-range in both RT and accuracy. These results are in accordance with previous research, which has repeatedly shown similar effects on both RT and accuracy as a result of decision biases (de Lange et al., 2013; Mulder et al., 2012).

In order to support the role of the CPP as a neural substrate of the decision variable, we expect these behavioural differences to be evident in the EEG waveform. Based on previous evidence, we hypothesised that the bias conditions would affect the starting point of the accumulation profile (Bode et al., 2012; Gao et al., 2011; Rorie et al., 2010). Since we expect the boundary to remain unaltered, a change in starting point implies a change in the baseline-to-boundary distance. Specifically, we expected that a bias towards a given response would increase the starting point towards the associated boundary, so that less evidence is needed for this response. The exact pattern these changes would evoke in the CPP waveforms of each condition is difficult to predict conceptually. Based on only a correct accumulator in a race model (i.e. the accumulator which integrates evidence for the correct alternative) we may expect that the 'uncued' decisions start around a given starting point  $z$ , while 'congruent' conditions have a higher starting point (i.e. closer to the correct boundary), and 'incongruent' decision have a lower starting point (i.e. at a larger distance to the correct boundary). Since a baseline correction is needed to generate the CPP waveform, a starting point difference would not be observed directly, but would instead lead to a difference in amplitude with higher starting

points leading to lower ERP peaks. This pattern would translate into the 'incongruent' CPP displaying the largest, and the 'congruent' CPP showing the smallest peak amplitude. However, we assume that different neural populations represent different accumulators and that the EEG signal recorded from the scalp is the sum of all accumulation in a race model, rather than a single accumulator. In this context, the expected amplitude differences are less clear. Since we expect that a bias leads to an increase in starting point in the cued accumulator alongside a decrease in the non-cued accumulator, the sum displayed in the CPP may in fact cancel out any difference to an unbiased process.

There are thus a number of possible outcomes which could, at least conceptually, be considered in line with sequential sampling models. This emphasises the importance of the approach implemented in the current study. In addition to the varying assumptions of different models complicating conceptual predictions, even simple sequential sampling models are often too complex to allow for accurate predictions based on reasoning alone. It is therefore particularly important to directly compare a signal to predictions made through model fits, in order to comment on its similarity to an accumulation process.

The pattern we observed in the CPP was somewhat similar to what might be expected for just a correct accumulator. There was no difference in slope between the conditions, but we found a clear difference in amplitude. The waveform associated with 'incongruent' decisions showed a higher amplitude than 'congruent' or 'uncued' profiles in both the stimulus and the response-locked data. The 'uncued' CPP also seemed to build up to a slightly higher plateau than the 'congruent' waveform, although this difference was not significant in our analysis. If, as we assume, these differences in amplitude are due to baseline differences, they indicate that, in correct trials, 'incongruent' trials have the lowest overall starting point, followed by 'uncued' trials, and lastly 'congruent' trials with the highest overall baseline. However, it is not clear why this difference is seen in the CPP which arguably represents the sum of all accumulators (but see below).

In order to evaluate to what extent this observed CPP pattern resembled the accumulation process as predicted by sequential sampling models, we fitted a simple race model to the behavioural data. Its estimated parameters were used to simulate the accumulation profile for each condition, and the resulting waveforms show that all three conditions are predicted to follow a very similar trajectory, only differing in amplitude. The order in which the amplitudes differ is identical to the one described by the CPP, with the highest amplitude seen for 'incongruent' decisions, followed by 'uncued' decisions, and 'congruent' waveforms showing the lowest amplitude.

Although both the simulated accumulation profile and the CPP display similar patterns, it is not immediately clear what caused this pattern. While, as outlined above, we expected this pattern for the correct accumulator, summing over the accumulators should remove any difference between the conditions. To aid our interpretation, we explored the accumulation profiles of both correct and incorrect accumulators in both correct and error trials separately and found that the differences between the conditions reported above were caused by dividing correct from error trials. While the sum of accumulation paths averaged over equally weighted correct and error trials showed, as predicted, no difference between conditions, correct trials showed that 'incongruent' trials accumulated higher (followed by 'uncued' and 'congruent' trials), while error trials displayed the reversed pattern. This is likely caused by a bias in inter-trial variability in starting point ( $z$ ) (and potentially intra-trial variability in accumulation;  $\sigma^2$ ). In the 'incongruent' condition for example, mean starting points are higher in the incorrect (cued) than the correct (non-cued) accumulator, which implies that the incorrect accumulator often wins, leading to error trials. Trials in which the correct accumulator wins are primarily trials in which, by chance, the incorrect starting point was further from the upper limit of the starting point distribution (and/or large noise in the correct accumulator pushed the correct accumulation profile towards the boundary), leading to a larger baseline-threshold distance. By averaging accumulation profiles over only correct trials (note that the sum of incorrect and correct accumulation profiles was generated, but averaged only over correct trials), we selected a biased sample, leading to the difference

between the waveforms reported above. Note that averaging the accumulation profile over all correct and error trials leads to a qualitatively similar pattern to the profile associated with correct trials, arguably due to high accuracy rates (the cancellation of any baseline effects described above is only seen with equal numbers of correct and error trials). This is also the case for the CPP waveform which does not change its shape when both correct and error trials remain in the average. Unfortunately, we can only speculate on the shape of the CPP associated with error trials, as the quality of the waveform was too low to confirm the same patterns that were observed in accumulation profile associated with error trials.

Nevertheless, the CPP and the simulated accumulation profile display similar patterns, suggesting similar underlying mechanisms, and supporting the role of the CPP as an accumulation signal. Further, these findings emphasise the importance of a direct comparison between the CPP and model predictions, as the patterns reported here are difficult to predict based on intuitive reasoning alone.

Note that, due to the design in this study, far fewer trials were obtained for 'incongruent' trials than 'uncued' or 'congruent' trials (although there were enough for each participant and each condition to generate useful ERP waveforms). This imbalance in trial numbers could be avoided by inducing decision biases using other manipulations, such as imbalanced rewards, rather than cues. Note however, that different implementations of decision bias may have different effects on decision-making (Diederich & Busemeyer, 2006; Feng et al., 2009; Leite & Ratcliff, 2011; Mulder et al., 2012; Summerfield & de Lange, 2014).

Overall, the different decision biases induced qualitatively similar changes in both the model predictions of accumulation profiles and the CPP waveforms. This evidence further supports the plausibility of the CPP as a neural correlate of the decision variable.

### 4.3. General Discussion

In this study, we aimed to test the role of the CPP as a neural substrate of the decision variable as predicted by sequential sampling models. The CPP is a centroparietal ERP component which has previously been suggested to display decision-related accumulation of evidence independent of sensory and motor processes (Kelly & O'Connell, 2013; O'Connell et al., 2012; Twomey et al., 2016). We were able to support its suitability as a decision-related EEG signal over other potential signals in Chapter 3, using a simple difficulty manipulation. Here, we built on this finding and tested the CPP and its similarity to the decision variable using more complex manipulations as well as model fits to predict accumulation profiles.

In particular, we aimed not only to explore the effect of previously untested manipulations on the CPP, but also to evaluate the resulting waveforms using sequential sampling modelling. Neural correlates of accumulation are often evaluated based on conceptual hypotheses drawing on abstract interpretations of sequential sampling models. However, the dynamics of even simple sequential sampling models are difficult to predict conceptually. We therefore used a race model to fit the behavioural data and compare the neural data to the predicted accumulation profile based on the estimated parameters.

In Experiment 1, we tested the impact of non-stationary evidence on the CPP waveform. Previous research had indicated that the CPP is susceptible to a change in evidence, a necessary feature of a signal which reflects the accumulation of evidence (O'Connell et al., 2012). Our results support this finding. While continuous evidence led to a gradual build-up of the CPP waveform, interrupted evidence caused a disruption in this build-up. Surprisingly, the two different interrupted conditions, one in which evidence was stopped, and one in which evidence was reversed, displayed very similar waveforms, even though they were associated with different behavioural patterns. Nevertheless, the pattern of the CPP closely resembled our model predictions. We fitted a race model to the data which accounted for the

changing evidence by using a different drift rate for each evidence state, and simulated its accumulation profiles for each condition. The model predictions showed qualitatively similar patterns to those observed in the CPP.

In Experiment 2, we followed the same approach, but using a manipulation of decision bias rather than non-stationary evidence. Previous research suggests that biases affect the starting point of accumulation, the effect of which on the EEG signal was unclear (Bode et al., 2012; Gao et al., 2011; Rorie et al., 2010). We found that the CPP differed in amplitude across bias conditions. In particular, the decisions in which a directional cue was incongruent with the following motion direction were associated with higher amplitudes than both decisions in which the cue was congruent with the motion and decisions in which there was no directional cue.

Once again, a race model was able to account for all behavioural data, in this case by varying only the starting points across bias conditions. The resulting accumulation profile predicted by the model showed qualitative similarities to the CPP waveforms. Both the EEG signal and the model prediction displayed a pattern in which profiles associated with different bias conditions differed only in amplitude, with the profiles of decisions with incongruent cues showing the highest amplitude, followed by uncued decisions, and trials with congruent cues showing the lowest amplitude. The model fits showed that these differences in amplitudes were not strictly the result of baseline differences, which in fact cancelled out on average, but were instead caused by a biased representation of variability parameters in correct trials.

Overall, the CPP showed waveform alterations for both manipulations, and importantly, displayed profiles which were qualitatively similar to accumulation profiles predicted by a sequential sampling model. Both the build-up profile and the absolute magnitude were shown to vary in the same way as the model predictions. These findings provide strong support for the role of the CPP as a neural substrate of the decision variable.

Despite the substantial similarity between the CPP and the predicted accumulation profiles, there were also differences worth noting. For example, in Experiment 1, the interruption in the 'stop' and 'reverse' conditions appears to cause a slight initial downward slope, while the model predicts a plateau which seems to retain a small positive slope. Additionally, in Experiment 2, the amplitude differences between the conditions are far more pronounced in the CPP than in the model predictions.

However, it is important to note that the CPP pattern is unlikely to replicate model predictions exactly for a number of reasons. Firstly, any model can, at best, be an approximation of true biological processes. This is the case here in particular, as we used a race model as a representation of sequential sampling models in general. This model was chosen as it requires only a minimal number of assumptions (compared to, for example, models which include leakage; Usher & McClelland, 2001), while still being physiologically plausible (as opposed to, for example, the Diffusion model which assumes a single accumulator which can become either positive or negative; Ratcliff & McKoon, 2008). While we suggest that the race model represents sequential sampling models as a group fairly well, it is likely that predicted accumulation profiles would differ slightly across different sequential sampling models.

A second reason for differences between the CPP and the model predictions lies in the nature of EEG recordings. EEG is measured from the scalp and can only record the sum of all electrical activity underneath each electrode. Since the brain is constantly performing accumulation-unrelated computations, the signal-to-noise ratio is low. Most of these computations are unlikely to be time-locked to the decisions and are therefore averaged out, and the impact of conducted activation from more distal sources is reduced using the current source density transform which increases the spatial selectivity of the data. Nevertheless, a proportion of noise remains. Therefore, even if the EEG component contains the activity of the neural populations which accumulate decision-related evidence (and these neural populations do so in a manner which resembles the model predictions exactly), the resulting ERP is likely to be

slightly distorted. For reasons like these, it is difficult to quantify the similarity between the CPP and the predicted accumulation<sup>16</sup>.

In summary, the current chapter provides strong support for the role of the CPP as a neural substrate of the decision variable. We have shown that the CPP is sensitive to two manipulations which influence decision-making behaviour, namely non-stationary evidence and decision biases. Importantly, we fitted a sequential sampling model to the behavioural data and simulated the resulting accumulation profiles. We found that the CPP waveform closely resembled the modelled accumulation. This indicates that the CPP seems to reflect the accumulation of evidence and remains a highly plausible correlate of the decision variable.

---

<sup>16</sup> Nevertheless, ongoing work in our lab continues to explore the similarity between neural signals and the model predictions and quantitatively compare different model predictions to the CPP.

## 5. Multiple-Alternative Decision-Making

For several decades, researchers have been exploring the mechanisms underlying perceptual decision-making, and there is now a consensus that the way perceptual decisions are made can be described by a family of models called sequential sampling models. Sequential sampling models state that to make a decision, sensory evidence from the environment is accumulated over time, until a set boundary is reached. At this point, the decision is made and the motor plan associated with a given boundary is executed. With these simple assumptions, sequential sampling models are able to account for behavioural decision-making data in a wide range of settings (Brown & Heathcote, 2008; Forstmann, Ratcliff, & Wagenmakers, 2016; Ratcliff & McKoon, 2008; Smith & Ratcliff, 2004; Usher & McClelland, 2001).

While all sequential sampling models share the assumption of the accumulation-to-bound processes described above, various models within this framework differ in a number of aspects defining this process. Generally speaking, there are two types of models: random walk models with a relative stopping rule, and accumulator models with an absolute stopping rule (Smith & Ratcliff, 2004). Random walk models assume that there is only one accumulator, in which all sensory evidence is accumulated to a single total. Accumulation begins at a starting point which is centred between two boundaries, each associated with a given alternative, and the accumulated evidence can become both positive or negative (e.g. Ratcliff & McKoon, 2008). Accumulator models on the other hand, assume that, in a choice between two alternatives, there are two accumulators, each accumulating the evidence in favour of a single alternative. The two accumulation processes race towards a common threshold and a decision is formed depending on which reaches the threshold first (Brown & Heathcote, 2008; Smith & Ratcliff, 2004). An example of an accumulator model is the leaky competing accumulator model (LCA; Usher & McClelland, 2001), which is arguably the most physiologically plausible of the sequential sampling models.

One major advantage of these models over random walk models is that they can be easily extended to decisions with any number of alternatives, by simply adding accumulators (e.g. Brown & Heathcote, 2008). Random walk models, such as the Diffusion model (Ratcliff & McKoon, 2008), on the other hand, offer no simple generalisation to multiple-alternative decision-making (although several attempts to extend the Diffusion model have been suggested; Krajbich & Rangel, 2011; Ratcliff et al., 2016; Ratcliff & Starns, 2013).

The ability of models of perceptual decision-making to apply to multi-alternative choices has received comparatively little attention. Although a large body of research has provided many findings shedding light on how we make perceptual decisions, virtually all of these findings have been based on two-alternative choices. While it is practical to reduce cognitive processes to their most basic form to study them in the lab, the ecological validity of the associated findings is questionable. Choices between two clearly defined, opposing alternatives are rare in everyday life, where we are more likely to face choices between a large number of potential responses with evidence supporting a subset of alternatives.

To date, only a small number of studies have explored multi-alternative perceptual decision-making. Studies which have explored this area have primarily focused on testing the ability of different models to account for more complex behavioural patterns associated with an increasing number of choice alternatives (Bogacz et al., 2007; Brown, Steyvers, & Wagenmakers, 2009; McMillen & Holmes, 2006; Nunes & Gurney, 2016; Roe, Busemeyer, & Townsend, 2001). Particular attention has been paid to the LCA model, which has successfully accounted for multi-alternative decision-making in a variety of settings, including standard motion discrimination tasks extended to three possible motion directions, multi-alternative decisions following non-stationary evidence, and value-based choices between several options (Bogacz et al., 2007; Ditterich, 2010; McMillen & Holmes, 2006; Tsetsos et al., 2010, 2011).

A human behavioural study on multi-alternative decisions was conducted by Niwa and Ditterich (2008), who presented three subjects with a three-alternative

random dot motion task, and found that a relatively simple model, based on a race between three accumulators, each accumulating the net evidence for a given alternative, was able to account for the behavioural data. However, it was noted that the behavioural data were not able to distinguish well between different types of sequential sampling models. In a follow-up study, Ditterich (2010) showed that several different models can explain the behavioural dataset, but found that, while different models make similar predictions for behavioural data, they differ in their internal dynamics and therefore in their predictions of a decision variable (i.e. the accumulation profile, described by sequential sampling models). He thereby highlighted the need to explore neural data as a correlate of the accumulation process, in order to gain insights into how we make perceptual multi-alternative decisions.

Only a small number of studies have recorded neural activity associated with decision-making with multiple alternatives. For binary decisions on the other hand, several neural signals have been studied and suggested to reflect the decision variable. For example, single-cell recordings in non-human primates have shown that firing rates of neurons in the lateral intraparietal area (LIP), but also the frontal eye field (FEF), and the superior colliculus (SC) display accumulation-to-bound characteristics in perceptual saccadic decision-making tasks (Gold & Shadlen, 2000, 2003; Paré & Wurtz, 2001; Roitman & Shadlen, 2002; Shadlen & Newsome, 2001).

Although a lot of research has been dedicated to studying neural correlates of decision-making, the vast majority of it focused solely on binary choices. Only a small number of studies have investigated the effects of multiple alternatives on neural correlates of the decision variable in non-human primates. In an early set of studies, Basso and Wurtz (1997, 1998) found that activity of monkey SC neurons decreased with the number of possible targets in a saccadic multi-target task. A decade later, this finding was explored more thoroughly and in the context of sequential sampling models by Churchland et al. (2008) who presented two monkeys with a two and a four-choice random dot motion task at different difficulty levels and recorded the firing rates from neurons in the LIP. Behavioural results showed that, as expected in accordance with Hick's law

(Hick, 1952), reaction times (RTs) were higher and accuracy scores were lower in the four-choice task, compared to the two-choice task. Importantly, Churchland et al. (2008) demonstrated a number of interesting patterns in the neurophysiological data. They were able to demonstrate that decisions with four alternatives show the same bounded accumulation profile, with firing rates reaching the same stereotyped level in both two and four-choice tasks. However, the firing rates associated with the two tasks differed in the beginning of the decision-making process as, in line with Basso and Wurtz (1997, 1998), four-choice decisions showed a large decrease in firing rate. This decreased level of activity at the beginning of the decision and the unaltered firing rate at response demonstrates a larger excursion extent in four-choice compared to two-choice tasks.

Higher decision boundaries, or more precisely, larger baseline-boundary distances, are associated with higher response caution, as more evidence has to be accumulated to make a decision, thereby improving the signal-to-noise ratio, but increasing decision times (Brown & Heathcote, 2008; Heitz, 2014; Ratcliff & Rouder, 1998). Since an increase in the number of alternatives increases the level of uncertainty associated with a given decision, this increase in response caution may be necessary for effective decision-making. Churchland et al. (2008) were able to account for their behavioural data using an accumulator model. It was later demonstrated that the data can also be explained by a recurrent cortical circuit model (Furman & Wang, 2008).

The finding of a reduction in firing rate in neurons associated with perceptual decision-making, with increasing numbers of alternatives has since been supported by a number of studies. Balan, Oristaglio, Schneider, and Gottlieb (2008) used a visual search task with two, four, or six elements while recording from LIP neurons, and found that firing rates decreased as elements were added to the display. Again, this difference was not seen at the time of the response. Similar findings have been reported for FEF neurons, as their firing rate during a visual-search task reduced as the number of visual elements increased (Cohen, Heitz, Woodman, & Schall, 2009). Another study using a saccadic colour-to-location task found the previously reported reduction in FEF

firing rate at the beginning of the trial, however, unlike previous studies, a reverse pattern was found at response time, with higher activity with higher numbers of alternatives (Lee & Keller, 2008).

While, as briefly summarised above, there are some studies investigating the effects of multi-alternative decisions on neural correlates of the decision variable in non-human primates, which, overall, seem to suggest a baseline decrease to be associated with an increasing number of alternatives, there is little corresponding data on human multi-alternative decision-making.

There are studies which have used functional magnetic resonance imaging (fMRI) to explore human decision-making with multiple alternatives. For example, Keuken et al. (2015) used a random dot motion task with three, five, or seven alternatives and found increased activity in the subthalamic nucleus with an increasing number of alternatives. Further, Daw, O'Doherty, Dayan, Dolan, and Seymour (2006) explored 'exploration-exploitation' behaviour using a multiple-choice decision-making task, and found that the frontopolar cortex and intraparietal sulcus showed increased activity during exploratory decisions.

However, we are not aware of any studies which directly investigated neural correlates of evidence accumulation in the human brain. A number of, primarily electroencephalographic (EEG) signals have been suggested to reflect the decision variable in the human brain in the context of binary decisions (although, to our knowledge, none have been explored in the context of multi-alternative decision-making). Among the most prominent are the event-related desynchronisation (ERD) in the beta frequency range (Donner et al., 2009; O'Connell et al., 2012; Siegel et al., 2011), an event-related potential (ERP) known as the centroparietal positivity (CPP; O'Connell et al., 2012), and the lateralised readiness potential (LRP; Kelly & O'Connell, 2013). Each of these signals has been suggested to show decision-related accumulation of evidence. Two of these signals, namely the LRP and the beta ERD, are motor preparation signals and therefore comparable to accumulation-related neural signals in non-human primates, which are typically recorded from oculomotor neurons. This implies that these signals, both from humans and non-human primates,

measure the decision-making process indirectly by tracking the preparation of the motor response which terminates the decision (i.e. saccades in monkeys and hand movements in humans). While this does not pose a problem in research with non-human primates which relies on single-cell recordings, electrophysiological recordings in humans are primarily restricted to EEG measures, which have low spatial resolution and therefore limited utility to research multi-alternative decision-making.

EEG is measured from the scalp and can therefore only record the sum of the electrical activity of all brain areas in the proximity of each electrode. It cannot track the activity of a specific region or neural population. However, signals of motor preparation are lateralised with any limb movement being processed in the contralateral hemisphere. This lateralisation implies that there is enough spatial distance between the regions preparing left and right-hand movements to be tracked individually by EEG recordings. For example, a hand movement is associated with a negativity over motor areas which is larger in the hemisphere contralateral to the movement (Ikeda & Shibasaki, 1992; Lang et al., 1991). By subtracting ipsilateral activity from contralateral recordings, any non-effector-specific activity is cancelled out, resulting in the LRP component (or, if power in the beta band is used, lateralised beta ERD), which tracks limb-specific motor preparation. This effector-specific nature of the LRP and other motor-related signals depends crucially on the lateralisation of the human motor cortex and on 'right vs left' movements. It cannot be extended to more than two response alternatives. Hence, it is unsurprising that the effects of multi-alternative decision-making on neural signals in the human brain remain largely unexplored.

In this experiment, we therefore aimed to rectify this and study the impact of multiple alternatives on a neural correlate of the decision variable in humans. Since motor-related EEG signals cannot be informative for decisions with more than two response alternatives, only the CPP remains as an established neural correlate of decision-making in the human EEG, which could potentially be extended to multi-alternative decisions. However, the CPP, even for binary decisions, does not allow for a distinction between response alternatives. It

arguably reflects the sum of all accumulators (see Chapter 4) and displays the same profile regardless of which response is chosen. Here, we therefore choose a different neural correlate of decision-making, which allows us to track the preparation of individual responses. For this purpose, we use transcranial magnetic stimulation (TMS).

TMS is a form of brain stimulation, which, when applied over the motor cortex, can induce electrical responses, called motor evoked potentials (MEPs), in the muscle associated with the stimulated region (Barker et al., 1985; Merton & Morton, 1980; Merton et al., 1982). Importantly, these evoked potentials can be used to index the level of motor preparation in the primary motor cortex or adjacent premotor areas (Bestmann et al., 2008; Hadar et al., 2012; Hadar et al., 2015; Kiers et al., 1997). It has been established that, given that a decision requires a motor response, motor preparation occurs throughout the decision-making process (Coles et al., 1985; Gluth et al., 2013; Hadar et al., 2012; Michelet et al., 2010) rather than in a serial fashion after the termination of the decision-making process, as previously suggested (Donders, 1969; Sternberg, 1969). Therefore, following the same logic as tracking motor-related EEG signals, which implies that signals of motor preparation display the same build-up as the accumulation profile itself, MEPs can be used as a correlate of the decision variable. This concept has already been shown in a number of studies. For example, Michelet et al. (2010) found that MEPs of responding muscles increased over the course of a decision before reaching a constant maximum immediately prior to the response. Similarly, Hadar et al. (2015) smoothed MEPs at different time points using a Gaussian kernel to generate a continuous signal of corticospinal excitability, and suggested that it reflects ongoing evidence accumulation. In their study, ambiguous faces were presented in a gender categorisation task and it was found that more difficult categorisations were associated with longer activations in the responding muscle than easy ones. Additionally, the authors fitted a sequential sampling model and revealed qualitative similarities between its prediction and the MEP signal, further supporting the validity of the MEP signal as a correlate of the decision variable.

Building on the approach used by Hadar et al. (2015), the current study set out to explore multi-alternative decision-making by tracking continuous MEP signals as a correlate of the decision variable. To this end, a colour-discrimination task with either two or four response alternatives was used. By mapping two separate responses, each recruiting a different dominant muscle, to each hand and measuring the activity of both muscles in the hand contralateral to the brain stimulation, we were able to record MEPs associated with each response separately (though not during the same trials; see Figure 5.2). Like Hadar et al. (2015), we evoked MEPs at random time points throughout the decision-making process and later smoothed them to generate a continuous readout of motor excitability. We hypothesised that, in line with its role as an accumulation-like signal, the MEP signal associated with the responding muscle would build up over the course of the decision and peak at the time of response. Importantly, based on evidence from non-human primates reviewed above, we hypothesised that there would be a baseline difference in the MEP signal between two and four-choice trials, with four-choice decisions leading to a reduction in baseline activity.

Since the approach of using a continuous MEP signal as a correlate of decision-making is still a novel one, we also included a manipulation of difficulty. The impact of difficulty on accumulation has been studied extensively (Mulder et al., 2014; Ratcliff & Rouder, 1998; Teodorescu & Usher, 2013) and has also been demonstrated in MEP signals (Hadar et al., 2015). We hypothesised that their findings would be replicated here.

To further test the role of the MEP signal as a correlate of the decision variable, and explore the effects of multiple alternatives, we fitted a sequential sampling model to the behavioural data and used the resulting parameter estimates to predict the accumulation profile associated with each accumulator. To this end, we used the LCA model (Usher & McClelland, 2001), as it is an accumulator model which lends itself to multiple-alternative decision-making more easily than a random walk model, and has been successfully applied to these decisions in a number of previous studies (Bogacz et al., 2007; Ditterich, 2010; McMillen & Holmes, 2006; Tsetsos et al., 2010, 2011).

Due to our unique approach, which allowed us to track the evolution of preparation of each response separately using MEPs, as well as predict the accumulation profile of each accumulator using the LCA, we were able to not only explore the decision variable with different numbers of response alternatives, but also directly compare the profile of the measured and predicted decision variable in a more detailed way.

## **5.1. Methods**

### **5.1.1. Participants**

We recruited a total of 13 participants (five males) with a mean age 26.23 ( $SD = 7.67$ ). Each participant took part in between two and four sessions (each lasting between one and three hours) and completed on average 4166 trials in total. Participants were recruited using poster advertisements and word of mouth, resulting in a sample which was primarily made up of students and staff at City, University of London. Three of the participants were researchers in the current project. All other participants were paid £ 8 per hour. All procedures were approved by the City, University of London Psychology Department Ethics Committee. Extensive information about the brain stimulation used was provided at least 24 hours before the first sessions. Additionally, each participant completed a medical screening questionnaire along with the standard informed consent, as well as a post-stimulation questionnaire.

### **5.1.2. Stimuli and Procedure**

Participants were asked to complete a colour-discrimination task. In each trial, an array of coloured pixels appeared on a screen. Each array consisted of pixels of four different colours (green, red, blue, yellow), and participants were asked to indicate which colour was most prevalent, using the corresponding one of four response buttons (see Figure 5.1).

### **5.1.2.1. Colour Calibration**

In order to ensure that the difficulty of the task did not vary excessively across different trials depending on which colour was dominant, it was important to match the perceived salience of the four colours. To this end, three participants (one male, mean age= 33.33 ( $SD = 7.09$ ), all researchers in the current project) completed a colour-matching task, using a Method of Adjustment procedure. Each participant was presented with an array of coloured pixels, which initially consisted of pixels of two different colours, one fixed colour (green), and one colour that could be adjusted to match the fixed colour in perceived salience, by increasing or decreasing its brightness using 'up' and 'down' keys on a keyboard. When participants found the appropriate colour intensity, the 'enter' key was pressed to confirm their selection and a third colour was added to the array. Again, participants were asked to adjust its brightness before the fourth colour was added and the procedure was repeated. The brightness was adjusted by converting the original colours into HSV colour space, in which colours are defined by the parameters hue, saturation, and value, and increasing/decreasing the 'value' parameter by a value of 0.05 for each 'up'/'down' press. Each participant completed 60 trials. The initial intensity as well as the order of the three colours that were to be adjusted (red, yellow, blue) were randomised across trials. The chosen colour intensities were averaged across trials and participants, resulting in the following colours that were used in the experiment: green (RGB [0 0.6 0]), red (RGB [0.8 0 0]), yellow (RGB [0.92 0.74 0]), blue (RGB [0.12 0.12 0.61]).

### **5.1.2.2. Stimuli and Experiment Setup**

All stimuli were written in Matlab (The Mathworks, Natick, U.S.A.), primarily using the Psychtoolbox extension (Brainard, 1997; Kleiner et al., 2007; Pelli, 1997), and presented on a Display++ LCD monitor (Cambridge Research Systems, Ltd., Rochester, UK, display size: 41 cm x 30 cm), operating at a refresh rate of 100 Hz and a resolution of 1240 x 786. Participants were seated at a distance of approximately 100 cm from the screen. Each trial presented a stimulus array of coloured pixels (6 x 6 degrees of visual angle; each coloured

pixel spanned 2 x 2 screen pixels, resulting in an array of 145 x 145 coloured pixels).

Participants held two digital response buttons interfaced via a 16 bit A/D card (National Instruments X-series PCIe-6323, sampling rate 100,000 Hz) in each hand, one between their thumb and index finger (pinch), and one in the palm of their hand, attached to a plastic cylinder (grasp; Hadar et al., 2012). The pinch response required participants to squeeze the small button using index finger and thumb, contracting the first dorsal interosseous (FDI) muscle, while the grasp response was made by tightly gripping the cylinder, activating the abductor digiti minimi (ADM) muscle. Each colour was mapped to one of the four response buttons. The colour-response mapping was randomised across participants.

In the experiment, each trial consisted of a cue (500 ms), the coloured stimulus array (2000 ms or until response), and a brief inter-stimulus interval (minimum 500 ms; see Figure 5.1 and section 5.1.3). The experiment consisted of both two and four-choice trials, as well as easy and hard trials. To manipulate the difficulty of the task, the percentage of pixels of the dominant colour varied between 33% (easy) and 30% (hard). The remaining colours each took up 22% and 23% of the array respectively. The cue at the beginning of each trial informed participants whether a given trial was a two or a four-choice trial by presenting either two or four coloured squares representing the possible choices. In two-choice trials, possible responses were either both in the same hand ('within') or both requiring the same movement ('between'), leading to four potential combinations ('within-left', 'within-right', 'between-pinch', 'between-grasp'; see Figure 5.1).

One third of trials were four-choice, one third were two-choice 'within', i.e. the two possible responses were on one hand (left pinch - left grasp, right pinch - right grasp), and one third of trials were two-choice 'between', i.e. responses from both hands were possible (left pinch - right pinch, left grasp - right grasp). The order of the trials was randomised. Note that the difference between the two and four-choice trials lay solely in the instructions conveyed by the cue, and

that the stimulus array and the percentage of the four colours within it did not change.

In the first session, participants completed 150 practice trials, to familiarise themselves with the task and the colour-response mapping. Participants completed between five and six experimental blocks per session, with each block consisting of 168 trials (plus additional trials to regulate TMS frequency; see section 5.1.3).

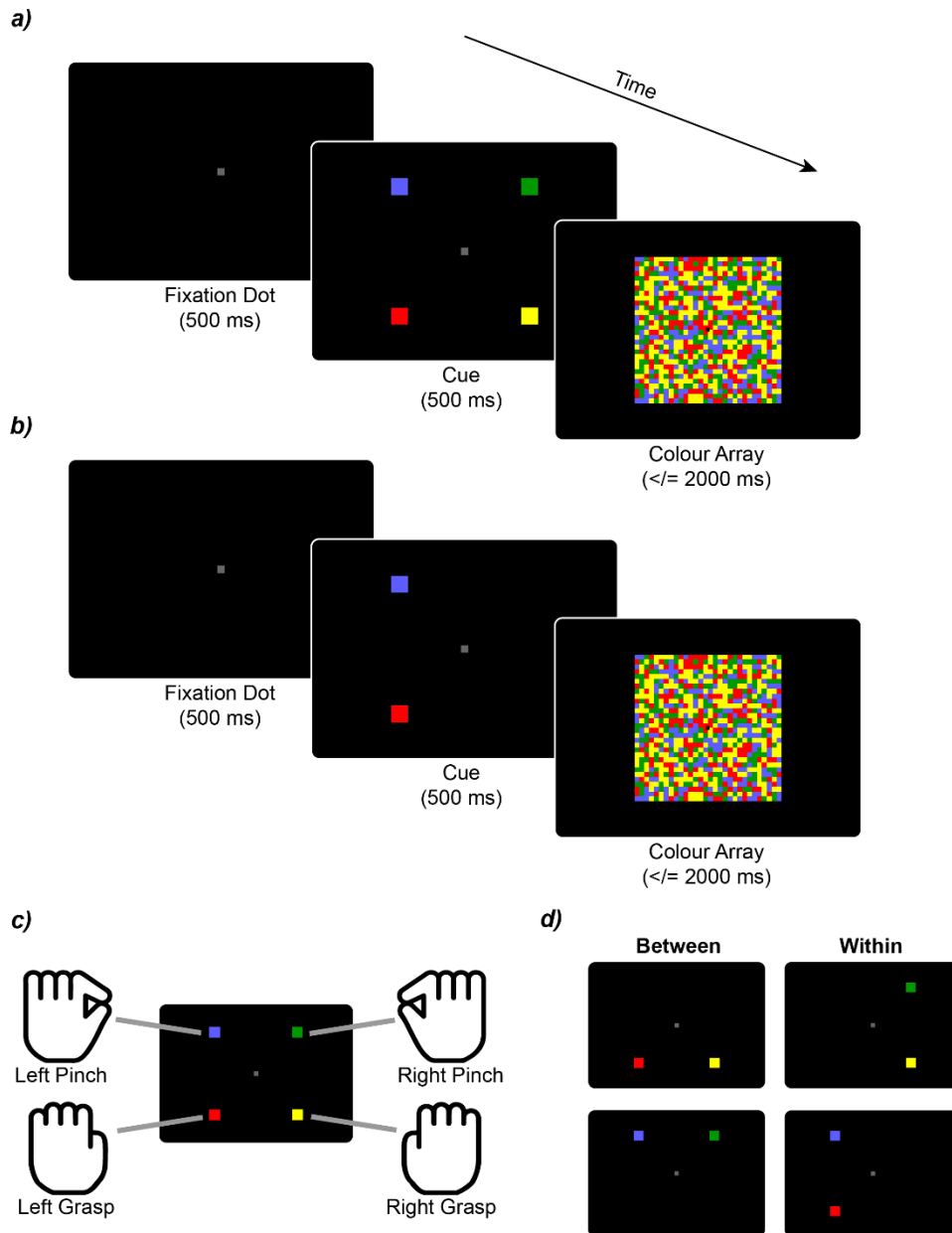


Figure 5.1: Colour discrimination task: each trial began with a fixation dot in the middle of the screen, followed by a cue which indicated which responses were possible in the following stimulus. Then, the colour array was displayed for 2000 ms or until the response. a) Four-choice task: all possible cues were displayed, indicating a four-choice trial; b) Two-choice task: only two of the possible cues were shown, indicating a two-choice trial. Here both cues are on the left-hand side, indicating that a left-hand response is required ('within' trial). c) Each cue/colour was associated with a specific response: the top right cue (here: green) was associated with a right-hand 'pinch' response, the top left cue (here: blue) was associated with a left-hand 'pinch' response, the bottom right cue (here: yellow) was associated with a right-hand 'grasp' response, and the bottom left cue (here: red) was associated with a left-hand 'grasp' response. Note that the colour-response mappings were randomised across participants while the cue location-response mapping remained the same; d) all possible two-choice combinations. In 'within' trials, both possible responses were on the same hand, while in 'between' trials, the two possible responses were on two hands but using the same response (pinch/grasp). Note that the size of the coloured pixels has been increased for illustration.

### 5.1.3. Stimulation and Recording

Participants' muscle activity was recorded using surface electromyography (EMG), recorded at a sampling rate of 1000 Hz via a 13 bit A/D Biometrics Datalink system (version 7.5, Biometrics Ltd., Ladysmith, VA, U.S.A., 2008) and band-pass filtered (20 to 450 Hz). Surface Ag/AgCl electrodes (22 mm x 28 mm, part No. SX230FW, Biometrics Ltd., Ladysmith, VA) were placed on the skin above the first dorsal interosseous (FDI), and the abductor digiti minimi (ADM) of each hand, as they contribute to the 'pinch' and 'grasp' responses respectively. Reference electrodes were placed at distances of approximately 2 cm to each of the four active electrodes. The recorded EMG signal of the right ADM and FDI was also passed to speakers placed on the left and right of the participant respectively, with noise informing participants that their muscles were not fully relaxed between responses.

During the experiment, single-pulse TMS was applied using a MagstimRapid<sup>2</sup> biphasic stimulator (The Magstim Co. Ltd., Whitland, UK). To induce motor evoked potentials (MEP) in both the ADM and the FDI of the right hand, a 70-mm figure-of-eight coil (external casing diameter approximately 90 mm for each loop) was positioned on the scalp over the left motor cortex. The exact location and stimulation intensity was adjusted for each participant individually and was set at approximately 110% of the resting motor threshold. The resting motor threshold was defined as the minimal intensity to elicit an MEP with a peak-to-peak amplitude of approximately 50  $\mu$ V in 50% of stimulations.

TMS pulses were planned in 57% of trials from each condition. In order to ensure a good distribution of TMS pulses during a baseline interval and over the course of the reaction time, TMS trials were divided into four equally frequent time bins between -200 and 700 ms relative to the stimulus onset (between 300 and 1200 ms relative to cue onset). Within a given bin, the exact stimulation time was drawn randomly for each trial. Since the experiment followed a single-pulse TMS protocol, the stimulation pulses were required to occur at a maximal frequency of 0.2 Hz. If, by chance, a planned pulse followed a previous one after less than 5000 ms, the task was adjusted in several ways. If the timespan

between the previous and the planned pulse was less than 5000 ms but more than 4000 ms, the inter-trial interval was increased in order to decrease the pulse frequency to its necessary limit. If, on the other hand, the duration between the last and the planned pulse was less than 4000 ms, the planned trial was replaced with the next planned stimulation free trial. If there were no stimulation free trials left, random stimulation free trials were generated in order to increase the interval between TMS pulses. Due to this method, an average of 434 trials were added per session, leading, in total, to an average of 1354 trials per session. Planned pulses were not delivered if a response had already been detected, as this precluded analysis of the resulting MEP (see below).

## 5.1.4. EMG Processing

### 5.1.4.1. Pre-processing

All EMG processing was performed in Matlab (The Mathworks, Natick, U.S.A.). Data from each trial were aligned to the stimulus onset and visually inspected. An algorithm applying the Teager-Kaiser energy operator (TKEO) was used to detect the onset time of muscle activity (EMG RT) associated with each response (Li & Aruin, 2005; Li, Zhou, & Aruin, 2007; Solnik, Rider, Steinweg, Devita, & Hortobágyi, 2010). The discrete TKEO  $\psi$  for a given EMG value  $x$  of the sample  $n$ , was defined as:

$$\psi[x(n)] = x^2(n) - x(n+1)x(n-1) \quad (5.1.)$$

A threshold-based method was used to identify the onset of muscle activity. The threshold was determined as:

$$T = \mu + h \sigma \quad (5.2.)$$

With  $\mu$  and  $\sigma$  representing the mean and standard deviation of a baseline period (-300 to 200 ms relative to cue onset), and  $h$  set to 3. Additionally, all trials were visually inspected and the EMG onset was adjusted manually if necessary. Visual inspection provided no information about the experimental condition of a given trial. Trials with muscular artifacts, no detectable EMG onset, or partial responses on more than one channel were excluded from further analysis (6.41% of all recorded trials).

We further excluded all trials with button RTs of more than or equal to 2000 ms or less than 180 ms, or EMG RTs of more than 1850 ms or less than 30 ms (< 1% of all recorded trials). The remaining EMG RTs were normalised by the median EMG RT per participant and per session.

In TMS trials, MEP amplitudes in both channels (FDI and ADM) of the right hand were defined as the difference between the minimal and maximal EMG values in a time window of 10 to 40 ms relative to stimulation time. Trials which showed muscular activity previous to the TMS pulse, defined by EMG amplitudes exceeding 50  $\mu$ V in a period of 200 ms preceding the stimulation, were excluded from further analysis (4.51% of all trials). Further, trials in which no MEP was visible or in which the amplitude of the MEP could not be accurately detected due to saturation were discarded (2.02% of all trials). Trials were also excluded if the participant's response preceded the planned TMS (4.36% of all trials).

In total, 17.53% of all recorded trials were discarded, leading to a total of 44,669 usable trials (note that 35.38% of TMS trials were excluded, with a total of 13,588 usable TMS trials remaining for analysis). The remaining MEP amplitudes were z-scored per muscle, session, and participant, in order to normalise the magnitudes of evoked responses which are likely to vary between muscles.

#### **5.1.4.2. Re-categorisation**

The channels (FDI and ADM) of correct trials were reclassified into one of four categories. MEPs recorded from correctly responding muscles were classed as 'Correct', while MEPs from the non-responding muscles were classified into three different error categories, 'Error1', 'Error2', and 'Error 3'.

MEPs were categorised as 'Error 1' if they were either non-responding but cued in two-choice trials, or non-responding but on the same hand as the correctly responding muscle in four-choice trials. 'Error 2' referred to MEPs from non-responding muscles in two-choice trials which were not cued but were either on

the same hand as the responding muscle ('two-choice between') or on the same muscle of the other hand ('two-choice within'), as well as to MEPs from the same muscle as the responding muscle but on the other hand in four-choice trials. Lastly, MEPs recorded from non-responding muscles which are neither on the same hand nor the same muscle on the other hand, as the responding muscle, were categorised as 'Error 3' (see Figure 5.2). For example, if a four-choice trial required the correct response 'right pinch', MEPs recorded from the right FDI (right pinch) were classed as 'Correct', MEPs recorded from the right ADM (right grasp) as 'Error 1', while the left FDI (left pinch) would be categorised as 'Error 2', and the left ADM (left grasp) as 'Error 3'. Note however, that only the left motor cortex was stimulated, eliciting MEPs in only the right hand. Therefore, any given trial only provided two MEPs which were sorted into two of the four categories.

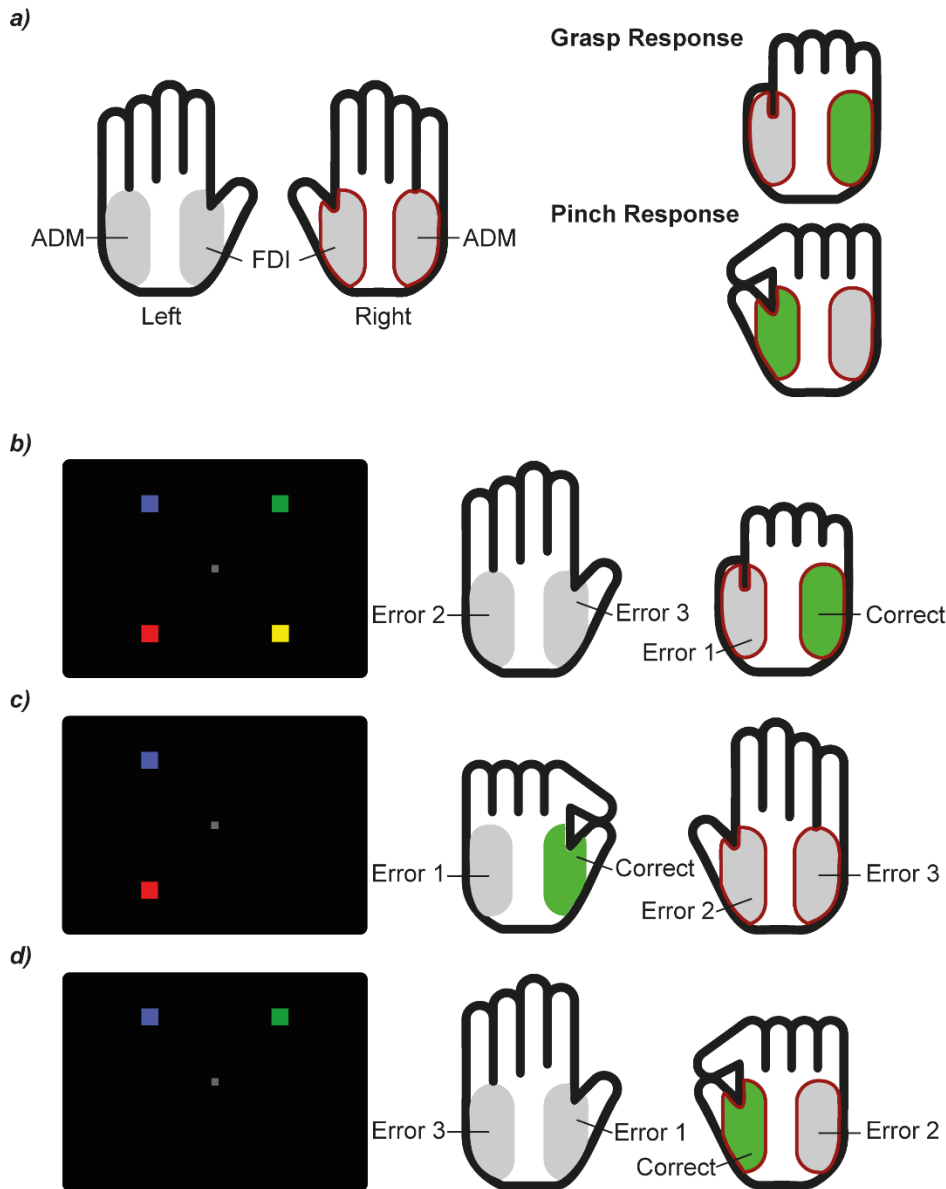


Figure 5.2: MEP categorisation: a) each hand performed pinch and grasp responses, recruiting the FDI and ADM muscle respectively. Non-responding FDI and ADM muscles are displayed in grey, and responding muscles are shown in green. MEPs were only recorded from the right hand (recorded muscles indicated by dark red border). b) four-choice trial resulting in a right grasp response. In four-choice trials, the responding muscle is labelled 'Correct', the non-responding muscle on the same hand is labelled 'Error 1', and the muscles on the non-responding hand are labelled 'Error 2' (for the same muscle as the responding one) and 'Error 3' (for the remaining muscle). Therefore, here, the recorded MEPs are classed as 'Correct' ('grasp' muscle, ADM), and 'Error 1' (passive 'pinch' muscle, FDI). c) Two-choice trial (within) resulting in a left pinch response. In 'within' two-choice trials, the responding muscle is classed as 'Correct', the non-responding but cued muscle is classed as 'Error 1' (here, the non-responding muscle on the same hand), the muscle corresponding to the responding muscle but on the opposite hand is labelled 'Error 2' and the remaining muscle is labelled 'Error 3'. Here, the recorded MEPs are classed as 'Error 3' ('grasp' muscle ADM), and 'Error 2' ('pinch' muscle FDI). d) Two-choice trial (between) resulting in a right pinch response. In 'between' two-choice trials, the responding muscle is classed as 'Correct', the non-responding but cued muscle is classed as 'Error 1' (here, the same muscle in the opposite hand), the non-responding muscle on the same hand is labelled 'Error 2' and the remaining muscle is labelled 'Error 3'. Here, the recorded MEPs are classed as 'Error 2' ('grasp' muscle ADM), and 'Correct' ('pinch' muscle FDI).

### 5.1.4.3. Smoothing

For each correct/error category and each condition, all MEPs associated with correct trials were pooled across participants and sessions. To this end, the stimulation times were normalised for each session and participant and expressed as a percentage of their median EMG RT (of stimulation free trials). Pooled MEPs were sorted in time and aligned to both the stimulus and the response, then smoothed (see Figure 5.3).

In order to generate a continuous signal, the amplitudes of the sorted MEPs were smoothed using a Gaussian kernel:

$$\hat{Y}(t) = \frac{\sum_{i=1}^N e^{-\frac{(t-t_i)^2}{2\sigma^2}} Y_i}{\sum_{i=1}^N e^{-\frac{(t-t_i)^2}{2\sigma^2}}} \quad (5.3.)$$

Where  $N$  is the number of MEPs, each being associated with a magnitude  $Y_i$  and a time  $t_i$ . The smoothed signal was calculated in time steps of 1% median EMG RT, using a smoothing kernel with a full-width half maximum of 5% median EMG RT.

A smoothed signal was generated for each time-lock (stimulus and response-locked), each correct/error category ('Correct', 'Error1', 'Error2', and 'Error3'), and each condition (number of alternatives: two/four, difficulty: easy/hard). Additionally, we generated a smoothed signal for the difference in MEP responses between the 'Correct' and the 'Error 1' muscles. This difference between a responding and a non-responding muscle cancels out any non-specific spinal influences which affect the MEPs of both muscles equally, and importantly, has therefore been suggested as the most suitable neurometric signal to reflect the decision variable in this context (Hadar et al., 2015).

Although we were able to generate smoothed MEP signals for each of the four responses ('Correct', 'Error1', 'Error2', and 'Error3'; see above), this was only possible by pooling MEP recordings from different trials. In order to take differences between MEP values and accurately remove any non-specific spinal effects, however, only MEPs recorded at the same time in the same trial can be used. Since the only trials in which we recorded MEPs for both 'Correct' and

'Error 1' responses simultaneously are four-choice trials in which the correct response is on the right hand, and two-choice 'within' trials, in which both cued responses are on the right hand, we selected these trials to create a smoothed MEP signal for the difference between the responding ('Correct') and non-responding (here: 'Error 1') trials.

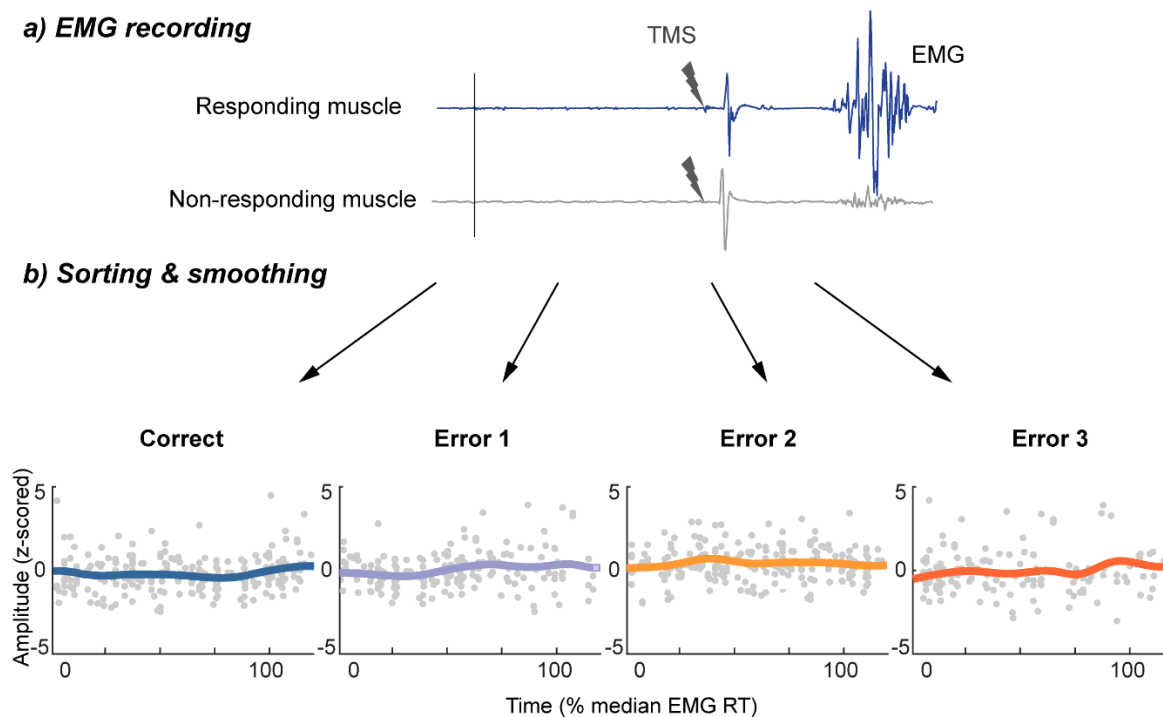


Figure 5.3: MEP processing: a) MEPs are recorded from two muscles (right FDI and right ADM, shown here as responding and non-responding) during each TMS trial; b) z-scored MEPs from each channel are sorted into one of four categories ('Correct', 'Error 1', 'Error 2', 'Error 3'; see Figure 5.2) and smoothed to generate a continuous MEP signal.

#### 5.1.4.4. Statistical Analysis

Based on previous research in non-human primates (Balan et al., 2008; Churchland et al., 2008; Cohen et al., 2009), we hypothesised that two-choice and four-choice trials would differ during the baseline period, with two-choice MEPs displaying higher amplitudes than four-choice MEPs. To test this, we conducted a paired t-test by first finding the mean absolute MEP size (for each participant) of all MEPs which were recorded prior to the stimulus onset and associated with a cued response. This means that, for four-choice trials, all MEPs during the baseline-period were used, while for two-choice trials, only MEPs from muscles categorised as 'Correct' or 'Error 1' were used.

We also expected a difference in the MEP signal depending on the difficulty of the task, with 'easy' trials displaying a steeper accumulation rate than 'hard' trials. To test this, we collapsed over two-choice and four-choice trials, and fitted a straight line to the stimulus-locked (between 50% and 90% median EMG RT) and response-locked (between -50% and -10% median EMG RT) MEP signal based on the difference between responding and non-responding muscles, for 'easy' and 'hard' trials. We then subtracted the resulting slope for 'hard' trials from the slope associated with 'easy' trials. We used a non-parametric permutation test with 1999 iterations to generate new sets of resampled 'easy' and 'hard' conditions (without replacement) and calculated the slope difference between them. The original slope difference was then compared to the resulting null distribution of differences.

### **5.1.5. Model**

We used the LCA model to fit the behavioural data (Usher & McClelland, 2001). The LCA is an accumulator model and is therefore easily extended to multiple alternatives. The accumulation traces are defined by a drift rate  $v$  as well as noise, and race towards a threshold  $A$ . The LCA is a comparatively complex sequential sampling model as it is designed to explain the accumulation process in a more neurophysiologically plausible way than other models within this framework. To this end, the LCA includes a leakage parameter  $k$ , aiming to account for the finding that neural excitatory input currents decay over time (Abbott, 1991; Hodgkin & Huxley, 1990; Stein, 1967). Although this effect is decreased by recurrent self-excitation in populations of neurons, Usher and McClelland (2001) argued that this passive decay means that information is not integrated perfectly and that leaky integrators are a more physiologically plausible model of evidence accumulation. Additionally, the LCA implements physiological evidence suggesting lateral inhibition between neuronal populations (Desimone, 1998; Reynolds et al., 1999), by including a parameter  $\beta$  for mutual inhibition between accumulators (see Figure 5.4).

Thus, in a binary decision involving the accumulators  $m$  and  $n$ , the change in activation in accumulator  $m$  is given by:

$$dx_m = I_m - k x_m - \beta x_n + N(0, \sigma^2) \quad (5.4.)$$

Where  $I$  is the input into the accumulator and  $N(0, \sigma^2)$  is noise drawn from a normal distribution with a mean of 0 and a standard deviation of  $\sigma$ . To further strengthen the neural plausibility of the LCA, the authors added a threshold function to prevent accumulation from dropping below zero, as the activity of a neuronal population, which accumulation arguably represents, cannot be negative:

$$x_m(t + 1) = \max(0, x_m(t) + dx_m) \quad (5.5.)$$

In accordance with other models, the LCA assumes that a decision is made when either of the accumulators reaches the threshold  $A$ , and the RT is made up of the time required to reach the threshold, and a non-decision time  $T_{er}$ , which accounts for sensory and motor processes before and after the accumulation process.

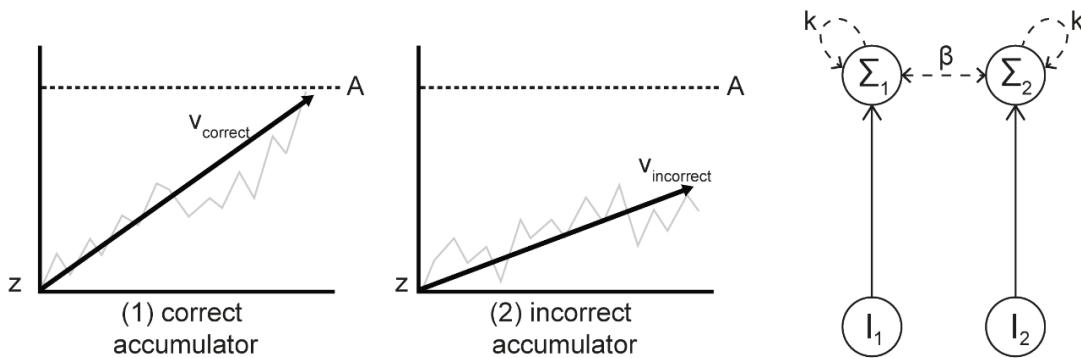


Figure 5.4: Standard LCA model: Left: two accumulators, one for the correct alternative, and one for the incorrect alternative, race towards a threshold  $A$ , starting at a starting point  $z$  (typically  $z = 0$ ) and increasing at a rate given by the drift rates  $v_{correct}$  and  $v_{incorrect}$  respectively. Right: Two accumulators  $\Sigma_1$  and  $\Sigma_2$  receive input  $I_1$  and  $I_2$ . The accumulation of a given accumulator is affected by leakage over time ( $k$ ) and by inhibition from the other accumulator ( $\beta$ ).

### 5.1.5.1. Model Fit

In order to apply the LCA to our data set, we tested a total of three models (see Table 5.1). In Model 1, we extended the model to include four accumulators. In a four-choice task, the drift rate of the correct accumulator was given by  $v_{correct}$ , while the drift rate for all other accumulators was given by  $v_{incorrect}$ . The starting point  $z_{four-choice}$  was set to 0, and along with the threshold  $A$  and the leakage  $k$ , equal across accumulators. The inhibition between accumulators was given by two parameters,  $\beta_1$  and  $\beta_2$ . Separate inhibition parameters are chosen depending on the anatomical adjacency of responses, with one parameter

describing inhibition between different muscles of the same hand or between the same muscles on each hand, and one describing the inhibition between different muscles on different hands. Specifically,  $\beta_2$  describes the inhibition induced by the evidence associated with the opposite response and opposite hand relative to a given accumulator, while inhibition between all other accumulators is given by  $\beta_1$  (see Figure 5.5). This means that the change in accumulation for each accumulator is given by:

$$\begin{aligned}
 dx_{Correct} &= I_{Correct} - k x_{Correct} - \beta_1 x_{Error1} - \beta_1 x_{Error2} - \beta_2 x_{Error3} + N(0, \sigma^2) \\
 dx_{Error1} &= I_{Error1} - k x_{Error1} - \beta_1 x_{Correct} - \beta_1 x_{Error3} - \beta_2 x_{Error2} + N(0, \sigma^2) \\
 dx_{Error2} &= I_{Error2} - k x_{Error2} - \beta_1 x_{Correct} - \beta_1 x_{Error3} - \beta_2 x_{Error1} + N(0, \sigma^2) \\
 dx_{Error3} &= I_{Error3} - k x_{Error3} - \beta_1 x_{Error1} - \beta_1 x_{Error2} - \beta_2 x_{Correct} + N(0, \sigma^2)
 \end{aligned}
 \tag{5.6.}$$

In two-choice decisions the same four-accumulator structure was used with the following exceptions: based on previously demonstrated baseline differences (e.g. Churchland et al., 2008), the two accumulators associated with the cued responses ('Correct' and 'Error 1'; see Figure 5.2) started the accumulation process at a starting point defined by  $Z_{two-choice-cued}$ , while the starting point of the other two accumulators ('Error 2' and 'Error 3')  $Z_{two-choice-uncued}$  was set to 0. The drift rate of the two accumulators associated with the non-cued responses ('Error 2' and 'Error 3'), was also set to 0, so that only noise was accumulated in these accumulators (see Figure 5.5 b).

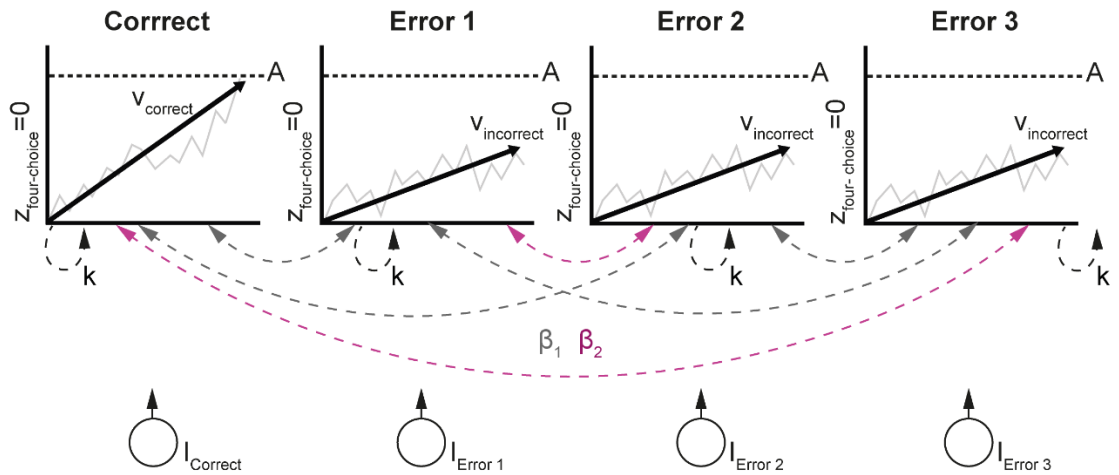
Lastly, the drift rates  $v_{correct}$  and  $v_{incorrect}$  varied across difficulty levels, leading to a model with a total of 10 free parameters ( $v\text{-easy}_{correct}$ ,  $v\text{-easy}_{incorrect}$ ,  $v\text{-hard}_{correct}$ ,  $v\text{-hard}_{incorrect}$ ,  $Z_{two-choice-cued}$ ,  $k$ ,  $\beta_1$ ,  $\beta_2$ ,  $\sigma^2$ ,  $T_{er}$ ). The threshold parameter  $A$  was used as a scaling parameter and set to 1. Model 1 is displayed in Figure 5.5.

By setting the drift rate of the non-cued accumulators to 0 in Model 1, we assume that attentional selection occurs at an early processing stage, gating the signal at a sensory level. Since this is based on speculation alone, we also tested a model without this assumption, Model 2. Model 2 is identical to Model 1, with the exception that the drift rate of the two uncued accumulators in two-

choice conditions ('Error 2' and 'Error 3') were not set to 0, but instead to the same  $v_{\text{incorrect}}$  as 'Error 1'. This resulted in a model with the same 10 free parameters as Model 1 ( $v\text{-easy}_{\text{correct}}$ ,  $v\text{-easy}_{\text{incorrect}}$ ,  $v\text{-hard}_{\text{correct}}$ ,  $v\text{-hard}_{\text{incorrect}}$ ,  $Z_{\text{two-choice-cued}}$ ,  $k$ ,  $\beta_1$ ,  $\beta_2$ ,  $\sigma^2$ ,  $T_{\text{er}}$ ).

Lastly, we also tested a model in which there was no difference in baseline between two-choice and four-choice conditions, but which introduced a difference in drift rate instead. This model, Model 3, is identical to Model 1 with the exception that the starting point is set to 0 for all conditions, and that two-choice and four-choice conditions have separate correct and incorrect drift rates ( $v\text{-easy-four}_{\text{correct}}$ ,  $v\text{-easy-four}_{\text{incorrect}}$ ,  $v\text{-easy-two}_{\text{correct}}$ ,  $v\text{-easy-two}_{\text{incorrect}}$ ,  $v\text{-hard-four}_{\text{correct}}$ ,  $v\text{-hard-four}_{\text{incorrect}}$ ,  $v\text{-hard-two}_{\text{correct}}$ ,  $v\text{-hard-two}_{\text{incorrect}}$ ). Note that, like in Model 1, the drift rates in uncued accumulators were set to 0. This resulted in a total of 13 free parameters for Model 3 ( $v\text{-easy-four}_{\text{correct}}$ ,  $v\text{-easy-four}_{\text{incorrect}}$ ,  $v\text{-easy-two}_{\text{correct}}$ ,  $v\text{-easy-two}_{\text{incorrect}}$ ,  $v\text{-hard-four}_{\text{correct}}$ ,  $v\text{-hard-four}_{\text{incorrect}}$ ,  $v\text{-hard-two}_{\text{correct}}$ ,  $v\text{-hard-two}_{\text{incorrect}}$ ,  $k$ ,  $\beta_1$ ,  $\beta_2$ ,  $\sigma^2$ ,  $T_{\text{er}}$ ).

a) **Four-choice decisions**



b) **Two-choice decisions**

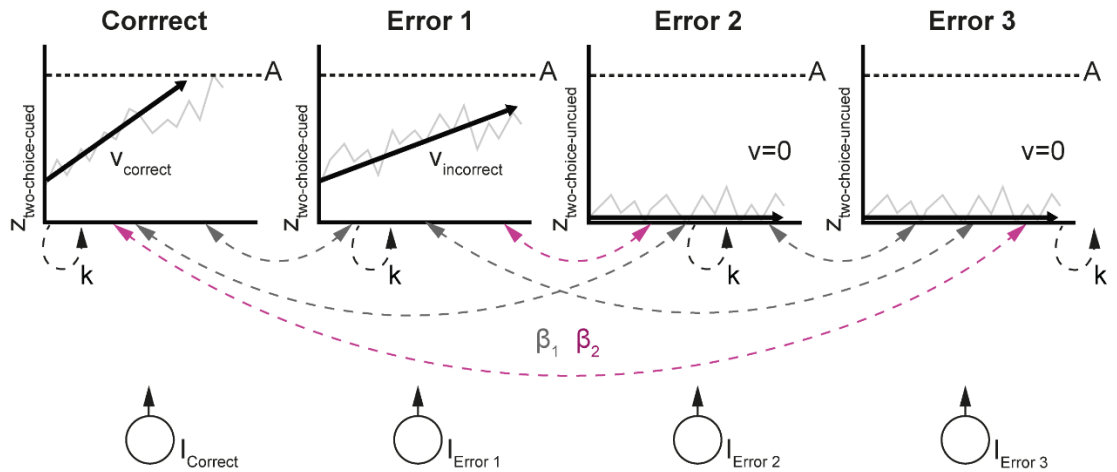


Figure 5.5: Model 1: LCA model applied to the current experiment: a) *Four-choice decisions*: four accumulators race towards a threshold  $A$ . Each accumulator receives input  $I$  and starts at a starting point  $Z_{\text{four-choice}} = 0$ . The accumulator associated with the correct alternative increases at a rate  $v_{\text{correct}}$  while all other accumulators increase at a rate given by  $v_{\text{incorrect}}$ . Each accumulator is affected by leakage over time ( $k$ , black, dashed arrows). Two inhibition parameters  $\beta_1$   $\beta_2$  define the inhibition between accumulators. Two accumulators representing different responses (pinch/grasp) on different hands inhibit each other with a strength of  $\beta_2$  (pink, dashed arrows). All other accumulators inhibit each other with a strength of  $\beta_1$  (grey, dashed arrows). b) *Two-choice decisions*: like a), but the two uncued responses ('Error 2' & 'Error 3') only accumulate noise, with a drift rate of 0. The starting points of the accumulators associated with the two responses which were cued increases to the positive value  $Z_{\text{two-choice-cued}}$ . The correct accumulator integrates evidence at a rate given by  $v_{\text{correct}}$  while the incorrect, but cued, accumulator ('Error 1') integrates evidence at a rate of  $v_{\text{incorrect}}$ . (Note that the only difference in Model 2 is in 'Error 2' & 'Error 3' in b, in which  $v$  is not 0, but  $v_{\text{incorrect}}$ . Model 3 on the other hand assumes all starting points to be 0, and that there is a separate set of  $v_{\text{correct}}$  and  $v_{\text{incorrect}}$  for two-choice and four-choice decisions).

To fit each model to the data, the normalised EMG RTs remaining after EMG processing were pooled across participants to estimate the model parameters at the group level. A total of 20,000 simulated EMG RTs were compared to the empirical data using Quantile Maximum Probability Estimation (Heathcote et al.,

2002) and parameter values were adjusted using a differential evolution algorithm implemented in Matlab (The Mathworks, Natick, U.S.A.; Price et al., 2005).

The three models were compared regarding their goodness of fit, by calculating two measures of fit which consider the likelihood as well as the number of free parameters of the model, namely the Bayesian information criterion (BIC, Schwarz, 1978) as well as the Akaike information criterion (AIC; Akaike, 1977). The model which best fitted the data according to these measures was then used to generate predictions of the accumulation profile.

#### **5.1.5.2. Model Prediction**

Once the best-fitting parameter values of the best model were estimated, we used the equations described above ((5.5.), (5.6.)) to simulate a total of 20,000 accumulation paths for each condition. Since we used EMG RTs rather than button RTs to fit the model (i.e. the time taken for movement of effectors was not included), we assume that virtually all of the estimated non-decision time described sensory processes. We therefore started the accumulation profile after a sensory delay given by  $T_{er}$ <sup>17</sup>.

Simulated MEPs were defined as the amplitude of a given accumulator at random MEP latencies (generated in the same way as described in section 5.1.3). Just as in the experimental data, only simulated MEPs that occurred before the decision was reached were retained. The simulated MEPs associated with correct decisions were then smoothed (in the same way as described in section 5.1.4.3) to create continuous MEP signals. Since the TMS paradigm used here allowed us to track each of the (up to) four responses

---

<sup>17</sup> It could be argued that a very small proportion of the non-decision time should be categorised as motor processing time to account for the brief interval in which the motor signal travels through the corticospinal tract. However, from comparing the timing of TMS pulses and MEPs, we estimate that this takes only approximately 30 ms. Since we compared model predictions and MEP signals on a qualitative basis only, we argue that this difference is negligible.

separately (though not simultaneously; see section 5.1.4.), we simulated and plotted the accumulation profile for each accumulator separately.

To create a prediction equivalent to the MEP signal reflecting the difference between the responding and the non-responding muscle of the same hand (see section 5.1.4.3), we also took the difference of only the MEPs classed as 'Correct' and 'Error 1' and generated a smooth signal per condition in the same way as described above.

Lastly, the resulting profiles were averaged within each condition and time-locked once to the onset of the decision-making process (stimulus-locked), and once to the EMG onset (response-locked).

## 5.2. Results

### 5.2.1. Behavioural Results

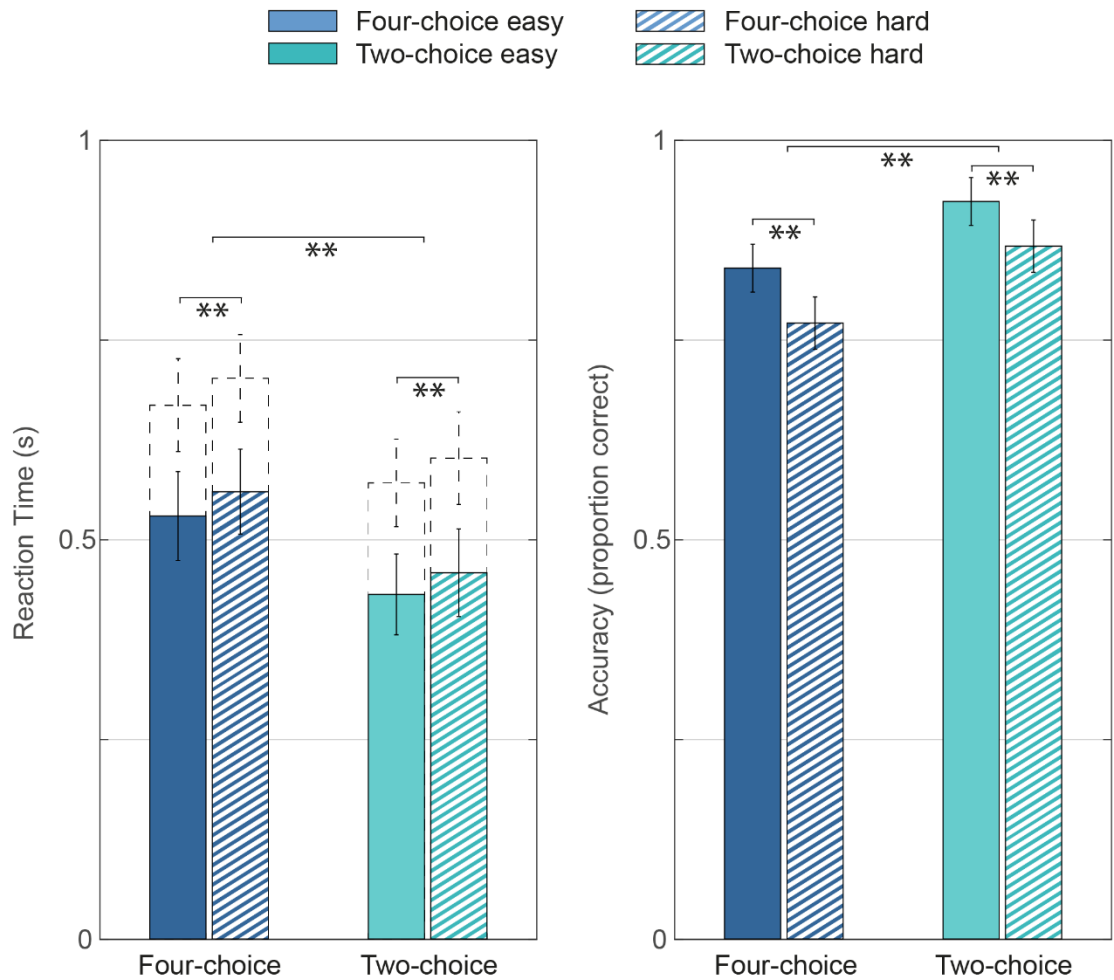
To analyse potential behavioural differences between conditions, only stimulation free trials (remaining after EMG and MEP processing) were used (see Figure 5.6 a)<sup>18</sup>. Since there were no significant differences between two-choice decisions involving one hand ('within') or two hands ('between') in RT, EMG RT or accuracy ( $p > .27$ ), we collapsed over all two-choice conditions. To explore the effects of 'Number of Alternatives' and 'Difficulty' on correct EMG RT, we used a two-by-two repeated measures ANOVA, with the levels 'two/four' and 'easy/hard'. We found a significant main effect of 'Number of Alternatives',  $F(1, 12) = 207.10$ ,  $p < .001$ ,  $\eta_p^2 = .95$ , with four alternatives ( $M = 544$  ms) being associated with longer reaction times than two alternatives ( $M = 445$  ms). Additionally, there was a significant main effect of Difficulty,  $F(1, 12) = 117.37$ ,  $p$

---

<sup>18</sup> Since the application of a TMS pulse alters response times, typically only stimulation free trials are used in the behavioural analysis. Since we reported some unexpected findings in the MEP data (see section 5.2.2.1), indicating no difference between 'easy' and 'hard' trials, we also analysed the EMG RT associated with TMS trials in order to rule out that the null finding in the MEP amplitude was caused by behavioural differences between TMS and stimulation free trials. An ANOVA exploring EMG RTs in TMS trials showed qualitatively similar findings to the ANOVA reported above (main effect of 'Number of Alternatives':  $p < .001$ , main effect of 'Difficulty':  $p < .001$ , interaction effect:  $p = .08$ ).

< .001,  $\eta_p^2 = .91$ , with 'hard' trials ( $M = 509$  ms) being associated with longer reaction times than 'easy' trials ( $M = 480$  ms). There was no significant interaction effect ( $p = .68$ ). Note that for this ANOVA, we used EMG onset time as RT. However, the same analysis with button RT as time of response led to qualitatively identical results (main effect of 'Number of Alternatives':  $p < .001$ , main effect of 'Difficulty':  $p < .001$ , interaction effect:  $p = .76$ ).

**a) Reaction Time & Accuracy**



**b) Errors**

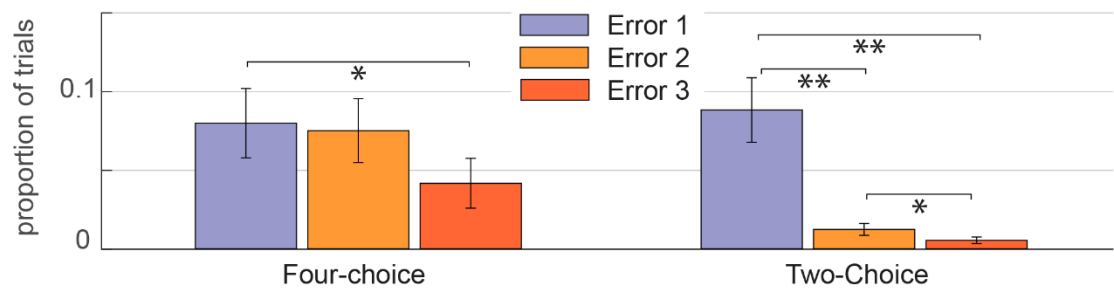


Figure 5.6: Behavioural results: a) response times (left) and accuracy (right) averages for all conditions. Response times are given in EMG RTs (button RTs are indicated in dashed lines). Error bars indicate 95% confidence intervals. b) Proportion of errors per error category for four-choice (left) and two-choice (right) trials. Error bars indicate 95% confidence intervals. \* indicates  $p < .05$ , \*\* indicates  $p < .001$ .

Since accuracy data do not meet the distributional assumptions required for a standard ANOVA, we used a generalised linear mixed-effects model in order to analyse the effects of our manipulations on participants' accuracies. Using the

‘fitglme’ function in Matlab (The Mathworks, Natick, U.S.A.), we used a model with a logistic link function and a binomial data model. Parameter estimates were based on a maximum likelihood method using Laplace approximation. We used the ‘maximal’ random effects structure (Barr et al., 2014), i.e. both manipulations, ‘Number of Alternatives’ and ‘Difficulty’, and their interaction were included as fixed effects, and both manipulations and their interactions within each participant and within each session were included as random effects (Wilkinson notation:  $Accuracy \sim 1 + \text{Number of Alternatives} * \text{Difficulty} + (1 + \text{Number of Alternatives} * \text{Difficulty} | \text{Participant}) + (1 + \text{Number of Alternatives} * \text{Difficulty} | \text{Session})$ )<sup>19</sup>. The ‘Number of Alternatives’ was a significant predictor,  $t(156) = 5.59, p < .001$ , with two-alternative trials ( $M = 89\%$ ) associated with higher accuracies than trials with four alternatives ( $M = 80\%$ ). Additionally, ‘Difficulty’ was a significant predictor,  $t(156) = 9.68, p < .001$ , with higher accuracy scores in easy ( $M = 88\%$ ) than in hard trials ( $M = 82\%$ ). The interaction between the ‘Number of Alternatives’ and ‘Difficulty’ was not a significant predictor,  $t(156) = 2.05, p = .052$ .

A further generalised linear mixed model was used to compare the proportions of the different error categories in the data (Figure 5.6 b). We used a model in which two predictors, ‘Number of Alternatives’ and ‘Error Category’, and their interaction were included as fixed effects, and both factors, and their interactions within each participant and within each session were included as random effects (Wilkinson notation:  $Accuracy \sim 1 + \text{Number of Alternatives} * \text{Error Category} + (1 + \text{Number of Alternatives} * \text{Error Category} | \text{Participant}) + (1 + \text{Number of Alternatives} * \text{Error Category} | \text{Session})$ ). We found that all fixed effects were significant predictors ( $p < .004$ ). To explore these effects, four further models were used. One model tested the fixed effect ‘Error Category’ on

---

<sup>19</sup> The dispersion parameter of the model,  $\phi = 2.08$ , was calculated by dividing the sum of squared Pearson residuals by the residual degrees of freedom (Venables & Ripley, 2002). This value indicates overdispersion, therefore, the  $p$ -values associated with the model may not be accurate. To test the reported effects, we therefore additionally conducted paired sign tests which confirmed that both the difference between ‘easy’ and ‘hard’, and between ‘two-choice’ and ‘four-choice’ trials were significant ( $p < .001$ ).

two-choice data alone. A second model was used to test the same effect, but with the reference set to a different level in order to evaluate the difference between all three levels of 'Error Category' ('Error 1', 'Error 2', 'Error 3'). Two further models were used in the same way but exploring four-choice data<sup>20</sup>.

In two-choice trials, all three levels of 'Error Category' differed significantly from each other,  $t(117) > 2.58$ ,  $p < .01$ , with most errors falling into the 'Error 1' category ( $M = 8\%$ ), and the least errors labelled 'Error 3' ( $M = .5\%$ ). In four-choice trials however, the only significant difference was seen between 'Error 1' and 'Error 3',  $t(117) = 2.27$ ,  $p = .03$ , with more errors in the 'Error 1' ( $M = 8\%$ ) than the 'Error 3' ( $M = 4\%$ ) category. There were no further significant differences in the four-choice condition,  $t(117) < 1.7$ ,  $p > .09$  (see Figure 5.6).

### 5.2.2. MEP Results

Smoothed MEP signals were generated for each muscle category ('Correct', 'Error 1', 'Error 2', 'Error 3') separately. The resulting signal is displayed in Figure 5.7. Note that two-choice traces were collapsed over 'within' and 'between' choices, since both displayed qualitatively similar patterns (see Appendix 7.2.). Visual inspection of the resulting MEP signals reveals that, as expected, in each condition, the 'Correct' muscle's activation increased over the course of the decision to a higher magnitude than all other muscles, while the 'Error 3' muscle showed the lowest amplitude and even decreased over time.

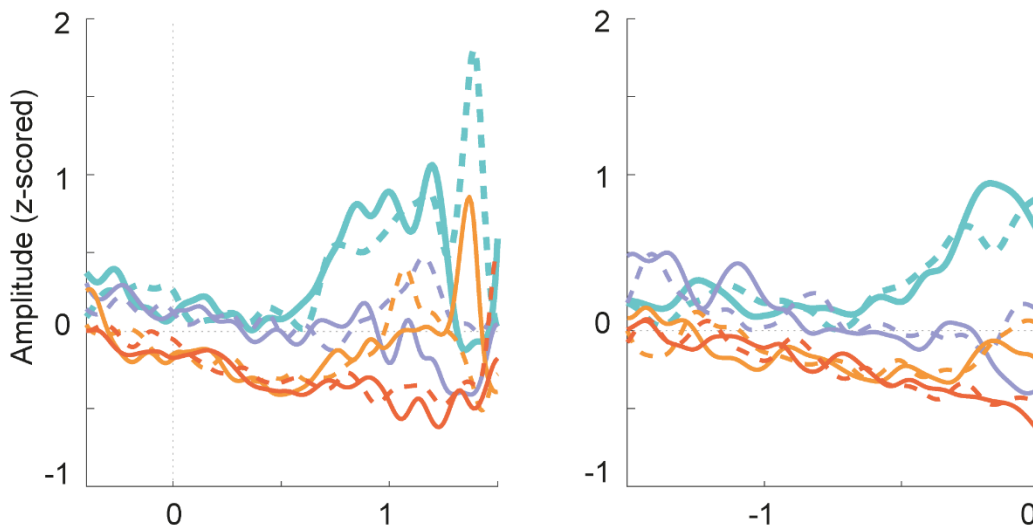
Contrary to our expectations, there was no visible difference between 'easy' (solid lines) and 'hard' (dashed lines) trials in any of the conditions. There were however, marked differences between two-choice and four-choice decisions. In the four-choice condition, 'Error 1' (same hand but different response relative to the responding muscle) and 'Error 2' (different hand but same response relative to the responding muscle) traces followed a virtually identical profile. In two-choice trials on the other hand, the two cued responses ('Correct' and 'Error 1')

---

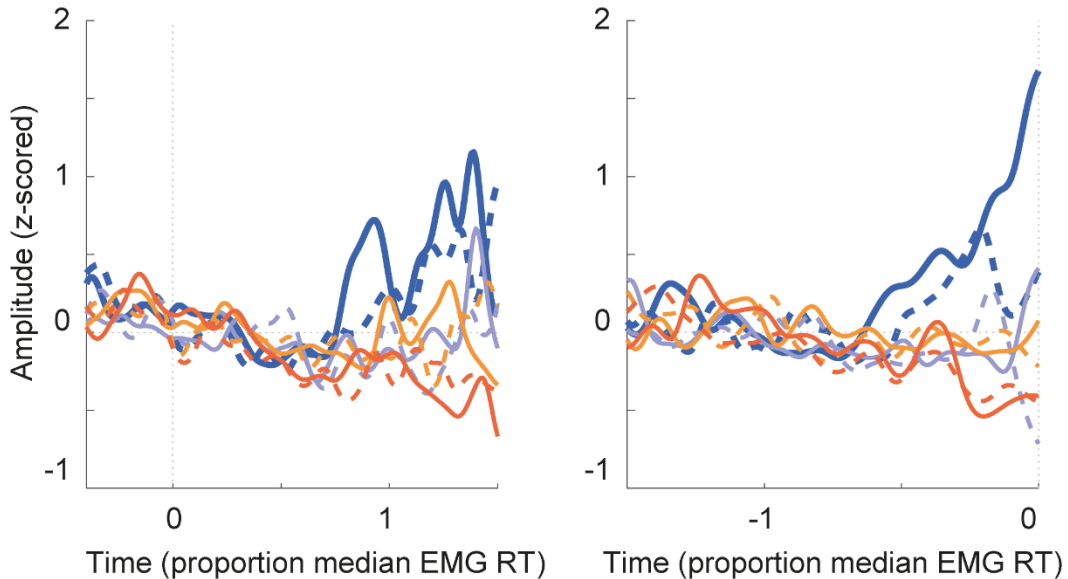
<sup>20</sup> The dispersion parameters of all models,  $\phi$ , were calculated by dividing the sum of squared Pearson residuals by the residual degrees of freedom (Venables & Ripley, 2002) and ranged between 1.14 and 1.25, indicating no problems of overdispersion.

are separated from the uncued response traces ('Error 2' and 'Error 3') throughout the beginning of the recording (note that the time of cue onset is prior to the onset of MEP recording). Only towards the end of the decision, arguably when the correct response is selected, does the 'Correct' muscle increase at a steeper rate while the 'Error 1' muscle decreases in amplitude.

**a) Two-Choice**



**b) Four-Choice**



- Two-Choice Correct Easy      - - - Two-Choice Correct Hard
- Four-Choice Correct Easy    - - - Four-Choice Correct Hard
- Error 1 Easy                    - - - Error 1 Hard
- Error 2 Easy                    - - - Error 2 Hard
- Error 3 Easy                    - - - Error 3 Hard

Figure 5.7: MEP results (smoothed MEP signal for each muscle category): stimulus-locked (left) and response-locked (right) smoothed signals are displayed separately for two-choice (a) and four-choice (b)

decisions. In each panel, easy (solid lines) and hard (dashed lines), as well as each correct/error category ('Correct', 'Error 1', 'Error 2', 'Error 3') are displayed separately.

Additionally, a smoothed signal for the difference between the responding and non-responding muscle (here: the difference between 'Correct' and 'Error 1') was generated (based on only a subset of trials; see section 5.1.4.3). The resulting profile is displayed in Figure 5.8, separately for stimulus-locked (left) and response-locked (right) signals, as well as four-choice (dark blue), two-choice (turquoise), 'easy' (solid lines), and 'hard' (dashed lines) conditions. Each profile displays a clear increase over the course of the decision, indicating an increasing difference between the activation profiles of the responding and the 'Error 1' muscles. Differences between 'easy' and 'hard', or four-choice and two-choice trials are not apparent.

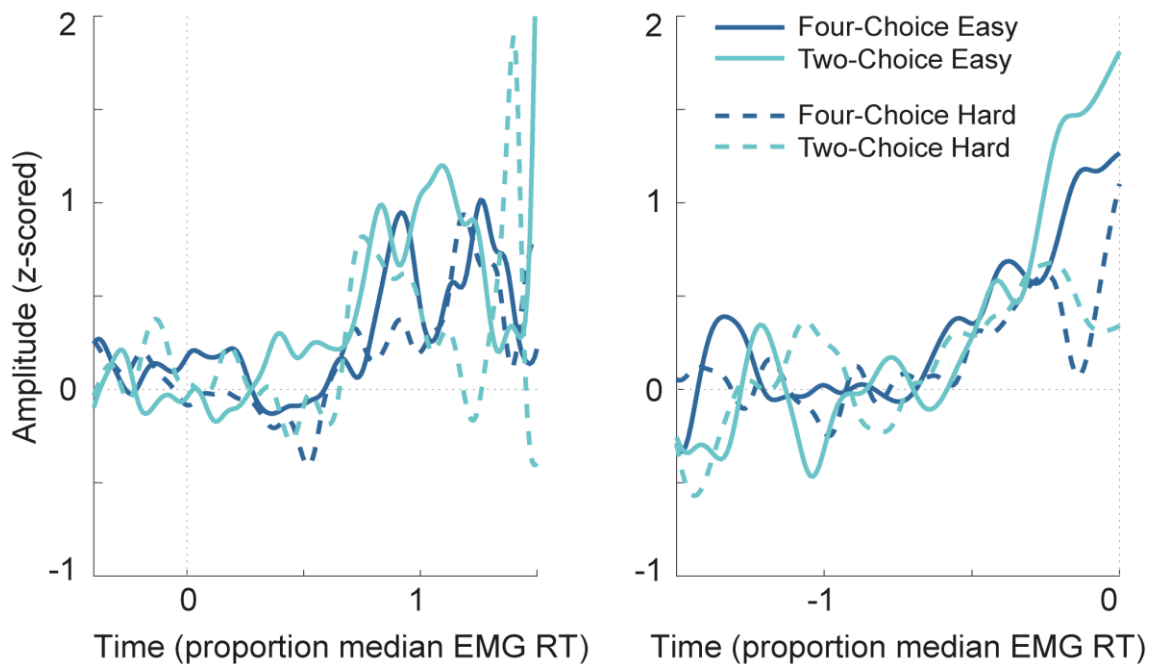


Figure 5.8: MEP results (smoothed MEP signals for the difference between responding and non-responding muscles): stimulus-locked (left) and response-locked (right) signals are displayed for four-choice (dark blue) and two-choice (turquoise), as well as easy (solid lines) and hard (dashed lines) separately. Note that each profile displays the difference between the MEPs which were simultaneously recorded in the 'Correct' and the 'Error 1' category.

### 5.2.2.1. Statistical Comparison

In order to test our hypothesis predicting a difference in baseline activity between two and four-choice decisions, we used a paired t-test to compare MEP amplitudes. Since there was no difference between two-choice 'within',

and two-choice ‘between’ MEP amplitudes ( $p > .48$ ), trials were pooled across both two-choice conditions. The t-test comparing two and four-choice baseline MEP sizes confirmed our hypothesis and showed that there was a significant difference in baseline amplitude,  $t(12) = 2.20$ ,  $p = .048$ ,  $d = .61$ , with two-choice trials showing larger MEP amplitudes ( $M = .22$ ) than four-choice trials ( $M = .13$ ).

Additionally, we tested the difference in slope between different difficulty levels using a permutation procedure. Comparing the slope difference in ‘easy’ and ‘hard’ trials to the null distribution of slope differences revealed that the original difference was not larger/smaller than the upper/lower 2.5% of the distribution, for either stimulus-locked or response-locked MEPs. This indicates that, contrary to our expectation, there was no slope difference between ‘easy’ and ‘hard’ trials ( $p > .05$ ).

To further explore this unexpected finding, we compared the slope between fast and slow responses. To this end, we performed a median split on the data in order to categorise it into fast and slow bins. We then used the same bootstrap method described above (see section 5.1.4.4), testing the difference in slope between ‘easy’ and ‘hard’ trials, to compare slopes of slow and fast trials. We found that slopes in fast trials were significantly higher than slopes in slow trials in both the stimulus-locked and the response-locked signal ( $p < .05$ ).

### **5.2.3. Model**

We fitted a total of three models to the EMG RT data. Model 1 (10 parameters) assumes that two-choice and four-choice trials are explained by the same drift rate, that there is no accumulation in uncued accumulators, and that cued two-choice trials have a free starting point. Model 2 (10 parameters) is identical to Model 1 but assumes that accumulation occurs in all accumulators. Lastly, Model 3 (13 parameters) is identical to Model 1, but assumes a drift rate difference, instead of a starting point difference, between two-choice and four-choice trials. Table 5.1 displays the BIC and AIC for each model, indicating their goodness of fit. The best (lowest) values were obtained for Model 1, indicating that this model provides the best account for the data. This suggests that

introducing multiple alternatives into a decision-making process primarily affects the baseline activity of the accumulation process. We therefore chose Model 1, and discarded the other models from the analysis. The resulting parameter estimates are displayed in Table 5.2.

Table 5.1: Model comparison: BIC and AIC values for each model. Model 1 has the lowest (best) BIC and AIC values (best BIC and AIC values in bold).

Model	Number of parameters	AIC	BIC	Parameters
<b>Model 1</b>	10	<b>141,600</b>	<b>141,680</b>	$v\text{-easy}_{correct}, v\text{-easy}_{incorrect}, v\text{-hard}_{correct}, v\text{-hard}_{incorrect}, z_{two\text{-choice-cued}}, k, \beta_1, \beta_2, \sigma^2, T_{er}$
Model 2	10	142,170	142,260	$v\text{-easy}_{correct}, v\text{-easy}_{incorrect}, v\text{-hard}_{correct}, v\text{-hard}_{incorrect}, z_{two\text{-choice-cued}}, k, \beta_1, \beta_2, \sigma^2, T_{er}$
Model 3	13	144,170	142,260	$v\text{-easy-four}_{correct}, v\text{-easy-four}_{incorrect}, v\text{-easy-two}_{correct}, v\text{-easy-two}_{incorrect}, v\text{-hard-four}_{correct}, v\text{-hard-four}_{incorrect}, v\text{-hard-two}_{correct}, v\text{-hard-two}_{incorrect}, k, \beta_1, \beta_2, \sigma^2, T_{er}$

Table 5.2: Estimated parameter values for the chosen model (Model 1): note that the response threshold  $A$  was set to 1 as a scaling parameter, and that the starting-point  $z$  was set to 0 for four-choice trials.

<b>Model 1: LCA Parameters</b>			
		Leakage ( $k$ )	0.000029
		Response threshold ( $A$ )	1
		Non-decision time ( $T_{er}$ )	0.2994
		Diffusion constant ( $\sigma^2$ )	0.4863
	Inhibition ( $\beta$ )	$\beta_1$	0.000022
		$\beta_2$	0.0408
	Starting point ( $z$ )	two-choice (cued)	0.2355
		four-choice/ two-choice (uncued)	0
Drift rate ( $v$ )	easy	correct	1.3199
		incorrect	0.2321
	hard	correct	1.1781
		incorrect	0.3413

The quality of the fit for each condition (left: four-choice, right: two-choice, top: easy, bottom: hard) is shown in Figure 5.9. The observed (circles) and

simulated (lines and crosses) normalised EMG RT distributions are summarised by five quantile estimates (from left to right: 10%, 30%, 50%, 70%, 90%), and the EMG RT (x-axis) and proportion of data (y-axis) associated with each quantile are displayed. Both correct responses (thick lines) and each error category ('Error1', 'Error 2', 'Error 3'; see Figure 5.2) are shown. The overlap between empirical and simulated quantiles indicates a good overall model fit. The mean difference between predicted and recorded EMG RT quantiles was approximately 2.5% median EMG RT for correct responses, confirming that the LCA was able to account for both two and four-choice decisions.

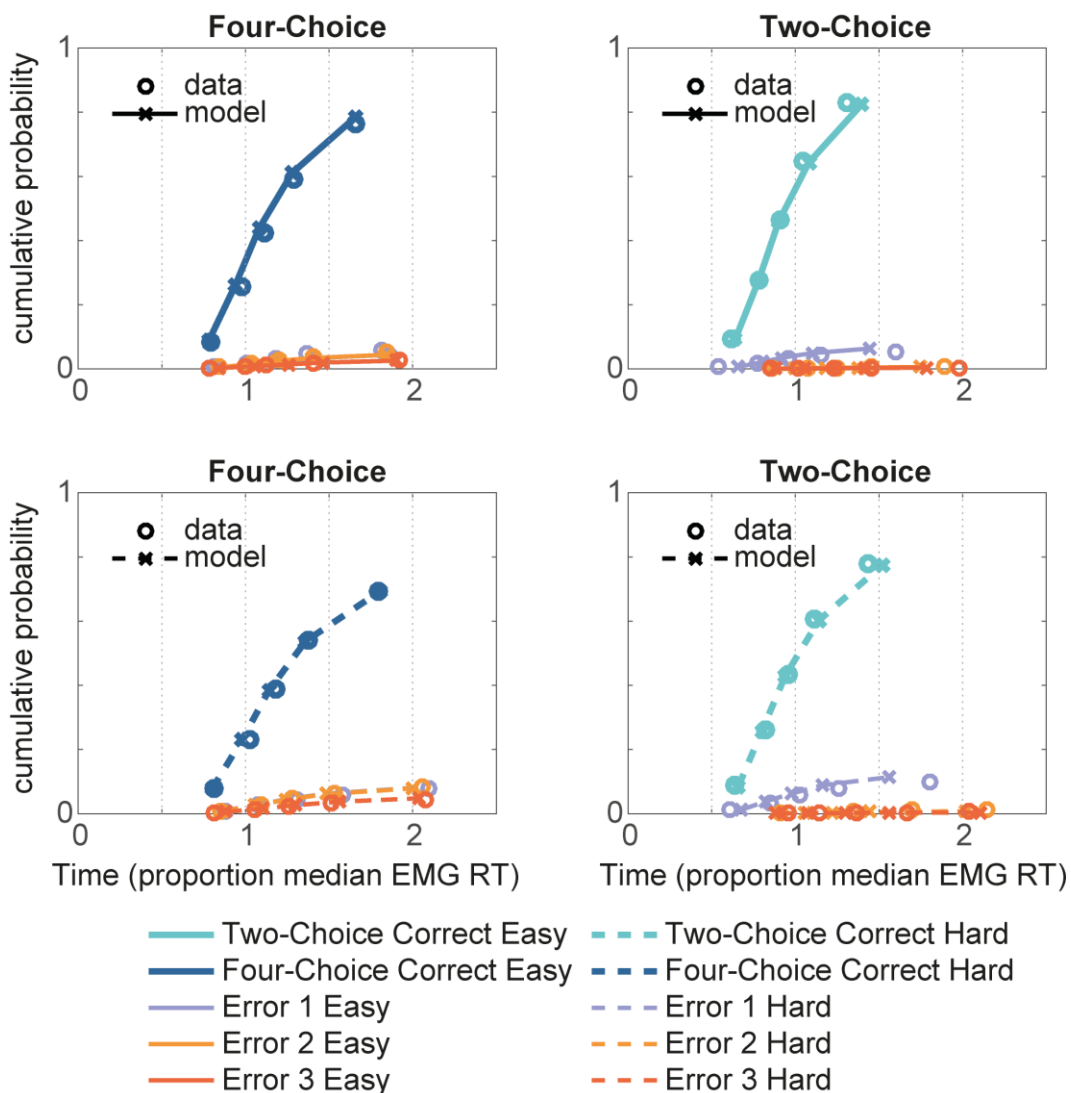
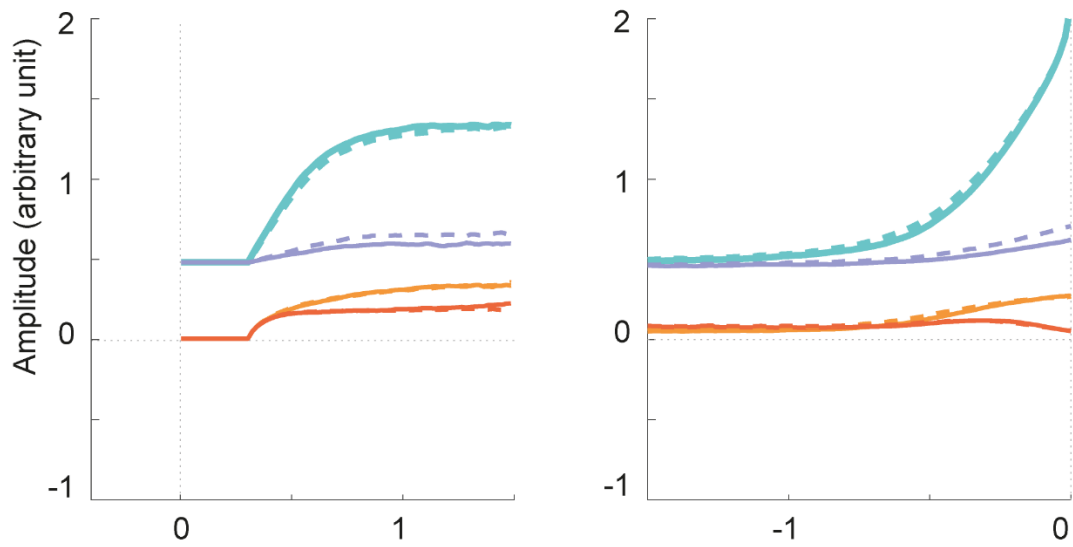


Figure 5.9: Model fit: quantiles estimated from behavioural data (circles) and LCA simulations (crosses and lines) for easy (top) and hard (bottom) decisions. For each condition, correct and incorrect quantiles are displayed separately.

The estimated parameters were used to simulate the average accumulation profile for each condition. Figure 5.10 displays the resulting stimulus-locked

(left) and response-locked (right) predictions for each condition and each accumulator (categorised as 'Correct', 'Error 1', 'Error 2', or 'Error 3'). For direct comparison, Figure 5.10 is displayed in the same format as Figure 5.7. Qualitatively similar patterns were observed in both the MEP signal (Figure 5.7) and the model predictions (Figure 5.10). Like the MEP signal, The LCA accumulation profiles show a higher increase of the 'Correct' accumulator than all other accumulators over the course of the decision in all conditions, while the 'Error 3' accumulator showed the lowest amplitude throughout. It can further be seen that in four-choice conditions, the accumulators associated with 'Error 1' and 'Error 2' display a virtually identical profile, while in two-choice conditions, the cued accumulators ('Correct' and 'Error 1') show a higher activation than the uncued accumulators ('Error 2' and 'Error 3'). Contrary to our hypotheses, there was no clear difference between 'easy' and 'hard' predicted accumulation profiles.

### a) Two-Choice



### b) Four-Choice

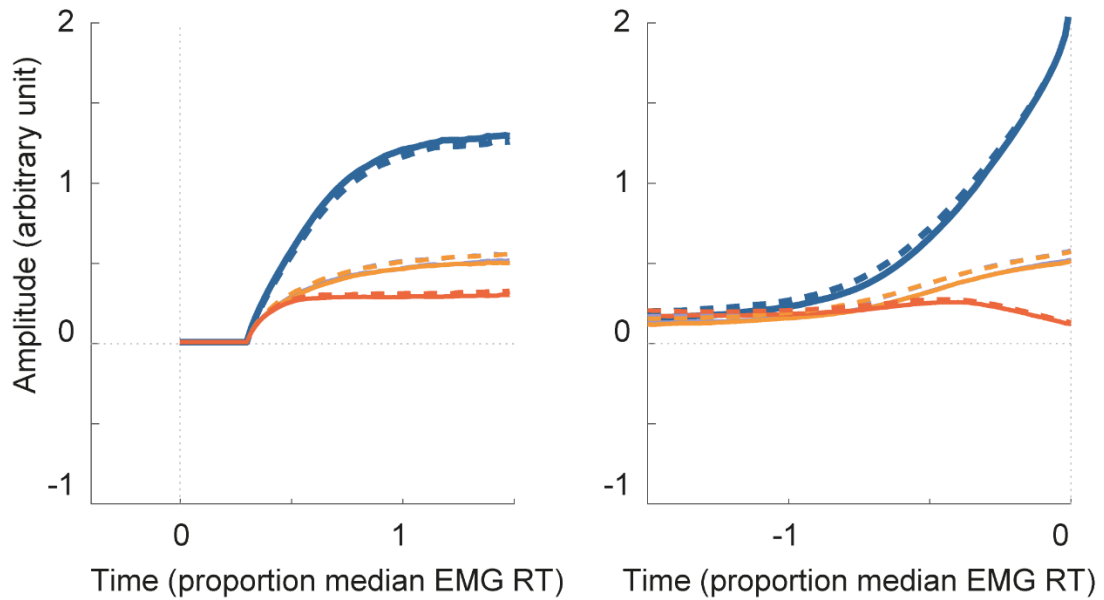


Figure 5.10: Decision variable (simulated): LCA predictions of the accumulation profile for two-choice (a) and four-choice (b) conditions, as well as easy (solid lines) and hard (dashed lines) conditions, locked to both the stimulus onset (left) and the EMG onset (right). For each condition, the accumulation profiles of all four accumulators (categorised into 'Correct', 'Error 1', 'Error 2', 'Error 3') are shown (note that in four-choice conditions, 'Error 1' and 'Error 2' traces are virtually identical). See Figure 5.7 to compare with the corresponding MEP signal.

Figure 5.11 shows the model predictions for the difference between the 'Correct' and the 'Error 1' accumulator for each condition. Overall, the observed patterns are comparable to those in the corresponding MEP signal (see Figure 5.8). However, there appear to be small differences in the model predictions (e.g. lower amplitude in hard trials in stimulus-locked predictions), which are not obvious, potentially due to a high level of noise, in the MEP signal.

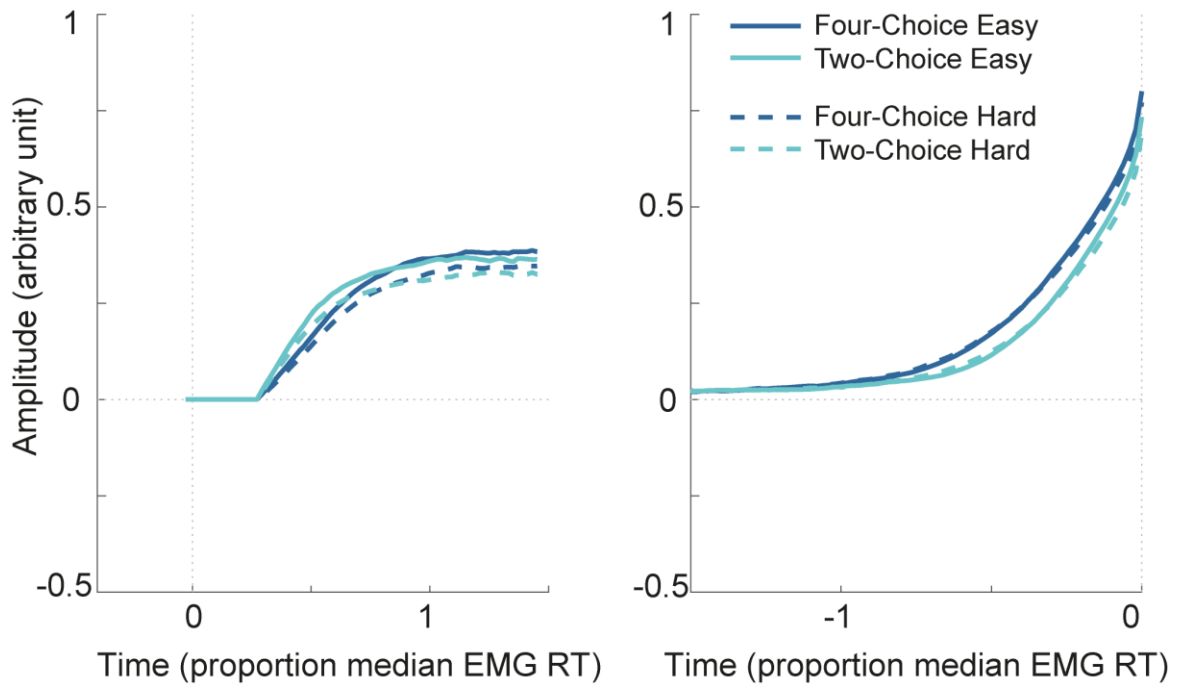


Figure 5.11: LCA Predictions of the difference between responding ('Correct') and non-responding ('Error 1') muscles: stimulus-locked (left) and response-locked (right) signals are displayed for four-choice (dark blue) and two-choice (turquoise), as well as easy (solid lines) and hard (dashed lines) separately. See Figure 5.8 to compare to the corresponding MEP signal.

### 5.3. Discussion

In this experiment, we set out to explore decision-making with multiple alternatives in humans. To this end, we asked participants to complete a colour-discrimination task with either two or four choices and applied TMS to induce MEPs in the hand muscles used to execute responses as a measure of corticospinal excitability resembling the decision variable. We hypothesised that, in line with previous research in monkeys, a difference in the number of choice alternatives would translate into a difference in baseline MEP size (Balan

et al., 2008; Churchland et al., 2008; Cohen et al., 2009). We also added a difficulty manipulation and expected that the MEP size (i.e. the corticospinal excitability) recorded from responding muscles would increase faster in easy than in hard trials.

Behavioural results showed that both the number of alternatives and the difficulty of the task had the expected effects on response times and accuracy scores. In line with previous research (Brown et al., 2009; Cohen et al., 2009; Hick, 1952), it was found that responses were faster and more accurate in two-choice compared to four-choice, and in easy compared to hard trials. Additionally, each error was classed into one of three categories. With a total of four possible responses (two movements per hand), either two or four of which were cued, each response was classed either as 'Correct', 'Error 1' (cued but incorrect in two-choice trials, and correct hand but incorrect movement in four-choice-trials), 'Error 2' (uncued and the correct/incorrect movement on the incorrect/correct hand in two-choice trials, and correct movement but on the incorrect hand in four-choice trials), or as 'Error 3' (incorrect movement and incorrect hand). We found, that in two-choice trials, 'Error 1' occurred more often than any other error, while in four-choice trials, 'Error 1' and 'Error 2' were roughly equal in frequency. These findings indicate that although the stimulus did not change, and the manipulation was implemented only by the cue, the two vs four-choice manipulation had a significant impact on participants' decision-making and affected not only the overall accuracy of responses but also the response selection of incorrect trials.

During decision-making, we used TMS to induce MEPs in the relevant muscles of the right hand. By stimulating at random time-points throughout the trial, pooling the data across participants, and smoothing the resulting data points, we were able to construct a continuous MEP signal for each condition and each correct/error category separately. This signal reflects corticospinal excitability and has previously been associated with decision-related evidence accumulation (Hadar et al., 2015). Typically, within a given condition, neural correlates of decision-making produce a single waveform per decision. An example is the EEG component CPP, which arguably reflects the sum of all

accumulators in a given decision (O'Connell et al., 2012; see Chapter 4). However, in the current experiment, tracking the evolution of preparation for each of the four potential responses ('Correct', 'Error 1', 'Error 2', 'Error 3') in each condition, allowed us to explore the behaviour of each of four associated accumulators and thereby provide a richer insight into the decision process than a single summary signal could provide.

To our knowledge, this is the first attempt to track a neural correlate of the decision variable for multi-alternative decision-making in humans with high temporal resolution. We are also not aware of any studies which have previously attempted to track the evolution of accumulation of each alternative in multi-alternative decision-making. In line with our hypotheses, we found that the 'Correct' MEP trace increased throughout the trial and peaked at the response, clearly separating from all profiles associated with incorrect responses. Importantly, we observed a difference in the trajectories of the incorrect responses between two and four-choice decisions. While there was no observable difference between 'Error 1' and 'Error 2' profiles in four-choice trials, or, in fact, any of the profiles during the first half of the trial, there was a clear separation in two-choice trials, where 'Correct' and 'Error 1' (both cued responses) showed a higher baseline amplitude than 'Error 2' and 'Error 3'. In fact, we showed that MEPs recorded from muscles associated with cued responses during the baseline period were significantly higher in two-choice decisions than in four-choice decisions. This finding is in line with previous evidence from non-human primates which has repeatedly shown a decrease in baseline firing rates of oculomotor neurons during saccadic decision-making with an increase in the number of alternatives (Basso & Wurtz, 1998; Churchland et al., 2008; Cohen et al., 2009; Lee & Keller, 2008).

It has previously been suggested that, in the context of sequential sampling models, this baseline effect implies a difference in the distance between the starting point and the threshold, which affects the signal-to-noise ratio (larger baseline-threshold distances imply that more evidence is necessary to terminate the accumulation process; Churchland et al., 2008). In four-choice decisions, in which uncertainty is inherently larger than in two-choice decisions,

an increase in the baseline-threshold distance may compensate for this uncertainty at the expense of response time.

Contrary to our hypotheses, we observed no difference between the MEP signals of easy and hard trials. Previous research has shown that manipulations of difficulty have strong effects on accumulation (Ho et al., 2009; Ratcliff & McKoon, 2008), as well as associated neural signals (Kelly & O'Connell, 2013; Roitman & Shadlen, 2002; see Chapter 3), including smoothed MEP signals like the ones used here (Hadar et al., 2015; see Chapter 2). The similarity between easy and hard waveforms in the current experiment may therefore lead one to question the role of the MEP signal as a correlate of the decision variable. However, it can be explained by the similarity in response times between easy and hard trials. Although easy decisions were associated with significantly shorter RTs, the difference was small compared to other experiments (see Chapter 4, Figure 4.4), and may have led to a similarity in RTs which is specific to our paradigm. In our task, the dominant colour in the easy condition of the colour discrimination task took up 33% of the display, compared to 30% in hard conditions. This difference may not have been large enough to induce visibly different accumulation rates. A post hoc analysis confirmed that, while there was no slope difference between easy and hard waveforms, fast decisions were associated with higher slopes than slow decisions, a typical finding for a decision variable, confirming the role of the MEP as a correlate of accumulation.

We fitted a sequential sampling model to the behavioural data in order to simulate the accumulation profile and directly compare it to the MEP signal. Here, we chose the LCA model for this purpose (Usher & McClelland, 2001). The LCA is an extension of a simple accumulator model, which includes leakage and inhibition parameters to model a more neurophysiologically plausible accumulation process than other sequential sampling models. This relatively complex model was chosen firstly because it has been shown to adequately account for multi-alternative decision-making in a number of previous studies (Bogacz et al., 2007; Ditterich, 2010; McMillen & Holmes, 2006; Tsetsos et al., 2010, 2011), secondly because it is an accumulator model which implies that it is easily extended to any number of choice alternatives

(Smith & Ratcliff, 2004; Usher & McClelland, 2001), and lastly because the decision-making required in the current experiment was comparatively complex, inducing behavioural patterns which go beyond those seen in typical binary choices and are unlikely to be accurately described by other sequential sampling models. In particular, the inhibition between accumulators appears a necessary characteristic of the model in order to explain the varying behaviours associated with the three different error categories. By allowing two inhibition parameters, as well as varying starting points for two-choice trials and varying drift rates for easy and hard decisions, the model was able to account for the behavioural data with complex anatomical linkages between effectors.

We tested a total of three different models and found that the best-fitting model assumed a difference in starting point between two-choice and four-choice trials, thereby supporting the findings of baseline difference observed in previous research in non-human primates (e.g. Churchland et al., 2008), as well as in our MEP results. Additionally, the model assumed that non-cued alternatives in two-choice trials had a drift rate of 0, indicating that attentional mechanisms gate the evidence at a sensory level, before accumulation occurs. Note that this was found, despite the fact that each stimulus contained all four colours, and the response options were determined by pre-stimulus cues alone. This finding is in line with previous research which demonstrated that a neural correlate of accumulation, namely the CPP only displays a build-up if the sensory evidence provided is directly relevant to the decision (O'Connell et al., 2012).

The estimated parameters of the chosen model were used to simulate accumulation profiles for each condition and each correct/error category separately. Crucially, the resulting profiles were qualitatively similar to those of the measured MEP signals. In both the simulated and the observed signal, there was a clear difference between error trajectories in two-choice and four-choice trials. We found that, in two-choice trials, 'Error 1' and 'Correct' profiles begin higher than 'Error 2' and 'Error 3' traces, while in four-choice trials, there is no baseline difference and 'Error 1' and 'Error 2' trials follow the same trajectory throughout the trial.

Importantly, reproducing the pattern of the MEP signal, there was no visible difference between easy and hard accumulation profiles predicted by the model. Although drift rates were free to vary in each difficulty condition, and confirmed that RT differences were due to a modulation of accumulation rates, with higher slopes for easier decisions, the difference in the resulting drift rates did not produce distinct accumulation profiles. Although this is somewhat surprising given the significant difference between easy and hard RTs, it supports the role of the MEP signal as an accumulation signal, as it showed the exact same pattern.

However, there were also marked differences between predicted and recorded accumulation signals, for at least two reasons. Firstly, like any model, the LCA can, at best, be an approximation of the true decision-making processes. This is an important point in this study, since we only used one model as representative of a family of models (sequential sampling models). We chose the model based on its previous application to multi-alternative decision-making and its ability to account for more complex decision-making processes, however, we must assume that other sequential sampling models or other implementations of our manipulations in the LCA may reveal slightly different patterns which should be explored in the future.

Secondly, it seems that the direct comparison of the model prediction is limited by the quality and nature of the MEP signal. While we assume that the MEP signal showing the difference between the responding and non-responding muscles is a relatively true reflection of cortical excitability (under the assumption that spinal contributions to the corticospinal signal are constant across effectors), the MEP signal displaying each response separately may still contain non-specific spinal influences. These spinal signals may, for example, explain the slow negative drift visible in the MEP signal associated with each response (Figure 5.7), which is not seen in the MEP signal reflecting the difference between two muscles (Figure 5.8) or the model predictions (Figure 5.10).

Additionally, the smoothed MEP signal used in this experiment is a labour-intensive signal to produce. In each TMS trial, MEPs at only a single time point are collected, and TMS can only be applied in a proportion of trials. Furthermore, a large proportion of TMS trials had to be discarded for a number of reasons. In addition to the standard removal of noisy trials (and in particular, trials in which participants' muscles were not fully relaxed prior to the stimulation) or trials with no, or very quick responses (i.e. trials in which it is unlikely that a decision-making process took place), a proportion of trials was lost due to the stimulation protocol. The planned TMS times for each trial were designed to ensure a good coverage of the whole RT distribution. This meant that in many cases, the response preceded the planned stimulation, leading to the exclusion of the trial.

Therefore, it is difficult to produce enough data to quantitatively compare smoothed MEP signals with model predictions, which can be based on any number of simulations. Nevertheless, it is important to note that high exclusion rates are typical for this type of experiment (Hadar et al., 2015), and we used a large number of trials to minimise its effects and produce a smoothed MEP signals which show qualitative differences between conditions, similar to those predicted by sequential sampling models. In spite of its limitations, the method used here provides a unique and detailed insight into the accumulation process during decision-making with multiple alternatives. It allowed us to not only track the dynamics of the decision variable, which was comparable to model simulations, but also explore the evolution of each response and each accumulator separately, thereby arguably providing richer data than any other method commonly used in research with human subjects.

Overall, the current study was able to demonstrate that multi-alternative decision-making in humans can be accounted for by sequential sampling models, and importantly, that smoothed MEP signals reflect the accumulation process. In addition, we showed that MEP signals can be used to track the evolution of preparation for each of four responses separately, giving insight into each of the four associated accumulators of a sequential sampling model. In addition, we demonstrated for the first time, that the number of choice

alternatives in a decision-making task affects the baseline activity of neural accumulation signals in humans.

## 6. General Discussion

The current project set out to explore human perceptual decision-making by combining neural data with sequential sampling models. Sequential sampling models explain decision-making reaction time (RT) data by assuming that sensory evidence accumulates over time until a decision threshold is reached and a response is executed (Ratcliff & McKoon, 2008; Ratcliff & Rouder, 1998; Usher & McClelland, 2001).

Although sequential sampling models were developed to explain behavioural decision-making data and make no claims about its neural underpinnings, a number of neural signals have been proposed to reflect the accumulation process predicted by these models. This similarity between model predictions and neural processes has primarily been shown in non-human primates, with firing rates in neurons in a range of oculomotor structures displaying accumulation-to-bound profiles in response to saccadic decisions (Huk & Shadlen, 2005; Roitman & Shadlen, 2002).

In humans, correlations between neural signals and sequential sampling models are less established. Nevertheless, a number of signals in the human brain have been suggested to be decision-related. One of these signals is the event-related potential (ERP) centroparietal positivity (CPP) which has been shown to reflect the accumulation of decision-relevant evidence and can be dissociated from sensory and motor processing (O'Connell et al., 2012). This signal has been reported to have promising properties, as it appears to be independent of both the modality of the sensory evidence and the associated response, suggesting that it reflects accumulation itself (O'Connell et al., 2012; Twomey et al., 2016). However, to date, few studies have attempted to replicate these findings.

Another neurometric measure which has been suggested to reflect the decision variable, i.e. the accumulation process predicted by sequential sampling models, is neural excitability in motor areas, measured through the amplitude of

motor-evoked potentials (MEPs) induced by transcranial magnetic stimulation (TMS; Hadar et al., 2015). While it has been claimed that the CPP reflects accumulation directly, this MEP signal is likely to be a down-stream representation of the integration of evidence. This is based on the concept that, during a decision, the accumulation progress is continuously fed forward into the motor system so that the level of evidence integration is reflected in the level of preparation of the associated motor response.

Although this signal displays accumulation indirectly, it has an advantage over EEG signals in that it allows us to track accumulation of each response alternative separately in multi-alternative decision-making paradigms. The CPP on the other hand, may display accumulation directly, but only tracks accumulation as a whole and cannot distinguish between response alternatives. By making use of both of these signals, depending on which is most informative for any given paradigm, many open questions regarding human perceptual decision-making can be addressed.

In this project, we used these neural signals to explore human perceptual decision-making by comparing them directly to predictions made by sequential sampling models. Specifically, we used accumulator models, i.e. sequential sampling models with an absolute stopping rule, in which evidence for each alternative is integrated in a separate accumulator and the accumulators race to a common threshold (Brown & Heathcote, 2008; Smith & Ratcliff, 2004; Usher & McClelland, 2001). We chose these models over random walk models, i.e. models with a relative stopping rule in which evidence for binary choices is integrated to a single total, due to their biological plausibility. The plausibility of random-walk models is limited, as they assume that accumulation can become negative, and it is not clear how activation of a neural population can decrease to arbitrary negative values. Separate accumulators assumed by accumulator models on the other hand, can be thought of as representations of the activity of separate neural populations, integrating evidence for a given alternative (Usher & McClelland, 2001). Additionally, random-walk models cannot be extended to account for decisions with multiple alternatives as easily as accumulator models (Ratcliff et al., 2016).

Note that, since, as described above, the MEP signal tracks each response alternative (i.e. the preparation of each muscle associated with a response) separately, we assume that the trajectory associated with each alternative is modelled by the associated accumulator of the accumulator model. In a binary choice, the difference wave reflecting the difference in MEP amplitude between the responding and the non-responding muscle is therefore assumed to be modelled by the difference between the two accumulators. The CPP on the other hand cannot distinguish between alternatives. We speculate that each alternative is accumulated in a separate neural population in proximity to centroparietal electrodes, but that, due to volume conduction, only the sum of all activity is recorded on the scalp. We therefore model the CPP as the sum of all accumulators in a model.

## **6.1. Summary**

Using these methods, we set out to explore the underlying mechanisms of human perceptual decision-making and specifically, address the questions (1) whether accumulation, as predicted by sequential sampling models, occurs in the human brain, (2) which signals are most suitable to track accumulation, given that it occurs, (3) what impact a number of manipulations have on these signals, and importantly, (4) to what extent modelled accumulation profiles resemble these signals (see Chapter 1). First, we will summarise the findings of each experimental chapter, before we describe how each of these questions was addressed by our studies in the following section (see section 6.2).

In Chapter 2, we explored the impact of the speed-accuracy trade-off (SAT) on perceptual decision-making. Participants were instructed to make easy and hard decisions either as quickly or as accurately as possible while we either recorded their EEG or used TMS to record MEPs. The SAT has traditionally been implemented in the sequential sampling model literature by adjusting the threshold parameter, with lower and higher thresholds associated with speed

and accuracy instructions respectively (Brown & Heathcote, 2008; Heitz, 2014; Ratcliff, 2002). We expected that this difference in the amount of evidence accumulated in each condition would translate into an amplitude difference in a neural substrate of the decision variable. However, evidence from studies using neurophysiological data from non-human primates have questioned this implementation of the SAT as they found no difference in amplitude of decision-related firing rates between SAT conditions, and instead found more widespread changes in activity (Heitz & Schall, 2012, 2013). Our results supported these neurophysiological findings. Although we found that both the CPP and the MEP signal displayed a gradual increase over the course of the decision, which increased at a rate depending on the difficulty of the decision and peaked at the response, supporting their roles as decision variable signals, we found no amplitude differences between speed and accuracy conditions in either of the neural signals.

We used two types of models to explain our data. First, we used a race model (i.e. an accumulator model) which, in line with the traditional approach, varied in threshold across SAT conditions. In our second model, we 'rescaled' the estimated parameters from the standard model. In line with previous neurophysiological findings suggesting more widespread changes in activity instead of specific amplitude differences (Heitz & Schall, 2012, 2013; Murphy et al., 2016), we set out to model a global modulation associated with the SAT using the rescaled model. To this end, we used the parameters estimated by the standard model (i.e. a model with variations in the threshold parameter), and rescaled the parameters in the speed condition so that the threshold in both SAT conditions was identical, and the original difference in threshold was transferred onto all other parameters. Note that this implementation of the SAT is conceptually different from the variation in threshold, but is mathematically identical and provides the same model fit to the RT data. We simulated mean accumulation profiles for each condition for each of the models. As expected, the original model with threshold changes led to accumulation profiles which differed in amplitude between SAT conditions. The accumulation profiles predicted by the rescaled model however, showed no amplitude differences and, in fact, replicated the pattern observed in the CPP and MEP signal. These

findings indicate that the SAT is associated not with a specific change in the amount of evidence required to make a decision, but with a global modulation of brain activity.

However, our interpretation of the findings crucially depends on the validity of the CPP and MEP signals as substrates of the decision variable. Given our findings which showed that the profiles displayed by the neurometric measures did not match the accumulation profile predicted by sequential sampling models using the traditional implementation of the SAT, it could perhaps be concluded that the neural signals used here do not display accumulation. Instead, we concluded that the neural signals reflect accumulation and that the model needs to be adjusted. We came to this conclusion for a number of reasons. Firstly, the neural signals displayed a number of other characteristics of the decision variable, such as the gradual build-up which peaked at the time of response, and the expected slope differences between easy and hard conditions. Secondly, we observed the same patterns of activity in two fundamentally different signals, one EEG signal which likely displays accumulation directly and one signal of corticospinal excitability displaying down-stream accumulation in form of motor preparation, each of which have previously been shown to reflect accumulation, and thus provide converging evidence for our interpretation (Hadar et al., 2015; O'Connell et al., 2012). Thirdly, similar findings, contradicting the traditional implementation of the SAT using threshold variations have been reported in previous studies using neural data in both human and non-human primates (Heitz & Schall, 2012, 2013; Murphy et al., 2016), further supporting our findings. And lastly, we were able to account for the neural signals by making only a small adjustment to the existing model, which implements a conceptually different explanation, namely a global modulation in activity, while remaining mathematically equivalent and without affecting the original model fit. We therefore conclude that both the CPP and the MEP signal are valid neural correlates of the decision variable, and importantly, that our results indicate that strategic changes in focus between speed and accuracy of perceptual decision-making are explained on a neural level not by a specific change in thresholds, but by a more global modulation of activity.

Nevertheless, it is important to note that, by observing no amplitude difference between speed and accuracy conditions, we identified a clear and somewhat unexpected difference between predictions made by sequential sampling models and neural data proposed to reflect the accumulation process. This necessarily questions the role of the neural signals used here, particularly since both the CPP and the MEP signal have not yet been supported by a large body of research. Therefore, to further strengthen our conclusions regarding the SAT, and to guide future work, we set out to test the role of the neural signals in Chapter 3. To this end, we tested a range of previously suggested neural correlates of the decision variable in order to identify the most suitable neural accumulation signal. We chose EEG signals since they, due to their temporal resolution, are the most appropriate measure to track the fast dynamics of the decision variable, and a variety of EEG signals have previously been proposed to reflect the accumulation process. Note that we did not test any other TMS methods as we are not aware of any alternative ways to generate accumulation-like signals to the one used in Chapter 2. However, we tested EEG signals, which, like the MEP signal used above, reflect motor preparation.

Specifically, we tested three of the most well-established neural correlates of the decision variable in the human brain, namely the CPP (Kelly & O'Connell, 2013; O'Connell et al., 2012; Twomey et al., 2016), the lateralised readiness potential (LRP; Kelly & O'Connell, 2013; Polanía et al., 2014), and event-related desynchronisation (ERD) in the beta frequency (both contralateral and lateralised; Donner et al., 2009; O'Connell et al., 2012). Note that some of these signals (e.g. beta ERD reported by Donner et al., 2009) were observed using magnetoencephalography (MEG) rather than EEG, but are equally observable in EEG (O'Connell et al., 2012).

In order to evaluate these signals and their roles as useful correlates of decision-making, we explored their profiles during decision-making with different levels of difficulty. The manipulation of difficulty was chosen as it is associated with very clear predictions regarding the shape of the accumulation profile. Unlike most other decision manipulations, difficulty is associated with a strong general consensus regarding its implementation in sequential sampling models

and its effects on the accumulation profile. Decision difficulty, i.e. the quality of sensory evidence, is known to be modelled by a variation in the drift rate parameter, i.e. the slope of the accumulation, with harder decisions being associated with lower accumulation rates (Donkin et al., 2009; Ratcliff & McKoon, 2008; Ratcliff & Rouder, 1998). Importantly, this modelled slope difference has been supported by a number of neural signals, reporting steeper build-up rates in neural activity for easy compared to hard decisions (de Lafuente et al., 2015; Hanks et al., 2011; Roitman & Shadlen, 2002). Together, these findings contribute to a large, unanimous body of research suggesting that any neural signal which claims to reflect decision-related accumulation must display slope differences associated with different levels of difficulty.

We tested to what extent the CPP, the LRP, and beta ERD displayed these slope differences. We were not able to replicate previous findings indicating that beta ERD reflects accumulation (Donner et al., 2009). We found no difference in beta power slope between easy and hard decisions, but speculate that this may be a task-specific finding, as longer RTs may be necessary to accurately detect beta ERD. Conversely, we found that the CPP displayed all expected characteristics, with easier decisions associated with steeper slopes, supporting its role as a neural correlate of the decision variable. The LRP findings were less clear, but the waveform overall displayed characteristics comparable to those observed in the CPP.

These findings indicate that, out of the three most commonly used EEG correlates of the decision variable, the CPP is the most suitable signal to track the evolution of the accumulation process, thereby supporting the findings described in Chapter 2. Additionally, we found that, in line with previous findings (Kelly & O'Connell, 2013) the LRP closely followed the CPP. Since the LRP has been shown to arise from supplementary motor areas (Ikeda & Shibasaki, 1992; Lang et al., 1991), this result supports the notion that accumulation is fed forward into motor areas in decisions requiring motor responses. Given the comparatively high spatial resolution of TMS, we can be confident that the MEP signal reported in Chapter 2 is an accurate reflection of excitability in motor areas (Bestmann & Krakauer, 2015; Hadar et al., 2012; Kiers et al., 1997). We

therefore argue that, if accumulation is represented in motor areas, as suggested by the LRP findings, it should also be visible in MEP amplitudes. The exploration of different EEG signals which have been claimed to reflect accumulation in Chapter 3 therefore arguably not only supports the role of the CPP as a neural correlate of the decision variable, but also gives some insight into accumulation in motor areas, indicating the validity of the MEP signal as a potential neural correlate of decision-making.

However, while the comparison of different EEG signals showed that the CPP is the most suitable neural substrate of the decision variable, it did so only in comparison to the LRP and beta ERD. We did not test the similarity of the CPP with predictions made by sequential sampling models directly, and although this is arguably not necessary given a simple and well-established manipulation such as difficulty, our results can only comment on the CPP's suitability over that of the other signals. It cannot give insight into the similarity of the CPP and the predictions made by sequential sampling models beyond what was already reported in the results of Chapter 2, i.e. that both the CPP and simulated accumulation profiles of a sequential sampling model vary in their build-up rate with easy decisions displaying a higher slope than hard decisions.

Therefore, having established the CPP as the most suitable out of three of the most commonly suggested EEG correlates of the decision variable, in Chapter 4, we set out to directly test its profile compared to model predictions in more complex settings. To this end, we explored decision-making with non-stationary evidence and biased decision-making in two separate experiments. In the first experiment, we used a motion discrimination task with easy and hard trials, in which the motion either continued in the same direction throughout the decision-making process, or was interrupted for a brief period by either random motion or motion in the opposite direction. In line with previous research (O'Connell et al., 2012), we found that the CPP was sensitive to these dynamic changes in evidence. However, contrary to our predictions, CPP waveforms associated with interruptions in evidence displayed similar profiles, regardless of whether the evidence was simply interrupted or reversed. A race model with intra-trial variation in drift rate accounted for the resulting behavioural data. We used the

parameters of the model to simulate the mean accumulation profile for each condition and directly compared the resulting waveform to the CPP. We found that the model predictions displayed a qualitatively similar pattern to the CPP waveform. Both profiles showed lower initial slopes in hard than in easy waveforms, and both profiles associated with un-interrupted evidence displayed the typical build-up over the course of the decision before peaking at the time of response, while profiles associated with interrupted and reversed evidence showed a dip in the build-up. We noted the unexpected similarity between the waveforms associated with the two interruption conditions in both the CPP and the model simulation, highlighting the necessity of using model-based approaches to explore more complex decision-making.

In the second experiment, motion discrimination trials were preceded by cues which either gave no information about the upcoming trial or pointed towards a specific direction, which was either congruent or incongruent with the motion direction of the upcoming trial. We found that the CPP differed in amplitude between the conditions, with incongruent waveforms displaying the highest amplitude, followed by uncued and lastly, congruent waveforms. We used a race model to account for the behavioural data and found that a model with varying starting points across conditions was able to explain the empirical RT distributions. The simulated accumulation profile associated with this model displayed the same patterns as the CPP, supporting the role of the CPP as a decision variable signal. However, the model also indicated that the amplitude differences observed were not strictly due to starting point differences across conditions (which cancelled out as we summed over cued and non-cued accumulators, i.e. increased and decreased starting points), but due to a selection bias caused by only considering correct trials.

Together, these findings support the role of the CPP as a correlate of the accumulation process. They also highlight the importance of combining modelling and neuroimaging approaches in order to gain interpretable insights into decision-making, as the shape of the accumulation profile is difficult to predict based on conceptual reasoning alone. Using a number of manipulations, including difficulty, speed stress, non-stationary evidence, and decision biases,

we have shown that the CPP reflects the decision variable and displays similar patterns to those predicted by sequential sampling models.

A further manipulation which is arguably of particular interest when studying perceptual decision-making in the most ecologically valid way possible, is the manipulation of the number of response alternatives. Since perceptual decisions are rarely made between two opposite alternatives outside of the lab, any decision-making model needs to be able to account for multi-alternative decision-making. There have been a number of attempts to explore sequential sampling models under these conditions, indicating that particularly the leaky competing accumulator model (LCA; Usher & McClelland, 2001), can explain multi-alternative decision-making in a number of paradigms (Bogacz et al., 2007; Nunes & Gurney, 2016; Roe et al., 2001). However, to our knowledge, neural correlates of the decision variable in perceptual decisions with multiple alternatives have not yet been explored in humans.

We therefore set out to explore the effects of four-choice compared to two-choice decisions on a neural substrate of accumulation in the human brain. However, although we confirmed the role of the CPP as a neural correlate of decision-making, we deemed a different neural signal more appropriate to explore decisions between multiple alternatives. As described above, the CPP tracks the evolution of the decision as a whole but cannot distinguish between different alternatives. To our knowledge, the CPP has not been used to track decisions between more than two alternatives, and although we speculate that it would track the sum of all accumulation, regardless of the number of alternatives, it cannot give a detailed insight into individual response alternatives which is arguably more important in multi-alternative decision-making. MEP signals on the other hand, can track the level of preparation associated with each response individually and therefore provide richer data, more appropriate to explore decisions with multiple alternatives.

We used a colour discrimination task in which participants were asked to identify the dominant one out of four colours. Each colour was associated with a different response muscle. A cue before each trial informed the participant

which out of the four colours were response options, thereby distinguishing between two-choice and four-choice trials. Besides the manipulation of the number of response options, we also manipulated difficulty by introducing easy and hard trials. By recording MEPs from two muscles during each TMS trial and pooling over trials, we were able to track the evolution of all four possible responses.

In line with previous findings from non-human primates (Churchland et al., 2008), we found that accumulation profiles displayed lower baselines in four-choice, compared to two-choice trials. However, contrary to our expectations, we found no difference in slope between easy and hard decisions. We used the LCA model to fit the data (Usher & McClelland, 2001). This model was chosen as it had previously been shown to account for decisions with multiple alternatives (Bogacz et al., 2007; Nunes & Gurney, 2016; Roe et al., 2001), but also due to its neurophysiological plausibility. The race model we used in previous experiments is a simplified version of the LCA and accounts well for decision-making data in many paradigms. The LCA differs from the race model primarily in its assumption of leakage of information over time, and lateral inhibition between accumulators, both of which arguably play a greater role in more complex decisions like those with multiple alternatives.

We found that a model with four accumulators, and varying inhibition parameters across response muscles, varying starting points across two-choice and four-choice trials, as well as varying drift rates for easy and hard decisions, was able to account for the behavioural data. The simulated accumulation profiles based on this model were similar to the MEP signals, confirming the baseline difference. Interestingly, like the MEP signal, the simulations did not show differences between easy and hard trials. Although drift rates (i.e. accumulation slopes) were free to vary across difficulty conditions, there was no visible difference in the accumulation profiles. On the one hand, this finding confirms the role of the MEP signals as an accumulation signal as it displays the same pattern as the model predictions, even when the results are unexpected. On the other hand however, we have previously claimed that the manipulation of difficulty has been associated with slope variations in a vast

body of both modelling and neuroimaging research, and that any neural correlate of the decision variable should display these variations.

However, in this particular case, the difference between easy and hard trials was likely not large enough to translate into a visible slope difference. Although the difficulty manipulation led to the expected behavioural differences, as well as differences in absolute drift rate values, these were not seen in the accumulation profile. We speculate that this is a task-specific finding. All other experiments reported in this project, which included a manipulation of difficulty, also included a calibration of difficulty for each participant, ensuring not only that each participant can complete the task, but also that easy and hard decisions are different from each other. This calibration did not take place in the colour discrimination task. Instead, the same difficulty levels were chosen for each participant, and although all participants were able to complete the task, the difference between easy and hard trials was likely too small. This is also supported by the comparatively small differences in the RTs associated with easy and hard trials. We therefore argue that although there was no visible slope difference between easy and hard decisions in the MEP signal, this finding is explained by a lack of difference between the conditions and does not question its role as a neural correlate of the decision variable, which was confirmed by model predictions.

Overall, this experiment was, to our knowledge, the first to track the decision variable associated with decisions with multiple alternatives in the human brain, and the first to demonstrate a baseline difference in activity associated with a variation in the number of response alternatives, which has previously been demonstrated in non-human primates (Balan et al., 2008; Basso & Wurtz, 1998; Churchland et al., 2008; Cohen et al., 2009).

## 6.2. Overall Findings

Based on the review of the literature in Chapter 1, we identified four main open questions we aimed to address in this project. In the following, we described the extent to which we answered these questions.

First, we asked the fundamental question of whether accumulation, as described by sequential sampling models, occurs in the human brain. Although accumulation-like processes have repeatedly been established in the neural activity of non-human primates (Gold & Shadlen, 2000; Roitman & Shadlen, 2002; Shadlen & Newsome, 1996, 2001), it remains somewhat unclear whether these findings based on anatomically different and over-trained monkeys can be applied to the human brain. Note also that sequential sampling models were designed to account for RT data and not to predict neural mechanisms. Although a variety of neural signals have been suggested to reflect this accumulation process in the human brain (Donner et al., 2009; O'Connell et al., 2012; Philiastides & Sajda, 2006; Twomey et al., 2015), a clear consensus regarding whether sequential sampling occurs in the human brain and how to record it is yet to be reached. Nevertheless, due to recent findings suggesting promising correlates of decision-making (Hadar et al., 2015; Kelly & O'Connell, 2013; O'Connell et al., 2012; Twomey et al., 2016), we hypothesised that accumulation-to-bound dynamics like those predicted by sequential sampling models occur in the human brain and can be observed using EEG and TMS methods.

The current project confirmed this hypothesis. We found that both EEG and TMS methods can be used to track accumulation-like signals in the human brain and utilised this in a variety of experiments. Specifically, both the CPP and the MEP signal displaying corticospinal excitability related to response preparation displayed a profile that is typical for the accumulation process suggested by sequential sampling models. Both signals build up gradually over the course of the decision and peak at the time of response, suggesting an accumulation-to-bound process. Therefore, in line with previous research

(Hadar et al., 2015; Kelly & O'Connell, 2013; O'Connell et al., 2012; Polanía et al., 2014), we argue that sequential sampling occurs in the human brain during perceptual decision-making and that the associated accumulation process can be observed using EEG and TMS methods.

The second question we aimed to address asked, given that decision-related accumulation can be observed in the human brain, which signals are most suitable to research this process. A large variety of signals stemming from a range of techniques, including functional magnetic resonance imaging (fMRI; Heekeren et al., 2004; Ho et al., 2009; Philiastides & Sajda, 2007), M/EEG (Dmochowski & Norcia, 2015; Donner et al., 2009; Kelly & O'Connell, 2013; O'Connell et al., 2012; Polanía et al., 2014; Twomey et al., 2015), and TMS (Hadar et al., 2015; Michelet et al., 2010) have previously been suggested to display characteristics of the decision variable. Due to its poor temporal resolution, fMRI is better suited to identify specific brain structures associated with decision-making, than to track the fast-evolving decision-variable, and was therefore not further considered. EEG approaches, on the other hand, benefit from a very high temporal resolution and are arguably the most appropriate method to track decision-related accumulation in humans. As indicated above, the ERP component CPP is of particular interest here, as it is one of the few EEG signals which is posited to track accumulation directly (O'Connell et al., 2012). Note that MEG and EEG record highly similar processes and although we chose EEG in the current project, many conclusions would arguably also apply to MEG data.

TMS approaches allowing for a dynamic tracking of decision-related response preparation, like the one suggested by Hadar et al. (2015) may provide additional insights, as the resulting MEP signals can arguably track individual responses, which is not possible using the CPP, which we argue represents the sum of all accumulation during a given decision. We therefore hypothesised on the one hand that the CPP can be used to track the decision variable, suggesting a parietal locus of accumulation, but on the other hand, that downstream accumulation can also be observed in motor areas which are related to the preparation of the response and can be tracked using MEP signals.

The results in this project confirmed this hypothesis. We found that the CPP can be used to track decision-related accumulation in a variety of paradigms, supporting previous research which identified it as a correlate of the decision variable (Kelly & O'Connell, 2013; O'Connell et al., 2012). In a direct comparison, we specifically identified the CPP to be the most suitable neural correlate of the decision variable, compared to other frequently suggested EEG signals (see Chapter 3). We also found that the motor-related LRP closely followed the profile of the CPP, supporting the notion that accumulation is continuously fed forward into the motor system.

Therefore, it is unsurprising that the MEP signal which displays the evolution of response preparation was also found to display the decision-related accumulation of evidence, supporting previous findings (Hadar et al., 2015). Although this signal tracks accumulation indirectly and depends on the association of the decision with a specific motor response, rendering the CPP as the more suitable signal to explore accumulation in most paradigms, it has an important advantage over the CPP. Since MEPs can be recorded from each response-relevant muscle separately, the MEP signal, unlike the CPP, can track the accumulation of each response alternative individually and is, to our knowledge, the only signal that can do so in decisions involving more than two response options in humans (see Chapter 5). We therefore conclude that both the CPP and the MEP signal are suitable signals to track the decision-related accumulation of evidence in the human brain, with the CPP displaying accumulation directly and the MEP signal showing the accumulation-dependent response preparation, and thereby complementing each other.

Thirdly, we aimed to explore how the signals we identified as neural correlates of the decision-making process respond to a number of manipulations, to further test their roles as decision variable signals. To this end, we chose a total of five different manipulations (difficulty, SAT instructions, continuity of evidence, decision bias, number of alternatives), each of which is known to affect behavioural decision-making, and has previously been explained using sequential sampling models. We hypothesised that the neural correlates of the

decision variable would be sensitive to these manipulations and display changes in their profile which are consistent with parameter changes which explain the associated behavioural changes.

The current findings largely supported these hypotheses. In a series of experiments, we recorded the CPP under a variety of conditions, including difficulty, non-stationary evidence, and decision biases (see Chapter 2-4). These manipulations have previously been associated with variations in the value of the accumulation slope (Ratcliff & McKoon, 2008), the continuity of the slope (Holmes et al., 2016), and the starting point of the accumulation (Leite & Ratcliff, 2011) in the modelling literature. We were able to demonstrate each of these changes in the accumulation profile in the CPP, supporting its role as a neural substrate of the decision variable. Additionally, we tested and observed the expected differences in the MEP signal in response to the manipulations of difficulty and a variation in the number of response alternatives (see Chapter 2, 5).

However, we also explored the impact of the SAT which is associated with a difference in threshold in the sequential sampling model literature (Brown & Heathcote, 2008), on both the CPP and the MEP signal, but did not observe the expected difference (see Chapter 1). As explained above, we nevertheless argue that both signals do in fact display the decision variable and that the notion of a threshold change to explain the SAT requires reconsideration.

Lastly, we addressed the question of how similar the identified neural substrates of the accumulation process are to the predictions made by sequential sampling models by directly applying the models to the data, rather than evaluating the neural signals based on intuitive predictions. As outlined in Chapter 1, we argue that, in order to disentangle human perceptual decision-making, a combination of often separated approaches, namely modelling of behavioural data and neuroimaging, is necessary. Increasingly complex experimental designs in particular require a combination of methods to inform each other. This combination is particularly important in order to evaluate a neural signal's role as a correlate of the decision variable, as interactions between parameters

often cause even simple sequential sampling models to predict accumulation profiles which are not predictable through intuitive reasoning alone. Equally, neural correlates of the decision variable can be used to inform sequential sampling models. This is particularly the case as sequential sampling models are designed to account for RT distributions rather than neural signals and can often explain the same data in a number of different ways, which lead to mathematically equivalent model fits, but qualitatively different accumulation profiles, which can only be evaluated using neural accumulation profiles.

We therefore fitted a sequential sampling model to each of our behavioural data sets and used the resulting parameters to simulate mean accumulation rates which we directly compared to the neural signals. Using this approach, the model fit was only influenced by the RT data and was never qualitatively changed to match the neural signal. Therefore, qualitative overlaps between the simulated and the empirical accumulation profile provided strong support for both the validity of the neural signal as a substrate of the decision variable, and the sequential sampling model as a neurally plausible model. By using this combination of approaches, we hypothesised that the waveforms of both the CPP and the MEP signal would display qualitative similarities to the simulated accumulation profile predicted by sequential sampling models.

We confirmed this hypothesis. In two experiments, the CPP displayed qualitatively similar patterns to those simulated by sequential sampling models (see Chapter 4). Similarly, the MEP signal was similar to simulated accumulation profiles, even in unexpected ways as neither the empirical nor the simulated profiles displayed the expected slope difference between easy and hard decisions (see Chapter 5). An exception is reported in Chapter 2, where both the CPP and the MEP signal displayed the same patterns but did not match the simulated accumulation profiles. However, since this is the only case in which the empirical and modelled profiles disagree, we used the neural findings to inform the model and adjusted it to match the neural signals without changing it mathematically. Together, these findings support the validity of the CPP and the MEP signal as neural correlates of the decision variable as well as the neural plausibility of sequential sampling models.

### 6.3. Limitations and Future Directions

Overall this project shed light on human perceptual decision-making by measuring a variety of potential neural correlates of the decision variable in the human brain and evaluating each in the context of sequential sampling models. Although this triangulation of methods, making use of behavioural data, mathematical modelling, and neuroimaging, is a strong approach, there are of course, a number of limitations.

One limitation, which is already discussed briefly above, is that our findings may appear somewhat unfalsifiable. It may seem like in this project, the chosen neural correlates of the decision variable (i.e. the CPP and the MEP signal) could not be questioned in their role, as different models (the LCA or a simpler race model) were chosen depending on which best fitted the data (see Chapter 4-5), and even altered when their predictions did not match the neural signal (Chapter 2). However, we argue that this claim is inaccurate for three reasons. Firstly, while we chose different models depending on which best fitted our data, we did so only with regards to the behavioural data. We aimed to choose the most simple yet neurophysiologically plausible representative of the sequential sampling model framework and used a more complex model (i.e. the LCA) only in experiments with particularly complex decisions (Chapter 5). In each experiment, a number of models were fitted to the data and the best model was chosen based on the quality of the fit to the behavioural data alone. The similarity between the prediction of the model and the neural signal made no contribution to the model selection. Secondly, we adjusted the model to fit the neural data in only one instance (Chapter 2). In this particular case, we had a number of reasons which are discussed more thoroughly above, including ongoing debate about the validity of the original model, which had repeatedly been questioned in previous literature. And thirdly, we have demonstrated that neural signals which have been suggested to reflect accumulation can in fact be falsified in Chapter 3, where we rejected a previously proposed neural decision variable.

An additional limitation of this project is that, while we have explored the evolution of accumulation over time in the human brain, we cannot answer the question of which brain regions are involved in this process. Although we have a good understanding of the structural origins of the MEP signals (Bestmann et al., 2008; Hadar et al., 2015; Rothwell et al., 1987), we do not assume that these structures accumulate evidence directly. The CPP on the other hand reflects accumulation but we have little information about its source. Although based on its recording site, a parietal source is likely, and supported by fMRI findings which have suggested parietal regions to be involved in evidence accumulation (see Mulder et al., 2014), EEG is not an appropriate method to gain insight into the structural origin of a given signal. While the decision variable in the human brain can be studied without having identified the location of its source, future work, e.g. using a combination of EEG and fMRI is necessary to localise the neural structures responsible for sequential sampling.

A further limitation is that we set out to explore decision-related accumulation in the human brain in the context of sequential sampling models as a whole. Although we necessarily chose specific models, namely two accumulator models (a race model without inhibition or leakage, and the LCA; Usher & McClelland, 2001), to fit the data, we interpreted the findings primarily with reference to the entire sequential sampling model framework, rather than a specific model. Note that, as discussed above, accumulator models were chosen due to their neural plausibility and extendibility to multi-alternative decision-making, and applied in this simple form where appropriate in order to make the least amount of assumption possible, and that the more complex version of the accumulator model (i.e. the LCA) was only used in experiments with more complex decision processes in which the additional leakage and inhibition parameters made an impact on the accumulation profile. Nevertheless, these models were used primarily as examples of sequential sampling models as a whole and were not directly compared to each other.

Although we argue that this method was appropriate here as we aimed to comment on whether accumulation as predicted by the sequential sampling model framework as a whole occurs in the human brain, and chose the most

appropriate representatives of this framework, we are aware and even provide evidence (see Chapter 2) that the choice of a specific model can have a large impact on the profile of the simulated accumulation path. Building on our findings, confirming the validity of the CPP and the MEP signal as neural correlates of accumulation, we therefore suggest that future work directly compares these neural signals to accumulation profiles from a variety of different sequential sampling models, thereby evaluating the neural plausibility of each of the models as well as shedding light on the underlying neural mechanisms of perceptual decision-making. For example, finding that the accumulation path predicted by a model with inhibition between accumulators displays more similarities to the CPP than a model without inhibition would not only indicate that the model with inhibition is a more appropriate model, but also that neural populations which integrate evidence for competing alternatives inhibit each other. We therefore propose that a direct model comparison would provide great insights into human perceptual decision-making.

## **6.4. Conclusion**

In summary, we set out to explore perceptual decision-making in the human brain in the context of sequential sampling models. Sequential sampling models assume that we make decisions by accumulating sensory evidence until a threshold is reached and a response is initiated. In a series of experiments, we demonstrated that these accumulation-to-bound processes occur in the human brain. We used a model-based approach, combining mathematical modelling of behavioural data and neuroimaging, by fitting sequential sampling models to empirical RT distributions and comparing associated simulated accumulation profiles with neural signals. Using this approach, we supported previous findings which indicated that the centroparietal ERP component CPP is a correlate of this accumulation process. Additionally, we confirmed that in decisions which require a specific motor response, accumulation is continuously fed forward into the motor system, and as a result, can be measured using an MEP signal reflecting the evolution of response preparation.

We found that the CPP shows qualitatively similar profiles to simulated accumulation profiles in decisions which vary in difficulty, the continuity of evidence, and decision biases, confirming not only its role as a neural correlate of decision-making, but also the validity of sequential sampling models on a neurophysiological level. Further, we gained new insights into the effect of speed stress on decision-making and suggest that this is not explained by a specific variation in threshold, but instead, by a global modulation in activity. Lastly, we explored, for the first time, the neural activity profile of each response alternative in a four-choice paradigm, and confirmed previous findings from non-human primates, suggesting that the number of alternatives influences the baseline activity of the accumulation process.

Overall, we showed that sequential sampling models apply not only to behavioural data but also account for neural processes in the human brain, and that these processes can be observed in both the CPP and the MEP signal. We have argued that a combination of modelling and neuroimaging is useful to gain a better understanding of human decision-making, and demonstrated that both approaches can inform each other. We suggest that future work makes use of these findings in order to directly compare different sequential sampling models and gain further insights into the underlying mechanisms of perceptual decision-making in the human brain.

## 7. Appendices

### 7.1. Appendix 1: Model Results for Normalised Data (Chapter 2, Experiment 1)

In Chapter 2 (see section 2.1), we compared the accumulation profile predicted by sequential sampling models to ERP waveforms. To this end, we fitted a model to RT data which was pooled across participants. We generated model predictions based on a standard model and a rescaled model and showed that the rescaled model is associated with accumulation profiles more similar to the EEG waveforms than the standard model.

Since we conducted the same experiment with TMS instead of ERP data (see section 2.2), which required the normalisation of data, including RTs, for consistency, we repeated the model comparison for the ERP data set with normalised data. To this end, we normalised each participant's RTs and ERPs by their median RT and followed the same steps as described in section 2.1.1.5. We found that the normalisation did not affect the results.

Table 7.1 displays the goodness of fit of three different models we fitted to the RT data. The best (lowest) BIC (Schwarz, 1978) was associated with Model 2, a model in which drift rate varied across difficulty conditions, and both the threshold and the starting point distribution varied across SAT conditions. The same model was shown to provide the best fit to the non-normalised data. The parameters for this model, as well as its rescaled version (see section 2.1.1.5.2) are displayed in Table 7.2.

Table 7.1: Model Comparison: BIC and AIC values for each model (best BIC and AIC values in bold).

Model	Number of parameters	Parameters	Experiment 1	
			BIC	AIC
Model 1	9	$v\text{-easy}_{correct}, v\text{-easy}_{incorrect}, v\text{-hard}_{correct}, v\text{-hard}_{incorrect}, A_{speed}, S_z, T_{er}, S_{Ter}, \sigma^2$	62,827	62,759
Model 2	10	$v\text{-easy}_{correct}, v\text{-easy}_{incorrect}, v\text{-hard}_{correct}, v\text{-hard}_{incorrect}, A_{speed}$	<b>62,741</b>	<b>62,665</b>

		$S_{z-speed}, S_{z-accuracy},$ $T_{er}, S_{Ter}, \sigma^2$		
<b>Model 3</b>	10	$v-easy_{correct}, v-easy_{incorrect},$ $v-hard_{correct}, v-hard_{incorrect},$ $A_{speed},$ $T_{er-speed}, T_{er-accuracy},$ $S_z, S_{Ter}, \sigma^2$	62,835	62,759

Table 7.2: Estimated parameter values for the chosen model (Model 2) and its rescaled version: note that the response threshold  $A$  in the 'accuracy' condition was set to 1 as a scaling parameter.

Parameters		Standard Model: parameter values per SAT Instruction		Rescaled Model: parameter values per SAT Instruction	
		<i>accuracy</i>	<i>speed</i>	<i>accuracy</i>	<i>speed</i>
Starting point variability ( $S_z$ )		0.216	0.644	0.216	0.741
Response threshold ( $A$ )		1	0.869	1	
Non-decision time ( $T_{er}$ )		0.531		0.531	
Non-decision time variability ( $S_{Ter}$ )		0.477		0.477	
Diffusion constant ( $\sigma^2$ )		0.585		0.585	0.673
Drift rate ( $\nu$ )	correct	easy	1.634	1.634	1.882
		hard	0.850	0.850	0.978
	incorrect	easy	0.210	0.210	0.242
		hard	0.039	0.039	0.045

Figure 7.1 displays the quality of the model fit, which is identical for both the standard and the rescaled model. The RT distribution is summarised by five quantile estimates (from left to right: 10%, 30%, 50%, 70%, 90%) for each condition separately. The overlap between empirical and modelled quantiles indicates that the model fitted the data well.

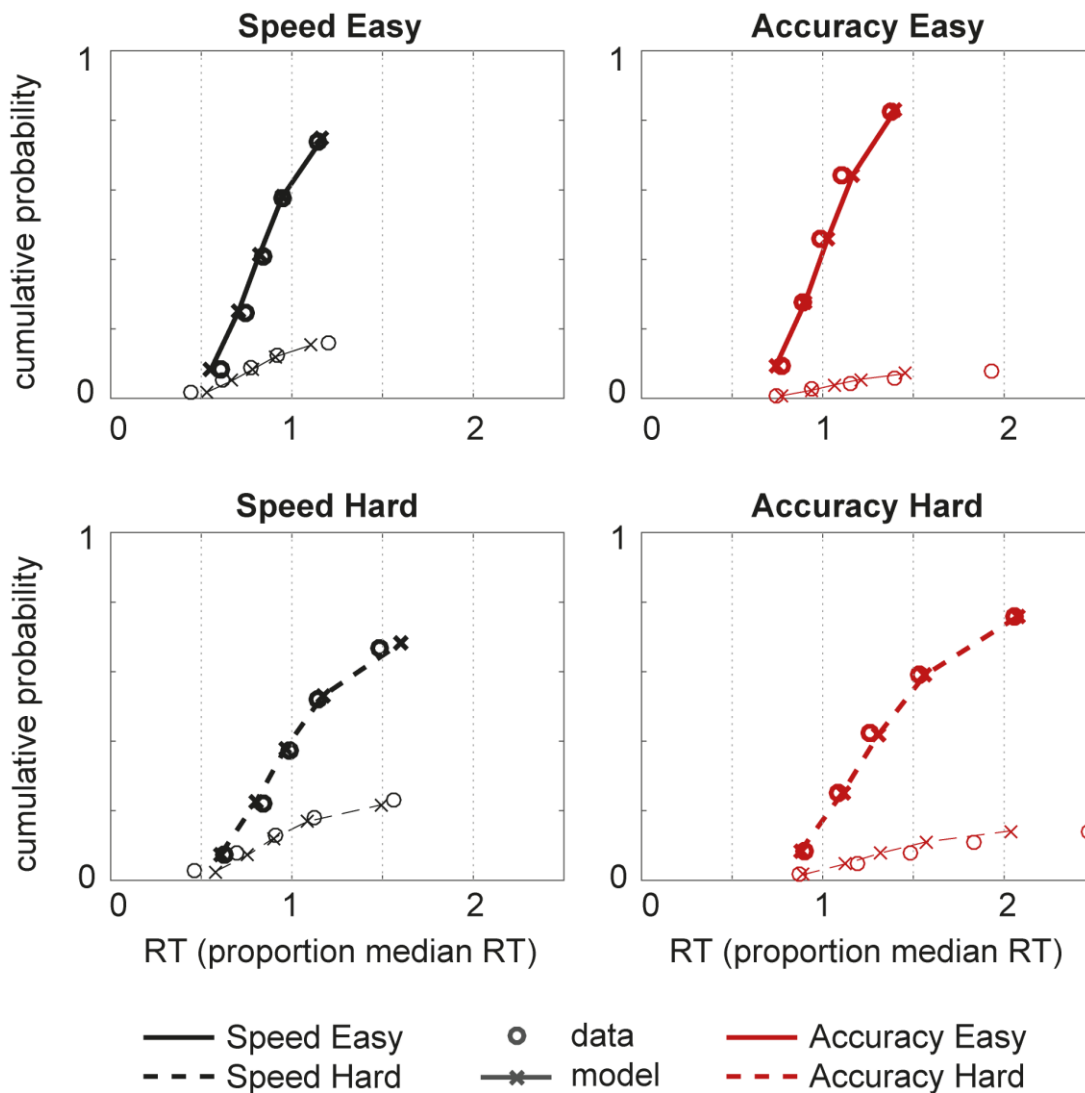


Figure 7.1: Model fit: quantiles estimated from behavioural data (circles) and Model 2 simulations (crosses and lines) for easy (top) and hard (bottom) decisions. For each condition, correct (thick) and incorrect (thin) quantiles are displayed separately. Note that the model fit is identical for the standard and the rescaled race model.

Figure 7.2 displays the normalised ERP (a), as well as the simulated accumulation profile for both the standard (b) and the rescaled (c) model. Visual inspection suggests that the rescaled model predicts profiles more similar to the ERP waveform than the standard model. The similarity of the rescaled model with the ERP was confirmed by a bootstrap test (see section 2.1.1.5.4) which showed that the mean squared errors between the ERP and the simulation was significantly lower for the rescaled model than the standard model ( $p < .05$ ).

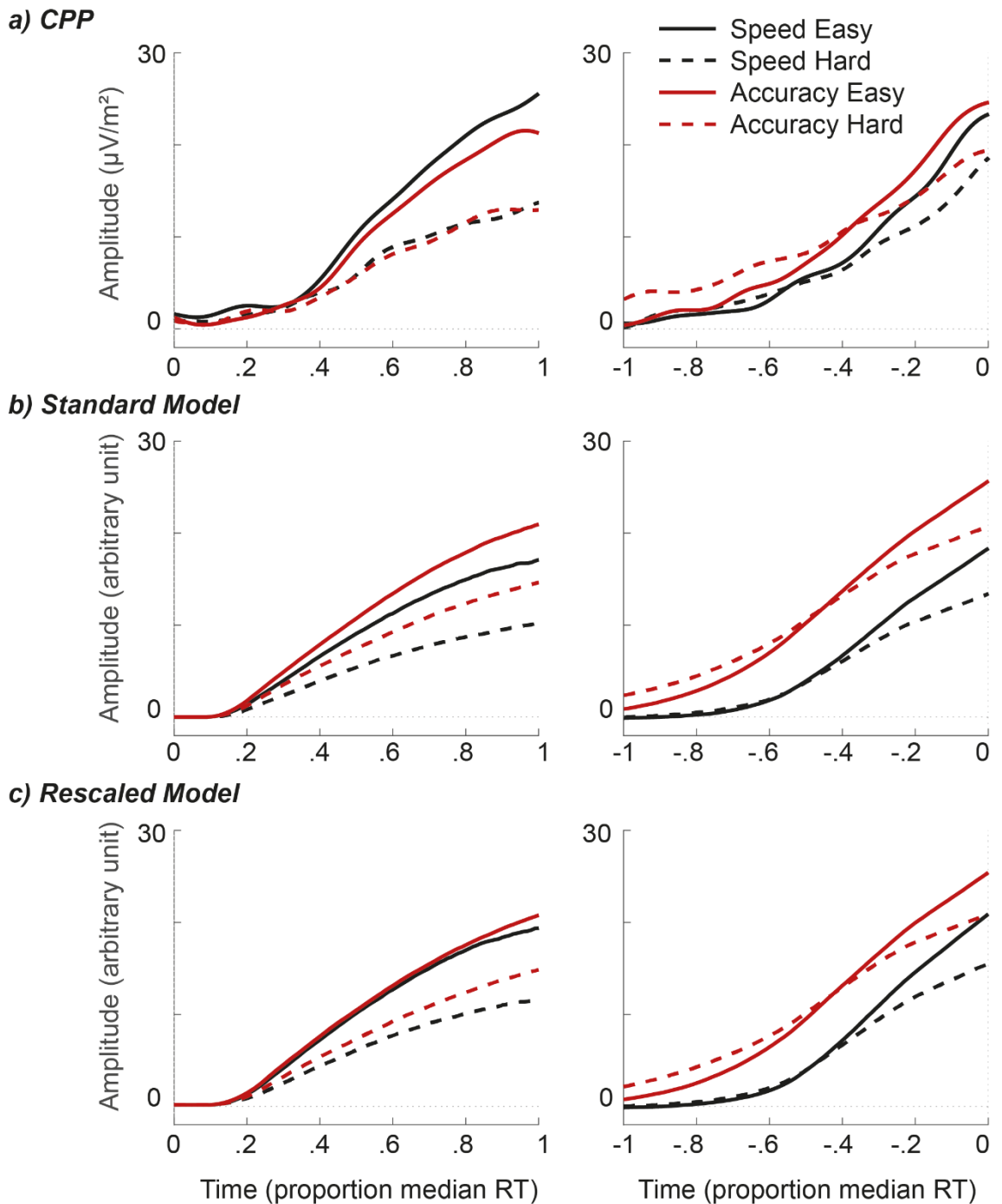
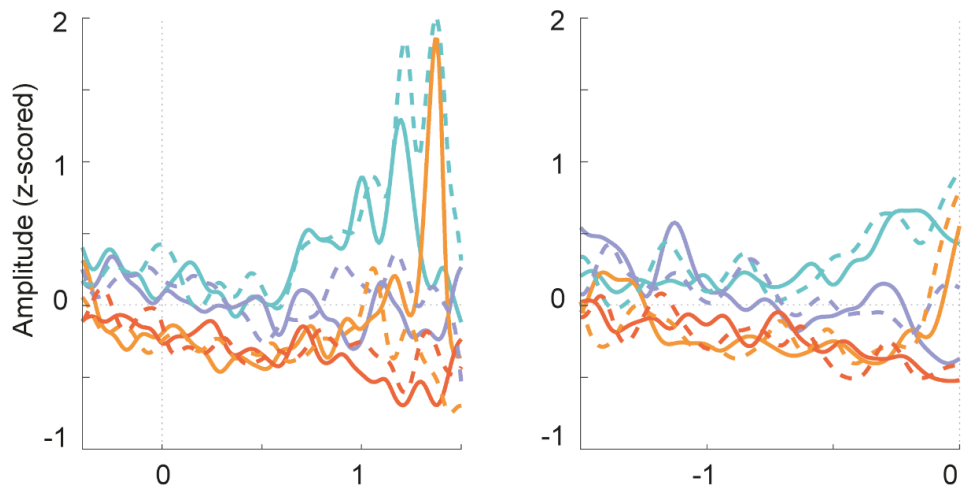


Figure 7.2: Decision variable (empirical and simulated): stimulus-locked (left) and response-locked (right) CPP for each condition. Note that the CPP here is a pooled average rather than a grand average. Additionally, the waveform has been low-pass filtered with a cut-off of 5 Hz for display only. b) accumulation profile (correct and incorrect accumulator summed) per condition as predicted by the standard race model. c) accumulation profile (correct and incorrect accumulator summed) per condition as predicted by the rescaled race model.

## **7.2. Appendix 2: Comparison of Two-choice ‘within’ and Two-choice ‘between’ Conditions (Chapter 5)**

In Chapter 5 (see section 5.2.2), we collapsed over all two-choice trials, including trials in which both response options were mapped to the same hand (within) and those in which the two options were mapped onto two hands (between). Figure 7.3 shows the MEP signals associated with within and between conditions separately. The two conditions do not display any visible qualitative differences.

**a) Two-Choice Between**



**b) Two-Choice Within**

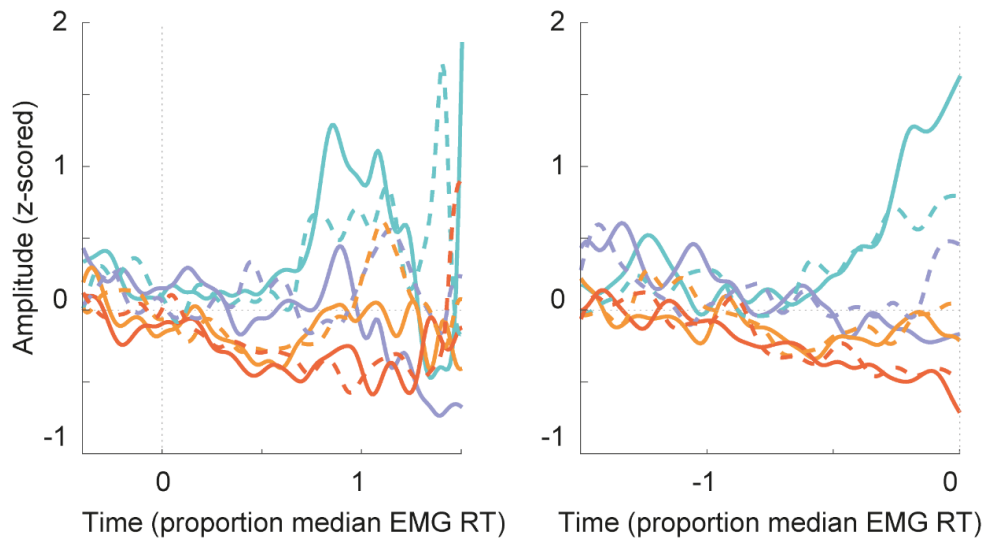


Figure 7.3: MEP results (smoothed MEP signal for each muscle category): stimulus-locked (left) and response-locked (right) smoothed signals are displayed separately for two-choice 'between' trials (trials with two response options on different hands, a) and 'within' trials (trials with two response options on the same hand b). Due to their similarity, we collapsed over 'within' and 'between' trials.

## 8. References

- Abbott, L. (1991). Firing-rate models for neural populations. In O. Benhar, C. Bosio, P. Giudice, & E. Tabet (Eds.), *Neural networks: From biology to high-energy physics* (pp. 179–196). Pisa, Italy: ETS Editrice.  
<http://doi.org/10.1.1.22.4635>
- Ahdab, R., Ayache, S. S., Brugières, P., Farhat, W. H., & Lefaucheur, J. P. (2016). The Hand Motor Hotspot is not Always Located in the Hand Knob: A Neuronavigated Transcranial Magnetic Stimulation Study. *Brain Topography*, 29(4), 590–597. <http://doi.org/10.1007/s10548-016-0486-2>
- Akaike, H. (1977). On entropy maximization principle. In P. R. Krishnaiah (Ed.), *Applications of Statistics* (pp. 27–41). Amsterdam.  
<http://doi.org/10.1007/s10955-006-9121-z>
- Balan, P. F., Oristaglio, J., Schneider, D. M., & Gottlieb, J. (2008). Neuronal correlates of the set-size effect in monkey lateral intraparietal area. *PLoS Biology*, 6(7), 1443–1458. <http://doi.org/10.1371/journal.pbio.0060158>
- Balci, F., Freestone, D., Simen, P., deSouza, L., Cohen, J. D., & Holmes, P. (2011). Optimal Temporal Risk Assessment. *Frontiers in Integrative Neuroscience*, 5(September), 1–15. <http://doi.org/10.3389/fnint.2011.00056>
- Barker, A. T., Jalinous, R., & Freeston, I. L. (1985). Non-Invasive Magnetic Stimulation of Human Motor Cortex. *The Lancet*, 325(8437), 1106–1107.  
[http://doi.org/10.1016/S0140-6736\(85\)92413-4](http://doi.org/10.1016/S0140-6736(85)92413-4)
- Barr, D. J., Levy, R., Scheepers, C., & Tily, H. J. (2014). Random effects structure for confirmatory hypothesis testing: Keep it maximal. *Journal of Memory and Language*, 68(3), 1–43.  
<http://doi.org/10.1016/j.jml.2012.11.001>
- Basso, M. A., & Wurtz, R. H. (1997). Modulation of neuronal activity by target uncertainty. *Nature*, 389(September), 66–69. <http://doi.org/10.1038/37975>
- Basso, M. A., & Wurtz, R. H. (1998). Modulation of neuronal activity in superior colliculus by changes in target probability. *The Journal of Neuroscience : The Official Journal of the Society for Neuroscience*, 18(18), 7519–7534.
- Benjamini, Y., & Hochberg, Y. (1995). Controlling the false discovery rate: a practical and powerful approach to multiple testing. *Journal of the Royal*

*Statistical Society*, 57(1), 289–300.

- Bestmann, S., Harrison, L. M., Blankenburg, F., Mars, R. B., Haggard, P., Friston, K. J., & Rothwell, J. C. (2008). Influence of Uncertainty and Surprise on Human Corticospinal Excitability during Preparation for Action. *Current Biology*, 18(10), 775–780. <http://doi.org/10.1016/j.cub.2008.04.051>
- Bestmann, S., & Krakauer, J. W. (2015). The uses and interpretations of the motor-evoked potential for understanding behaviour. *Experimental Brain Research*, 233(3), 679–689. <http://doi.org/10.1007/s00221-014-4183-7>
- Blair, R. C., & Karniski, W. (1993). An alternative method for significance testing of waveform difference potentials, 518–524.
- Bode, S., Sewell, D. K., Lilburn, S., Forte, J. D., Smith, P. L., & Stahl, J. (2012). Predicting Perceptual Decision Biases from Early Brain Activity. *Journal of Neuroscience*, 32(36), 12488–12498. <http://doi.org/10.1523/JNEUROSCI.1708-12.2012>
- Bogacz, R., Brown, E., Moehlis, J., Holmes, P., & Cohen, J. D. (2006). The physics of optimal decision making: A formal analysis of models of performance in two-alternative forced-choice tasks. *Psychological Review*, 113(4), 700–765. <http://doi.org/10.1037/0033-295X.113.4.700>
- Bogacz, R., Usher, M., Zhang, J., & McClelland, J. L. (2007). Extending a biologically inspired model of choice: multi-alternatives, nonlinearity and value-based multidimensional choice. *Philosophical Transactions of the Royal Society B: Biological Sciences*, 362(1485), 1655–1670. <http://doi.org/10.1098/rstb.2007.2059>
- Bogacz, R., Wagenmakers, E. J., Forstmann, B. U., & Nieuwenhuis, S. (2010). The neural basis of the speed-accuracy tradeoff. *Trends in Neurosciences*, 33(1), 10–16. <http://doi.org/10.1016/j.tins.2009.09.002>
- Brainard, D. H. (1997). The Psychophysics Toolbox. *Spatial Vision*, 10, 433–436. <http://doi.org/10.1163/156856897X00357>
- Britten, K., Newsome, W., Shadlen, M. N., Celebrini, S., & Movshon, J. (1996). A relationship between behavioural choice and the visual responses of neurons in macaque MT. *Visual Neuroscience*, 13, 87–100. <http://doi.org/10.1017/S095252380000715X>
- Brown, S. D., & Heathcote, A. (2008). The simplest complete model of choice response time: Linear ballistic accumulation. *Cognitive Psychology*, 57(3),

153–178. <http://doi.org/10.1016/j.cogpsych.2007.12.002>

- Brown, S., Steyvers, M., & Wagenmakers, E. J. (2009). Observing evidence accumulation during multi-alternative decisions. *Journal of Mathematical Psychology*, *53*(6), 453–462. <http://doi.org/10.1016/j.jmp.2009.09.002>
- Bruce, C. J., & Goldberg, M. E. (1985). Primate frontal eye fields. I. Single neurons discharging before saccades. *Journal of Neurophysiology*, *53*(3), 603–35. Retrieved from <http://www.ncbi.nlm.nih.gov/pubmed/3981231>
- Chen, M. Y., Jimura, K., White, C. N., Todd Maddox, W., & Poldrack, R. A. (2015). Multiple brain networks contribute to the acquisition of bias in perceptual decision-making. *Frontiers in Neuroscience*, *9*(MAR), 1–13. <http://doi.org/10.3389/fnins.2015.00063>
- Chittka, L., Dyer, A. G., Bock, F., & Dornhaus, A. (2003). Psychophysics: Bees trade off foraging speed for accuracy. *Nature*, *424*(6947), 388–388. <http://doi.org/10.1038/424388a>
- Churchland, A. K., Kiani, R., & Shadlen, M. N. (2008). Decision-making with multiple alternatives. *Nature Neuroscience*, *11*(6), 693–702. <http://doi.org/10.1038/nn0708-851c>
- Cisek, P., & Kalaska, J. F. (2005). Neural correlates of reaching decisions in dorsal premotor cortex: Specification of multiple direction choices and final selection of action. *Neuron*, *45*(5), 801–814. <http://doi.org/10.1016/j.neuron.2005.01.027>
- Cisek, P., Puskas, G. A., & El-Murr, S. (2009). Decisions in Changing Conditions: The Urgency-Gating Model. *Journal of Neuroscience*, *29*(37), 11560–11571. <http://doi.org/10.1523/JNEUROSCI.1844-09.2009>
- Cohen, J. Y., Heitz, R. P., Woodman, G. F., & Schall, J. D. (2009). Neural Basis of the Set-Size Effect in Frontal Eye Field: Timing of Attention During Visual Search. *Journal of Neurophysiology*, *101*(4), 1699–1704. <http://doi.org/10.1152/jn.00035.2009>
- Coles, M. G. H., Gratton, G., Bashore, T. R., Eriksen, C. W., & Donchin, E. (1985). A Psychophysiological Investigation of the Continuous Flow Model of Human Information Processing. *Journal of Experimental Psychology: Human Perception and Performance*, *11*(5), 529–553.
- Daw, N. D., O'Doherty, J. P., Dayan, P., Dolan, R. J., & Seymour, B. (2006). Cortical substrates for exploratory decisions in humans. *Nature*, *441*(7095),

- 876–9. <http://doi.org/10.1038/nature04766>
- de Lafuente, V., Jazayeri, M., & Shadlen, M. N. (2015). Representation of accumulating evidence for a decision in two parietal areas. *The Journal of Neuroscience: The Official Journal of the Society for Neuroscience*, *35*(10), 4306–18. <http://doi.org/10.1523/JNEUROSCI.2451-14.2015>
- de Lange, F. P., Rahnev, D. A., Donner, T. H., & Lau, H. (2013). Prestimulus Oscillatory Activity over Motor Cortex Reflects Perceptual Expectations. *Journal of Neuroscience*, *33*(4), 1400–1410. <http://doi.org/10.1523/JNEUROSCI.1094-12.2013>
- Delorme, A., & Makeig, S. (2004). EEGLAB: An open source toolbox for analysis of single-trial EEG dynamics including independent component analysis. *Journal of Neuroscience Methods*, *134*(1), 9–21. <http://doi.org/10.1016/j.jneumeth.2003.10.009>
- Desimone, R. (1998). Visual attention mediated by biased competition in extrastriate visual cortex. *Philosophical Transactions of the Royal Society B: Biological Sciences*, *353*(1373), 1245–1255. <http://doi.org/10.1098/rstb.1998.0280>
- Diederich, A. (2008). A further test of sequential-sampling models that account for payoff effects on response bias in perceptual decision tasks. *Perception & Psychophysics*, *70*(2), 229–256. <http://doi.org/10.3758/PP.70.2.229>
- Diederich, A., & Busemeyer, J. R. (2006). Modeling the effects of payoff on response bias in a perceptual discrimination task: bound-change, drift-rate-change, or two-stage-processing hypothesis. *Perception & Psychophysics*, *68*(2), 194–207. <http://doi.org/10.3758/BF03193669>
- Ditterich, J. (2010). A comparison between mechanisms of multi-alternative perceptual decision making: Ability to explain human behavior, predictions for neurophysiology, and relationship with decision theory. *Frontiers in Neuroscience*, *4*(NOV), 1–24. <http://doi.org/10.3389/fnins.2010.00184>
- Ditterich, J., Mazurek, M. E., & Shadlen, M. N. (2003). Microstimulation of visual cortex affects the speed of perceptual decisions. *Nature Neuroscience*, *6*(8), 891–898. <http://doi.org/10.1038/nn1094>
- Dmochowski, J. P., & Norcia, A. M. (2015). Cortical components of reaction-time during perceptual decisions in humans. *PLoS ONE*, *10*(11), 1–18. <http://doi.org/10.1371/journal.pone.0143339>

- Donchin, E., & Heffley, E. F. (1978). Multivariate analysis of event-related potential data: A tutorial review. In E. Callaway, P. Tueting, & S. H. Koslow (Eds.), *Event-Related Brain Potentials in Man* (pp. 349–441). New York: Academic Press.
- Donders, F. C. (1969). On the speed of mental processes. *Acta Psychologica*, 30, 412–431. [http://doi.org/10.1016/0001-6918\(69\)90065-1](http://doi.org/10.1016/0001-6918(69)90065-1)
- Donkin, C., Averell, L., Brown, S., & Heathcote, A. (2009). Getting more from accuracy and response time data: methods for fitting the linear ballistic accumulator. *Behavior Research Methods*, 41(4), 1095–1110. <http://doi.org/10.3758/BRM.41.4.1095>
- Donner, T. H., Siegel, M., Fries, P., & Engel, A. K. (2009). Buildup of Choice-Predictive Activity in Human Motor Cortex during Perceptual Decision Making. *Current Biology*, 19(18), 1581–1585. <http://doi.org/10.1016/j.cub.2009.07.066>
- Dorris, M. C., & Munoz, D. P. (1998). Saccadic probability influences motor preparation signals and time to saccadic initiation. *The Journal of Neuroscience*, 18(17), 7015–7026.
- Doyle, L. M. F., Yarrow, K., & Brown, P. (2005). Lateralization of event-related beta desynchronization in the EEG during pre-cued reaction time tasks. *Clinical Neurophysiology*, 116(8), 1879–1888. <http://doi.org/10.1016/j.clinph.2005.03.017>
- Dufau, S., Grainger, J., & Ziegler, J. C. (2012). How to say “no” to a nonword: A leaky competing accumulator model of lexical decision. *Journal of Experimental Psychology: Learning, Memory, and Cognition*, 38(4), 1117–1128. <http://doi.org/10.1037/a0026948>
- Feng, S., Holmes, P., Rorie, A., & Newsome, W. T. (2009). Can Monkeys choose optimally when faced with noisy stimuli and unequal rewards? *PLoS Computational Biology*, 5(2). <http://doi.org/10.1371/journal.pcbi.1000284>
- Forstmann, B. U., Anwander, A., Schafer, A., Neumann, J., Brown, S., Wagenmakers, E.-J., ... Turner, R. (2010). Cortico-striatal connections predict control over speed and accuracy in perceptual decision making. *Proceedings of the National Academy of Sciences*, 107(36), 15916–15920. <http://doi.org/10.1073/pnas.1004932107>

- Forstmann, B. U., Dutilh, G., Brown, S., Neumann, J., von Cramon, D. Y., Ridderinkhof, K. R., & Wagenmakers, E.-J. (2008). Striatum and pre-SMA facilitate decision-making under time pressure. *Proceedings of the National Academy of Sciences of the United States of America*, *105*(45), 17538–42. <http://doi.org/10.1073/pnas.0805903105>
- Forstmann, B. U., Ratcliff, R., & Wagenmakers, E.-J. (2016). Sequential Sampling Models in Cognitive Neuroscience: Advantages, Applications, and Extensions. *Annual Review of Psychology*, *67*, 641–66. <http://doi.org/10.1146/annurev-psych-122414-033645>
- Forstmann, B. U., Wagenmakers, E.-J., Eichele, T., Brown, S., & Serences, J. T. (2011). Reciprocal Relations Between Cognitive Neuroscience and Cognitive Models : Opposites Attract ? *Trends in Cognitive Sciences*, *15*(6), 272–9. <http://doi.org/10.1016/j.tics.2011.04.002>. Reciprocal
- Frank, M. J., Gagne, C., Nyhus, E., Masters, S., Wiecki, T. V., Cavanagh, J. F., & Badre, D. (2015). fMRI and EEG Predictors of Dynamic Decision Parameters during Human Reinforcement Learning. *Journal of Neuroscience*, *35*(2), 485–494. <http://doi.org/10.1523/JNEUROSCI.2036-14.2015>
- Furman, M., & Wang, X. J. (2008). Similarity Effect and Optimal Control of Multiple-Choice Decision Making. *Neuron*, *60*(6), 1153–1168. <http://doi.org/10.1016/j.neuron.2008.12.003>
- Gao, J. F., Zheng, C. X., & Wang, P. (2010). Online Removal of Muscle Artifact from Electroencephalogram Signals Based on Canonical Correlation Analysis. *Clinical Eeg and Neuroscience*, *41*(1), 53–59.
- Gao, J., Tortell, R., & McClelland, J. L. (2011). Dynamic integration of reward and stimulus information in perceptual decision-making. *PLoS ONE*, *6*(3). <http://doi.org/10.1371/journal.pone.0016749>
- Gluth, S., Rieskamp, J., & Büchel, C. (2013). Classic EEG motor potentials track the emergence of value-based decisions. *NeuroImage*, *79*(May), 394–403. <http://doi.org/10.1016/j.neuroimage.2013.05.005>
- Gold, J. I., & Shadlen, M. N. (2000). Representation of a perceptual decision in developing oculomotor commands. *Nature*, *404*(6776), 390–394. <http://doi.org/10.1038/35006062>
- Gold, J. I., & Shadlen, M. N. (2003). The influence of behavioral context on the

representation of a perceptual decision in developing oculomotor commands. *The Journal of Neuroscience*, 23(2), 632–651.  
<http://doi.org/10.1038/35006062>

Gold, J. I., & Shadlen, M. N. (2007). The Neural Basis of Decision Making. *Annual Review of Neuroscience*, 30, 535–574.  
<http://doi.org/10.1146/annurev.neuro.29.051605.113038>

Goldfarb, S., Leonard, N. E., Simen, P., Caicedo-Nunez, C. H., & Holmes, P. (2014). A comparative study of drift diffusion and linear ballistic accumulator models in a reward maximization perceptual choice task. *Frontiers in Neuroscience*, 8(8 MAY), 1–11.  
<http://doi.org/10.3389/fnins.2014.00148>

Groppe, D. M., Urbach, T. P., & Kutas, M. (2011). Mass univariate analysis of event-related brain potentials/fields I: A critical tutorial review. *Psychophysiology*, 48(12), 1711–1725. <http://doi.org/10.1111/j.1469-8986.2011.01273.x>

Hadar, A. A., Makris, S., & Yarrow, K. (2012). The truth-telling motor cortex: Response competition in M1 discloses deceptive behaviour. *Biological Psychology*, 89(2), 495–502.  
<http://doi.org/10.1016/j.biopsycho.2011.12.019>

Hadar, A., Rowe, P., Di Costa, S., Jones, A., & Yarrow, K. (2015). Motor-evoked potentials reveal a motor-cortical readout of evidence accumulation for sensorimotor decisions. *Journal of Vision*, 15(12), 49.  
<http://doi.org/10.1167/15.12.49>

Hanes, D. P., & Schall, J. D. (1996). Neural Control of Voluntary Movement Initiation. *Science*, 274(5286), 427–430.

Hanks, T. D., Kiani, R., & Shadlen, M. N. (2014). A neural mechanism of speed-accuracy tradeoff in macaque area LIP. *eLife*, 2014(3), 1–17.  
<http://doi.org/10.7554/eLife.02260>

Hanks, T. D., Mazurek, M. E., Kiani, R., Hopp, E., & Shadlen, M. N. (2011). Elapsed Decision Time Affects the Weighting of Prior Probability in a Perceptual Decision Task. *Journal of Neuroscience*, 31(17), 6339–6352.  
<http://doi.org/10.1523/JNEUROSCI.5613-10.2011>

Hawkins, G. E., Forstmann, B. U., Wagenmakers, E.-J., Ratcliff, R., & Brown, S. D. (2015). Revisiting the evidence for collapsing boundaries and urgency

- signals in perceptual decision-making. *The Journal of Neuroscience : The Official Journal of the Society for Neuroscience*, 35(6), 2476–84.  
<http://doi.org/10.1523/JNEUROSCI.2410-14.2015>
- Hawkins, G. E., Wagenmakers, E.-J., Ratcliff, R., & Brown, S. D. (2015). Discriminating evidence accumulation from urgency signals in speeded decision making. *Journal of Neurophysiology*, jn.00088.2015.  
<http://doi.org/10.1152/jn.00088.2015>
- Heathcote, A., Brown, S., & Mewhort, D. J. K. (2002). Quantile maximum likelihood estimation of response time distributions. *Psychonomic Bulletin and Review*, 9(2), 1–31. <http://doi.org/10.3758/BF03196299>
- Heathcote, A., & Love, J. (2012). Linear deterministic accumulator models of simple choice. *Frontiers in Psychology*, 3(AUG), 1–19.  
<http://doi.org/10.3389/fpsyg.2012.00292>
- Heekeren, H. R., Marrett, S., Bandettini, P. A., & Ungerleider, L. G. (2004). A general mechanism for perceptual decision-making in the human brain. *Nature*, 431(7010), 859–862. <http://doi.org/10.1038/nature02966>
- Heitz, R. P. (2014). The speed-accuracy tradeoff: History, physiology, methodology, and behavior. *Frontiers in Neuroscience*, 8(8 JUN), 1–19.  
<http://doi.org/10.3389/fnins.2014.00150>
- Heitz, R. P., & Schall, J. D. (2012). Neural Mechanisms of Speed-Accuracy Tradeoff. *Neuron*, 76(3), 616–628.  
<http://doi.org/10.1016/j.neuron.2012.08.030>
- Heitz, R. P., & Schall, J. D. (2013). Neural chronometry and coherency across speed-accuracy demands reveal lack of homomorphism between computational and neural mechanisms of evidence accumulation. *Philosophical Transactions of the Royal Society of London. Series B, Biological Sciences*, 368(1628), 20130071.  
<http://doi.org/10.1098/rstb.2013.0071>
- Hick, W. E. (1952). On the rate of gain of information. *Quarterly Journal of Experimental Psychology*, 4(1), 11–26. [http://doi.org/10.1016/0022-0965\(78\)90002-4](http://doi.org/10.1016/0022-0965(78)90002-4)
- Ho, T. C., Brown, S., & Serences, J. T. (2009). Domain General Mechanisms of Perceptual Decision Making in Human Cortex. *Journal of Neuroscience*, 29(27), 8675–8687. <http://doi.org/10.1523/JNEUROSCI.5984-08.2009>

- Hodgkin, A. L., & Huxley, A. F. (1990). A quantitative description of membrane current and its application to conduction and excitation in nerve. *Bulletin of Mathematical Biology*, *52*(1–2), 25–71. <http://doi.org/10.1007/BF02459568>
- Holmes, W. R., Trueblood, J. S., & Heathcote, A. (2016). A new framework for modeling decisions about changing information: The Piecewise Linear Ballistic Accumulator model. *Cognitive Psychology*, *85*, 1–29. <http://doi.org/10.1016/j.cogpsych.2015.11.002>
- Horwitz, G. D., Batista, A. P., & Newsome, W. T. (2004). Representation of an abstract perceptual decision in macaque superior colliculus. *Journal of Neurophysiology*, *91*(5), 2281–2296. <http://doi.org/10.1152/jn.00872.2003>
- Huk, A. C., & Shadlen, M. N. (2005). Neural Activity in Macaque Parietal Cortex Reflects Temporal Integration of Visual Motion Signals during Perceptual Decision Making. *J. Neurosci.*, *25*(45), 10420–10436. <http://doi.org/10.1523/JNEUROSCI.4684-04.2005>
- Ikeda, A., & Shibasaki, H. (1992). Invasive recording of movement-related cortical potentials in humans. *Journal of Clinical Neurophysiology*, *9*(4), 509–520.
- Ivanoff, J., Branning, P., & Marois, R. (2008). fMRI evidence for a dual process account of the speed-accuracy tradeoff in decision-making. *PLoS ONE*, *3*(7). <http://doi.org/10.1371/journal.pone.0002635>
- Jasper, H. H. (1958). The ten-twenty electrode system of the International Federation. *Electroencephalography and Clinical Neurophysiology*, *10*, 371–375.
- Jasper, H., & Penfield, W. (1949). Electroencephalograms in man : Effect of voluntary movement upon the electrical activity of the precentral gyrus. *Archiv Fur Psychatrie Und Zeitschrift Neurologie*, *183*, 163–174. <http://doi.org/10.1007/BF01062488>
- Kaiser, J., Birbaumer, N., & Lutzenberger, W. (2001). Event-related beta desynchronization indicates timing of response selection in a delayed-response paradigm in humans. *Neuroscience Letters*, *312*(3), 149–152. [http://doi.org/10.1016/S0304-3940\(01\)02217-0](http://doi.org/10.1016/S0304-3940(01)02217-0)
- Kaiser, J., Lennert, T., & Lutzenberger, W. (2007). Dynamics of oscillatory activity during auditory decision making. *Cerebral Cortex*, *17*(10), 2258–2267. <http://doi.org/10.1093/cercor/bhl134>

- Karsilar, H., Simen, P., Papadakis, S., & Balci, F. (2014). Speed accuracy trade-off under response deadlines. *Frontiers in Neuroscience*, *8*(248), 1–18. <http://doi.org/10.3389/fnins.2014.00248>
- Kayser, A. S., Buchsbaum, B. R., Erickson, D. T., & Esposito, M. D. (2010). The Functional Anatomy of a Perceptual Decision in the Human Brain. *Journal of Neurophysiology*, *103*, 1179–1194. <http://doi.org/10.1152/jn.00364.2009>.
- Kayser, J., & Tenke, C. E. (2006). Principal components analysis of Laplacian waveforms as a generic method for identifying ERP generator patterns: II. Adequacy of low-density estimates. *Clinical Neurophysiology*, *117*(2), 369–380. <http://doi.org/10.1016/j.clinph.2005.08.033>
- Kelly, S. P., & O'Connell, R. G. (2013). Internal and external influences on the rate of sensory evidence accumulation in the human brain. *J Neurosci*, *33*(50), 19434–19441. <http://doi.org/10.1523/JNEUROSCI.3355-13.2013>
- Keuken, M. C., Van Maanen, L., Bogacz, R., Schäfer, A., Neumann, J., Turner, R., & Forstmann, B. U. (2015). The subthalamic nucleus during decision-making with multiple alternatives. *Human Brain Mapping*, *36*(10), 4041–4052. <http://doi.org/10.1002/hbm.22896>
- Kiani, R., Hanks, T. D., & Shadlen, M. N. (2008). Bounded integration in parietal cortex underlies decisions even when viewing duration is dictated by the environment. *J Neurosci*, *28*(12), 3017–3029. <http://doi.org/10.1523/JNEUROSCI.4761-07.2008>
- Kiani, R., & Shadlen, M. N. (2009). Representation of confidence associated with a decision by neurons in the parietal cortex. *Science (New York, N. Y.)*, *324*(2009), 759–764. <http://doi.org/10.1126/science.1169405>
- Kiers, L., Fernando, B., & Tomkins, D. (1997). Facilitatory effect of thinking about movement on magnetic motor-evoked potentials. *Electroencephalography and Clinical Neurophysiology - Electromyography and Motor Control*, *105*(4), 262–268. [http://doi.org/10.1016/S0921-884X\(97\)00027-1](http://doi.org/10.1016/S0921-884X(97)00027-1)
- Klein-Flugge, M. C., & Bestmann, S. (2012). Time-Dependent Changes in Human Corticospinal Excitability Reveal Value-Based Competition for Action during Decision Processing. *Journal of Neuroscience*, *32*(24), 8373–8382. <http://doi.org/10.1523/JNEUROSCI.0270-12.2012>
- Klein, P.-A., Olivier, E., & Duque, J. (2012). Influence of Reward on

Corticospinal Excitability during Movement Preparation. *The Journal of Neuroscience*, 32(50), 18124–18136.

<http://doi.org/10.1523/JNEUROSCI.1701-12.2012>

Kleiner, M., Brainard, D. H., Pelli, D. G., Broussard, C., Wolf, T., & Niehorster, D. (2007). What's new in Psychtoolbox-3? *Perception*, 36, S14.

<http://doi.org/10.1068/v070821>

Kornhuber, H. H., & Deecke, L. (1965). Hirnpotentialänderungen bei Willkürbewegungen und passiven Bewegungen des Menschen: Bereitschaftspotential und reafferente Potentiale. *Pflügers Archiv Für Die Gesamte Physiologie Des Menschen Und Der Tiere*, 284(1), 1–17.

<http://doi.org/10.1007/BF00412364>

Krajbich, I., & Rangel, A. (2011). Multialternative drift-diffusion model predicts the relationship between visual fixations and choice in value-based decisions. *Proceedings of the National Academy of Sciences of the United States of America*, 108(33), 13852–7.

<http://doi.org/10.1073/pnas.1101328108>

Kruee, G. K., Podell, J. E., & Ronco, P. G. (1954). Effect of number of alternatives and set on the visual discrimination of numerals. *Journal of Experimental Psychology*, 48(1), 75–80. <http://doi.org/10.1037/h0055644>

Kubaneck, J., Snyder, L. H., Brunton, B. W., Brody, C. D., & Schalk, G. (2013). A low-frequency oscillatory neural signal in humans encodes a developing decision variable. *Neuroimage*, 83, 795–808.

<http://doi.org/10.1016/j.neuroimage.2013.06.085>

Kühn, A. A., Williams, D., Kupsch, A., Limousin, P., Hariz, M., Schneider, G. H., ... Brown, P. (2004). Event-related beta desynchronization in human subthalamic nucleus correlates with motor performance. *Brain*, 127(4), 735–746. <http://doi.org/10.1093/brain/awh106>

Lagarias, J. C., Reeds, J. A., Wright, M. H., & Wright, P. E. (1998). Convergence Properties of the Nelder--Mead Simplex Method in Low Dimensions. *SIAM Journal on Optimization*, 9(1), 112–147.

<http://doi.org/10.1137/S1052623496303470>

Lang, W., Cheyne, D., Kristeva, R., Beisteiner, R., Lindinger, G., & Deecke, L. (1991). Three-dimensional localization of SMA activity preceding voluntary movement. A study of electric and magnetic fields in a patient with

- infarction of the right supplementary motor area. *Experimental Brain Research*, 87, 688–695.
- Lee, K.-M., & Keller, E. L. (2008). Neural Activity in the Frontal Eye Fields Modulated by the Number of Alternatives in Target Choice. *Journal of Neuroscience*, 28(9), 2242–2251.  
<http://doi.org/10.1523/JNEUROSCI.3596-07.2008>
- Leite, F. P., & Ratcliff, R. (2011). What cognitive processes drive response biases? A diffusion model analysis. *Judgment and Decision Making*, 6(7), 651–687. <http://doi.org/https://doi.org/10.1371/journal.pone.0146769>
- Li, X., & Aruin, A. (2005). Muscle activity onset time detection using teager-kaiser energy operator. *Conference Proceedings : ... Annual International Conference of the IEEE Engineering in Medicine and Biology Society. IEEE Engineering in Medicine and Biology Society. Conference*, 7, 7549–7552.  
<http://doi.org/10.1109/IEMBS.2005.1616259>
- Li, X., Zhou, P., & Aruin, A. S. (2007). Teager-kaiser energy operation of surface EMG improves muscle activity onset detection. *Annals of Biomedical Engineering*, 35(9), 1532–1538. <http://doi.org/10.1007/s10439-007-9320-z>
- Lo, C.-C., Wang, C.-T., & Wang, X.-J. (2015). Speed-accuracy tradeoff by a control signal with balanced excitation and inhibition. *Journal of Neurophysiology*, 114, 650–661. <http://doi.org/10.1152/jn.00845.2013>
- Lopez-Persem, A., Domenech, P., & Pessiglione, M. (2016). How prior preferences determine decision-making frames and biases in the human brain. *eLife*, 5(NOVEMBER2016), 1–20. <http://doi.org/10.7554/eLife.20317>
- Luce, R. D. (1986). *Response Times: Their Role in Inferring Elementary Mental Organization*. New York: Oxford University Press.
- Maris, E., & Oostenveld, R. (2007). Nonparametric statistical testing of EEG- and MEG-data. *Journal of Neuroscience Methods*, 164(1), 177–190.  
<http://doi.org/10.1016/j.jneumeth.2007.03.024>
- Marshall, J. A. R., Bogacz, R., & Gilchrist, I. D. (2012). Consistent Implementation of Decisions in the Brain. *PLoS ONE*, 7(9).  
<http://doi.org/10.1371/journal.pone.0043443>
- Matthews, P. M., & Jezzard, P. (2004). Functional magnetic resonance imaging. *J. Neurol. Neurosurg. Psychiatry*, 75(1), 6–12. <http://doi.org/978-0-87893->

- Maunsell, J. H., & Van Essen, D. C. (1983). Functional properties of neurons in middle temporal visual area of the macaque monkey. II. Binocular interactions and sensitivity to binocular disparity. *Journal of Neurophysiology*, *49*(5), 1148–1167.
- McMillen, T., & Holmes, P. (2006). The dynamics of choice among multiple alternatives. *Journal of Mathematical Psychology*, *50*(1), 30–57.  
<http://doi.org/10.1016/j.jmp.2005.10.003>
- Merton, P. A., & Morton, H. B. (1980). Stimulation of the cerebral cortex in the intact human subject. *Nature*, *285*(5762), 227–227.  
<http://doi.org/10.1038/285227a0>
- Merton, P. a, Hill, D. K., Morton, H. B., & Marsden, C. D. (1982). Scope of a technique for electrical stimulation of human brain, spinal cord, and muscle. *The Lancet*, *2*(8298), 597–600. [http://doi.org/10.1016/S0140-6736\(82\)90670-5](http://doi.org/10.1016/S0140-6736(82)90670-5)
- Michelet, T., Duncan, G. H., & Cisek, P. (2010). Response Competition in the Primary Motor Cortex: Corticospinal Excitability Reflects Response Replacement During Simple Decisions. *Journal of Neurophysiology*, *104*(1), 119–127. <http://doi.org/10.1152/jn.00819.2009>
- Miletic, S., Turner, B. M., Forstmann, B. U., & Van, L. (2017). Parameter Recovery for the Leaky Competing Accumulator Model. *Journal of Mathematical Psychology*, *67*, 25–50.  
<http://doi.org/https://doi.org/10.1016/j.jmp.2016.12.001>
- Milosavljevic, M., Malmaud, J., & Huth, A. (2010). The Drift Diffusion Model can account for the accuracy and reaction time of value-based choices under high and low time pressure. *Judgement and Decision Making*, *5*(6), 437–449. <http://doi.org/10.2139/ssrn.1901533>
- Mulder, M. J., van Maanen, L., & Forstmann, B. U. (2014). Perceptual decision neurosciences - a model-based review. *Neuroscience*, *277*, 872–884.  
<http://doi.org/10.1016/j.neuroscience.2014.07.031>
- Mulder, M. J., Wagenmakers, E.-J., Ratcliff, R., Boekel, W., & Forstmann, B. U. (2012). Bias in the Brain: A Diffusion Model Analysis of Prior Probability and Potential Payoff. *Journal of Neuroscience*, *32*(7), 2335–2343.  
<http://doi.org/10.1523/JNEUROSCI.4156-11.2012>

- Murphy, P. R., Boonstra, E., & Nieuwenhuis, S. (2016). Global gain modulation generates time-dependent urgency during perceptual choice in humans. *Nature Communications*, 7(May), 13526.  
<http://doi.org/10.1038/ncomms13526>
- Newsome, W., Britten, K., & Movshon, J. (1989). Neuronal correlates of a perceptual decision. *Nature*. <http://doi.org/doi:10.1038/341052a0>
- Nichols, T. E., & Holmes, A. P. (2001). Nonparametric Permutation Tests for {PET} functional Neuroimaging Experiments: A Primer with examples. *Human Brain Mapping*, 15(1), 1–25. <http://doi.org/10.1002/hbm.1058>
- Nieuwenhuis, S., Aston-Jones, G., & Cohen, J. D. (2005). Decision making, the P3, and the locus coeruleus--norepinephrine system. *Psychological Bulletin*, 131(4), 510–532. <http://doi.org/10.1037/0033-2909.131.4.510>
- Niwa, M., & Ditterich, J. (2008). Perceptual decisions between multiple directions of visual motion. *The Journal of Neuroscience*, 28(17), 4435–4445. <http://doi.org/10.1523/JNEUROSCI.5564-07.2008>
- Noorbaloochi, S., Sharon, D., & McClelland, J. L. (2015). Payoff Information Biases a Fast Guess Process in Perceptual Decision Making under Deadline Pressure: Evidence from Behavior, Evoked Potentials, and Quantitative Model Comparison. *J. Neurosci.*, 35(31), 10989–11011.  
<http://doi.org/10.1523/JNEUROSCI.0017-15.2015>
- Noppeney, U., Ostwald, D., & Werner, S. (2010). Perceptual Decisions Formed by Accumulation of Audiovisual Evidence in Prefrontal Cortex. *Journal of Neuroscience*, 30(21), 7434–7446.  
<http://doi.org/10.1523/JNEUROSCI.0455-10.2010>
- Nunes, L. F., & Gurney, K. (2016). Multi-alternative decision-making with non-stationary inputs. *Royal Society Open Science*, 3(8).  
<http://doi.org/10.1098/rsos.160376>
- O’Connell, R. G., Dockree, P. M., & Kelly, S. P. (2012). A supramodal accumulation-to-bound signal that determines perceptual decisions in humans. *Nature Neuroscience*, 15(12), 1729–35.  
<http://doi.org/10.1038/nn.3248>
- Oostenveld, R., Fries, P., Maris, E., & Schoffelen, J. M. (2011). FieldTrip: Open source software for advanced analysis of MEG, EEG, and invasive electrophysiological data. *Computational Intelligence and Neuroscience*,

2011. <http://doi.org/10.1155/2011/156869>

- Osman, A., Lou, L., Muller-Gethmann, H., Rinkenauer, G., Mattes, S., & Ulrich, R. (2000). Mechanisms of speed-accuracy tradeoff: Evidence from covert motor processes. *Biological Psychology*, *51*(2–3), 173–199. [http://doi.org/10.1016/S0301-0511\(99\)00045-9](http://doi.org/10.1016/S0301-0511(99)00045-9)
- Palmer, J., Huk, A. C., & Shadlen, M. N. (2005). The effect of stimulus strength on the speed and accuracy of a perceptual decision. *Journal of Vision*, *5*(5), 1. <http://doi.org/10.1167/5.5.1>
- Paré, M., & Wurtz, R. H. (2001). Progression in Neuronal Processing for Saccadic Eye Movements From Parietal Cortex Area LIP to Superior Colliculus. *Journal of Neurophysiology*, *85*(6), 2545–2562. Retrieved from <http://jn.physiology.org/content/85/6/2545.full#ref-list-1>  
<http://jn.physiology.org/content/85/6/2545#cite>  
<http://jn.physiology.org/content/85/6/2545.full>  
<http://jn.physiology.org/>
- Pelli, D. G. (1997). The VideoToolbox software for visual psychophysics: transforming numbers into movies. *Spatial Vision*. <http://doi.org/10.1163/156856897X00366>
- Perri, R. L., Berchicci, M., Spinelli, D., & Di Russo, F. (2014). Individual differences in response speed and accuracy are associated to specific brain activities of two interacting systems. *Frontiers in Behavioral Neuroscience*, *8*(July), 251. <http://doi.org/10.3389/fnbeh.2014.00251>
- Pfurtscheller, G. (1981). Central beta rhythm during sensorimotor activities in man. *Electroencephalography and Clinical Neurophysiology*, *51*(3), 253–264. [http://doi.org/10.1016/0013-4694\(81\)90139-5](http://doi.org/10.1016/0013-4694(81)90139-5)
- Pfurtscheller, G., & Lopes, F. H. (1999). Event-related EEG / MEG synchronization and desynchronization : basic principles. *Clinical Neurophysiology*, *110*, 1842–1857. [http://doi.org/10.1016/S1388-2457\(99\)00141-8](http://doi.org/10.1016/S1388-2457(99)00141-8)
- Philiastides, M. G., Auksztulewicz, R., Heekeren, H. R., & Blankenburg, F. (2011). Causal role of dorsolateral prefrontal cortex in human perceptual decision making. *Current Biology*, *21*(11), 980–983. <http://doi.org/10.1016/j.cub.2011.04.034>
- Philiastides, M. G., Heekeren, H. R., & Sajda, P. (2014). Human Scalp

- Potentials Reflect a Mixture of Decision-Related Signals during Perceptual Choices. *Journal of Neuroscience*, 34(50), 16877–16889.  
<http://doi.org/10.1523/JNEUROSCI.3012-14.2014>
- Philiastides, M. G., Ratcliff, R., & Sajda, P. (2006). Neural Representation of Task Difficulty and Decision Making during Perceptual Categorization: A Timing Diagram. *Journal of Neuroscience*, 26(35), 8965–8975.  
<http://doi.org/10.1523/JNEUROSCI.1655-06.2006>
- Philiastides, M. G., & Sajda, P. (2006). Temporal characterization of the neural correlates of perceptual decision making in the human brain. *Cerebral Cortex*, 16(4), 509–518. <http://doi.org/10.1093/cercor/bhi130>
- Philiastides, M. G., & Sajda, P. (2007). EEG-Informed fMRI Reveals Spatiotemporal Characteristics of Perceptual Decision Making. *Journal of Neuroscience*, 27(48), 13082–13091.  
<http://doi.org/10.1523/JNEUROSCI.3540-07.2007>
- Platt, M. L., & Glimcher, P. W. (1999). Neural correlates of decision variables in parietal cortex. *Nature*, 400(6741), 233–238. <http://doi.org/10.1038/22268>
- Ploran, E. J., Nelson, S. M., Velanova, K., Donaldson, D. I., Petersen, S. E., & Wheeler, M. E. (2007). Evidence Accumulation and the Moment of Recognition: Dissociating Perceptual Recognition Processes Using fMRI. *Journal of Neuroscience*, 27(44), 11912–11924.  
<http://doi.org/10.1523/JNEUROSCI.3522-07.2007>
- Polanía, R., Krajbich, I., Grueschow, M., & Ruff, C. C. (2014). Neural Oscillations and Synchronization Differentially Support Evidence Accumulation in Perceptual and Value-Based Decision Making. *Neuron*, 82(3), 709–720. <http://doi.org/10.1016/j.neuron.2014.03.014>
- Price, K. V., Storn, R. M., & Jouni, L. A. (2005). *Differential Evolution: A Practical Approach to Global Optimization*. Heidelberg: Springer Berlin Heidelberg. <http://doi.org/10.1038/155531c0>
- Pritchard, W. S. (1981). Psychophysiology of P300. *Psychological Bulletin*, 89(3), 506–540. <http://doi.org/10.1037/0033-2909.89.3.506>
- Rao, V., DeAngelis, G. C., & Snyder, L. H. (2012). Neural correlates of prior expectations of motion in the lateral intraparietal and middle temporal areas. *The Journal of Neuroscience : The Official Journal of the Society for Neuroscience*, 32(29), 10063–74.

<http://doi.org/10.1523/JNEUROSCI.5948-11.2012>

- Ratcliff, R. (1978). A theory of memory retrieval. *Psychological Review*, 85(2), 59–108. <http://doi.org/10.1037/0033-295X.85.2.59>
- Ratcliff, R. (2002). A diffusion model account of response time and accuracy in a brightness discrimination task: Fitting real data and failing to fit fake but plausible data. *Psychonomic Bulletin & Review*, 9(2), 278–291. <http://doi.org/10.3758/BF03196283>
- Ratcliff, R., Cherian, A., & Segraves, M. (2003). A Comparison of Macaque Behavior and Superior Colliculus Neuronal Activity to Predictions From Models of Two-Choice Decisions. *Journal of Neurophysiology*, 90(3), 1392–1407. <http://doi.org/10.1152/jn.01049.2002>
- Ratcliff, R., Gomez, P., & McKoon, G. (2004). A diffusion model account of the lexical decision task. *Psychological Review*, 111(1), 159–182. <http://doi.org/10.1037/0033-295X.111.1.159>
- Ratcliff, R., & McKoon, G. (2008). The diffusion decision model: theory and data for two-choice decision tasks. *Neural Computation*, 20(4), 873–922. <http://doi.org/10.1162/neco.2008.12-06-420>
- Ratcliff, R., Perea, M., Colangelo, A., & Buchanan, L. (2004). A diffusion model account of normal and impaired readers. *Brain and Cognition*, 55(2), 374–382. <http://doi.org/10.1016/j.bandc.2004.02.051>
- Ratcliff, R., Philiastides, M. G., & Sajda, P. (2009). Quality of evidence for perceptual decision making is indexed by trial-to-trial variability of the EEG. *Proceedings of the National Academy of Sciences of the United States of America*, 106(16), 6539–6544. <http://doi.org/10.1073/pnas.0812589106>
- Ratcliff, R., & Rouder, J. N. (1998). Modeling Response Times for Two-Choice Decisions. *Psychological Science*, 9(5), 347–356.
- Ratcliff, R., & Smith, P. L. (2004). A comparison of sequential sampling models for two-choice reaction time. *Psychological Review*, 111(2), 333–367. <http://doi.org/10.1016/j.pestbp.2011.02.012>
- Ratcliff, R., Smith, P. L., Brown, S. D., & McKoon, G. (2016). Diffusion Decision Model: Current Issues and History. *Trends in Cognitive Sciences*, 20(4), 260–281. <http://doi.org/10.1016/j.tics.2016.01.007>
- Ratcliff, R., & Starns, J. J. (2013). Modeling confidence judgments, response times, and multiple choices in decision making: recognition memory and

- motion discrimination. *Psychological Review*, 120(3), 697–719.  
<http://doi.org/10.1037/a0033152>
- Ratcliff, R., Thapar, A., College, B. M., & Mckoon, G. (1992). Effects of aging and IQ on item and associative memory. *Journal of Experimental Psychology*, 140(3), 464–487. <http://doi.org/10.1037/a0023810>
- Ratcliff, R., Thapar, A., & McKoon, G. (2004). A diffusion model analysis of the effects of aging on recognition memory. *Journal of Memory and Language*, 50(4), 408–424. <http://doi.org/10.1016/j.jml.2003.11.002>
- Ratcliff, R., Thapar, A., & McKoon, G. (2010). Individual differences, aging, and IQ in two-choice tasks. *Cognitive Psychology*, 60(3), 127–157.  
<http://doi.org/10.1016/j.cogpsych.2009.09.001>
- Reynolds, J. H., Chelazzi, L., & Desimone, R. (1999). Competitive mechanisms subserve attention in macaque areas V2 and V4. *The Journal of Neuroscience : The Official Journal of the Society for Neuroscience*, 19(5), 1736–1753.
- Rinkenauer, G., Osman, A., Ulrich, R., Muller-Gethmann, H., & Mattes, S. (2004). On the locus of speed-accuracy trade-off in reaction time: inferences from the lateralized readiness potential. *Journal of Experimental Psychology. General*, 133(2), 261–82. <http://doi.org/10.1037/0096-3445.133.2.261>
- Roe, R. M., Busemeyer, J. R., & Townsend, J. T. (2001). Multialternative decision field theory: A dynamic connectionst model of decision making. *Psychological Review*, 108(2), 370–392. <http://doi.org/10.1037/0033-295X.108.2.370>
- Roitman, J. D., & Shadlen, M. N. (2002). Response of neurons in the lateral intraparietal area during a combined visual discrimination reaction time task. *The Journal of Neuroscience : The Official Journal of the Society for Neuroscience*, 22(21), 9475–9489. [http://doi.org/10.1016/S0377-2217\(02\)00363-6](http://doi.org/10.1016/S0377-2217(02)00363-6)
- Romo, R., Hernandez, A., & Zainos, A. (2004). Neuronal correlates of a perceptual decision in ventral premotor cortex. *Neuron*, 41(1), 165–173.  
<http://doi.org/S0896627303008171> [pii]
- Rorie, A. E., Gao, J., McClelland, J. L., & Newsome, W. T. (2010). Integration of sensory and reward information during perceptual decision-making in

- Lateral Intraparietal Cortex (LIP) of the macaque monkey. *PLoS ONE*, 5(2).  
<http://doi.org/10.1371/journal.pone.0009308>
- Rothwell, J. C., Day, B. L., Thompson, P. D., Dick, J. P., & Marsden, C. D. (1987). Some experiences of techniques for stimulation of the human cerebral motor cortex through the scalp. *Neurosurgery*, 20(1), 156–163.
- Schurger, A., Sitt, J. D., & Dehaene, S. (2012). An accumulator model for spontaneous neural activity prior to self-initiated movement. *Proceedings of the National Academy of Sciences*, 109(42), E2904–E2913.  
<http://doi.org/10.1073/pnas.1210467109>
- Schwarz, G. E. (1978). Estimating the dimension of a model. *Annals of Statistics*, 6(2), 461–464.  
<http://doi.org/10.1214/aos/1176344136>.MR468014
- Segraves, M. A. (1992). Activity of monkey frontal eye field neurons projecting to oculomotor regions of the pons. *Journal of Neurophysiology*, 68(6), 1967–1985.
- Selen, L. P. J., Shadlen, M. N., & Wolpert, D. M. (2012). Deliberation in the Motor System: Reflex Gains Track Evolving Evidence Leading to a Decision. *Journal of Neuroscience*, 32(7), 2276–2286.  
<http://doi.org/10.1523/JNEUROSCI.5273-11.2012>
- Servant, M., White, C., Montagnini, A., & Burle, B. (2015). Using Covert Response Activation to Test Latent Assumptions of Formal Decision-Making Models in Humans. *Journal of Neuroscience*, 35(28), 10371–10385. <http://doi.org/10.1523/JNEUROSCI.0078-15.2015>
- Shadlen, M. N., & Newsome, W. T. (1996). Motion perception: seeing and deciding. *Proceedings of the National Academy of Sciences of the United States of America*, 93(January), 628–633.  
<http://doi.org/10.1073/pnas.93.2.628>
- Shadlen, M. N., & Newsome, W. T. (2001). Neural Basis of a Perceptual Decision in the Parietal Cortex (Area LIP) of the Rhesus Monkey. *Journal of Neurophysiology*, 86(4), 1916–1936.
- Siegel, M., Engel, A. K., & Donner, T. H. (2011). Cortical Network Dynamics of Perceptual Decision-Making in the Human Brain. *Frontiers in Human Neuroscience*, 5(February), 1–12. <http://doi.org/10.3389/fnhum.2011.00021>
- Smith, P. L., & Ratcliff, R. (2004). Psychology and neurobiology of simple

- decisions. *Trends in Neurosciences*, 27(3), 161–168.  
<http://doi.org/10.1016/j.tins.2004.01.006>
- Smith, P. L., Ratcliff, R., & Wolfgang, B. J. (2004). Attention orienting and the time course of perceptual decisions: Response time distributions with masked and unmasked displays. *Vision Research*, 44(12), 1297–1320.  
<http://doi.org/10.1016/j.visres.2004.01.002>
- Solnik, S., Rider, P., Steinweg, K., Devita, P., & Hortobágyi, T. (2010). Teager-Kaiser energy operator signal conditioning improves EMG onset detection. *European Journal of Applied Physiology*, 110(3), 489–498.  
<http://doi.org/10.1007/s00421-010-1521-8>
- Spaniol, J., Voss, A., Bowen, H. J., & Grady, C. L. (2011). Motivational incentives modulate age differences in visual perception. *Psychology and Aging*, 26(4), 932–939. <http://doi.org/10.1037/a0023297>
- Stein, R. B. (1967). Some Models of Neuronal Variability. *Biophysical Journal*, 7(1), 37–68. [http://doi.org/10.1016/S0006-3495\(67\)86574-3](http://doi.org/10.1016/S0006-3495(67)86574-3)
- Sternberg, S. (1969). The discovery of processing stages: Extensions of Donders' method. *Acta Psychologica*, 30, 276–315.  
[http://doi.org/10.1016/0001-6918\(69\)90055-9](http://doi.org/10.1016/0001-6918(69)90055-9)
- Summerfield, C., & de Lange, F. P. (2014). Expectation in perceptual decision making: neural and computational mechanisms. *Nature Reviews Neuroscience*, 15(11), 745–756. <http://doi.org/10.1038/nrn3838>
- Summerfield, C., & Koechlin, E. (2010). Economic value biases uncertain perceptual choices in the parietal and prefrontal cortices. *Frontiers in Human Neuroscience*, 4(November), 208.  
<http://doi.org/10.3389/fnhum.2010.00208>
- Summerfield, C., & Tickle, H. (2015). The P300 as a build-to-threshold variable (Commentary on Twomey et al.). *European Journal of Neuroscience*, 42(1), 1635. <http://doi.org/10.1111/ejn.12944>
- Sutton, S., Braren, M., Zubin, J., & John, E. R. (1965). Evoked-Potential Correlates of Stimulus Uncertainty. *Science*, 150(3700), 1187–1188.  
<http://doi.org/10.1126/science.150.3700.1187>
- Teodorescu, A. R., & Usher, M. (2013). Disentangling decision models: from independence to competition. *Psychological Review*, 120(1), 1–38.  
<http://doi.org/10.1037/a0030776>

- Thapar, A., Ratcliff, R., & McKoon, G. (2003). A diffusion model analysis of the effects of aging on letter discrimination. *Psychology and Aging, 18*(3), 415–429. <http://doi.org/10.1037/0882-7974.18.3.415>
- Thompson, K. G., Bichot, N., & Schall, J. D. (1997). Dissociation of visual discrimination from saccade programming in the frontal eye field. *Journal of Neurophysiology*. Retrieved from <http://jn.physiology.org/content/77/2/1046.short>
- Thura, D., Beauregard-Racine, J., Fradet, C.-W., & Cisek, P. (2012). Decision making by urgency gating: theory and experimental support. *Journal of Neurophysiology, 108*(11), 2912–2930. <http://doi.org/10.1152/jn.01071.2011>
- Thura, D., & Cisek, P. (2016). Modulation of Premotor and Primary Motor Cortical Activity during Volitional Adjustments of Speed-Accuracy Trade-Offs. *Journal of Neuroscience, 36*(3), 938–956. <http://doi.org/10.1523/JNEUROSCI.2230-15.2016>
- Tosoni, A., Galati, G., Romani, G. L., & Corbetta, M. (2008). Sensory-motor mechanisms in human parietal cortex underlie arbitrary visual decisions. *Nature Neuroscience, 11*(12), 1446–1453. <http://doi.org/10.1038/nn.2221>.
- Tsetsos, K., Usher, M., & Chater, N. (2010). Preference reversal in multiattribute choice. *Psychological Review, 117*(4), 1275–1291. <http://doi.org/10.1037/a0020580>
- Tsetsos, K., Usher, M., & McClelland, J. L. (2011). Testing multi-alternative decision models with non-stationary evidence. *Frontiers in Neuroscience, 5*(MAY), 1–18. <http://doi.org/10.3389/fnins.2011.00063>
- Turner, B. M., & Sederberg, P. B. (2014). A generalized, likelihood-free method for posterior estimation. *Psychonomic Bulletin & Review, 21*(2), 227–250. <http://doi.org/10.3758/s13423-013-0530-0>
- Twomey, D. M., Kelly, S. P., & Connell, R. G. O. (2016). Abstract and Effector-Selective Decision Signals Exhibit Qualitatively Distinct Dynamics before Delayed Perceptual Reports. *The Journal of Neuroscience, 36*(28), 7346–7352. <http://doi.org/10.1523/JNEUROSCI.4162-15.2016>
- Twomey, D. M., Murphy, P. R., Kelly, S. P., & O'Connell, R. G. (2015). The classic P300 encodes a build-to-threshold decision variable. *European Journal of Neuroscience, 42*(1), 1636–1643.

- <http://doi.org/10.1111/ejn.12936>
- Tzagarakis, C., Ince, N. F., Leuthold, A. C., & Pellizzer, G. (2010). Beta-Band Activity during Motor Planning Reflects Response Uncertainty. *Journal of Neuroscience*, *30*(34), 11270–11277.  
<http://doi.org/10.1523/JNEUROSCI.6026-09.2010>
- Ulehla, Z. J. (1966). Optimality of perceptual decision criteria. *Journal of Experimental Psychology*, *71*(4), 564–9. Retrieved from <http://www.ncbi.nlm.nih.gov/pubmed/5909083>
- Urai, A. E., & Pfeffer, T. (2014). An action-independent signature of perceptual choice in the human brain. *The Journal of Neuroscience*, *34*(15), 5081–5082. <http://doi.org/10.1523/JNEUROSCI.0477-14.2014>
- Usher, M., & McClelland, J. L. (2001). The time course of perceptual choice: The leaky, competing accumulator model. *Psychological Review*, *108*(3), 550–592. <http://doi.org/10.1037/0033-295X.108.3.550>
- van Veen, V., Krug, M. K., & Carter, C. S. (2008). The neural and computational basis of controlled speed-accuracy tradeoff during task performance. *Journal of Cognitive Neuroscience*, *20*(11), 1952–1965.  
<http://doi.org/10.1162/jocn.2008.20146>
- van Vugt, M. K., Simen, P., Nystrom, L. E., Holmes, P., & Cohen, J. D. (2012). EEG oscillations reveal neural correlates of evidence accumulation. *Frontiers in Neuroscience*, (JULY), 1–13.  
<http://doi.org/10.3389/fnins.2012.00106>
- van Vugt, M. K., Simen, P., Nystrom, L., Holmes, P., & Cohen, J. D. (2014). Lateralized readiness potentials reveal properties of a neural mechanism for implementing a decision threshold. *PLoS ONE*, *9*(3).  
<http://doi.org/10.1371/journal.pone.0090943>
- Vaughan, H. G., Costa, L. D., & Ritter, W. (1968). Topography of the human motor potential. *Electroencephalography and Clinical Neurophysiology*, *25*(1), 1–10. [http://doi.org/10.1016/0013-4694\(68\)90080-1](http://doi.org/10.1016/0013-4694(68)90080-1)
- Venables, W. N., & Ripley, B. D. (2002). *Modern Applied Statistics with S*. New York: Springer. <http://doi.org/10.1007/978-0-387-21706-2>
- Voss, A., Nagler, M., & Lerche, V. (2013). Diffusion models in experimental psychology: A practical introduction. *Experimental Psychology*, *60*(6), 385–402. <http://doi.org/10.1027/1618-3169/a000218>

- Watson, A. P., & Pelli, D. G. (1983). QUEST: A Bayesian adaptive psychometric method *ANDREW*, 33(2), 113–120.
- Wenzlaff, H., Bauer, M., Maess, B., & Heekeren, H. R. (2011). Neural Characterization of the Speed-Accuracy Tradeoff in a Perceptual Decision-Making Task. *Journal of Neuroscience*, 31(4), 1254–1266.  
<http://doi.org/10.1523/JNEUROSCI.4000-10.2011>
- Wickelgren, W. A. (1977). Speed-Accuracy Tradeoff and Information Processing Dynamics. *Acta Psychologica*, 41, 67–85.
- Wyart, V., de Gardelle, V., Scholl, J., & Summerfield, C. (2012). Rhythmic Fluctuations in Evidence Accumulation during Decision Making in the Human Brain. *Neuron*, 76(4), 847–858.  
<http://doi.org/10.1016/j.neuron.2012.09.015>
- Zaepffel, M., Trachel, R., Kilavik, B. E., & Brochier, T. (2013). Modulations of EEG Beta Power during Planning and Execution of Grasping Movements. *PLoS ONE*, 8(3). <http://doi.org/10.1371/journal.pone.0060060>
- Zhou, X., Wong-Lin, K., & Philip, H. (2009). Time-varying perturbations can distinguish among integrate-to-threshold models for perceptual decision making in reaction time tasks. *Neural Computation*, 21(8), 2336–62.  
<http://doi.org/10.1162/neco.2009.07-08-817>